

**FUNDAMENTAL STUDY OF CATIONIC DOPED CALCIUM PHOSPHATE BASED
SCAFFOLDS AND COATINGS FOR BONE TISSUE ENGINEERING**

by

Satish Sanjay Singh

B. S. Chemical Engineering, University of Florida, 2008

Submitted to the Graduate Faculty of
Swanson School of Engineering in partial fulfillment
of the requirements for the degree of
Doctor of Philosophy

University of Pittsburgh

2014

UNIVERSITY OF PITTSBURGH
SWANSON SCHOOL OF ENGINEERING

This dissertation was presented

by

Satish Sanjay Singh

It was defended on

June 20th, 2014

and approved by

Ipsita Banerjee, Ph.D., Assistant Professor, Department of Chemical Engineering

Steven R. Little, Ph.D., Associate Professor, Department of Chemical Engineering

Kacey G. Marra, Ph.D., Associate Professor, Department of Surgery

Dissertation Director: Prashant N. Kumta, Ph.D., Edward R. Weidlein Chair Professor,

Departments of Bioengineering, Chemical Engineering, Mechanical Engineering and

Materials Science

Copyright © by Satish Sanjay Singh

2014

FUNDAMENTAL STUDY OF CATIONIC DOPED CALCIUM PHOSPHATE BASED SCAFFOLDS AND COATINGS FOR BONE TISSUE ENGINEERING

Satish Sanjay Singh, PhD

University of Pittsburgh, 2014

Calcium phosphates (CaPs) are widely studied as scaffolds for hard tissue regeneration due to their similar composition to the inorganic component of native mineralized tissues. Unfortunately, their poor mechanical properties and the limited dissolution of hydroxyapatite (HA), the most ubiquitous CaP in bone tissue engineering, restricts their application to the treatment of non-load bearing defects. In order to improve patient outcomes, a major emphasis has been placed on the controlled delivery of growth factors, such as bone morphogenic proteins (BMPs), from CaPs, to accelerate regeneration and recruit cells capable of resorbing HA. However, the added expense, poor shelf life, and the unknown side effects of treatment with increased amounts of growth factors are the major limitations of this approach.

In an attempt to reduce the requirement to deliver increased amounts of growth factors, more resorbable CaP phases, such as β -tricalcium phosphate (β -TCP), have been studied. Recent work has shown that scaffolds prepared with β -TCP may be at least equally capable of inducing *in vivo* bone regeneration in comparison to autologous bone grafts and BMP-2, delivered from a collagen sponge. This favorable response is believed to be due to the capability of β -TCP to degrade in a more clinically relevant time frame, similar to the rate at which native tissues are regenerated, and release bioactive Ca^{2+} and PO_4^{3-} ions in close proximity to the defect site.

In addition to Ca^{2+} and PO_4^{3-} , mineralized tissues are composed of several other elements which play a key role in regulating their structure and function. Therefore, in the current work

the influence of ionic substitutions using two biologically relevant cations, Mg^{2+} and Sr^{2+} , in CaPs on their physicochemical and biological properties was studied. It was hypothesized that β -TCP scaffolds prepared with various amounts of Mg^{2+} and Sr^{2+} would provide microenvironments suitable for promoting osteogenic differentiation in comparison to commercially available β -TCP. In addition to bulk scaffolds, cationic substituted β -TCP was explored as a bioactive coating on a biodegradable metallic substrate. The influence of coating composition and structure on corrosion protection and cytocompatibility was assessed. Finally, the influence of cationic substitution on the physicochemical properties and cytocompatibility of an injectable self-setting HA cement was also evaluated.

TABLE OF CONTENTS

LIST OF TABLES	XIV
LIST OF FIGURES	XVII
PREFACE.....	XXX
1.0 INTRODUCTION.....	1
1.1 BONE DEVELOPMENT, STRUCTURE, AND REPAIR.....	1
1.1.1 Osteoblasts.....	3
1.1.2 Osteoclasts	4
1.1.3 Osteocytes.....	6
1.2 OVERVIEW OF BONE TISSUE ENGINEERING.....	6
1.3 SYNTHETIC MATERIALS USED IN BONE TISSUE ENGINEERING ...	8
1.3.1 Polymers	8
1.3.1.1 Natural Polymers	9
1.3.1.2 Synthetic Polymers.....	11
1.3.2 Metals.....	13
1.3.2.1 Non-Degradable Metals.....	13
1.3.2.2 Biodegradable Metals	14
1.3.3 Non-Calcium Phosphate Based Ceramics.....	15
1.4 CALCIUM PHOSPHATES IN BONE TISSUE ENGINEERING.....	17

1.4.1	Calcium Phosphate Phases	18
1.4.2	Formation of Clinically Relevant Forms of Calcium Phosphate	20
1.4.2.1	Calcium Phosphate Granules.....	20
1.4.2.2	Preformed Porous Scaffolds.....	21
1.4.2.3	Calcium Phosphate Self Setting Cements	22
1.4.2.4	Calcium Phosphate Coatings	24
1.4.3	Limitations of Calcium Phosphates	27
1.4.4	Ionic Substitution in Calcium Phosphates	27
2.0	THESIS GOALS	30
2.1	SPECIFIC AIM 1	30
2.2	SPECIFIC AIM 2	32
2.3	SPECIFIC AIM 3	34
2.4	SPECIFIC AIM 4	35
3.0	SYNTHESIS AND CHARACTERIZATION OF MAGNESIUM SUBSTITUTED B-TRICALCIUM PHOSPHATE	38
3.1	INTRODUCTION	38
3.2	MATERIALS AND METHODS	40
3.2.1	Synthesis of Magnesium Substituted β -Tricalcium Phosphate	40
3.2.2	X-Ray Diffraction and Rietveld Refinement.....	41
3.2.3	Thermal Stability	42
3.2.4	Elemental Analysis	42
3.2.5	Scaffold Preparation.....	43
3.2.6	Scaffold Pore Size Distribution and Protein Adsorption.....	43

3.2.7	Cell Culture and Maintenance	44
3.2.8	Cell Viability	44
3.2.9	Alkaline Phosphatase Activity	45
3.2.10	Osteogenic Gene Expression.....	47
3.2.11	Statistical Analysis.....	47
3.3	RESULTS AND DISCUSSION	48
3.3.1	Powder Characterization	48
3.3.1.1	X-Ray Diffraction.....	48
3.3.1.2	Thermal Analysis	51
3.3.1.3	Rietveld Refinement.....	55
3.3.2	Scaffold Characterization	60
3.3.2.1	Pore Size Distribution and Total Pore Volume	60
3.3.2.2	Protein Adsorption.....	62
3.3.2.3	Cell Viability	64
3.3.2.4	Ionic Concentrations in Culture Media	67
3.3.2.5	Alkaline Phosphatase Activity	68
3.3.2.6	Osteogenic Gene Expression	70
3.4	CONCLUSIONS.....	73
4.0	SYNTHESIS AND CHARACTERIZATION OF MAGNESIUM-STRONTIUM CO-SUBSTITUTED B-TRICALCIUM PHOSPHATE.....	75
4.1	INTRODUCTION	75
4.2	MATERIALS AND METHODS	77
4.2.1	Synthesis of Mg and Mg-Sr Co-Substituted β -Tricalcium Phosphate.....	77

4.2.2	Powder Characterization	78
4.2.3	Scaffold Preparation.....	79
4.2.4	Cell Culture and Maintenance	79
4.2.5	Cell Proliferation	80
4.2.6	Live/dead Staining	80
4.2.7	Chemical Analysis of Culture Media	81
4.2.8	Alkaline Phosphatase Activity	81
4.2.9	Indirect Cell Culture	81
4.2.10	Osteogenic Protein Expression.....	82
4.2.11	Transforming Growth Factor- β Signaling PCR Array	84
4.2.12	Statistical Analysis.....	84
4.3	RESULTS AND DISCUSSION	86
4.3.1	Powder Characterization	86
4.3.1.1	Phase Composition	86
4.3.1.2	Elemental Composition.....	87
4.3.1.3	Thermal Stability	88
4.3.1.4	Particle Size and Density	90
4.3.2	In-Vitro Cytocompatibility	95
4.3.2.1	Cell Proliferation.....	95
4.3.2.2	Chemical Analysis of Culture Media	97
4.3.2.3	Osteogenic Protein Expression	100
4.3.2.4	Indirect Cell Culture.....	103
4.3.2.5	Transforming Growth Factor-β Signaling PCR Array.....	104

4.4	CONCLUSIONS.....	109
5.0	SYNTHESIS AND CHARACTERIZATION OF AMORPHOUS CALCIUM MAGNESIUM PHOSPHATES.....	110
5.1	INTRODUCTION	110
5.2	MATERIALS AND METHODS	112
5.2.1	Synthesis of pH Modified β -TCMP	112
5.2.2	Characterization of Amorphous β -TCMP Powder	113
5.2.3	The Formation of β -TCP and β -TCMP Scaffolds	113
5.2.4	Human Mesenchymal Stem Cell Culture and Maintenance	113
5.2.5	Cell Proliferation	114
5.2.6	Alkaline Phosphatase Activity	114
5.2.7	qRT-PCR.....	115
5.2.8	Media Supplementation with Mg^{2+} and PO_4^{3-} Ions	116
5.2.9	MTT Assay	116
5.2.10	Osteoimage Mineralization Assay.....	117
5.2.11	Statistical Analysis.....	117
5.3	RESULTS AND DISCUSSION	118
5.3.1	Characterization of Amorphous β -TCMP	118
5.3.2	Cell Proliferation on Amorphous β -TCMP.....	127
5.3.3	Ionic Concentrations in Culture Media.....	129
5.3.4	Osteogenic Differentiation on Amorphous β -TCMP.....	132
5.3.5	Influence of Mg^{2+} and PO_4^{3-} Concentration on Proliferation.....	135
5.3.6	Influence of Mg^{2+} and PO_4^{3-} Concentration on Mineralization	137

5.4	CONCLUSIONS.....	140
6.0	CATIONIC SUBSTITUTED CALCIUM PHOSPHATE COATINGS ON BIODEGRADABLE MAGNESIUM ALLOYS.....	142
6.1	INTRODUCTION	142
6.2	MATERIALS AND METHODS	144
6.2.1	Substrate Preparation, Pretreatment, and Coating Formation	144
6.2.2	Coating Characterization.....	145
6.2.3	Corrosion Experiments	146
6.2.3.1	Hydrogen Evolution.....	146
6.2.3.2	Immersion Test.....	146
6.2.3.3	Electrochemical Corrosion Testing	147
6.2.4	In-Vitro Cytocompatibility	147
6.2.4.1	Cell Culture and Maintenance.....	147
6.2.4.2	Cell Proliferation.....	148
6.2.4.3	Osteogenic Gene Expression	149
6.2.4.4	Osteogenic Protein Expression	149
6.2.4.5	Statistical Analysis	150
6.3	RESULTS AND DISCUSSION	151
6.3.1	Pretreatment Characterization	151
6.3.2	Coating Structural Characterization.....	156
6.3.3	Corrosion Protection	161
6.3.3.1	Hydrogen Evolution and Immersion Test	161
6.3.3.2	Electrochemical Corrosion Testing.....	165

6.3.4	In-Vitro Cytocompatibility	166
6.3.4.1	Live/Dead Staining.....	166
6.3.4.2	DNA Concentration	167
6.3.4.3	Osteogenic Gene and Protein Expression	169
6.4	CONCLUSIONS	175
7.0	MURINE OSTEOBLASTIC AND OSTEOCLASTIC DIFFERENTIATION ON STRONTIUM RELEASING HYDROXYAPATITE FORMING BONE CEMENTS	177
7.1	INTRODUCTION	177
7.2	MATERIALS AND METHODS	179
7.2.1	Synthesis of Strontium Substituted Dicalcium Phosphate Dihydrate	179
7.2.2	Powder Characterization	179
7.2.3	Cement Scaffold Characterization.....	180
7.2.4	Cell Culture and Maintenance	181
7.2.4.1	MC3T3-E1 Cell Culture	181
7.2.4.2	RAW 264.7 Cell Culture.....	182
7.2.5	MC3T3-E1 Cell Proliferation	182
7.2.6	Alkaline Phosphatase Activity	183
7.2.7	Osteogenic Protein Expression	183
7.2.8	Tartrate Resistant Acidic Phosphatase (TRAP) Activity	184
7.2.9	RAW264.7 Morphology	184
7.2.10	Statistical Analysis.....	185
7.3	RESULTS AND DISCUSSION	185
7.3.1	Dicalcium Phosphate Dihydrate Characterization.....	185

7.3.2	Cement Scaffold Characterization.....	188
7.3.2.1	Setting Time.....	188
7.3.2.2	Phase Composition.....	190
7.3.2.3	Elemental Composition of Cement Scaffolds	195
7.3.2.4	Wet Compressive Strength and % Porosity	196
7.3.2.5	MC3T3-E1 Proliferation	197
7.3.2.6	Ionic Concentrations in Media.....	199
7.3.2.7	MC3T3-E1 Osteogenic Differentiation	201
7.3.2.8	RAW 264.7 TRAP Activity and Morphology.....	204
7.4	CONCLUSIONS.....	207
8.0	GENERAL CONCLUSIONS AND FUTURE WORK	208
	APPENDIX A.....	215
	APPENDIX B.....	220
	APPENDIX C.....	240
	APPENDIX D.....	272
	BIBLIOGRAPHY.....	280

LIST OF TABLES

Table 1.1	The advantages and disadvantages of the synthetic materials used in bone tissue engineering.	18
Table 1.2	The properties of the calcium phosphate phases widely studied in bone tissue engineering [83].	19
Table 1.3	A summary of the advantages and disadvantages of the various processes used to deposit calcium phosphate coatings on metallic substrates.	25
Table 1.4	The elemental composition of enamel, dentin, and bone [118].	28
Table 3.1	The molar amounts of calcium and magnesium chloride dissolved in 100 ml of DI water and used in the precipitation of DCPD by adding drop wise to 100 ml of 0.05 M Na ₂ HPO ₄ at room temperature.	41
Table 3.2	Calcium site positions and occupancy factors for β-TCP from Dickens et. al. ...	41
Table 3.3	qRT-PCR genes and primer sequences used for MC3T3-E1 mouse preosteoblasts	47
Table 3.4	BET surface areas and true density of β-TCMP powders after precipitating, refluxing for two hours, and heat treatment to 600°C.	57
Table 4.1	Amounts of Ca ²⁺ , Mg ²⁺ , and Sr ²⁺ containing precursors used in the precipitation of Mg and Mg-Sr doped CaHPO ₄ •2H ₂ O.	78
Table 4.2	Elemental analysis of as prepared Mg and Mg-Sr doped β-TCP.	87

Table 4.3	Surface area and true density of Mg and Mg-Sr doped β -TCP after precipitating, refluxing, and heat treatment to 600°C.	94
Table 5.1	The qRT-PCR primer sequences used to determine the gene expression of GAPDH, RUNX2, collagen-1, and osteocalcin.....	115
Table 5.2	The elemental composition of 50% Mg DCPD and the powders collected after refluxing 50% Mg DCPD at a pH of 4, without pH modification, and at a pH of 8.	122
Table 6.1	The molar concentrations of the salts used to prepare coating solutions. A (Ca+Sr)/P of 1.67 was maintained for all conditions and the Sr/(Ca+Sr) ratio was varied between 0, 5, and 10%.....	145
Table 6.2	The qRT-PCR primer sequences used for mouse preosteoblast cell line MC3T3-E1.....	149
Table 6.3	The qRT-PCR primer sequences used for human mesenchymal stem cells.	149
Table 6.4	ICP elemental analysis of pretreated coatings formed after immersion in Na ₂ HPO ₄ . Coatings from 9 samples were collected and analyzed.....	156
Table 6.5	ICP elemental analysis of CaP coatings formed after immersion in solutions containing various amounts of Ca ²⁺ , Sr ²⁺ , and PO ₄ ³⁻ . Coatings from 9 samples were collected and analyzed.	159
Table 6.6	Corrosion data collected from hydrogen evolution experiments and potentiodynamic polarization tests. Three repeats for each condition were performed for electrochemical corrosion experiments.	162
Table 7.1	The elemental compositions of DCPD precipitated with and without Sr, determined using ICP.	188

Table 7.2	The setting times at 37°C for cements prepared with a 55:45 TTCP:DCPD ratio by weight and a P/L ratio of 2.2 g ml ⁻¹	190
Table 7.3	The elemental composition of cement powders after setting and after immersion in PBS at 37°C for 7 days.	195
Table 7.4	The wet compressive strength and % porosity of cement samples after incubation in PBS at 37°C for 1 and 7 days. The % porosity was calculated using the formula $1-(\rho_A/\rho_T)$, where ρ_A is the apparent density and ρ_T is the true density.	196
Table A.1	BET surface areas of β -TCMP prior to forming DCPD cements and the surface area of the cement powders after setting.	218
Table B.1	The phosphating bath ionic concentrations	222

LIST OF FIGURES

Figure 1.1	The hierarchical organization of bone at multiple length scales. At the macroscopic level, the cortical bone forms a dense outer layer which encapsulates the trabecular, or spongy, bone within the marrow cavity. At the microscopic level, both trabecular and cortical bone are comprised of lamellar type structures. At the nanoscale, bone is a composite of collagen fibers and plates of mineral dispersed between these fibers providing structural reinforcement [16].	3
Figure 1.2	On the left of the figure, osteoclasts are derived from hematopoietic stem cells and quiescent osteoclast precursors (QoP). On the right of the figure, osteoblasts are formed from mesenchymal stem cells, pericytes, and lining cells. On the bottom of the figure, osteocytes are entrapped within the bone matrix and directly communicate with osteoblasts and osteoclasts [19].	5
Figure 1.3	The mechanical properties of some of the more common materials used in bone tissue engineering in comparison to mineralized tissues [46].	10
Figure 1.4	An example of an injectable calcium phosphate self-setting cement prior to and after setting using cylindrical molds of varying size.	23
Figure 3.1	Powder X-ray diffraction data collected from i) DCPD (JCPDS 09-0077) and DCPD precipitated ii) 35%, iii) 40%, iv) 45%, and v) 50% Mg.	46

Figure 3.2	Powder X-ray diffraction data collected from i) β -TCP (JCPDS 09-0169) and β -TCMP after refluxing with ii) 35%, iii) 40%, iv) 45%, and v) 50% Mg.....	50
Figure 3.3	Thermogravimetric analysis and differential scanning calorimetry data collected from powder samples prepared with 35 and 50% Mg.....	52
Figure 3.4	Powder X-ray diffraction data collected from samples prepared using i) 35, ii) 40, iii) 45, and iv) 50% Mg after heat treatment to 750°C ($\text{Ca}_2\text{P}_2\text{O}_7$ JCPDS 03-0421 and $\text{Mg}_2\text{P}_2\text{O}_7$ JCPDS 05-0582).....	53
Figure 3.5	SEM images of powder samples prepared with a) 35% and b) 50% Mg after heat treatment to temperatures greater than 750°C.	54
Figure 3.6	Powder X-ray diffraction data collected from i) β -TCP (JCPDS 09-0169) and β -TCMP after refluxing and heat treatment to 600°C with ii) 35%, iii) 40%, iv) 45%, and v) 50% Mg.....	56
Figure 3.7	The effect of varying the Mg^{2+} concentration in β -TCMP synthesis on lattice parameters a and c	58
Figure 3.8	A comparison of the mol. % of Mg^{2+} calculated from Rietveld refinement and measured using elemental analysis.....	59
Figure 3.9	The pore size distribution of scaffolds prepared using commercially available β -TCP, 35% β -TCMP, and 50% β -TCMP measured using Hg porosimetry.....	61
Figure 3.10	The total protein measured from scaffolds after incubation in FBS.....	62
Figure 3.11	Coomassie blue staining illustrating the size distribution of proteins adsorped to scaffold surfaces.	63
Figure 3.12	MC3T3-E1 a) live/dead staining and b) SEM images on scaffolds prepared using i) commercially available β -TCP, ii) 35% β -TCMP, and iii) 50% β -TCMP.....	65

Figure 3.13	MC3T3-E1 proliferation on β -TCMP scaffolds determined using the MTT assay after 3 and	66
Figure 3.14	The a) pH and b) Ca^{2+} , c) Mg^{2+} , and d) PO_4^{3-} concentrations in cell culture media during the MC3T3-E1 proliferation experiments.....	68
Figure 3.15	Alkaline phosphatase activity measured after 7, 14, and 21 days in osteogenic media normalized with respect to DNA concentration. A p value of < 0.05 was considered significant.....	69
Figure 3.16	qRT-PCR gene expression of a) collagen 1, b) osteocalcin, and c) runx2 for MC3T3-E1 cells cultured on commercially available β -TCP and β -TCMP scaffolds after 14 and 21 days in osteogenic media. All conditions were normalized to undifferentiated cells. A p value of < 0.05 was considered significant.....	71
Figure 4.1	The signaling pathways involved in regulating MSC differentiation on natural hydroxyapatite scaffolds [160].	76
Figure 4.2	X-ray diffraction data collected from as prepared i) DCPD (JCPDS 09-0077), ii) 35-15%, iii) 40-10%, iv) 45-5%, and 50% Mg and Mg-Sr doped DCPD.....	83
Figure 4.3	X-ray diffraction data collected from as prepared i) β -TCP (JCPDS 09-0169), ii) 35-15%, iii) 40-10%, iv) 45-5%, and 50% Mg and Mg-Sr doped β -TCP.....	85
Figure 4.4	DTA-TGA data collected from samples prepared with 50% Mg and 35-15% Mg-Sr doped β -TCP while heating in air at a rate of $10^\circ\text{C min}^{-1}$ up to 1000°C	89
Figure 4.5	X-ray diffraction data collected from i) β -TCP (JCPDS 09-0169), ii) 35-15%, iii) 40-10%, iv) 45-5%, and v) 50% Mg and Mg-Sr β -TCP heat treated to 600°C ...	91

Figure 4.6	<p>TEM images of 35-15% Mg-Sr doped β-TCP after heat treatment to 600°C at a magnification a) 6,000X and b) 40,000X and 50% Mg doped β-TCP after heat treatment to 600°C at a magnification of c) 6,000X and d) 40,000X. The crystalline and amorphous regions observed in the areas from which the Fast Fourier Transform Diffraction Patterns (FFT-DPs) were collected are illustrated using the symbols ‘X’ and ‘A’, respectively. 93</p>
Figure 4.7	<p>Cell viability was assessed after 3 and 9 days in growth media using the MTT assay. The data collected for all conditions was normalized to that of commercially available β-TCP. 96</p>
Figure 4.8	<p>Live/dead staining of hMSCs seeded on scaffolds prepared with a) 35-15% Mg-Sr β-TCP and b) β-TCP after 3 days and SEM images of hMSCs after 3 days on samples prepared using c) 35-15% Mg-Sr β-TCP and d) β-TCP. 97</p>
Figure 4.9	<p>The ionic concentrations of a) Ca^{2+}, b) Sr^{2+}, c) Mg^{2+}, and d) PO_4^{3-} in culture media throughout the experiment. 98</p>
Figure 4.10	<p>Alkaline phosphatase (ALP) activity measured from hMSCs after culturing for 14 and 21 days in osteogenic media on β-TCP prepared with various amounts of Mg and Mg-Sr. A p value of < 0.05 was considered significant. 100</p>
Figure 4.11	<p>The intracellular expression of osteopontin (OPN) and osteoprotegrin (OPG) of hMSCs cultured for 21 days in osteogenic media a) directly and b) indirectly on β-TCP prepared with various amounts of Mg and Mg-Sr. A p value of < 0.05 was considered significant. 102</p>
Figure 4.12	<p>The gene expression of a) BMP and its receptors b) TGF-β and its receptors, c) SMAD proteins, and d) the ECM components and transcription factors either up</p>

	or downregulated by more than 50% cultured on 50% Mg β -TCP in comparison to commercially available β -TCP. The markers with C_t values of less than 30 were reported.	105
Figure 4.13	The interaction of genes in the Cellular Development network analyzed using Ingenuity Pathway Analysis. The red filled shapes correspond to the up-regulated genes while the blank ones were not found in the input list. The genes with a fold change greater than or equal to 2 in comparison to β -TCP were included in the analysis.	107
Figure 5.1	The pH with respect to time while refluxing DCPD precipitated with 35 and 50% Mg.....	119
Figure 5.2	X-ray diffraction data collected from i) β -TCP (JCPDS 09-0169), 50% Mg DCPD refluxed at ii) a pH of 4, iii) with no pH modification, and iv) a pH of 8.	121
Figure 5.3	FT-IR spectra collected from commercially available i) DCPD, ii) β -TCP, iii) 50% β -TCMP, and iv) 50% β -TCMP refluxed at a pH of 8.....	124
Figure 5.4	Powder X-ray diffraction of i) β -TCP (JCPDS 09-0169), ii) as prepared amorphous β -TCMP, amorphous β -TCMP heat treated to iii) 200°C, iv) 400°C, and v) 600°C.	126
Figure 5.5	hMSC proliferation on scaffolds prepared using commercially available β -TCP, 50% β -TCMP, and fully amorphous 50% β -TCMP refluxed at a pH of 8.....	128
Figure 5.6	The ionic concentrations of a) Ca^{2+} , b) Mg^{2+} , and c) PO_4^{3-} in culture media after up to 21 days in growth media released from β -TCP, β -TCMP, and A β -TCMP scaffolds.	131

Figure 5.7	The alkaline phosphatase activity of hMSCs cultured directly on β -TCP, β -TCMP, and A β -TCMP containing scaffolds with growth media (GM) and differentiation media (DM) after 14 and 21 days.	133
Figure 5.8	qRT-PCR results collected from hMSCs cultured on β -TCMP and amorphous β -TCMP constructs after 14 days in osteogenic media. The data presented is normalized to that determined for hMSCs cultured on scaffolds prepared using commercially available β -TCP.	134
Figure 5.9	MTT cell viability data collected from hMSCs cultured in growth media (GM) supplemented with 5 mM Mg, 5 mM PO ₄ , 5 mM Mg and 5 mM PO ₄ , and differentiation, or osteogenic, media (DM). The data presented is normalized with respect to that collected for the cells cultured in growth media after 1 day. hMSCs cultured in GM with 10% DMSO was used as a negative control.	135
Figure 5.10	A proposed scheme for the stages of osteogenic differentiation. Active proliferation typically occurs for up to one week. The first regulatory transition during the differentiation process result in matrix formation which the second concludes with matrix maturation and mineralization [18].	136
Figure 5.11	The staining of the mineral formed by hMSCs cultured in media supplemented with a) 5 mM Mg, b) 5 mM PO ₄ , c) 5 mM Mg and 5 mM PO ₄ , and d) osteogenic or differentiation media after 14 days.	138
Figure 5.12	The staining of the mineral formed by hMSCs cultured in media supplemented with a) 5 mM Mg, b) 5 mM PO ₄ , c) 5 mM Mg and 5 mM PO ₄ , and d) osteogenic or differentiation media after 21 days.	139

Figure 5.13	The quantification of the mineral formed in the presence of growth media supplemented with various amounts of Mg and PO ₄ ions. The data collected was normalized with respect to that collected for cells cultured in growth media after 14 days.	140
Figure 6.1	a) Optical images of AZ31 after immersion in Na ₂ HPO ₄ and heat treatments as well as SEM images of the substrate surface after b) immersion in Na ₂ HPO ₄ , c) heat treatment to 350°C, and d) heat treatment to 400°C (Scale bars are 2 μm).	151
Figure 6.2	ATR-FTIR spectra collected from samples after a) Na ₂ HPO ₄ treatment, b) heat treatment to 350°C, and c) heat treatment to 400°C.	153
Figure 6.3	XRD collected from coatings formed on AZ31 after i) Na ₂ HPO ₄ treatment, ii) heat treatment to 350°C, and iii) heat treatment to 400°C. (Na ₂ HPO ₄ (JCPDS 01-0997), Mg ₃ PO ₄ •8H ₂ O (JCPDS 33-0877), and MgO (JCPDS 04-0829)).	155
Figure 6.4	XRD collected from CaP coatings formed on pretreated AZ31 after heat treatment to a) 350°C and b) 400°C and immersion in solutions prepared with i) 0, ii) 5, and iii) 10% Sr/(Ca+Sr) ratios (β-TCP (JCPDS 09-0169) and HA (JCPDS 09-0432)).	158
Figure 6.5	The morphology of CaP coatings formed on substrates pretreated to 350°C prepared with a) no Sr and b) 10% Sr; substrates pretreated at 400°C with c) no Sr and d) 10% Sr.....	160
Figure 6.6	The thickness of CaP coatings formed on substrates pretreated to a) 350 and b) 400°C with no Sr.....	161

Figure 6.7	a) pH measurements and b) elemental analysis of culture media after incubation with coated and uncoated samples for up to 21 days.....	164
Figure 6.8	Live/dead staining on culture plastic, Sr0-350, Sr5-350, and Sr10-350 after 3 (a-d) and 7 (e-h) days of culture with MC3T3-E1 cells.....	167
Figure 6.9	An SEM image of MC3T3-E1 cells after 3 days of culture on Sr10-350.	168
Figure 6.10	DNA concentration measured from a) MC3T3-E1 preosteoblast cells and b) hMSCs after 3 and 7 days of culture in growth media on AZ31 coated and uncoated substrates.....	170
Figure 6.11	qRT-PCR gene expression data showing the expression of osteopontin (OPN) and osteocalcin (OCN) of a) MC3T3-E1 cells and b) hMSCs cultured on coated samples normalized with respect to cells cultured on bare AZ31.	172
Figure 6.12	Osteocalcin (OCN) concentration measured from lysed hMSCs after 18 days of culture in osteogenic media.	174
Figure 7.1	The X-ray diffraction patterns of i) DCPD (JCPDS 09-0077), ii) undoped DCPD, iii) 5% Sr DCPD, and iv) 10% Sr DCPD after drying under vacuum.....	187
Figure 7.2	The microstructure of DCPD particles precipitated a) without Sr, b) with 5% Sr, and c) with 10% Sr.	189
Figure 7.3	X-ray diffraction patterns of i) DCPD (JCPDS 09-0077), ii) TTCP (JCPDS 25-1137), iii) HA (JCPDS 09-0432), and cement samples after setting prepared with iv) undoped DCPD, v) 5% Sr DCPD, and vi) 10% Sr DCPD.....	192
Figure 7.4	X-ray diffraction patterns of i) DCPD (JCPDS 09-0077), ii) TTCP (JCPDS 25-1137), iii) HA (JCPDS 09-0432), and cement samples after 3 days in PBS prepared with iv) undoped DCPD, v) 5% Sr DCPD, and vi) 10% Sr DCPD....	193

Figure 7.5	The weight % of a) HA, b) DCPD, and c) TTCP in cement samples after setting and after immersion in PBS at 37°C for 1, 3, and 7 days determined using Rietveld refinement.	194
Figure 7.6	MC3T3-E1 cell proliferation determined using the alamarblue assay after culturing on cements prepared using undoped, 5, and 10% Sr DCPD for up to 15 days in growth media.	198
Figure 7.7	The a) pH and concentrations of b) Ca ²⁺ , c) Sr ²⁺ , and d) PO ₄ ³⁻ in culture media during MC3T3-E1 viability experiments on cements prepared with undoped, 5% Sr, and 10% Sr DCPD.	200
Figure 7.8	Alkaline phosphatase activity and osteogenic protein expression after 21 days of MC3T3-E1 cells cultured a)-b) directly on cement scaffolds and c)-d) indirectly with cement scaffolds in osteogenic media.	203
Figure 7.9	Tartrate resistant acidic phosphatase (TRAP) activity of RAW 264.7 cells cultured directly on cement scaffolds in media supplemented with 50 ng*ml ⁻¹ of RANKL.....	205
Figure 7.10	Cytoskeletal staining of RAW 264.7 cells cultured a) on culture plastic, and directly on cement scaffolds prepared with b) undoped DCPD, c) 5% Sr DCPD, and d) 10% Sr DCPD in media supplemented with 50 ng*ml ⁻¹ of RANKL for 10 days.....	206
Figure 8.1	The a) alkaline phosphatase activity and b) OPN expression of hMSCs cultured with scaffolds prepared using β-TCP and a calcium magnesium silicate bioceramic (akerminate) [223].	213

Figure A.1	The setting times of DCPD forming cements prepared using deionized water and a powder to liquid ratio of 2 g ml ⁻¹ at 37°C.	217
Figure B.1	FT-IR spectra of iv) β-TCP, iii) PB1, ii) PB2, and i) PB3 coated samples as prepared on a) AZ31 and b) Mg-4Y. Also included are the FT-IR spectra of iv) uncoated, iii) PB1, ii) PB2, and i) PB3 samples after incubation for one week in DMEM on c) AZ31 and d) Mg-4Y are also shown.	227
Figure B.2	SEM images of Mg4Y samples coated in a) PB1 and b) PB3 as well as EDX plots taken from Mg4Y samples coated in c) PB1 and d) PB3. EDX mapping was also performed illustrating the distribution of Ca (blue), P (green), and Si (pink) for (e) AZ31 coated in PB3 and (f) Mg-4Y coated in PB3. Scale bars are 500 μm.	230
Figure B.3	The ICP-OES measurements of a) Mg, b) Zn, and c) Al in collected DMEM from AZ31 coated and uncoated samples as well as d) Mg and e) Y from MgY coated and uncoated samples.	231
Figure B.4	Live/dead imaging at a magnification of 10X of a) uncoated AZ31 and AZ31 immersed in b) PB1, c) PB2, and d) PB3 as well as uncoated e) Mg4Y and Mg4Y immersed in f) PB1, g) PB2, and h) PB3 after 3 days of culture.	237
Figure B.5	SEM images of fixed samples at a magnification of 500X on a) uncoated AZ31 and AZ31 immersed in b) PB1, c) PB2, and d) PB3 as well as uncoated e) Mg4Y and Mg4Y immersed in f) PB1, g) PB2, and h) PB3 after 3 days of culture. ...	238
Figure C.1	FT-IR spectra of (a) Ca(NO ₃) ₂ ·4H ₂ O, (b) P ₂ O ₅ , (c) tetraethyl orthosilicate (TEOS), (d) dried gel of x = 0, (e) dried gel of x = 1, (f) dried gel of x = 2, and (g) dried gel of x = 3.	248

Figure C.2	The DSC and TG curves of the as dried gels.....	251
Figure C.3	X-ray diffraction patterns of coated samples heat treated to 450°C, 24 h, in argon together with the standard diffraction patterns (a) JCPDS# 9-169 of β -tricalcium phosphate (β -TCP), (b) $x = 0$, (c) JCPDS #9-432 for hydroxyapatite, (d) $x = 1$, (e) $x = 2$, and (f) $x = 3$	254
Figure C.4	FTIR spectra for the standard β -tricalcium phosphate (β -TCP), standard hydroxyapatite (HA) powders and gel coated substrates treated to 450°C, 24 h, in argon (a) β -TCP (HIMED, New York, USA), (b) $x = 0$, (c) HA (ACROS organics), (d) $x = 1$, (e) $x = 2$, and (f) $x = 3$	255
Figure C.5	SEM micrographs at different magnifications and EDX results on the coated substrates heat treated to 450°C, 24 h, argon, (a) SEM of $x = 0$ coatings; scale bar = 100 μ m, (b) SEM of $x = 0$ coatings; scale bar = 10 μ m, (c) SEM of $x = 0$ coatings; scale bar = 500 nm, (d) SEM of $x = 2$ coatings; scale bar = 100 μ m, (e) SEM of $x = 2$ coatings; scale bar = 10 μ m, (f) SEM of $x = 2$ coatings; scale bar = 500 nm, (g) EDX spectrum of $x = 0$ coatings, and (h) EDX spectrum of $x = 2$ coatings.	258
Figure C.6	SEM micrographs at different magnifications and EDX results on the coated substrates heat treated to 450°C, 24 h, argon, (a) SEM of $x = 0$ coatings; scale bar = 100 μ m, (b) SEM of $x = 0$ coatings; scale bar = 10 μ m, (c) SEM of $x = 0$ coatings; scale bar = 500 nm, (d) SEM of $x = 2$ coatings; scale bar = 100 μ m, (e) SEM of $x = 2$ coatings; scale bar = 10 μ m, (f) SEM of $x = 2$ coatings; scale bar = 500 nm, (g) EDX spectrum of $x = 0$ coatings, and (h) EDX spectrum of $x = 2$ coatings.	260

Figure C.7	SEM images of the pristine Mg4Y, CaPs coated (x=0) and Si-CaPs coated (x=3) substrates after incubation in DMEM for different times. The scale bar for all the images is 100 m.	262
Figure C.8	MC3T3-E1 cells were seeded onto uncoated, CaPs coated (x=0) and Si-CaPs coated (x=2) substrates, and tissue culture polystyrene plate, incubated for 24h and 72h, and double-stained to be green for live cells and red for dead cells. The scale bar for all the images is 100 m.....	266
Figure C.9	Plots of (a) live to dead MC3T3-E1 cells ratio and (b) % area coverage by live MC3T3-E1 cells for bare metal (Mg4Y). CaPs coated (x = 0) and Si-CaPs coated (x = 1, 2, and 3) substrates together with tissue culture plastics as control.....	267
Figure C.10	SEM images of MC3T3-E1 cells on (a) CaPs coated (x=0) substrate at day 1, (b) CaPs coated (x=0) substrate at day 3, (c) CaPs coated (x=0) substrate at day 3, arrow showing cell junction and extension that bridges the crack in the porous films, and (d) Si-CaPs coated (x = 3) substrate at day 3.....	269
Figure D.1	Tafel plots of MAO treated AZ31 for coatings deposited after various amounts of time in Hank's buffer solution kept at 37°C.	275
Figure D.2	The microstructure of a) MAO coated AZ31 after 10 minutes, b) the CaP coating formed on top of MAO treated AZ31, and c) the CaP coating formed in the presence of 10% Sr on MAO treated AZ31 at 1000X.....	276
Figure D.3	The microstructure of a) MAO coated AZ31 after 10 minutes, b) the CaP coating formed on top of MAO treated AZ31, and c) the CaP coating formed in the presence of 10% Sr on MAO treated AZ31 at 2000X.....	277

Figure D.4 Live/dead staining of MC3T3-E1 cells on a) tissue culture plastic, b) MAO treated AZ31, c) CaP coated MAO treated AZ31, and d) SrCaP coated MAO treated AZ31 after 3 days of culture. Scale bars are 200 μm 278

Figure D.5 Live/dead staining of MC3T3-E1 cells on a) tissue culture plastic, b) MAO treated AZ31, c) CaP coated MAO treated AZ31, and d) SrCaP coated MAO treated AZ31 after 7 days of culture. Scale bars are 200 μm 279

PREFACE

First and foremost I would like to thank my thesis advisor, Dr. Prashant N. Kumta, for his guidance and support throughout the past 6 years. Dr. Kumta, through your mentorship I have grown significantly not only as a scientist but also professionally and I will forever be grateful for this opportunity which you have provided me. I would also like to thank Dr. Ipsita Banerjee for her mentorship and significant input throughout the past few years. Dr. Banerjee, I have learned a tremendous amount from you through our regular meetings and your guidance has been invaluable.

I would also like thank all of the members of the Kumta Lab, specifically Dr. Abhijit Roy and Boeun Lee. Abhijit, I thank you for your mentorship throughout my time in the lab, on both personal and professional issues, and the assistance you provided me in planning and conducting many of my experiments. Boeun, it was truly a pleasure getting to work with you. I thank you for training me in cell culture and helping to troubleshoot and standardize many of the *in vitro* experiments I was required to perform and initially had no background in doing. I would also like to thank all of the members of the Banerjee lab. I would especially like to acknowledge Dr. Maria Jaramillo for training me in many of the molecular biology techniques I used in performing this work.

Finally, I would like to thank my family. Without the support from my parents and sisters in the difficult times when I questioned whether or not this was the right path for me none of this

would have been attainable. Last and certainly not least, I would like to thank my fiancé, Portia, for always believing in me. I cannot thank you enough for your continued support and the companionship you have provided me with throughout graduate school and I look forward to starting our new life together.

1.0 INTRODUCTION

1.1 BONE DEVELOPMENT, STRUCTURE, AND REPAIR

During embryonic development, the mineralized tissues of the skeleton are formed by two distinct processes, endochondral and intramembranous ossification [1]. During endochondral ossification, rather than directly forming bone tissue, cell aggregates first form cartilage. The differentiation of the perichondral derived cells to form osteoblasts then results in the mineralization of cartilage and subsequent formation of mature bone tissues [2]. This process occurs for all of the bones which comprise the appendicular skeleton, such as the pelvis, clavicle and the bones of the legs and arms. In contrast, during intramembranous ossification, aggregates of mesenchymal stem cells differentiate to form bone forming cells, or osteoblasts, without forming cartilage as an intermediate [3]. The majority of the bones which comprise the axial skeleton, such as the rib cage and the vertebral column, are formed by endochondral ossification [4]. Interestingly, the bones which comprise the skull and mandible are formed by both endochondral and intramembranous ossification. Despite these differences in origin, the bone tissues in the skull are indistinguishable from those found elsewhere in the body [5].

The primary role of bone tissue is to provide structural support and protection to more fragile organs and tissues. Mineralized tissues, which include bone, enamel, and dentin, consist of both organic and inorganic components and possess a hierarchical structure at multiple length

scales, all of which contribute to their function, illustrated in Figure 1.1 [6]. The major inorganic component of mineralized tissues consists of carbonated hydroxyapatite (HA) while type-I collagen is the major organic component [7]. The carbonated HA found in bone tissues is composed of 2-6 nm thick elongated crystals [8]. These relatively small elongated crystals ensure that the mineral component of bone is less sensitive to flaws [9]. Subtle variations in the composition and hierarchical structure of mineralized tissues exist depending on their function. For example, the mineral content of dentin is slightly higher than that of bone. As a result, dentin has a reduced toughness or ability to absorb energy in a plastic range in comparison to bone [10, 11].

Despite the impressive structural and mechanical properties of mineralized tissues, failure due to either disease or trauma often leads to the formation of fractures and defects. Once a defect or fracture is formed, a series of events take place in an attempt to regenerate the native bone tissues and restore complete function. This process begins with the formation of a hematoma, or blood clot [3]. Hematoma formation results in the migration of mesenchymal stem cells to the defect site. Once mesenchymal stem cells have migrated to the defect, a soft callus composed of cartilage is initially formed [12]. The cartilage is then slowly mineralized and replaced by bone as a result of the differentiation of mesenchymal stem cells to osteoblasts and is eventually remodeled by osteoclasts, or bone resorbing cells [13]. Irrespective of the formation of a defect, bone tissue is constantly remodeled throughout life [14, 15]. Subtle variations in the homeostasis of this remodeling process lead to the occurrence of various bone diseases. The origins and roles of the three major cell types involved in the function of bone tissues will be described in the following sections.

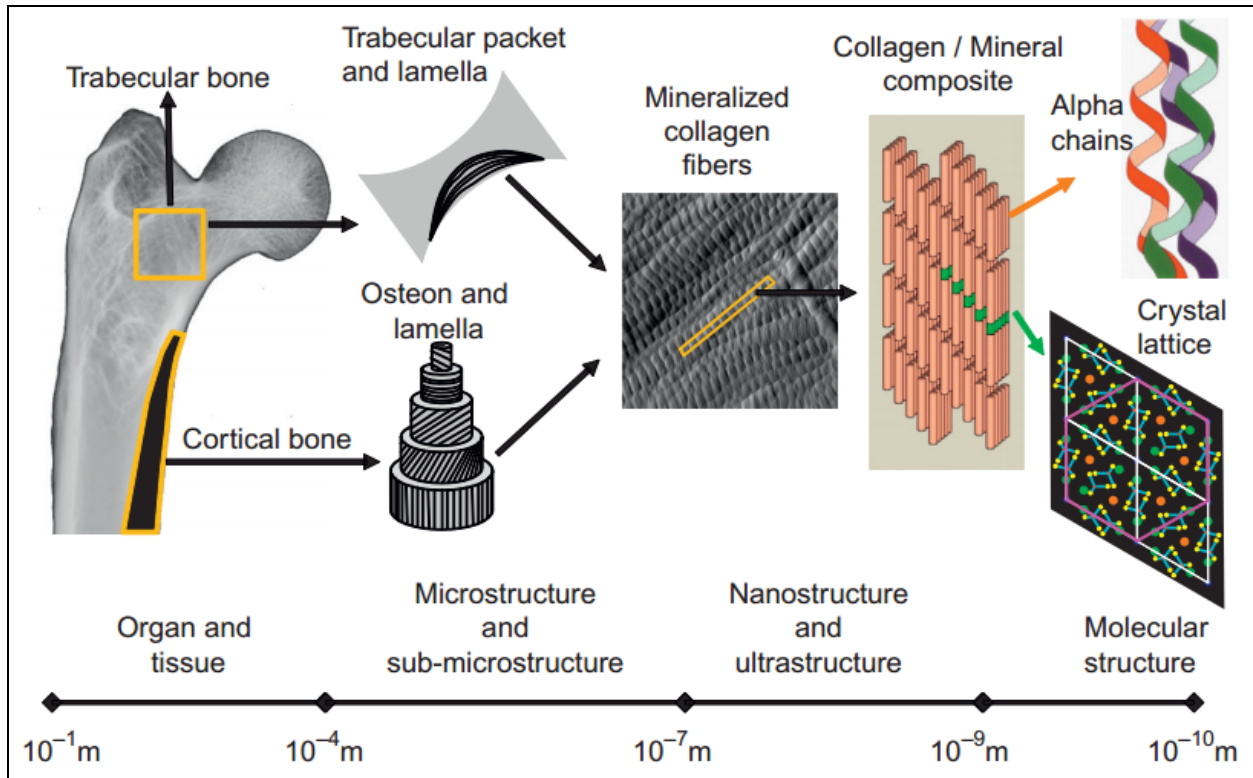


Figure 1.1 The hierarchical organization of bone at multiple length scales. At the macroscopic level, the cortical bone forms a dense outer layer which encapsulates the trabecular, or spongy, bone within the marrow cavity. At the microscopic level, both trabecular and cortical bone are comprised of lamellar type structures. At the nanoscale, bone is a composite of collagen fibers and plates of mineral dispersed between these fibers providing structural reinforcement [16].

1.1.1 Osteoblasts

Osteoblasts are the cells found in bone tissue which are responsible for the formation of the organic non-mineralized bone matrix [17]. The sources for osteoblast precursor cells include mesenchymal stem cells, adipocytes, lining cells, and perivascular pericytes contiguous to a bone wound (Figure 1.2) [13]. Mature osteoblasts express proteins such as alkaline phosphatase (ALP), type I collagen (Col-1), bone sialoprotein (BSP), and osteocalcin (OCN) [18, 19]. Due to their role in the formation of mineralized tissues, osteoblast precursor cell interaction with

synthetic scaffold materials is most often studied in the development of materials for the regeneration of mineralized tissues. In addition to bone formation, osteoblasts secrete signaling molecules, such as osteoprotegerin (OPG), which play a key role in also regulating the resorption of mineralized tissues [20].

1.1.2 Osteoclasts

Osteoclasts are the cells responsible for the resorption of mineralized tissues. They are derived from quiescent osteoclast precursors and hematopoietic progenitors which also give rise to both macrophages and monocytes (Figure 1.2) [21]. Mature osteoclasts form large multinucleated motile cells and are relatively rare in comparison to the other cell types found in bone. Receptor activator of nuclear factor kappa-B ligand (RANKL) is a molecule necessary for the formation of mature osteoclasts from monocyte precursor cells [22]. The interactions *in vivo* between RANKL and OPG play an important role in regulating both the resorption and formation of mineralized tissues. During resorption, osteoclast podosomes form a dense ring resulting in the formation of a sealing zone that tightly anchors the osteoclast to the mineral surface [23]. The compartment beneath the cell is resorbed due to the acidic environment created. As a result of the harsh conditions required to resorb bone tissues, osteoclasts are capable of functioning in extremely harsh environments with an extremely low pH [19]. In addition to their morphology, mature osteoclasts are often characterized by their increased expression of tartarate resistant acidic phosphatase (TRAP) [24].

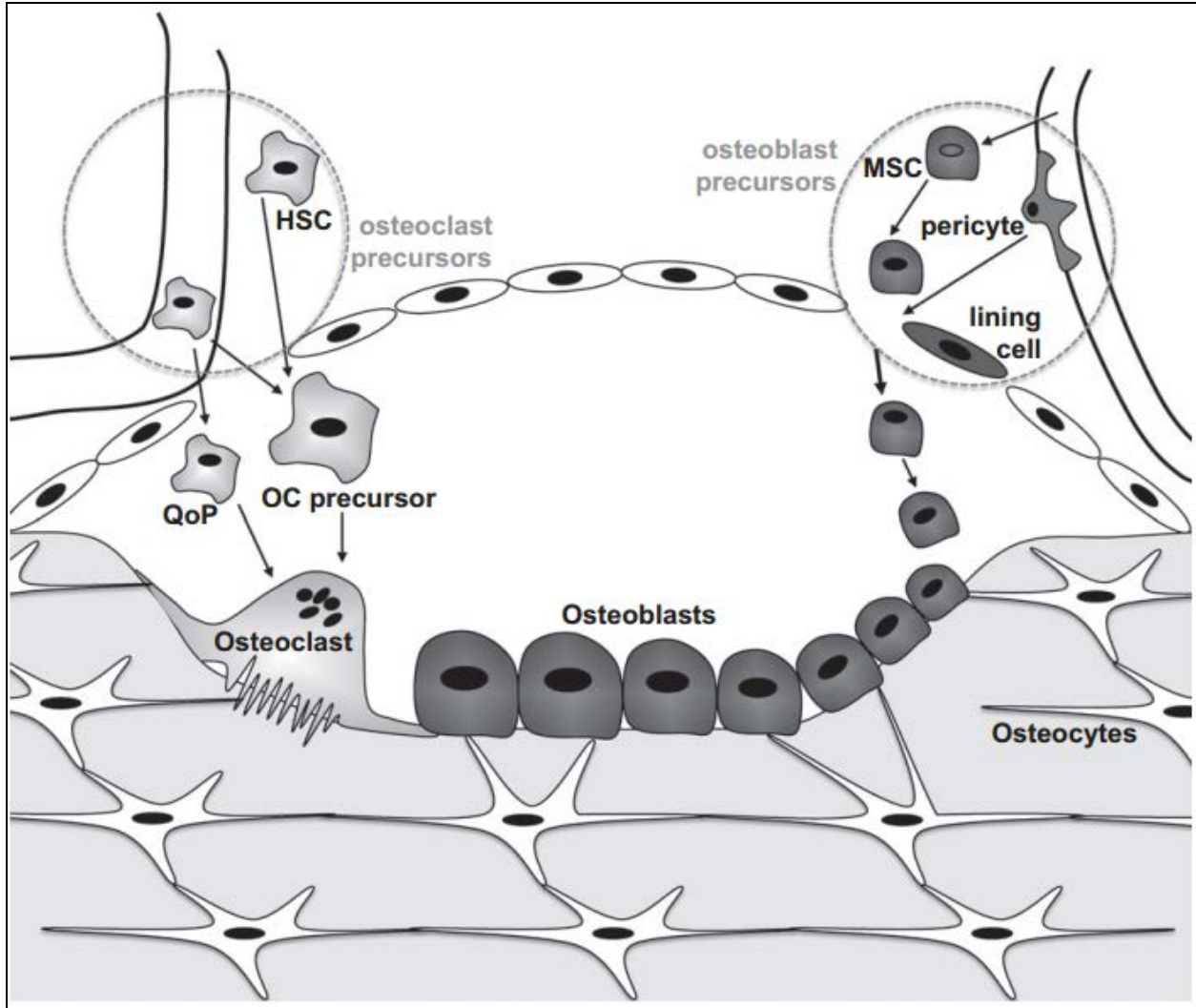


Figure 1.2 On the left of the figure, osteoclasts are derived from hematopoietic stem cells and quiescent osteoclast precursors (QoP). On the right of the figure, osteoblasts are formed from mesenchymal stem cells, pericytes, and lining cells. On the bottom of the figure, osteocytes are entrapped within the bone matrix and directly communicate with osteoblasts and osteoclasts [19].

1.1.3 Osteocytes

Osteocytes are terminally differentiated osteoblasts which are entrapped within the bone matrix (Figure 1.2). They are the most abundant cell type found in bone [21]. The function of osteocytes remains largely unknown since they have not been studied as much as either osteoblasts or osteoclasts. However, they have been shown to be sensitive to mechanical stimulation [25]. As a result of their sensitivity to mechanical stimulation, they are believed to play a role in the signaling of both, bone formation and resorption. A direct link between osteocytes and bone formation was discovered when it was observed that mature osteocytes secrete sclerostin, a potent inhibitor of bone formation [26]. Osteocytes have also been observed to secrete OPG, which is involved in the regulation of bone resorption through interactions with RANKL and its receptor [27]. Due to the fact that these cells account for as much as 90% of the cell population found in bone, a greater understanding of their function and the mechanisms through which they regulate bone formation and resorption is required.

1.2 OVERVIEW OF BONE TISSUE ENGINEERING

Bone loss as a result of disease and trauma affects millions globally. Furthermore, the projected increase in life expectancy in more developed countries is expected to increase the occurrence of both musculoskeletal and dental diseases [28]. Bone grafts are often required to treat the defects caused by both disease and trauma in instances where natural bone healing, described in Section 1.1, is insufficient to restore complete function. They are routinely used in procedures such as alveolar ridge augmentation, sinus augmentation, and spinal fusions, to name a few. Autologous

bone grafts, or autografts, are the current gold standard for the treatment of a myriad of bone defects [29]. Unfortunately, donor site morbidity, increased recovery time due to the multiple surgical procedures often required, and limitations on the amount of material that can be harvested are the major limitations of this approach [7].

Allografts are an alternative option to autografts. However, in addition to some of the disadvantages previously outlined, the risk for disease transmission and variation in the quality of the graft material, depending on donor health and age also exist [30]. The 3D structure, cells, and extracellular matrix (ECM) proteins such as bone morphogenic proteins (BMPs), insulin-like growth factor (IGF), transforming growth factor β (TGF- β), vascular endothelial growth factor (VEGF), and platelet derived growth factor (PDGF) in these harvested tissues enhance their capability to induce bone formation, or osteoinductivity, and remain a challenge to mimic synthetically [31].

In an attempt to maintain osteoinductivity, while reducing the risk for disease transmission, allografts have been processed to produce a demineralized bone matrix (DBM) which retains much of the proteinaceous content of native bone [32]. Unfortunately, the 3D structure, cells, and the ensuing mechanical properties are commonly lost during the demineralization process. DBM has been further processed to form injectable pastes, sheets, and other clinically relevant constructs resulting in DBM based products being used in approximately 20% of current bone grafting procedures [33]. However, batch to batch variation exists with DBM based products due to the varying quality of donor tissues. Protein conformation may also change depending on the demineralizing process and, similar to autografts and allografts, the amount of graft material that can be produced is limited by the amount of donor material available [34, 35].

As a result, a need for improved bone grafting technologies currently exists. Ideally, bone grafts should be capable of both inducing and supporting bone regeneration. They should also provide sufficient mechanical stability throughout the regeneration process and degrade at a similar rate with which mineralized tissues are regenerated. In addition, neither the graft material nor its degradation products should put patients at risk of an undesired immune response, particularly when a substantial amount of graft material is necessary. Therefore, it remains a challenge to develop bone grafts which satisfy all of these criteria. However, through advances in the synthesis and processing of synthetic materials, using techniques such as 3D printing and bioreactors, significant improvements in the performance of synthetic based bone graft substitutes have been made. As a result, synthetic materials, either on their own or in combination with naturally derived products, such as DBM, may have the potential to satisfy the criteria outlined for the next generation of bone graft materials. The advantages and limitations of the synthetic materials currently used as bone graft substitutes will be described in Section 1.3.

1.3 SYNTHETIC MATERIALS USED IN BONE TISSUE ENGINEERING

1.3.1 Polymers

Polymeric materials have been widely used in bone tissue engineering. Although their mechanical properties may not be ideal for the temporary replacement of mineralized tissues (Figure 1.3), their capability to degrade and deliver both cells and biological molecules in a controlled manner to a defect site is particularly of interest [36, 37]. The polymers studied in

bone regeneration can be classified into two categories, natural and synthetic polymers. These materials will be discussed in the following two sections.

1.3.1.1 Natural Polymers

Natural polymers can be classified into either protein or polysaccharide derived based on their origin. A few of the more common naturally derived polymers from both protein and polysaccharide sources used in bone tissue engineering include chitosan, alginate, hyaluronic acid, silk, fibrin, and collagen [38-40]. Due to their structural similarity to ECM proteins, particularly with respect to protein derived natural polymers, these materials are considered biocompatible and in some cases can also be classified as bioactive [41]. Many natural polymers have also been demonstrated to be biodegradable. Unfortunately, in addition to their poor mechanical properties, batch to batch variation exists depending on the source of the material. As a result, additives in the form of either plasticizers or particulates are often combined with natural polymers to enhance their mechanical properties and functionality among other desired biofunctional characteristics [42].

Collagen, due to its abundance in the human body, is perhaps the most widely used natural polymer for bone tissue engineering applications [43]. Bone tissue itself is a composite of collagen fibrils reinforced with mineral particles (Figure 1.1) [7]. As a result, type I collagen is the most abundant extracellular protein found in bone [44]. Collagen based coatings, hydrogels, and scaffolds have all been studied in the regeneration of mineralized tissues. One of the major disadvantages of collagen is the relatively high degree of swelling collagen undergoes upon exposure to physiological environments [45]. As a result, chemical modifications, usually in the form of cross-linking, are required to tailor the swelling and degradation characteristics of collagen based coatings, hydrogels, and scaffolds.

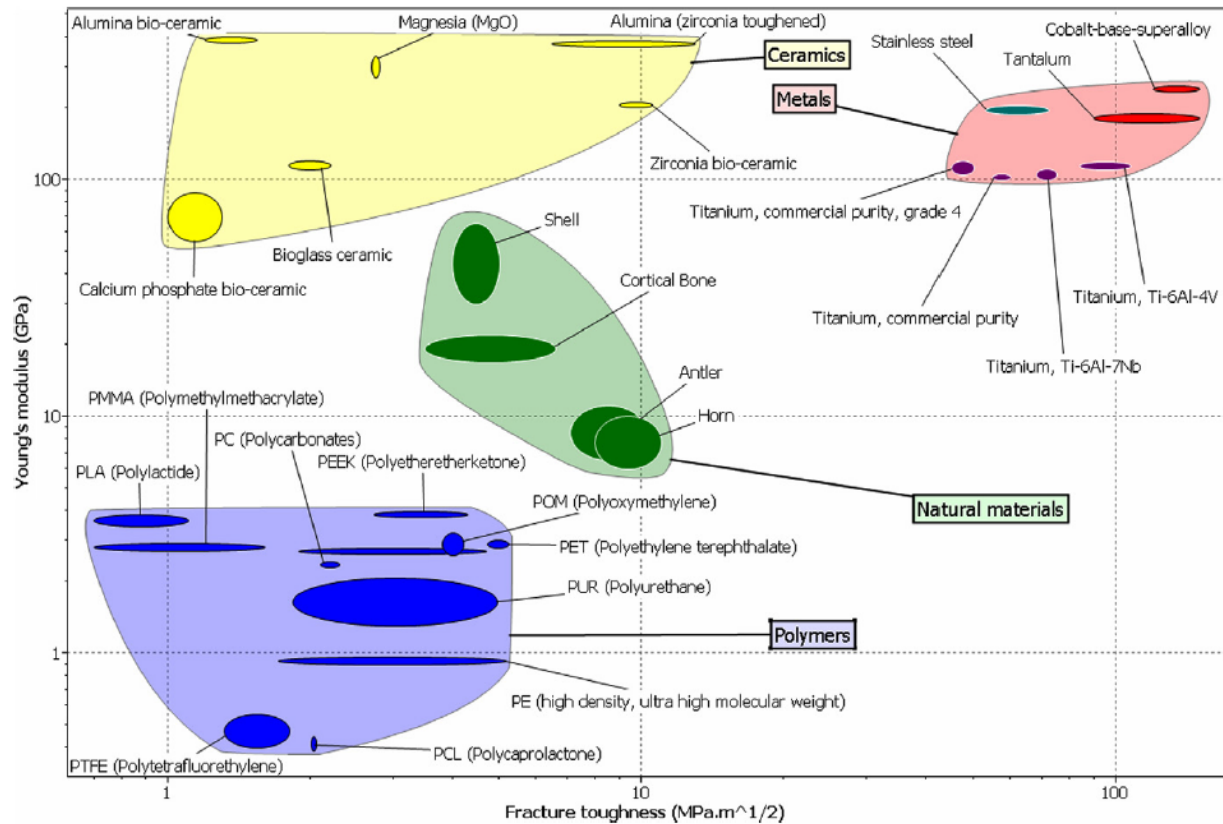


Figure 1.3 The mechanical properties of some of the more common materials used in bone tissue engineering in comparison to mineralized tissues [46].

Of the non-protein derived natural polymers, chitosan is one of the more abundantly studied natural polymers in bone tissue engineering [41]. Chitosan is a linear polysaccharide derived during the deacetylation of the shells of crustaceans [47]. Similar to collagen, chitosan coatings, hydrogels, and scaffolds have been studied in the regeneration of mineralized tissues. Acidic conditions are however required to dissolve chitosan and a viscous gel is formed upon increasing the solution pH to near physiological conditions. Due to the cationic nature of chitosan, the electrostatic interactions between chitosan and negatively charged structural molecules, such as glycosaminoglycans and proteoglycans, have been used to achieve the sustained release of these and other bioactive molecules [48]. Interestingly, chitosan has also

been shown to possess antimicrobial properties [49]. This is particularly of interest in bone tissue engineering since infection is a major cause of bone graft failure.

In summary, natural polymers provide several beneficial properties for applications in bone tissue engineering. Unfortunately, the mismatch in mechanical properties of naturally derived polymeric scaffolds with mineralized tissues limits their wider application. In addition, their expense, depending on the source and procedure required to isolate these molecules, provides further challenges. As a result, these materials are often used in combination with either metallic or ceramic biomaterials rather than on their own for applications in bone tissue engineering.

1.3.1.2 Synthetic Polymers

In comparison to natural polymers, synthetic polymers are of interest in bone tissue engineering due to the capability to chemically modify their structure leading to greater control with respect to degradation, swelling, and mechanical properties. As a result of chemical modification, synthetic polymer scaffolds with significantly increased mechanical properties can be prepared in comparison to natural polymers. Synthetic polymers also provide a reduced risk of batch to batch variation in comparison to natural polymers and are more flexible with respect to the processing techniques that can be utilized [50]. Some of the more common synthetic polymers used in bone tissue engineering include poly(methyl methacrylate) (PMMA), poly(lactic-co-glycolic) acid (PLGA), polycaprolactone (PCL), and polyethylene glycol (PEG), to name a few [51].

Similar to natural polymers, synthetic polymers have been processed to form coatings, hydrogels, and scaffolds. One of the more interesting applications of synthetic polymers in bone tissue engineering is the use of PMMA bone cements [52]. Upon mixing a powder and a liquid

component which contain methylmethacrylate, the monomer of PMMA, and initiators of the PMMA polymerization reaction, a viscous paste is formed. Over time, the paste hardens as the polymerization reaction proceeds. These cements are widely used in spinal surgical procedures, such as percutaneous vertebroplasty [53]. One of the major drawbacks of PMMA bone cements is the exothermic polymerization reaction of PMMA. The recorded temperatures during the polymerization reaction can exceed 70°C leading to concerns over the health of the surrounding tissues upon exposure to such elevated temperatures [54]. In addition, antibiotics and other drugs loaded into these bone cements intended for delivery during healing may become denatured during the polymerization process. However, PMMA, once fully polymerized, is extremely biocompatible but exhibits poor integration with surrounding bone tissues and limited resorption leading to long term complications [55].

In addition to their application in bone cements, synthetic polymers are most often utilized for their tunable degradation properties which facilitate the controlled delivery of therapeutic agents [56]. This capability has been widely used with degradable PLGA which can be processed to form particles of varying size to deliver ECM proteins, such as BMP-2 [57]. Although biocompatible and biodegradable, a major disadvantage of these synthetic polymers is that these materials on their own are not considered bioactive, in contrast to many of the protein derived natural polymers. As a result, either expensive growth factors with limited shelf lives, such as BMP-2 and VEGF, or bioactive particles are required in combination with synthetic polymers to achieve the desired therapeutic response [51, 58].

The wide ranging tunable properties of synthetic polymers make them an attractive choice of material for bone tissue engineering applications. Unfortunately, their poor bioactivity is a major disadvantage in comparison to naturally derived polymers and other choices of

material. As a result, similar to naturally derived polymers, synthetic polymers are often used in combination with either metallic or ceramic biomaterials rather than on their own for applications in bone tissue engineering.

1.3.2 Metals

In contrast to natural and synthetic polymers, metals are capable of providing the mechanical stability necessary to support load bearing bone defects, illustrated in Figure 1.3 [46, 59, 60]. As a result, they are frequently used in hip implants, knee replacements, and spinal procedures. Several non-degradable metallic alloy based medical devices have been approved by the FDA for bone fixation. On the other hand, degradable metallic alloys, although having been reported since the early 1900s, are only recently gaining increased attention in bone tissue engineering [61]. To date, a degradable metallic device for the treatment of bone defects is yet to be approved by the FDA. A brief overview of the developments in both non-degradable and degradable metallic alloys for the treatment of bone defects will be discussed in the following two sections.

1.3.2.1 Non-Degradable Metals

Non-degradable metals, such as stainless steel, titanium and its alloys, and cobalt-chrome alloys, are known for their exceptional biocompatibility with mineralized tissues [62]. As a result, they have been machined to form screws, plates, and constructs of varying sizes and geometries for a wide range of applications in both orthopedic and craniofacial bone fixation. Non-degradable metals are generally considered bio-inert. Therefore, relatively large amounts of material can be used without inducing an undesired foreign body response. In order to facilitate the increased

integration with bone tissues, also referred to as osseointegration, bioactive coatings containing either growth factors or ceramic particles are often required [63, 64].

As previously mentioned in Section 1.1, degradability is one of the desired properties of the ideal bone tissue engineering scaffold. Due to the fact that this classification of metallic biomaterials does not degrade, complications exist for many metallic implants after longer periods due to the mismatch in mechanical properties between metallic biomaterials and native mineralized tissues [65]. In addition, the accumulation of non-degradable wear debris from these implants can lead to an undesired inflammatory response. As a result, follow up surgeries are often required after the implantation of non-degradable metallic scaffolds [61]. However, their desirable mechanical properties and relatively inert characteristics in comparison to both polymers and ceramics make them a necessity in the current treatment of load bearing bone defects.

1.3.2.2 Biodegradable Metals

Biodegradable metals have only recently gained significant attention for a wide range of clinical applications in addition to both orthopedic and craniofacial bone regeneration. The alloys developed to date which are considered biodegradable are typically either Mg or Fe based [62]. Mg and Fe can both be found in the human body. Mg^{2+} is the fourth most abundant cation in the human body and is involved in several key enzymatic reactions [66]. It is also necessary for cell proliferation and ATP synthesis [67]. Interestingly, the role of Mg^{2+} ions on the differentiation of osteoblast progenitor cells and human mesenchymal stem cells towards mature osteoblasts, or bone forming cells, remains poorly understood [68]. Fe^{2+} ions are involved in both the storage and activation of molecular oxygen and can be found in a wide number of Fe containing enzymes and proteins [69]. Upon degradation, Fe based alloys may release both Fe^{2+} and Fe^{3+}

ions. Unfortunately, hemoglobin containing Fe^{3+} rather than Fe^{2+} is incapable of binding oxygen [70]. As a result, Mg based alloys are more commonly studied for bone tissue engineering applications.

The degradation of Mg alloys occurs through corrosion mechanisms where $\text{Mg}(\text{OH})_2$ and H_2 gas are formed as the corrosion products, illustrated in Equation 1.1. The majority of alloys developed to date undergo a rapid and uncontrolled corrosion *in vivo*. This is primarily due to the presence of Cl^- ions which destabilize the protective $\text{Mg}(\text{OH})_2$ passivation layer initially formed upon exposure to physiological environments during the corrosion process.

Equation 1.1



Therefore, a substantial emphasis has been placed on tailoring the corrosion properties of Mg based alloys either by the application of protective coatings, by the modification of the alloy microstructure, or by the development of new alloy compositions which form more stable hydroxides upon exposure to Cl^- containing environments.

1.3.3 Non-Calcium Phosphate Based Ceramics

Ceramic materials are widely studied in bone tissue engineering applications either on their own or as bioactive components in combination with polymers and metals. Many of these materials are degradable and capable of supporting the regeneration of bone tissue, or considered osteoconductive [29]. In addition, several ceramic systems in recent years have been demonstrated to be osteoinductive in relevant animal models while very few polymers or metals have demonstrated this capability [71]. Unfortunately, in contrast to metals, ceramic based biomaterials are incapable of supporting load bearing bone defects and are relatively brittle

(Figure 1.3) [72]. Bioceramics can be described as either calcium phosphate (CaP) based or non-calcium phosphate based. However, CaPs are more widely used in bone tissue engineering than any other ceramic material due to their chemical similarity to the mineral component of native bone tissues [7]. Non-CaP based ceramic materials will be described in the current section while CaPs will be discussed in Section 1.4.

Zirconia, magnesia, and alumina are ceramic materials widely used in the regeneration of mineralized tissues. However, the most widely used non-CaP based ceramic materials in bone tissue engineering are silicate based bioactive glasses. These amorphous materials are prepared using either melt-quenching or sol-gel based approaches [73]. The favorable interactions of these materials with bone tissues were first described by Hench and coworkers [74]. Bioactive glasses are believed to support bone formation due to the release of bioactive dissolution products, such as silicate ions, and subsequent formation of a hydroxycarbonate apatite layer on their surface upon exposure to physiological environments [75, 76]. Due to their capability to support rapid mineralization, bioactive glass powders are often used in toothpaste formulations for the treatment of hypersensitivity [77]. While many different compositions have been reported, the bioactive glass prepared using 46.1 mol. % SiO_2 , 24.4 mol. % Na_2O , 26.9 mol. % CaO , and 2.6 mol. % P_2O_5 , also referred to as Bioglass 45S5, is the most well-known and has been FDA approved for use in the regeneration of mineralized tissues in various forms [78].

The processing of bioactive glasses to form granules and porous scaffolds has led to an increased clinical acceptance. A more detailed description of the techniques used to form porous bioceramics scaffolds will be provided in Section 1.4.2. Unfortunately, the inability to mold bioactive glass based scaffolds into the desired shapes to fill irregularly shaped bone defects and their poor degradation rate has restricted their wider use [74]. Sintering at elevated temperatures

is required to enhance the mechanical stability of ceramic scaffolds. However, many of the traditionally used bioactive glass compositions cannot be sintered without inducing their crystallization which alters their dissolution behavior and subsequent bioactivity.

1.4 CALCIUM PHOSPHATES IN BONE TISSUE ENGINEERING

As mentioned previously, CaPs are more widely used in bone tissue engineering than any other ceramic material due to their chemical similarity to the mineral component of native bone tissues. In addition to the advantages outlined for non-CaP based ceramics, including bioactive glasses, CaPs can also be processed to form self-setting injectable bone cements which can be delivered in a minimally invasive fashion to fill irregularly shaped bone defects. CaP based self-setting cements will be described in Section 1.4.2.3. The use of a wide range of CaP phases, which will be described in the following Section, enables the formation of CaP based scaffolds with varying rates of degradation which can be tailored for specific applications. A summary of the advantages and disadvantages of the synthetic materials discussed to treat bone defects thus far is illustrated in Table 1.1.

Table 1.1 The advantages and disadvantages of the synthetic materials used in bone tissue engineering.

Scaffold Material	Advantages	Disadvantages
Naturally Derived Polymers	Excellent biocompatibility and in some cases bioactivity. Mimics the structure of native extracellular matrix. Can be used as controlled release vehicles	Poor mechanical properties. Expense and batch to batch variation depending on the source and procedure required to isolate these molecules.
Synthetic Polymers	Improved processing capabilities in comparison to naturally derived polymers. Can be used as controlled release vehicles and processed to form injectable cements.	Poor mechanical properties. Limited bioactivity. Exothermic setting reaction of PMMA cements.
Non-degradable Metals	Exceptional biocompatibility with native host tissues. Improved mechanical properties in comparison to polymers. Can support load bearing defects.	Non-degradability and mismatch in mechanical properties with native tissues. Accumulation of wear debris.
Degradable Metals	Degradability under <i>in vivo</i> conditions. Can support load bearing defects. Little or no accumulation of wear debris is anticipated due to degradability.	Uncontrolled corrosion and the potential release of large amounts of undesired corrosion products, such as H ₂ .
Non-Calcium Phosphate Ceramics	Excellent integration with mineralized tissues. Releases bioactive ions near the implantation site.	Incapable of supporting load bearing defects. Slow rate of degradation <i>in vivo</i> . Cannot be processed to form self-setting injectable cements. Crystallization at high temperatures.
Calcium Phosphate Ceramics	Excellent integration with mineralized tissues. Releases bioactive ions near the implantation site. Can be processed to form injectable self-setting cements.	Incapable of supporting load bearing defects. Slow degradation of HA containing scaffolds <i>in vivo</i> .

1.4.1 Calcium Phosphate Phases

The CaP phases widely studied in the development of synthetic bone graft substitutes are illustrated in Table 1.2. Interestingly, of the 7 phases listed in Table 1.2, only 3 are stable under aqueous conditions. Dicalcium phosphate dihydrate (DCPD) is stable under acidic conditions while calcium deficient hydroxyapatite (CDHA) and HA are stable under neutral and basic conditions, respectively. The instability under aqueous conditions of tetracalcium phosphate (TTCP), β -tricalcium phosphate (β -TCP), α -tricalcium phosphate (α -TCP), and dicalcium phosphate anhydrous (DCPA) indicates that these phases cannot be synthesized under aqueous conditions. Therefore, alternative approaches, such as solid state synthesis and sol-gel based techniques, have been developed [79, 80]. However, DCPD, CDHA, and HA can be prepared

under aqueous conditions using chemical precipitation techniques with controlled conditions of temperature, pH, and concentration [81, 82].

Table 1.2 The properties of the calcium phosphate phases widely studied in bone tissue engineering [83].

Abbreviation	Name	Chemical Formula	Ca/P	pK _{sp} @ 25°C	pH Stability
TTCP	Tetracalcium phosphate	Ca ₄ (PO ₄) ₂ O	2	38-44	-
HA	Hydroxyapatite	Ca ₅ (PO ₄) ₃ OH	1.67	116.8	9.5-12
β-TCP	β-tricalcium phosphate	Ca ₃ (PO ₄) ₂	1.5	28.9	-
α-TCP	α-tricalcium phosphate	Ca ₃ (PO ₄) ₂	1.5	25.5	-
CDHA	Calcium deficient hydroxyapatite	Ca _{10-x} (HPO ₄) _x (PO ₄) _{6-x} (OH) _{2-x}	1.5	85.1	6.5-9.5
DCPD	Dicalcium phosphate dihydrate	CaHPO ₄ •2H ₂ O	1	6.59	2-6
DCP	Dicalcium phosphate anhydrous	CaHPO ₄	1	6.90	-

Due to their instability under aqueous conditions, TTCP, β-TCP, and α-TCP are also known to hydrolyze to form CDHA upon exposure to physiological conditions [84, 85]. With respect to DCP and DCPD, additional Ca²⁺ ions are required to provide the stoichiometry needed to form CDHA under aqueous conditions [86].

In addition to pH stability, a wide range in the solubility of the phases listed can be observed. DCP and DCPD are the most soluble phases while CDHA and HA are the least soluble. The increased solubility of DCPD, DCP, β-TCP, and α-TCP are particularly of interest in regenerative medicine due to their capability to degrade under physiological conditions through dissolution in addition to cell mediated degradation [87-89]. Unfortunately, the relatively rapid and acidic degradation products of DCP and DCPD may also lead to an undesired inflammatory response. However, the release of Ca²⁺ and PO₄³⁻ ions during CaP

degradation is known to support the differentiation of osteoblast progenitor cells and mesenchymal stem cells towards mature osteoblasts which favors regeneration [90].

1.4.2 Formation of Clinically Relevant Forms of Calcium Phosphate

Calcium phosphates have been processed into various forms to enhance their wider clinical application in the treatment of orthopedic, craniofacial, and dental bone defects. A few of the more widely used forms include granules, preformed porous scaffolds, injectable self-setting cements, and coatings. The development and applications of these forms of calcium phosphate will be discussed in the following sections.

1.4.2.1 Calcium Phosphate Granules

CaP granules are aggregates of CaP powders typically ranging from a few hundred microns to less than 5 mm in diameter. This form of calcium phosphate is widely used in dental and craniofacial applications since they can be tightly packed into bone defects while allowing the flow of biological fluids throughout the defect [74]. CaP granules are typically made porous by the addition of highly soluble salts which are leached out prior to implantation. The formation of porous rather than dense scaffolds allows the infiltration of cells and various physiological fluids more closely mimicking the 3D structure of mineralized tissues [7].

CaP granules are often composed of HA, β -TCP, or a biphasic mixture of HA and β -TCP. The sieving of either sintered dense CaP tablets or fully set CaP cements, which will be described in Section 1.4.2.3, is performed to achieve the desired particle size distribution. Prior to implantation, it is common for clinicians to combine CaP granules with blood to accelerate regeneration and improve their handling properties [91]. CaP granules are also often combined

with polymeric components, which can serve as binders and drug delivery vehicles [92, 93]. The addition of polymeric components provides improved mechanical stability and allows the composite mixture to be easily molded to fill irregularly shaped defects.

1.4.2.2 Preformed Porous Scaffolds

Porous rather than dense scaffolds are favored in bone tissue engineering. Ideally, a large number of macropores, considered to be greater than 10 μm , are required to allow the host cells to infiltrate the scaffold. The pores formed should also be interconnected to increase the interaction of host cells within the scaffold and to enhance the transport of both nutrients and waste [94, 95]. Therefore, several techniques to form porous bulk ceramic scaffolds, larger than the granules describe in Section 1.4.2.1, have been developed. One approach is to combine CaP powders with particles which are either highly soluble or volatile and can be lost to create pores either during sintering or upon exposure to aqueous environments from sintered CaP scaffolds [96]. Although scaffolds with a well-defined pore size distribution can be formed using this technique, the formation of interconnected pores is not guaranteed.

3D printing is an approach used to process CaP powders into structures with a controlled architecture enabling the formation of interconnected pores [97]. Scaffolds are constructed by using a print head containing a binder solution that builds up a desired 3D structure using CaP powders. When using a polymeric binder solution, subsequent heat treatment is required to sinter the scaffold and burn off the remaining organic binder solution. However, the need to sinter scaffolds after 3D printing can be avoided when using CaP powders that undergo a cement-like setting reaction upon exposure to the binder solution [98]. One major advantage of 3D printing is that patient specific bone grafts can be prepared. However, since these scaffolds are preformed, they cannot be molded prior to implantation to fill bone defects. In most cases, heat treatment to

temperatures in excess of 800°C is required to achieve adequate sintering and mechanical properties. Processing at such temperatures also restricts the capability to incorporate either proteins or growth factors prior to implantation.

1.4.2.3 Calcium Phosphate Self Setting Cements

Similar to the polymeric PMMA cements, described in Section 1.3.1.2, CaP powders can be combined with aqueous solutions to form a workable paste. The exposure to aqueous environments initiates the dissolution of CaP powders followed by the precipitation of crystals of either HA (Equation 1.2) or DCPD (Equation 1.3) which become intricately embedded within the initial precursors with an invariable moderate rise in temperature sufficient to cause the bonding of the particles resulting in the solidification or setting of the paste. HA forming CaP cements were first discovered by Brown and Chow in the 1980s while DCPD forming cements were introduced by Lemaitre in the 1990s [99, 100].

Equation 1.2



Equation 1.3



In both cases, they have since been engineered to form injectable pastes which can be administered in a minimally invasive fashion to fill irregularly shaped bone defects and fully set in the presence of physiological fluids (Figure 1.4). HA forming cements are more widely studied than DCPD forming cements due to their improved mechanical stability and less acidic setting conditions. However, as previously described, DCPD cements are much more degradable in comparison to HA forming cements [101].

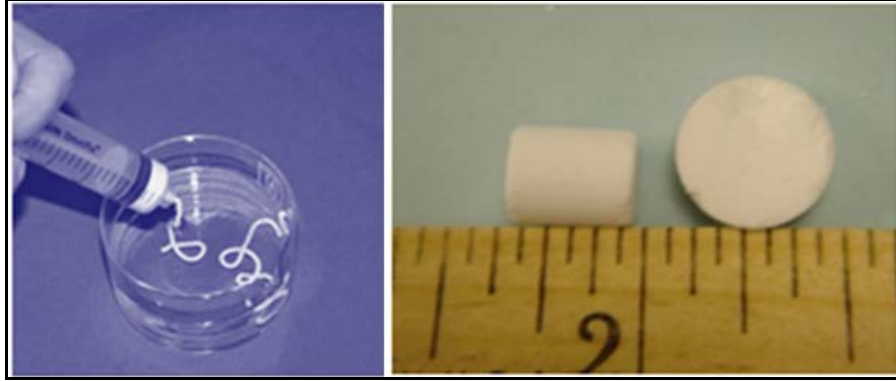


Figure 1.4 An example of an injectable calcium phosphate self-setting cement prior to and after setting using cylindrical molds of varying size.

HA forming cements have been prepared using a wide range of precursors due to the hydrolysis of several CaP phases to form HA under physiological conditions. They are most commonly prepared either by the hydrolysis of α -TCP or an acid-base reaction between TTCP and either DCPD or DCPA. The cements formed using these reaction mechanisms exhibit compressive strengths which range from 10-100 MPa [83, 102]. Therefore, they are incapable of supporting load bearing defects (Figure 1.3). Nonetheless, their similar compressive strengths to that of spongy, or trabecular bone, which is approximately 10 MPa, limits the risk for implant rejection due to a mismatch in mechanical properties as is commonly observed with both metallic and polymeric biomaterials in bone tissue engineering [83].

Although CaP cements were first developed for over thirty years ago, several key advancements have only recently been reported. One of the more recent advances in CaP cements is the development of premixed cements. These cements are packaged in the form of a premixed paste, rather than separate liquid and powder components, and can be directly administered without mixing and set in the presence of blood and other physiological fluids [103]. The controlled delivery of growth factors and drugs from injectable CaP cements, either

with or without polymeric carriers, is also a field with significant potential [104]. Due to the brittle nature of CaP cements, reinforcement with polymeric fibers to increase the flexural strength and achieve mechanical properties closer to that of native mineralized tissues is also widely studied [105].

1.4.2.4 Calcium Phosphate Coatings

Calcium phosphate coatings are often applied to metallic bone fixation devices to enhance their integration with mineralized tissues [106, 107]. Several approaches to deposit a wide range of calcium phosphate phases on metallic substrates have therefore been developed. Although many of these techniques have been optimized for the deposition of calcium phosphate coatings on non-degradable metals, they have only recently been applied to degradable magnesium and iron based alloy substrates. These processes include aqueous biomimetic approaches, organic based sol-gel methods, electrochemical techniques, and plasma assisted techniques [108-110]. A summary of the advantages and disadvantages of each of these techniques is described in Table 1.3.

Table 1.3 A summary of the advantages and disadvantages of the various processes used to deposit calcium phosphate coatings on metallic substrates.

Coating Technique	Advantages	Disadvantages
Aqueous Biomimetic Methods	Can be performed under physiological conditions. Capable of incorporating biological molecules during the coating process. Coatings can be deposited on porous 3D scaffolds.	Coating process requires relatively long periods of time. Acidic or basic pretreatment is often required. Coating adhesion is relatively poor.
Organic Sol-Gel Based Methods	Coatings can be deposited on porous 3D scaffolds. Homogeneous coatings can be formed using techniques such as dip or spin coating. The coating process is relatively quick.	Heat treatment to decompose organic precursors is required. Therefore, biological molecules cannot be simultaneously incorporated.
Electrochemical Methods	Coatings can be deposited on porous 3D scaffolds. High temperature processing and alloy pretreatments are not required. Coatings can be deposited very quickly.	Coating adhesion to the substrate is relatively poor without heat treatment.
Plasma Assisted Methods	Very homogeneous and dense coatings with excellent adhesion to the substrate can be formed. Coatings are deposited relatively quickly. Coating crystallinity can be easily adjusted.	Cannot be used to coat 3D porous scaffolds due to line of sight deposition. Coating deposition is often performed under vacuum conditions at elevated temperatures.

Biomimetic coatings are deposited by immersing metallic substrates in solutions containing Ca^{2+} and PO_4^{3-} ions kept at physiological temperatures for extended periods of time [111]. Pretreatment with either acidic or basic precursors is often required when using biomimetic approaches to form a highly reactive layer which calcium phosphates are subsequently deposited on [112]. Although biological molecules can be incorporated during the coating process due to the relatively mild conditions, the coatings formed often have a very poor adhesion to the substrate unless further heat treatment is performed.

An alternative approach to deposit calcium phosphates is the use of organic solvents by the sol-gel method [79]. Calcium and phosphate containing precursors when dissolved separately in organic solvents and combined are capable of forming a viscous sol-gel in the absence of moisture. The further heat treatment of this gel results in the decomposition of the organic components and the formation of calcium phosphate nanoparticles [113]. The sol-gel formed has been dispersed on metallic substrates using processes, such as either dip coating or spin coating,

and heat treated to sufficient temperatures to fully decompose the organic components resulting in the formation of homogeneous calcium phosphate coatings. Unfortunately, biological molecules cannot be integrated using this approach due to the high temperature processing required [108]. Furthermore, the relatively low melting temperature of biodegradable Mg alloys leads to further complications.

Electrochemical processes are more suitable for depositing calcium phosphate coatings on degradable alloys than sol-gel based methods since high temperature processing is not required [109]. Techniques such as electrophoretic deposition and cathodic deposition are widely studied [114, 115]. In both cases, metallic substrates are immersed in solutions containing Ca^{2+} and PO_4^{3-} ions and an electrical potential is applied. The coatings formed are typically homogeneous and can be formed in a relatively short period of time after applying an electrical potential. Although heat treatment after the formation of the coating is not required, heat treatment has been found to substantially improve the coating adhesion to the substrate providing the mechanical stability necessary for surgical implantation [116].

Plasma assisted methods, which include plasma spraying, magnetron sputtering, pulsed laser deposition, and ion beam assisted deposition are some of the more widely used techniques to deposit calcium phosphates on non-degradable metals, such as titanium [110]. These procedures are performed under vacuum conditions and at various temperatures to adjust the crystallinity of calcium phosphate coating formed [64]. Due to the processing conditions, dense homogeneous coatings with excellent adhesion to the substrate can be formed [117]. However, plasma assisted methods deposit calcium phosphates on metallic substrates by line of sight. Therefore, it is difficult to deposit homogeneous calcium phosphate coatings on 3D porous scaffolds using this approach.

1.4.3 Limitations of Calcium Phosphates

Although CaP scaffolds have been demonstrated to be biodegradable, osteoconductive, and osteoinductive, several limitations, in addition to their relatively poor mechanical properties, currently exist. HA is the most widely used CaP phase in the regeneration of mineralized tissues. Unfortunately, the poor solubility and limited cell mediated degradation of HA often leads to the formation of cracks throughout HA scaffolds. This is due to a mismatch between the rate of degradation of the scaffold and the rate of regeneration of the native mineralized tissues. As a result, more soluble CaP phases, such as DCPD and β -TCP, have gained increasing interest. However, their rates of resorption may also not be ideal for many applications. Although they are cheaper and provide a lower risk of undesired side effects, CaPs alone are also unable to regenerate mineralized tissues as rapidly as scaffolds containing the ECM proteins described in Section 1.1. Therefore, techniques to improve the bioactivity of CaP scaffolds and cell recruitment to the defect site enhancing the differentiation of osteoblast progenitor cells using reduced concentrations of expensive growth factors and ECM molecules remains a topic of interest.

1.4.4 Ionic Substitution in Calcium Phosphates

One approach to address the limitations of CaP scaffolds, outlined in Section 1.4.3, is the use of ionic substitutions. The inorganic components of mineralized tissues are composed of several elements in addition to Ca and P, which are known to play a key role in regulating both their structure and function. The elemental compositions dentin, enamel, and bone are illustrated in Table 1.4 [118]. A few of the more noticeable differences are the reduced CO_3^{2-} and F^- content in

enamel in comparison to dentin and bone and the increased amount of Mg in dentin. In an attempt to mimic the structure and composition of native mineralized tissues, the synthesis of ionic substituted CaP scaffolds for bone tissue engineering applications has been explored.

Table 1.4 **The elemental composition of enamel, dentin, and bone [118].**

	Enamel	Dentin	Bone
Ca (wt. %)	37.6	40.3	36.6
P (wt. %)	18.3	18.6	17.1
CO ₃ (wt. %)	3.0	4.8	4.8
Mg (wt. %)	0.2	1.1	0.6
Sr (wt. %)	0.03	0.04	0.05
F (wt. %)	0.01	0.07	0.1

The biologically most relevant cationic substitutions for Ca²⁺ include Mg²⁺, Sr²⁺, and Zn²⁺. Sr²⁺ is specifically of interest since oral supplements of containing strontium have been shown to increase bone density and are currently used in the treatment of osteoporotic patients. Unfortunately, larger doses of strontium have also been shown to cause rickets disease, defective bone mineralization, and renal failure [119]. *In vitro*, Sr²⁺ has been shown to enhance osteogenic differentiation. However, the role of strontium in modulating these mechanisms remains unknown [118]. Cationic substitutions with Mg²⁺ are also of interest since, similar to Sr²⁺, Mg²⁺ also influences osteoblast and osteoclast activity [118]. Furthermore, the increasing interest in the use of biodegradable Mg alloys in bone tissue engineering suggests that a greater understanding of the role of Mg²⁺ in regulating osteogenic differentiation is needed. Thus the present thesis has been outlined with the major goals to primarily address several of the issues discussed above comprising bulk scaffold type materials. These aspects, both in terms of

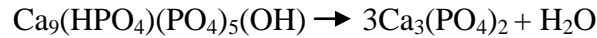
material characteristics as well as the *in vitro* biological response, will be discussed in the subsequent chapters.

2.0 THESIS GOALS

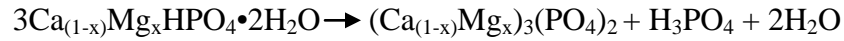
2.1 SPECIFIC AIM 1

SYNTHESIS AND CHARACTERIZATION OF MAGNESIUM SUBSTITUTED B-TRICALCIUM PHOSPHATE

Background: Single phase β -TCP cannot be synthesized under aqueous conditions due to its instability in aqueous environments. However, the substitution of Ca^{2+} with Mg^{2+} ions in the β -TCP crystal structure is known to stabilize β -TCP under aqueous conditions and enhances the temperature at which β -TCP converts to α -TCP enabling increased sintering and densification [120]. Sintering is required in the manufacturing of commercially available β -TCP granules and 3D printed scaffolds to provide the mechanical stability necessary for clinical use. The traditional synthesis of Mg^{2+} substituted β -TCP (β -TCMP) requires either precipitating Mg^{2+} substituted CDHA and heat treating the precipitate formed to at least 800°C (Equation 2.1) or the hydrolysis of single phase DCPD or DCPA in the presence of Ca^{2+} and Mg^{2+} ions at moderate temperatures ($\sim 100^\circ\text{C}$) (Equation 2.2) [121, 122]. The lower temperature synthesis technique described in Equation 2.2 is much less studied although low temperature synthesis procedures typically form high surface area nanoparticles rather than micron sized particles offering the advantage to study the influence of the nanoscale surface with respect to *in vitro* cytocompatibility.

Equation 2.1**Equation 2.2**

In previous work by Lee et al., rather than adding Ca^{2+} and Mg^{2+} ions during the hydrolysis of DCPA or DCPD (Equation 2.3), Mg^{2+} was introduced during the formation of DCPD prior to performing the hydrolysis reaction [81].

Equation 2.3

For the single composition reported, it was concluded that β -TCMP was the only crystalline phase formed. However, the authors did not evaluate either the *in vitro* or *in vivo* biocompatibility of the β -TCMP prepared using this synthesis approach. This therefore formed the basis of the present work.

Goals:

- To synthesize β -TCMP using the approach described by Lee et al. [81] for a wide range of compositions and determine whether or not single phase β -TCMP was formed.
- To study the role of β -TCMP composition on the *in vitro* proliferation and differentiation of osteoblast progenitor cells.

Hypothesis: Mg^{2+} substitution in β -TCP will vary the physicochemical properties of β -TCP based scaffolds resulting in improved cytocompatibility in comparison to scaffolds prepared using commercially available β -TCP. The synthesis of β -TCMP with increased Mg^{2+} concentrations will result in the formation of multiple phases rather than single phase β -TCMP. The formation of multiple rather than single phase β -TCMP will vary the dissolution profile and surface properties of β -TCMP scaffolds. The release of bioactive Mg^{2+} , Ca^{2+} , and PO_4^{3-} ions at

different rates will influence the osteogenic differentiation of osteoblast progenitor cells towards mature osteoblasts. The results obtained and subsequent discussion pertaining to this Specific Aim will be presented in Chapter 3 of this thesis.

2.2 SPECIFIC AIM 2

SYNTHESIS AND CHARACTERIZATION OF MAGNESIUM-STRONTIUM CO-SUBSTITUTED B-TRICALCIUM PHOSPHATE

Background: The optimum scaffold composition determined in Specific Aim 1 which supports increased cell proliferation and differentiation will be compared with scaffolds prepared with both Mg^{2+} and Sr^{2+} . Sr^{2+} concentrations between 0.01 and 0.1 mM in cell culture media have been found to promote the osteogenic differentiation of human mesenchymal stem cells through Wnt and MAPK signaling pathways by activating calcium sensing receptors (CaSRs) [123, 124]. Sr^{2+} containing supplements prepared using strontium ranelate are also currently prescribed to osteoporotic patients since they have been shown to increase bone density. However, excessive amounts of Sr^{2+} can also cause Rickets and renal failure [119]. Therefore, the incorporation of Sr^{2+} ions into bioactive glasses, biodegradable metals, and calcium phosphate scaffolds have been studied to provide a sustained release of Sr^{2+} locally at the defect site [76, 125]. In comparison to Mg^{2+} , Sr^{2+} ions have an increased solubility in CaPs due to a similar ionic radius with Ca^{2+} ions [118]. While Mg^{2+} and Sr^{2+} co-substituted β -TCP has been prepared using the method described in Equation 2.1, the use of DCPD hydrolysis at moderate temperatures of $\sim 100^\circ\text{C}$ to synthesize

Mg²⁺ and Sr²⁺ co-substituted β -TCP using the reaction mechanisms described in Equation 2.2 and Equation 2.3 is yet to be reported.

Goals:

- To compare the influence of Mg²⁺ and Sr²⁺ doping on the cytocompatibility of β -TCP scaffolds.
- To determine whether chemical cues, due to the dissolution of the scaffold, or physical cues, such as surface characteristics, influence the differentiation of osteoblast progenitor cells.
- To study the role of cationic substitution on TGF- β and BMP signaling on β -TCP scaffolds.
- To evaluate the roles of individual ions on supporting the osteogenic differentiation of osteoblast progenitor cells.

Hypothesis: The co-substitution of β -TCP with Mg²⁺ and Sr²⁺ will result in increased cell proliferation in comparison to the scaffolds prepared using Mg²⁺ substituted β -TCP, described in Specific Aim 1, due to the release of Sr²⁺ ions in addition to Mg²⁺. The supplementation of culture media with either Mg²⁺ or Sr²⁺ has previously been shown to support differentiation [126]. However, work evaluating the cytocompatibility of nano-sized co-substituted β -TCP is yet to be reported. Therefore, it is hypothesized that both the chemical and the physical cues provided by the scaffold will support differentiation through TGF- β and BMP signaling. Chapters 4 and 5 of this thesis will focus on the results and discussion related to this Specific Aim.

2.3 SPECIFIC AIM 3

EVALUATION OF MAGNESIUM AND STRONTIUM SUBSTITUTED B-TRICALCIUM PHOSPHATES AS COATINGS ON BIODEGRADABLE MAGNESIUM ALLOYS

Background: Degradable Mg based alloys have shown promise as an alternative to widely used non-degradable metallic biomaterials such as titanium and stainless steel [127]. Unfortunately, the majority of Mg alloys developed to date undergo rapid and uncontrolled corrosion under physiological conditions resulting in the accumulation of hydrogen gas, a corrosion product, near the implant site. In an attempt to improve bioactivity while also providing corrosion control for orthopedic and dental applications, CaP based coatings have been explored [108, 128]. CaPs have been deposited using a wide range of approaches. Some of the more widely used techniques include biomimetic approaches, sol-gels, pulsed laser deposition, and electrophoretic deposition [108, 129]. The limitations of many of the existing approaches are the need for heat treatment at elevated temperatures, the slow deposition process, and the inability to coat 3D porous scaffolds. The use of cationic substituted CaPs as coatings on biodegradable alloys is yet to be studied in detail [128]. The deposition of either strontium phosphates or Sr²⁺ doped CaPs on Mg alloys has only recently been reported [130, 131]. In addition to the improved cytocompatibility of cationic substituted CaPs in comparison to undoped CaPs, the variation in solubility in comparison to undoped CaPs may also lead to improved corrosion protection.

Goals:

- To deposit Mg^{2+} and Sr^{2+} substituted β -TCP coatings, similar to the materials studied in Specific Aims 1 and 2, on a biodegradable magnesium alloy.
- To study the influence of alloy pretreatment on CaP coating properties.
- To evaluate the influence of CaP coating composition on corrosion protection.
- To evaluate the influence of CaP coating composition on cytocompatibility.

Hypothesis: CaP coatings with similar compositions to the powders synthesized in Specific Aims 1 and 2 will be deposited on a biodegradable Mg alloy. The incorporation of Sr^{2+} into CaP coatings through an aqueous approach can reduce coating solubility providing increased corrosion control and cytocompatibility in comparison to undoped CaP coatings. Chapter 6 of this thesis will focus on all of the details related to this Specific Aim.

2.4 SPECIFIC AIM 4

SYNTHESIS AND CHARACTERIZATION OF CATIONIC SUBSTITUTED SELF-SETTING CALCIUM PHOSPHATE CEMENTS

Background: HA self-setting cement formulations are widely used in craniofacial and orthopedic bone regeneration [101]. A few of the major disadvantages of HA forming cements include their poor *in vivo* resorption and limited radiopacity. The incorporation of Sr^{2+} into CaP scaffolds was previously found to enhance the solubility of HA *in vitro* and enhance the radiopacity of CaP cements [132]. Therefore, several approaches have been utilized to incorporate Sr^{2+} ions into HA forming cements. These reported methods have included the use of

highly soluble Sr^{2+} salts, such as SrCO_3 and $\text{SrCl}_2 \cdot 6\text{H}_2\text{O}$ in addition to the precursors for HA forming cements described in Section 1.4.2.3 [124, 133]. However, the incorporation of Sr^{2+} ions into the CaP cements when using this approach is dependent upon the relative solubility of Sr^{2+} containing precursors in comparison to CaP precursors during the setting reaction. The use of cationic substituted CaP precursors rather than Sr^{2+} salts is much less studied although this may be a more efficient route to incorporate Sr^{2+} ions ensuring the sustained release of Sr^{2+} from these scaffolds once implanted.

Goals:

- To synthesize and characterize Sr^{2+} substituted DCPD by precipitation in aqueous conditions using the approaches studied in Specific Aims 1 and 2.
- To develop Sr^{2+} substituted HA forming self-setting cements which provide a sustained release of Sr^{2+} ions.
- To study the role of Sr^{2+} content on cement handling, setting, and mechanical properties.
- To study the role of cement composition on cell proliferation, osteoblastic, and osteoclastic differentiation.

Hypothesis: Sr^{2+} substitution can be used to improve the handling properties and solubility of HA forming cements while also improving cytocompatibility. The use of Sr^{2+} containing CaP precursors rather than Sr^{2+} containing salts will enhance the incorporation of Sr^{2+} into HA forming cements rather than using Sr^{2+} containing salts. The incorporation of increased amounts of Sr^{2+} into the final setting product will result in the sustained release of Sr^{2+} ions from these scaffolds. The resulting increased Sr^{2+} concentration will enhance the proliferation and

differentiation of both osteoblast and osteoclast progenitors. Chapter 7 of this thesis will focus on all of the details related to this Specific Aim.

3.0 SYNTHESIS AND CHARACTERIZATION OF MAGNESIUM SUBSTITUTED B-TRICALCIUM PHOSPHATE

3.1 INTRODUCTION

In order to improve the mechanical stability of β -TCP scaffolds, Mg^{2+} substitution has previously been explored since it is known to increase the temperature at which the β -TCP to α -TCP conversion occurs, enabling improved sintering and densification [120, 134]. Due to the instability of β -TCP under aqueous conditions, it can only be synthesized either by solid state methods or by the heat treatment of CDHA to temperatures of 800°C or more [82]. In contrast, β -TCMP has been synthesized under aqueous conditions by precipitation, hydrolysis, and hydrothermal techniques, in addition to the non-aqueous methods used to synthesize β -TCP [7, 81, 135]. As a result, β -TCMP with a wide range of particle sizes and varying crystallinity, both of which are known to influence degradation, cell proliferation, and differentiation, can be synthesized, in comparison to β -TCP [36, 107].

In addition to the capability of Mg^{2+} to stabilize β -TCP under aqueous conditions, Mg^{2+} deficiency has been shown to cause bone fragility and osteoporosis [136]. Mg^{2+} therapy has also been shown to increase bone mass in patients suffering from postmenopausal osteoporosis [137]. Despite this evidence to suggest that Mg^{2+} plays a critical role in bone metabolism, the exact role of Mg^{2+} in bone remodeling remains poorly understood. However, several studies have reported

a relationship between Mg^{2+} and parathyroid hormone levels [119, 138]. With respect to β -TCMP, it has been shown that β -TCMP scaffolds are capable of supporting cell attachment and proliferation [139]. However, fewer studies have explored the role of Mg^{2+} substitution in β -TCP on osteogenic differentiation [140, 141]. The few *in vivo* studies performed to date with β -TCMP scaffolds have shown that in a murine dental alveolus model β -TCP was found to support increased bone regeneration in comparison to β -TCMP. However, β -TCMP based scaffolds have been shown to support bone regeneration in both rat and rabbit femur models [138, 142, 143]. As a result, further work is warranted to more accurately determine the role of Mg^{2+} substitution in β -TCP on both *in vitro* and *in vivo* biocompatibility.

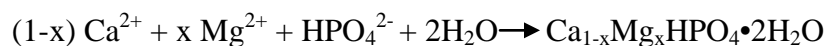
Previous work by Lee et al. using a novel low temperature aqueous synthesis approach has shown that upon refluxing Mg^{2+} substituted DCPD, synthesized with a 50% $Mg/(Ca+Mg)$ molar ratio, β -TCMP with a relatively high surface area of approximately $200\text{ m}^2\text{ g}^{-1}$ can be formed [81]. An elemental analysis of β -TCMP produced by this method indicated that the $Mg/(Ca+Mg)$ molar ratio was close to 30 mol. %, although previous reports using Rietveld refinement have confirmed that the maximum possible Mg^{2+} substitution in the β -TCP structure is approximately 14 mol. % [122, 134]. To date, the structural refinement and *in vitro* cytocompatibility of β -TCMP synthesized using this method is yet to be reported. Therefore, this low temperature approach reported by Lee et al. was employed to generate β -TCMP with varying levels of substitution. Rietveld refinement was used to evaluate the actual level of ionic substitution in β -TCMP while varying the $Mg/(Ca+Mg)$ ratio during synthesis. The effect of Mg^{2+} substitution on the physicochemical properties, cytocompatibility, and the capability to support the osteogenic differentiation of the MC3T3-E1 mouse preosteoblast cell line was studied in detail.

3.2 MATERIALS AND METHODS

3.2.1 Synthesis of Magnesium Substituted β -Tricalcium Phosphate

The detailed molar amounts used for the synthesis of β -TCMPs are illustrated in Table 3.1. Briefly, a 100 ml solution consisting of mixtures of $\text{CaCl}_2 \cdot 2\text{H}_2\text{O}$ (ACS Reagent $\geq 99.0\%$, Acros Organics) and $\text{MgCl}_2 \cdot 6\text{H}_2\text{O}$ (ACS Reagent, $\geq 99.0\%$, Acros Organics) was added dropwise under constant stirring to 100 ml of a 0.5 M solution of disodium hydrogen phosphate (Na_2HPO_4 , $\geq 99.0\%$ Sigma-Aldrich) at room temperature. The mixture was stirred for 15 minutes prior to centrifuging and washing the collected precipitate with deionized water. The reaction illustrated in Equation 3.1 is believed to proceed. In all cases, the $(\text{Ca}+\text{Mg})/\text{P}$ mole ratio was kept constant at a value of 1, corresponding to DCPD. The washed precipitate was then dispersed in 200 ml of deionized water and was refluxed for 2 hours following the previously published report which has shown that for a $\text{Mg}/(\text{Ca}+\text{Mg})$ ratio of 50%, refluxing for 2 hours resulted in the highest surface area [81]. While refluxing, the hydrolysis reaction illustrated in Equation 2.3 is believed to proceed resulting in the formation of β -TCMP. After refluxing, the powders were collected by centrifugation and were once again washed with deionized water prior to drying overnight at 60°C .

Equation 3.1



Where $0.35 \leq x \leq 0.50$

Table 3.1 The molar amounts of calcium and magnesium chloride dissolved in 100 ml of DI water and used in the precipitation of DCPD by adding drop wise to 100 ml of 0.05 M Na₂HPO₄ at room temperature.

Mol. % Mg	CaCl₂•2H₂O (moles)	MgCl₂•6H₂O (moles)
35%	0.0325	0.0175
40%	0.0300	0.0200
45%	0.0275	0.0225
50%	0.0250	0.0250

3.2.2 X-Ray Diffraction and Rietveld Refinement

Phase analysis was performed using X-ray diffraction (XRD). XRD was performed using a Philips X-Pert PRO diffractometer employing Cu K α radiation ($\lambda=1.5406$ Å) with a Si-detector (X'celerator). The X-ray generator was operated at 45 kV and 40 mA at a 2θ range of 10-70° with a step size of 0.0167° and a time per step of 3s. Quantitative analysis of phase composition and Mg substitution was performed using Rietveld refinement. The structural model of ICSD card number 6191 [144] was used for the undoped β -TCP and is described in further detail in Table 3.2. ICSD card numbers 15326 and 22225 were used for Mg₂P₂O₇ and Ca₂P₂O₇, respectively.

Table 3.2 Calcium site positions and occupancy factors for β -TCP from Dickens et. al.

	x	y	z	Occ. Factor	Wyckoff Position
Ca1	-0.2766	-0.1421	0.1658	1	18b
Ca2	-0.3836	-0.1775	-0.0336	1	18b
Ca3	-0.2721	-0.1482	0.0606	1	18b
Ca4	0	0	-0.0850	0.491	6a
Ca5	0	0	-0.2658	0.999	6a

X'Pert HighScore Plus version 3.0d was used to perform Rietveld refinements. The refined parameters were scale factor, zero displacement, background as Chebyshev polynomial of fifth grade and 1/x function, crystallite size, micro-strain, lattice parameters, and occupancy factors. Rietveld refinements were performed using the pseudo-Voigt peak shape model. Mg atoms were inserted into Ca(4) and Ca(5) lattice sites and a constraint that the sum of the occupancy factors for these sites be equal to 0.491 and 0.999, respectively, was applied [122].

3.2.3 Thermal Stability

Thermogravimetric analysis (TGA) and differential scanning calorimetry (DSC) were performed using a Netzsch STA 409 PC DTA/TGA instrument to analyze the weight loss and phase stability of the refluxed powders during heat treatment. The measurements were performed by heating samples in air up to 1000°C at a heating rate of 10°C min⁻¹. The analysis of the ceramic powders was performed using a platinum crucible.

3.2.4 Elemental Analysis

An elemental analysis of the powders formed after precipitation and after refluxing was performed using inductively coupled plasma optical emission spectrometry (ICP-OES, iCAP duo 6500, Thermo Scientific). The powders were first dissolved in diluted HNO₃ solutions and the concentrations of Ca²⁺, Mg²⁺, and PO₄³⁻ in solution was determined using known standards. A minimum of four batches were analyzed independently. The mean and standard deviation for each composition was reported.

3.2.5 Scaffold Preparation

13 mm diameter β -TCMP pellets were formed by uniaxial compression (Carver, Wabash, IN). Briefly, 0.35 g of powder was compressed with an applied load of 2,500 psi. All β -TCMP pellets were heat treated to 600°C for 4 hours prior to use in any further experiments. Commercially available β -TCP (HIMED, Old Bethpage, NY, $\geq 53 \mu\text{m}$) was similarly uniaxially pressed and heat treated to 1000°C for 4 hours to be used as a control. Heat treated pellets were used for all of the subsequent experiments described.

3.2.6 Scaffold Pore Size Distribution and Protein Adsorption

The pore size distribution and total pore volume of sintered β -TCMP and β -TCP pellets was analyzed using mercury porosimetry (Autopore IV 9500, Micromeritics). To study protein adsorption on β -TCMP and β -TCP pellets, pellets were first washed with PBS followed by incubation in fetal bovine serum (FBS, Atlanta Biologicals, Lawrenceville, GA) for 24 hours at 37°C. After incubation, the samples were washed twice with PBS and incubated for half an hour in a lysis buffer (CellLytic M Lysis Reagent, Sigma Aldrich) on a platform shaker at room temperature. The lysis buffer was collected and the concentration of the proteins adsorbed to the surface of the pellets was measured using the BCA assay (Peirce BCA Protein Assay Kit, Thermo Scientific). Further analysis of the adsorbed proteins was performed using SDS-polyacrylamide gel electrophoresis and Coomassie Blue staining (ChemiDoc XRS Molecular Imager, Bio-Rad).

3.2.7 Cell Culture and Maintenance

Murine preosteoblast cell line, MC3T3-E1, was obtained from ATCC (Manassas, VA). Cells were cultured under 37°C, 5% CO₂, and 95% relative humidity in minimum essential medium alpha (α -MEM, Gibco, Grand Island, NY) containing 10% FBS and 1% penicillin streptomycin (P/S, Gibco, Grand Island, NY). Cells after third passage were used in experiments and were seeded at a density of 50,000 cells per pellet/scaffold. For differentiation studies, cells were cultured on samples, as previously described, for up to 7 days. After 7 days, growth media supplemented with 10 mM β -glycerophosphate, 50 μ M ascorbic acid, and 100 nM dexamethasone was used to induce differentiation.

3.2.8 Cell Viability

Cell viability was assessed using live/dead staining (Invitrogen, Live/Dead Staining Kit) and the MTT assay (Vybrant MTT Cell Proliferation Assay Kit, Invitrogen, Carlsbad, CA). After 3 days of culture on heat treated pellets, samples were washed with phosphate buffered saline (PBS) and incubated for 40 minutes with the live/dead stain. After incubation, the samples were once again gently washed with PBS prior to imaging using fluorescence (Olympus CKX41). Cells were then fixed with 4% paraformaldehyde and were subjected to alcohol dehydration followed by sputter coating with palladium (Cressington sputter coater 108A) in order to observe cell morphology by scanning electron microscopy (Philips XL30 FEG ESEM).

The MTT assay was used to quantitatively determine cell proliferation after 3 and 9 days. 1 ml of culture media was added to each well along with 100 μ L of a 12 mM MTT stock solution in PBS. Samples were incubated for 4 hours during which water soluble MTT is reduced to

insoluble formazan inside living cells. 100 μ l of a 0.1 g/ml solution of sodium dodecyl sulfate in 0.01 M hydrochloric acid was then added to each well to solubilize formazan and the samples were incubated for an additional 15 hours. 100 μ l aliquots were removed from each well and added to a 96 well plate. Absorbance was then measured at a wavelength of 570 nm.

3.2.9 Alkaline Phosphatase Activity

Cells were lysed using the CellLytic M lysis buffer according to the manufacturer's protocol. 30 μ L of cell lysate was added to 170 μ L of 1 g L⁻¹ p-nitrophenyl phosphate (pNPP) dissolved in 0.2 M tris buffer (SIGMAFASTTM p-Nitrophenyl phosphate tablets, Sigma Aldrich). Samples were then incubated for 1 h at 37°C prior to stopping the reaction with 20 μ L of 0.3 N NaOH. The concentration of p-nitrophenyl (pNP) in solution after 1 h was determined by measuring the absorbance at a wavelength of 405 nm. pNP standards were prepared by diluting in 0.02 N NaOH. Alkaline phosphatase (ALP) activity was normalized with respect to DNA concentration which was measured using the Quant-iT PicoGreen Kit (Invitrogen, Carlsbad, CA) according to the manufacturer's protocol.

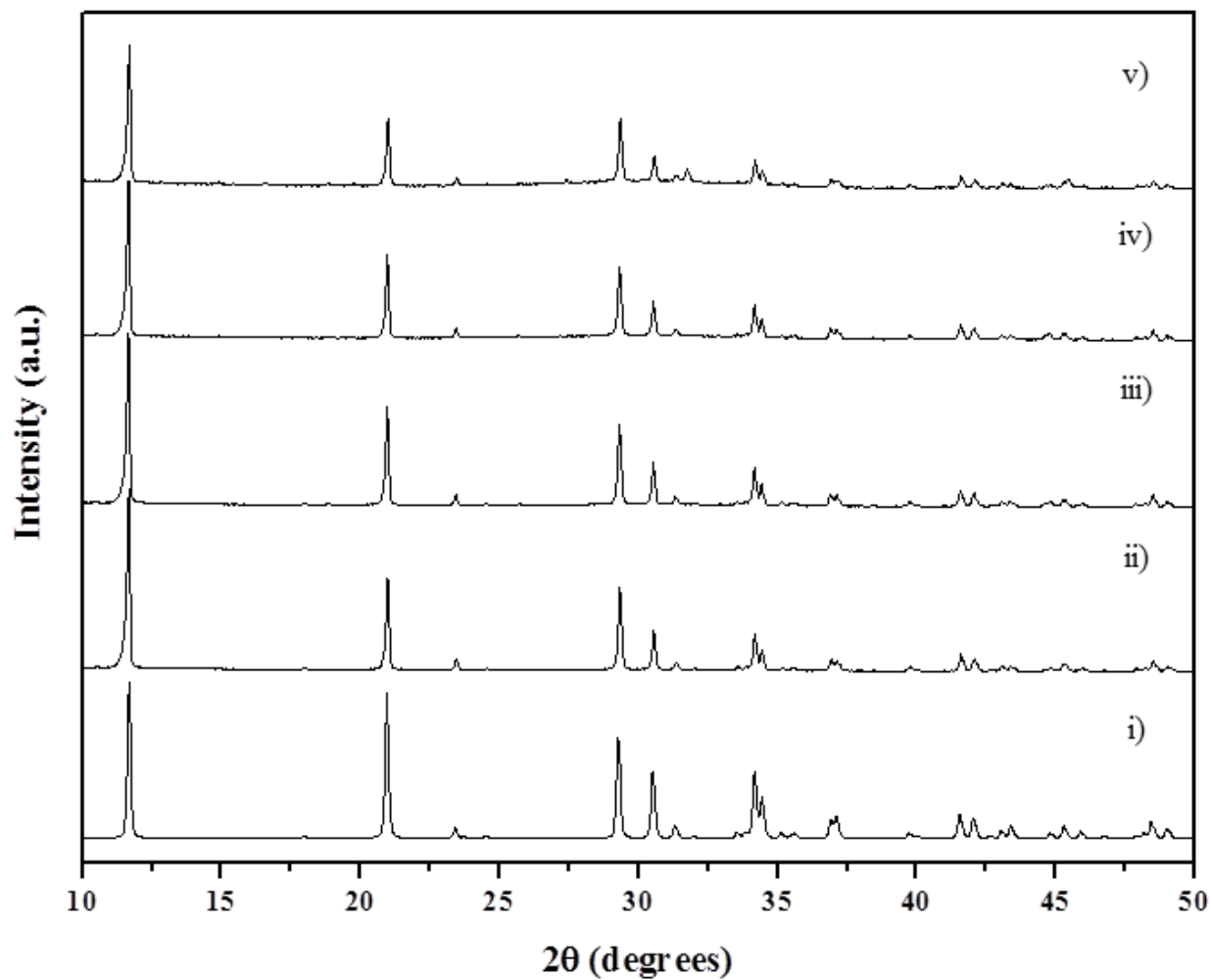


Figure 3.1 Powder X-ray diffraction data collected from i) DCPD (JCPDS 09-0077) and DCPD precipitated ii) 35%, iii) 40%, iv) 45%, and v) 50% Mg.

Table 3.3 qRT-PCR genes and primer sequences used for MC3T3-E1 mouse preosteoblasts

	Forward Primer (5'-3')	Reverse Primer (5'-3')
GAPDH	AGGAGTATATGCCCGACGTG	TCGTCCACATCCACACTGTT
COL1	ATGGAGACAGGTCAGACCTGTGT	CAGGCTTCCTGCCAGTACCT
OCN	GGGAGACAACAGGGAGGAAAC	TCGGTCATGCTCTCTCCAAAC
RUNX2	CCCAGCCACCTTTACCTACA	TATGGAGTGCTGCTGGTCTG

3.2.10 Osteogenic Gene Expression

After 14 and 21 days of culture in osteogenic media, RNA extraction was performed using the NucleoSpin RNA II kit (Macherey Nagel, Bethlehem, Pa) according to the manufacturer's protocol. RNA concentration was determined by measuring absorbance at 260 and 280 nm, respectively, using a BioRad SmartSpec spectrophotometer. Reverse transcription was then performed using the ImProm II Promega Reverse Transcription Kit according to the manufacturer's protocol. Primers for GAPDH, osteocalcin, collagen-I, and runx2 were used in qRT-PCR experiments (Table 3.3) and each sample was measured in triplicate using Brilliant II SYBR Green Master Mix (Agilent Technologies).

3.2.11 Statistical Analysis

Five independent batches for each condition described in Table 3.1, were prepared. Unless otherwise mentioned, analyses were performed independently for each batch. Accordingly, the average and standard deviation were reported. Statistical significance was determined using a one way analysis of variance (ANOVA). The Tukey-Kramer test was used for all pairwise comparisons. A p value < 0.05 was considered significant.

3.3 RESULTS AND DISCUSSION

3.3.1 Powder Characterization

3.3.1.1 X-Ray Diffraction

X-ray diffraction was performed to determine the crystallinity and phase composition of the powder samples formed both after precipitating and refluxing in the presence of various Mg^{2+} concentrations (Table 3.1). After precipitating DCPD in the presence of various Mg^{2+} concentrations and drying overnight at 60°C , DCPD (JCPDS 09-0077) was the only crystalline phase formed when using up to 50% $\text{MgCl}_2 \cdot 6\text{H}_2\text{O}$ (Figure 3.1). The powders were then dispersed in deionized water and boiled with reflux for up to two hours. A similar analysis of the phase composition was performed. Specifically of interest was to determine whether or not samples prepared with 35-45% Mg were capable of stabilizing β -TCMP under aqueous conditions, as was previously observed for samples prepared with 50% Mg [81]. The XRD spectra of powder samples prepared with 35-50% Mg after refluxing and washing is illustrated in Figure 3.2. The peaks observed for all compositions closely resembled that of β -TCP (JCPDS 09-0169) and no other crystalline phases were detected. A slight peak shift to increased 2θ values was also observed between β -TCP and the β -TCMPs. In comparing the XRD spectra collected for the various β -TCMPs, little or no peak shift was observed between conditions despite varying the Mg^{2+} concentration used during synthesis.

The peak shift observed for the β -TCMPs in comparison to β -TCP is most likely due to a decrease in lattice size as a result of smaller 0.065 nm Mg^{2+} ions substituting for larger 0.099 nm Ca^{2+} ions in the β -TCP crystal structure [118]. Therefore, the similar peak positions observed for the β -TCMPs suggests that similar amounts of Mg^{2+} were retained in the β -TCMP formed after

refluxing despite varying Mg^{2+} concentration. Interestingly, upon increasing Mg^{2+} concentration, an increase in the full width half maxima (FWHM) was also observed. A similar increase in FWHM and loss of crystallinity was observed when synthesizing β -TCMP with increased Mg^{2+} concentrations using a hydrothermal technique [135]. As a result of the increased FWHM, it is difficult to confirm the presence of amorphous content for samples prepared with 50% Mg. However, little or no amorphous content was observed in the XRD spectra of samples prepared with 35%-45% Mg. Traditional β -TCMP synthesis methods, such as the heat treatment of CDHA and solid state synthesis, require heat treatment to at least 800°C in order to form β -TCMP [121]. However, by refluxing Mg^{2+} substituted DCPD, precipitated with $Mg/(Ca+Mg)$ molar ratios of 35-50%, β -TCMP can be synthesized under aqueous conditions at temperatures near 100°C, similar to previous reports using hydrothermal and hydrolysis techniques [135, 145].

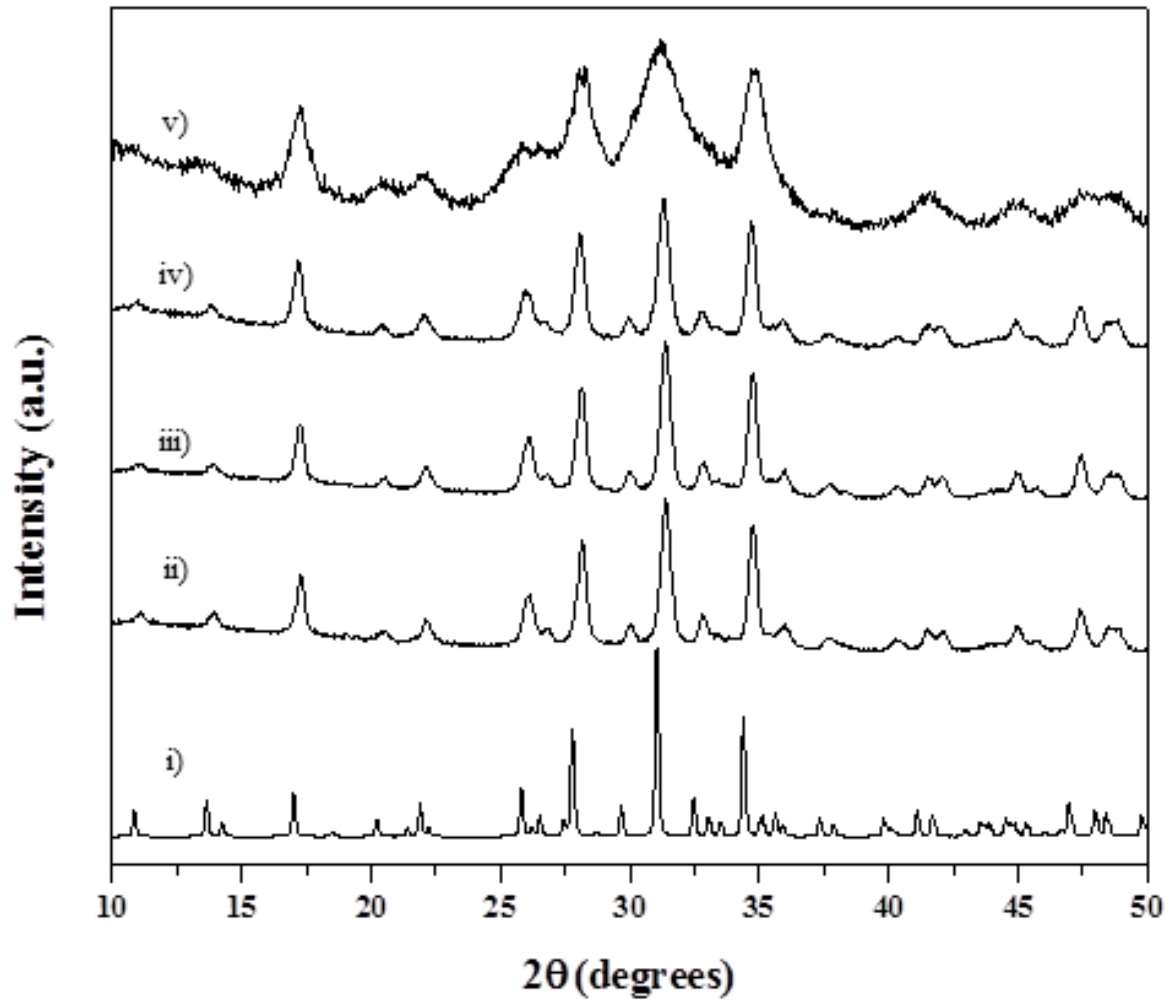


Figure 3.2 Powder X-ray diffraction data collected from i) β -TCP (JCPDS 09-0169) and β -TCMP after refluxing with ii) 35%, iii) 40%, iv) 45%, and v) 50% Mg.

3.3.1.2 Thermal Analysis

Thermal analysis was performed in order to further characterize the phase purity of the refluxed powders since the presence of amorphous content could not be confirmed by XRD. The TGA and DSC curves collected from samples prepared with 35 and 50% Mg are illustrated in Figure 3.3. For samples prepared with 35% Mg, an endothermic peak near 100°C, due to the evaporation of moisture adsorbed to the surface of powder samples, was observed. Interestingly, near 750°C a sharp exothermic peak was also observed. For samples prepared with 50% Mg, a similar peak between 100-150°C, indicative of the evaporation of adsorbed moisture, was observed. However, it was of much greater intensity in comparison to the peak observed for samples prepared with 35% Mg. At increased temperatures, a sharp exothermic peak near 750°C was also observed. Similar to the peak indicative of the evaporation of adsorbed moisture, the peak observed near 750°C was also of much greater intensity in comparison to the peak observed at a similar temperature for samples prepared with 35% Mg. Similar patterns were also observed for samples prepared with 40 and 45% Mg.

The exothermic peak at 750°C observed for both samples could be due to the crystallization of an amorphous phase, which was not previously detected by XRD, the phase separation of β -TCMP, or the reconstitutive phase transformation of β -TCMP. Mg^{2+} substitution was previously found to increase the thermal stability of β -TCP since it increased the temperature at which β -TCP converts to α -TCP [134]. Therefore, it is highly unlikely that a phase separation or a phase transformation of β -TCMP is occurring, since for all compositions β -TCMP was the only crystalline phase detected. Considering these aspects, it can be assumed that the exothermic peak arises due to the presence of an amorphous phase. The greater peak intensity

for samples prepared with 50% Mg suggests the formation of increased amorphous content upon increasing Mg^{2+} concentration.

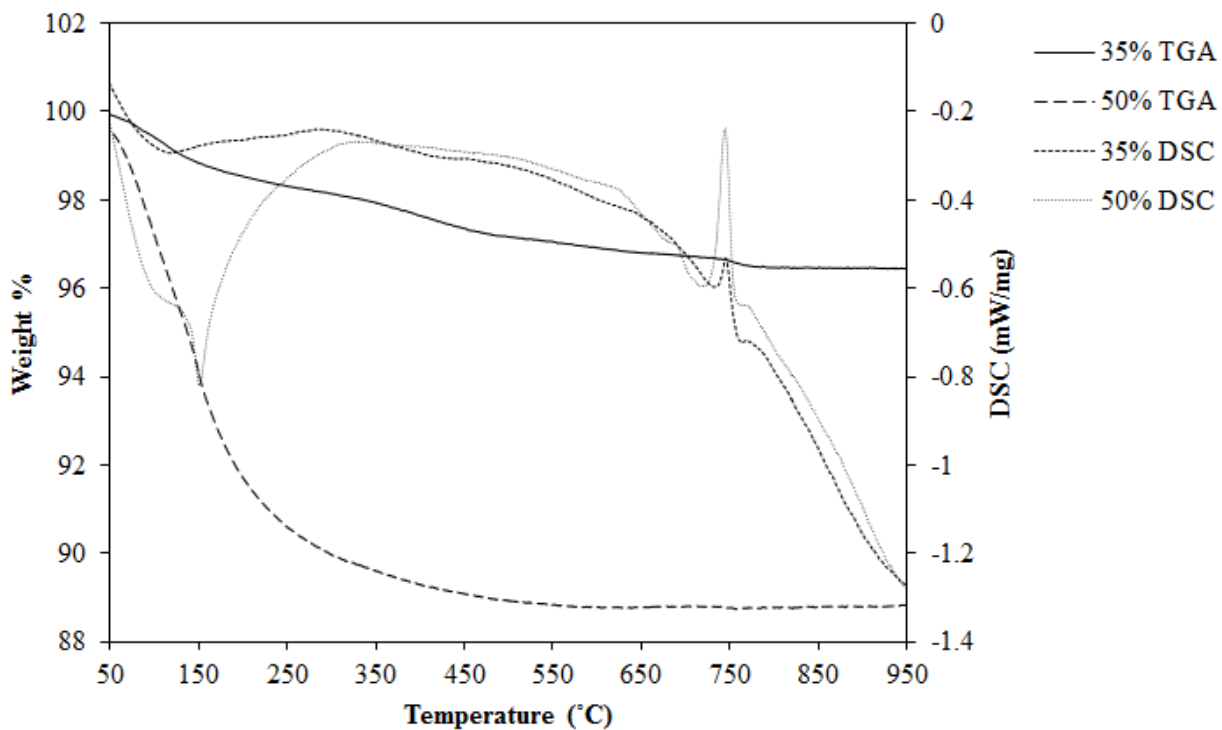


Figure 3.3 Thermogravimetric analysis and differential scanning calorimetry data collected from powder samples prepared with 35 and 50% Mg.

In order to confirm the presence of amorphous phases, the refluxed powder samples were heat treated to 750°C for 4 hours and analyzed using XRD and SEM (Figure 3.4). XRD results indicated that in addition to β -TCMP, $Ca_2P_2O_7$ and $Mg_2P_2O_7$, were formed after heat treatment to 750°C (Figure 3.4). SEM images of these heat treated samples illustrated the formation of sintered particles for samples prepared with 35% Mg (Figure 3.5 a)). However, for samples prepared with 50% Mg, two distinct morphologies were observed (Figure 3.5 b)). Similar sintered particles, as were observed for samples prepared with 35% Mg, along with much smaller

evenly distributed particles, believed to be due to the formation of increased amounts of $\text{Mg}_2\text{P}_2\text{O}_7$, were also observed.

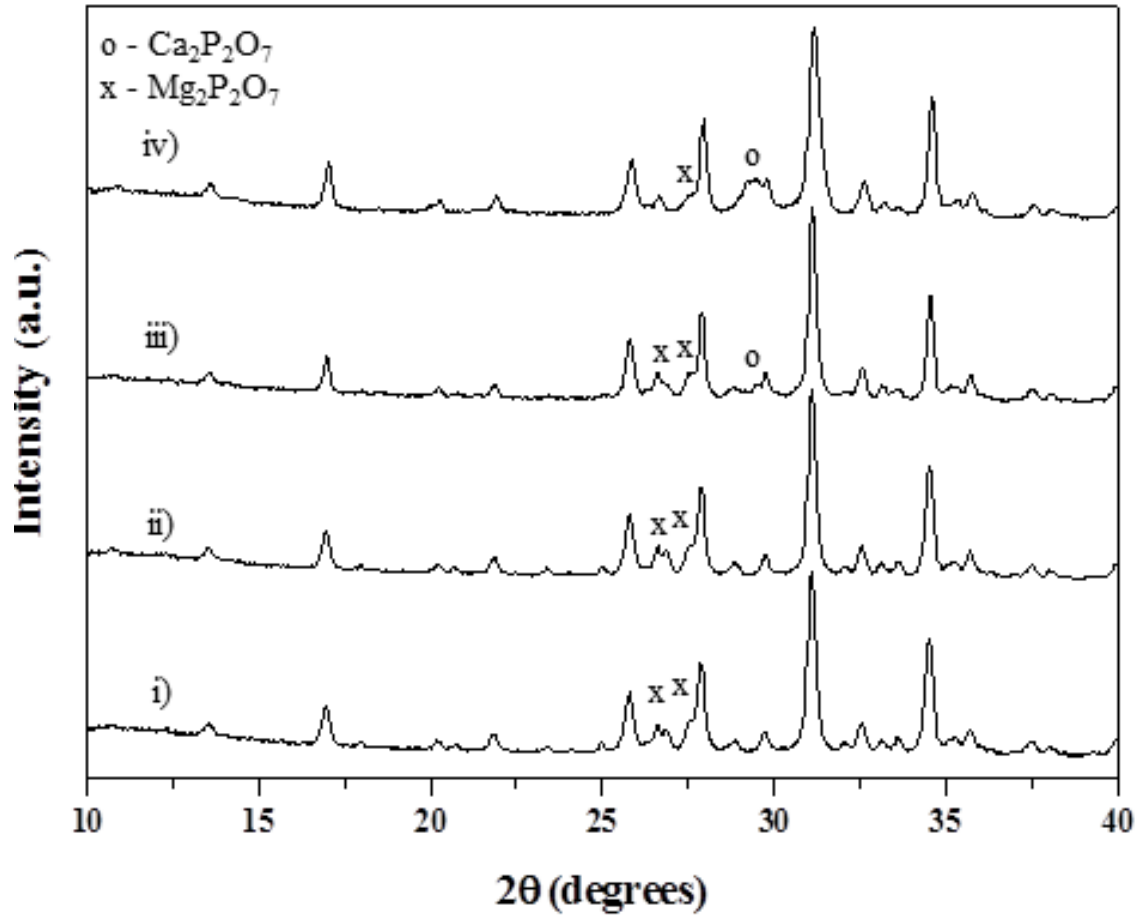


Figure 3.4 Powder X-ray diffraction data collected from samples prepared using i) 35, ii) 40, iii) 45, and iv) 50% Mg after heat treatment to 750°C ($\text{Ca}_2\text{P}_2\text{O}_7$ JCPDS 03-0421 and $\text{Mg}_2\text{P}_2\text{O}_7$ JCPDS 05-0582).

Heat treatment to 600°C was also performed (Figure 3.6). Similar to the XRD spectra collected after refluxing, a peak shift to greater 2θ values was observed and β -TCP was the only crystalline phase detected. A slight increase in FWHM could also still be observed after heat treatment to 600°C for samples prepared with 50% Mg in comparison to powder samples

prepared with 35-45% Mg. The BET surface area after precipitating, refluxing, and heat treatment to 600°C was also determined (Table 3.4). Surface area increased after refluxing upon increasing Mg²⁺ concentration for all conditions and a maximum surface area of 200 m²*g⁻¹ was measured, similar to previous studies [81].

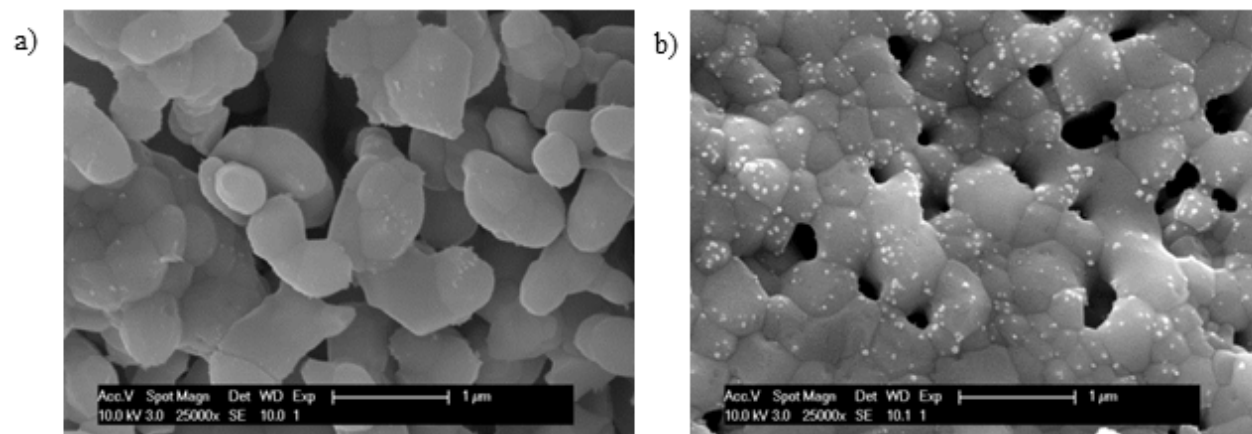


Figure 3.5 SEM images of powder samples prepared with a) 35% and b) 50% Mg after heat treatment to temperatures greater than 750°C.

After heat treatment to 600°C, both surface area and true density decreased with increasing Mg²⁺ concentration. These results confirmed that β-TCMPs synthesized using this method can be processed and subsequently heat treated at temperatures of up to 600°C retaining β-TCMP as the only crystalline phase.

In summary, thermal analysis and heat treatment confirmed the formation of amorphous phases after refluxing. However, the level of Mg²⁺ substitution and weight % of the crystalline and amorphous phases formed after refluxing remains unknown. The amorphous phase appears to form Mg₂P₂O₇ and Ca₂P₂O₇ upon heat treatment to 750°C, maintaining a (Ca+Mg)/P ratio of 1, which was kept constant during synthesis prior to refluxing. Therefore, it appears that Mg²⁺

doped DCPD first forms an amorphous intermediate phase which converts into β -TCMP during refluxing. In previous work where β -TCMP was synthesized by the hydrolysis of DCPD or dicalcium phosphate (DCP), Ca^{2+} and Mg^{2+} containing solutions were added to solutions containing dissolved DCPD or DCP while refluxing ensuring that a $(\text{Ca}+\text{Mg})/\text{P}$ stoichiometric ratio of 1.5, that of β -TCP, was maintained [145]. In the current work, additional Ca^{2+} and Mg^{2+} ions were not added while refluxing Mg^{2+} doped DCPD, resulting in the formation of H_3PO_4 as a by-product. pH measurements after refluxing and prior to washing ranged between 3.7-5.8. More basic pH values were obtained for samples prepared with increased Mg^{2+} concentrations, suggesting a lower conversion. As a result of the poor conversion for samples prepared with increased Mg^{2+} concentrations, it is likely that increased amorphous content was also formed.

3.3.1.3 Rietveld Refinement

For CaPs, Rietveld refinement has typically been used to study biphasic substituted mixtures of HA and β -TCP and more recently even co-substituted β -TCP [82, 146, 147]. In the current work, five batches for each condition were prepared and were analyzed independently by Rietveld refinement to observe variations in lattice parameters, to determine the amount of Mg^{2+} retained in the β -TCP crystal structure, and to estimate the weight % of amorphous content formed. The occupancies of Ca(4) and Ca(5) sites were included in the refined parameters since it is known that Mg^{2+} ions preferentially occupy these two sites within the β -TCP crystal structure [144, 148]. Ca(5), which is coordinated with six oxygen atoms, is initially occupied by Mg^{2+} followed by Ca(4), which is coordinated with three oxygen atoms [149].

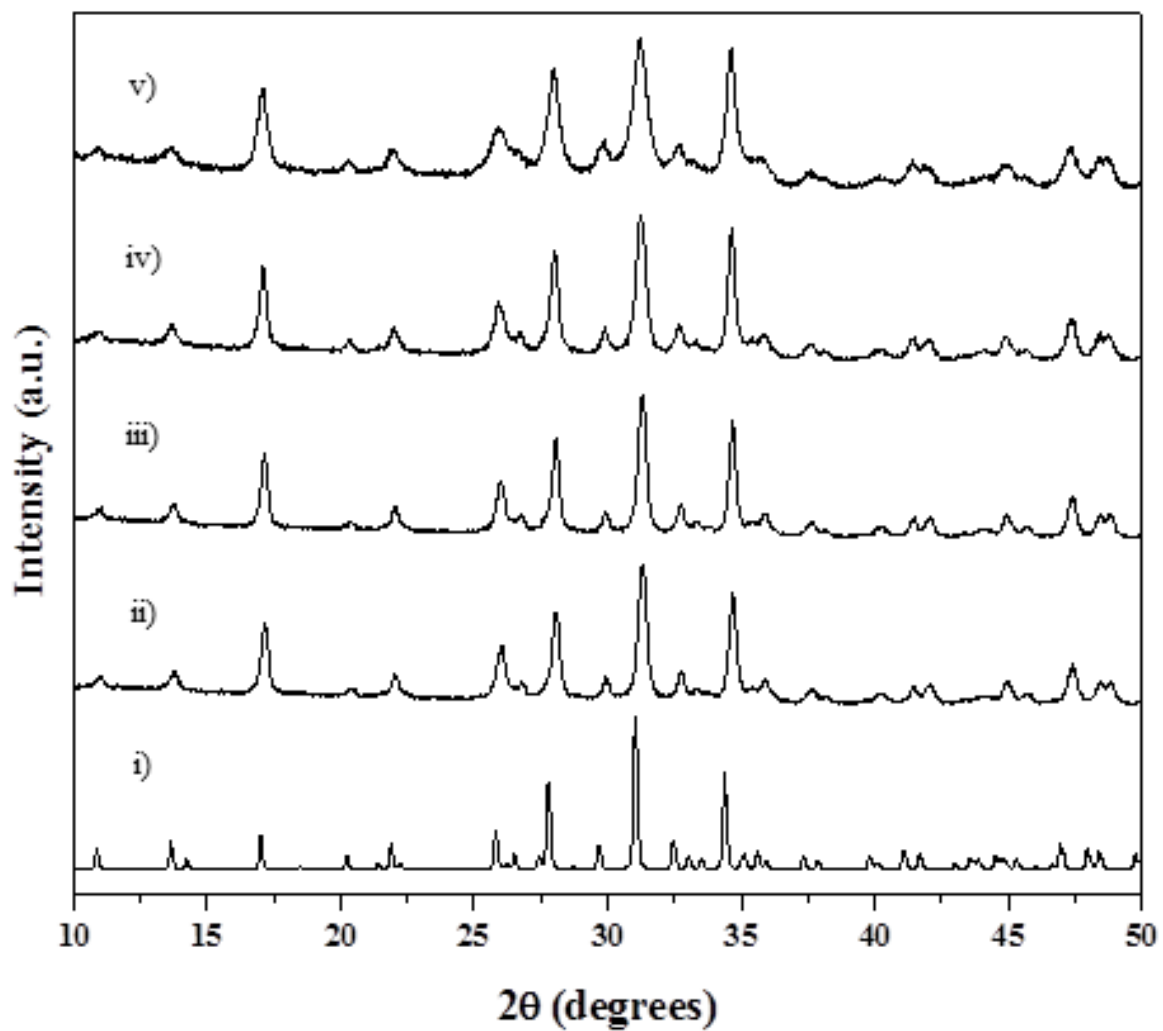


Figure 3.6 Powder X-ray diffraction data collected from i) β -TCP (JCPDS 09-0169) and β -TCMP after refluxing and heat treatment to 600°C with ii) 35%, iii) 40%, iv) 45%, and v) 50% Mg.

Table 3.4 BET surface areas and true density of β -TCMP powders after precipitating, refluxing for two hours, and heat treatment to 600°C.

Mol. % Mg in synthesis	BET Surface Area After Precipitating (m²/g)	BET Surface Area After Refluxing (m²/g)	BET Surface Area After Heat Treatment to 600°C (m²/g)	ρ After Heat Treatment to 600°C (g/ml)
35%	31.86	77.69	16.50	3.087 ± 0.010
40%	40.74	158.83	13.60	3.056 ± 0.010
45%	56.13	180.01	14.75	3.035 ± 0.006
50%	28.84	207.96	9.21	3.002 ± 0.010

Refinement results indicated a decrease in lattice size compared to undoped β -TCP for all conditions studied (Figure 3.7). A steady decrease in lattice parameter a was observed upon increasing the Mg²⁺ concentration used during synthesis. A similar trend was observed for lattice parameter c , although it was observed to increase for samples prepared with 50% Mg. Previous work by Enderle et. al. has found that the lattice parameter a constantly decreases up to 14 mol. % Mg²⁺ substitution whereas the lattice parameter c decreases up to 10 mol. % Mg²⁺ substitution and then increases until it approaches 14% substitution [134]. Similar to Enderle et al a slight increase in the lattice parameter c was also observed in the current study and is believed to be due to Mg²⁺ preferably occupying the Ca(5) site and not occupying the Ca(4) site until the Ca(5) site is near full occupancy. This result indicates an increased Mg²⁺ substitution for samples prepared with 50% Mg in comparison to those prepared with 35-45% Mg. However, the substitution level appears to be similar for all conditions based on the limited range of variation of lattice parameters in comparison to that observed in other studies analyzing β -TCMP synthesized via high temperature approaches [121, 122].

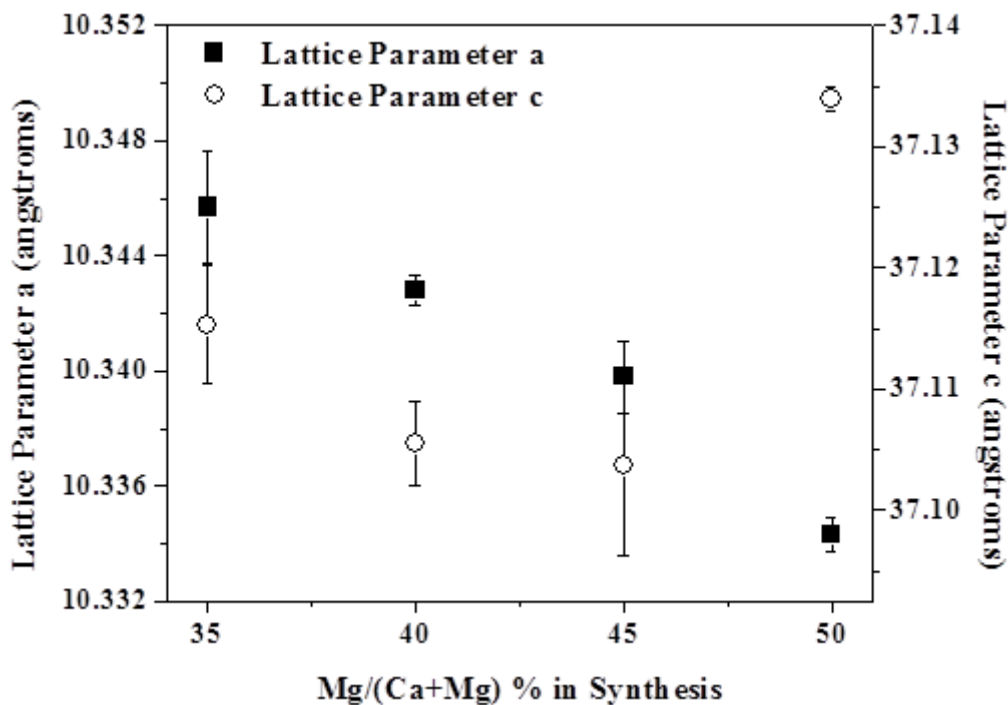


Figure 3.7 The effect of varying the Mg^{2+} concentration in β -TCMP synthesis on lattice parameters a and c .

Mg^{2+} substitution was calculated based on the refined occupancy factors using Rietveld refinement and was compared with the mol. % of Mg determined by elemental analysis (Figure 3.8). As the Mg^{2+} concentration in synthesis was increased, there was a greater deviation between the $\text{Mg}/(\text{Ca}+\text{Mg})$ molar ratio determined by Rietveld refinement in comparison to that determined using elemental analysis. Samples prepared with 50% Mg had the maximum Mg^{2+} substitution of roughly 13 mol. %, which was lower than the maximum possible Mg^{2+} substitution of 14% in β -TCP [122]. However, the total mol. % of Mg^{2+} for samples prepared with 50% Mg, measured by elemental analysis, was almost twice that which was determined by Rietveld refinement. Interestingly, β -TCMP synthesized with 35% Mg had a fairly similar result for $\text{Mg}/(\text{Ca}+\text{Mg})$ ratio from both the elemental analysis and computational methods.

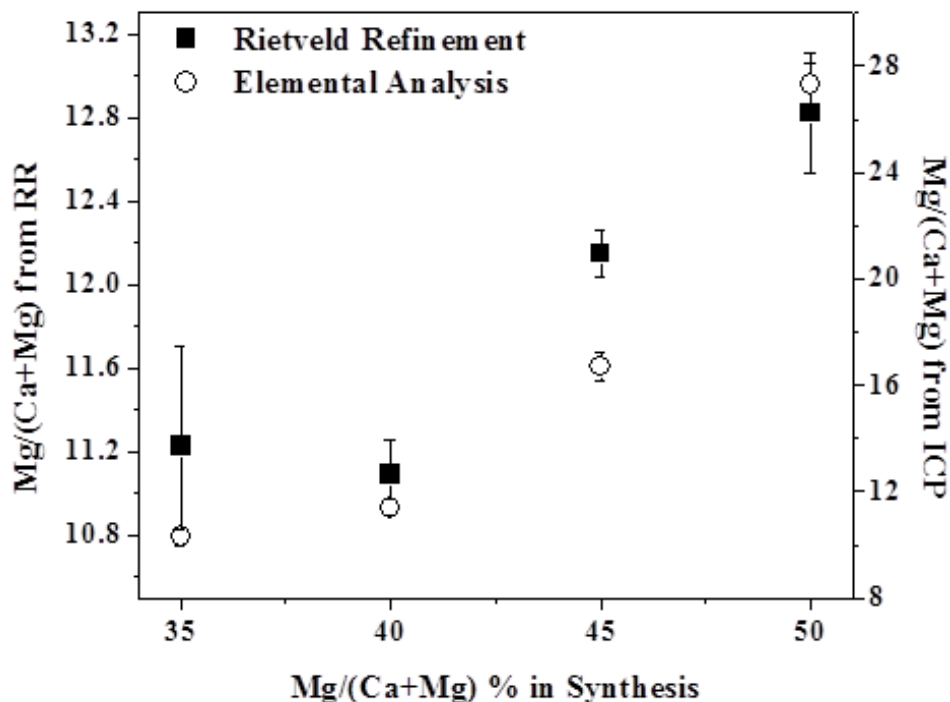


Figure 3.8 A comparison of the mol. % of Mg^{2+} calculated from Rietveld refinement and measured using elemental analysis.

This discrepancy between elemental analysis and Rietveld refinement results suggests that the excess Mg^{2+} is retained in the amorphous phase. Assuming that an amorphous phase has formed for samples prepared with 35% Mg due to the exothermic peak observed in thermal analysis, the similarity in $Mg/(Ca+Mg)$ ratio determined by experimental and computational methods suggests that the amorphous content for this condition is either relatively small or has a similar composition to the crystalline content. As previously mentioned, upon heat treatment the amorphous phase appears to crystallize and form $Ca_2P_2O_7$ and $Mg_2P_2O_7$ (Figure 3.4). In order to estimate the amorphous content, Rietveld refinement was used to quantitatively determine the composition of the mixture after heat treatment to $750^\circ C$ and indirectly ascertain the amorphous phase content. Surprisingly, for samples prepared with 35% Mg, as much as 15% by weight

consisted of $\text{Ca}_2\text{P}_2\text{O}_7$ with traces of $\text{Mg}_2\text{P}_2\text{O}_7$ whereas for samples prepared with 50% Mg, 20% by weight consisted of $\text{Mg}_2\text{P}_2\text{O}_7$ with traces of $\text{Ca}_2\text{P}_2\text{O}_7$. This result indicates the variation in composition of the amorphous phase upon varying the Mg^{2+} concentration in synthesis, and confirms the formation of increased amorphous content.

Using this low temperature aqueous method, high surface area β -TCMP, with 11-13% Mg substitution along with amorphous calcium magnesium phosphate was synthesized. Similar to β -TCP, amorphous calcium phosphate (ACP) has also been shown to be a relevant material for a wide range of applications in hard tissue regeneration [150, 151]. ACP exists *in vivo* and is believed to be a precursor for the nucleation and growth of HA crystals which are formed during mineralization, along with DCPD and octacalcium phosphate (OCP) [152]. Previous work has shown that Mg^{2+} substitution reduces the solubility of β -TCP thereby restricting the release of bioactive Ca^{2+} , Mg^{2+} , and PO_4^{3-} ions [137]. Therefore, the formation of a highly soluble amorphous calcium magnesium phosphate phase in addition to β -TCMP may positively influence cytocompatibility in comparison to traditionally synthesized single phase β -TCMP. As a result, further study is warranted to determine the influence of the amorphous content formed on the proliferation and differentiation of osteoblast progenitor cells in the presence of β -TCMP.

3.3.2 Scaffold Characterization

3.3.2.1 Pore Size Distribution and Total Pore Volume

Refluxed β -TCMP powders were uniaxially pressed to form 13 mm diameter pellets and were heat treated to 600°C for 4 hours prior to use in any further experiments. Commercially available β -TCP was similarly processed and used as a control. Heat treatment to 600°C was performed to provide sufficient mechanical stability during handling and under aqueous conditions while

avoiding the formation of multiple crystalline phases, observed after heat treatment to 750°C. The pore size distribution and total pore volume of the scaffolds formed after uniaxial compression and heat treatment was determined to compare the surface area exposed in scaffolds formed using various β -TCMPs and β -TCP powders.

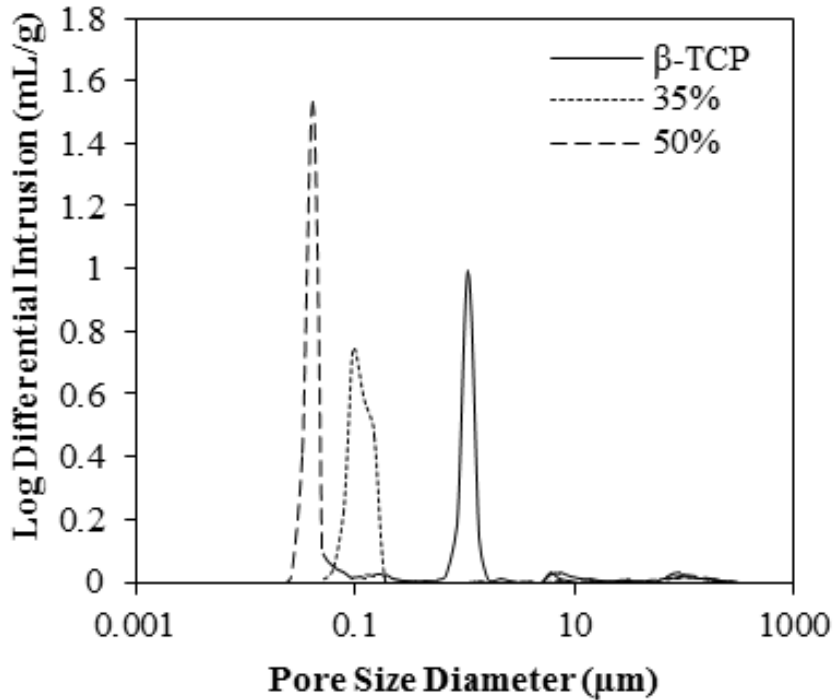


Figure 3.9 The pore size distribution of scaffolds prepared using commercially available β -TCP, 35% β -TCMP, and 50% β -TCMP measured using Hg porosimetry.

In Figure 3.9, the pore size distribution of pellets prepared with β -TCP, 35%, and 50% β -TCMP is illustrated. For scaffolds prepared with commercially available β -TCP, the mean pore size is approximately 1 μm . For those prepared with 35 % β -TCMP, a mean pore size of 100 nm was obtained while a value of 40 nm was measured for scaffolds prepared with 50% β -TCMP. Despite the decreased mean pore size, the total intrusion volume for pellets prepared with 50% β -

TCMP was 0.25 ml g^{-1} and that for samples prepared with β -TCP was 0.15 ml g^{-1} , suggesting a greater total pore volume for scaffolds prepared with 50% β -TCMP.

The increased mean pore size for pellets prepared using commercially available β -TCP is due to the larger particle size of high temperature synthesized β -TCP in comparison to the β -TCMPs prepared in the study. An increased BET surface area was measured for β -TCMP prepared with 50% Mg in comparison to 35% Mg (Table 3.4), suggesting a decrease in particle size. As a result of the decreased particle size, a smaller mean pore size was obtained for pellets prepared using 50% Mg powders when using the same applied load. The near two-fold increase in intrusion volume for samples prepared with 50% Mg in comparison to β -TCP suggests that increased volumes of cell culture media and physiological fluids may interact with pellets prepared using 50% Mg, potentially leading to increased protein adsorption and cell attachment.

3.3.2.2 Protein Adsorption

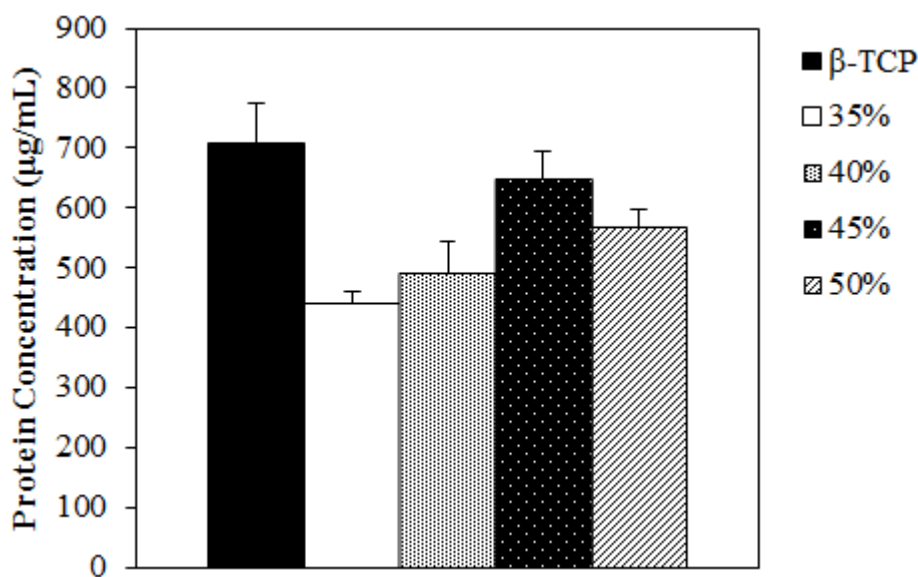


Figure 3.10 The total protein measured from scaffolds after incubation in FBS.

Protein adsorption is known to influence cell attachment and proliferation as well as the activation and inhibition of the nucleation and growth of mineral phases [153]. Material properties such as phase purity, crystallinity, composition, microstructure, surface morphology, particle size, shape, and texture have all been shown to have a strong influence on protein adsorption [154]. Heat treated scaffolds were incubated overnight in FBS and rinsed with PBS prior to immersing in a lysis buffer to collect the adsorbed proteins. The concentration of total protein in the solutions collected is illustrated in Figure 3.10. Interestingly, despite a reduced total pore volume in comparison to β -TCMP scaffolds, increased protein concentrations were measured from commercially available β -TCP. In comparing the β -TCMPs, increased protein concentrations were measured from those prepared with increased Mg^{2+} concentrations (45-50%). Similar trends observed in protein concentration were also observed using Coomassie Blue staining (Figure 3.11). While the variation of physical properties, such as porosity and total pore volume, may influence protein adsorption, it appears that the chemical properties of bulk β -TCP scaffolds facilitate increased protein adsorption, despite the near 50% lower total pore volume in comparison to 50% β -TCMP.

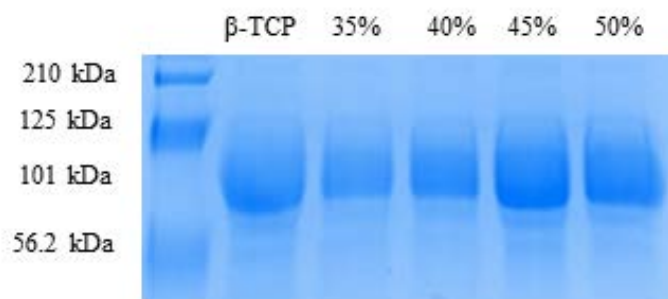


Figure 3.11 Coomassie blue staining illustrating the size distribution of proteins adsorbed to scaffold surfaces.

3.3.2.3 Cell Viability

Uniaxially pressed and heat treated β -TCMP and β -TCP pellets were sterilized by rinsing in ethanol and allowed to dry while exposed to UV. Once sterile, they were soaked overnight in culture media prior to seeding MC3T3-E1 mouse preosteoblast cells. Cell viability on these scaffolds was initially assessed using live/dead staining after 3 days of culture (Figure 3.12 a) i-iii)). A relatively high live cell density was observed on pellets prepared with commercially available β -TCP after 3 days of culture while much fewer dead cells were detected (Figure 3.12 a) i)). In comparison to β -TCP, much fewer live cells were observed on pellets prepared with 35% Mg (Figure 3.12 a) ii)). However, similar to scaffolds prepared using β -TCP, a relatively high live cell density was observed on scaffolds prepared with 50% Mg and much fewer dead cells were detected. Cell morphology after 3 days was observed using SEM (Figure 3.12 b) (i-iii)). Cells seeded on β -TCP exhibited a broad morphology whereas those on scaffolds prepared with 35% Mg appeared rather elongated (Figure 3.12 b) i-ii)). A similar broad morphology was observed on scaffolds prepared using 50% Mg in comparison to commercially available β -TCP, despite the formation of increased amorphous content (Figure 3.12 b) iii)).

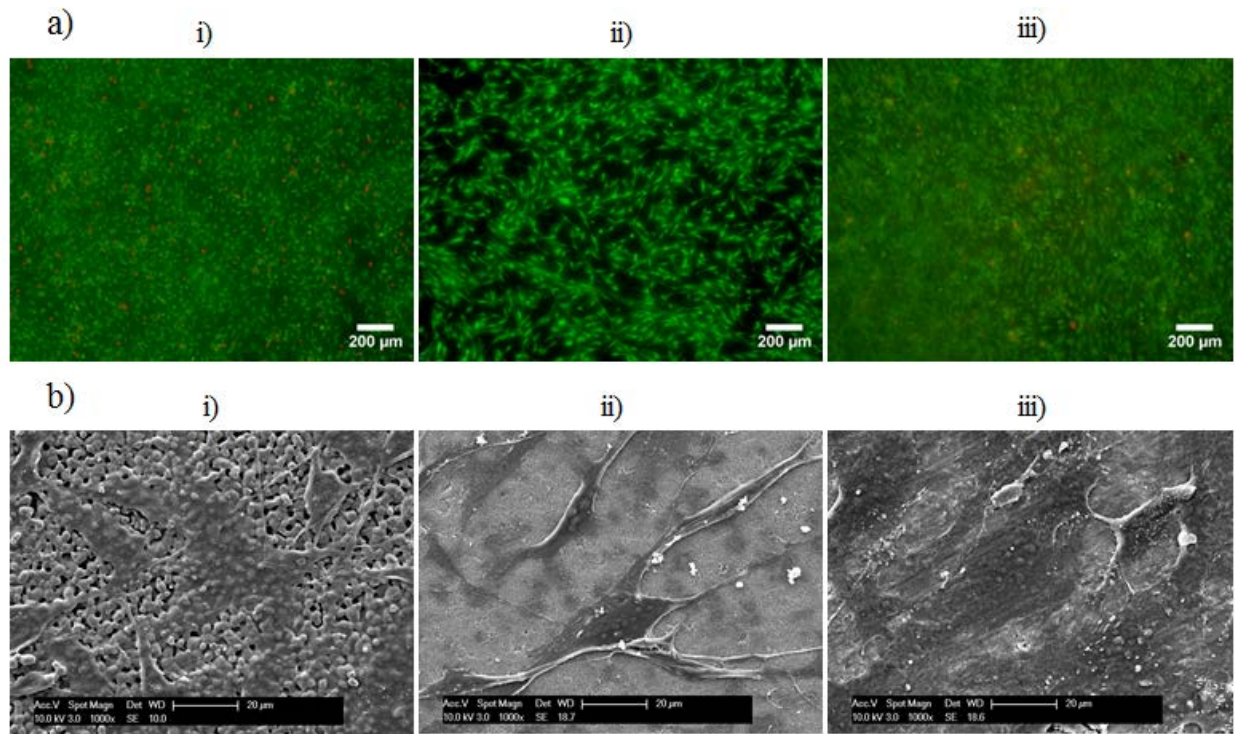


Figure 3.12 MC3T3-E1 a) live/dead staining and b) SEM images on scaffolds prepared using i) commercially available β -TCP, ii) 35% β -TCMP, and iii) 50% β -TCMP.

The MTT assay was used to quantitatively analyze cell proliferation after live dead staining confirmed that cells could indeed attach and proliferation on β -TCMPs (Figure 3.13). Initially, cells cultured on β -TCP were most proliferative. However, after 9 days those cultured on substrates prepared with 50% Mg exhibited an increased proliferation in comparison to β -TCP and all other β -TCMPs. Previous studies have found that increased concentrations of Mg^{2+} ions in cell culture media can adversely influence the MTT assay [155]. In order to compensate for any interference, substrates without cells were used as controls in this experiment. The potential increased Mg^{2+} concentrations were not observed to influence the MTT assay.

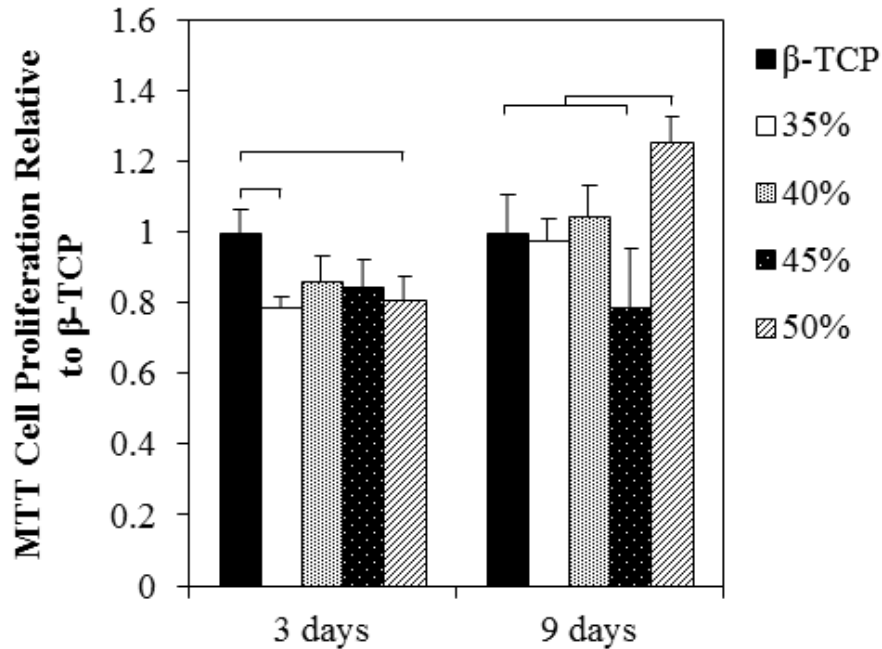


Figure 3.13 MC3T3-E1 proliferation on β -TCMP scaffolds determined using the MTT assay after 3 and 9 days of culture. A p value of < 0.05 was considered significant.

Previous studies have reported that Mg^{2+} ions act as a mitogenic factor, supporting enhancing cellular proliferation, *in vitro* [135]. Therefore, the increased proliferation observed on scaffolds prepared using β -TCMP synthesized with 50% Mg may be due to the release of increased Mg^{2+} ions into the surrounding culture media. Since a similar level of Mg^{2+} substitution in the β -TCP structure was determined by Rietveld refinement, if there is indeed an increased Mg^{2+} concentration in culture media it is most likely due to the dissolution of increased Mg^{2+} rich amorphous content. It has also previously been reported that Mg^{2+} substitution reduces the solubility of β -TCP, confirming that increased Mg^{2+} concentrations in culture media would be due to the dissolution of amorphous rather than crystalline phases [137].

3.3.2.4 Ionic Concentrations in Culture Media

The pH and ionic concentrations of cell culture media were analyzed throughout the 9 day culture period in the presence of MC3T3-E1 cells to confirm the release of increased Mg^{2+} and PO_4^{3-} ions into culture media. The pH measurements generally varied from 7.8-8.4 and were similar among most groups (Figure 3.14 a)). A more noticeable difference was observed for Ca^{2+} concentration (Figure 3.14 b)). For samples prepared with β -TCP, there was a near two-fold increase in Ca^{2+} concentration at earlier time points in comparison to media collected from β -TCMP based scaffolds. The Ca^{2+} concentration in media collected from β -TCMP pellets steadily increased throughout the experiment. After 7 days, similar Ca^{2+} concentrations were measured for both β -TCMP and β -TCP based scaffolds. Mg^{2+} and PO_4^{3-} measurements (Figure 3.14 c) and d)) exhibited quite similar trends throughout the 9 day period. In general, increased Mg^{2+} and PO_4^{3-} concentrations were measured in the media collected from samples prepared with 50% Mg throughout the 9 day experiment.

The similar trend in Mg^{2+} and PO_4^{3-} concentrations for samples prepared with elevated Mg^{2+} concentrations is likely due to the dissolution of larger amounts of Mg^{2+} rich amorphous phosphate phases, as previously described. The basal concentrations of Ca^{2+} , Mg^{2+} , and PO_4^{3-} in culture media were roughly 1.8, 0.8, and 1 mM, respectively. The sharp decrease in Ca^{2+} concentration from basal levels for β -TCMPs is most likely due to the biomimetic precipitation of CaPs from the culture media under slightly basic conditions. The gradual increase in Ca^{2+} concentration suggests that less surface modification is occurring at later time points. Therefore, it is likely that the reduced proliferation observed at earlier time points on β -TCMPs in comparison to β -TCP is due to the significant surface modification occurring and increased proliferation was observed once scaffold surfaces stabilized (Figure 3.13).

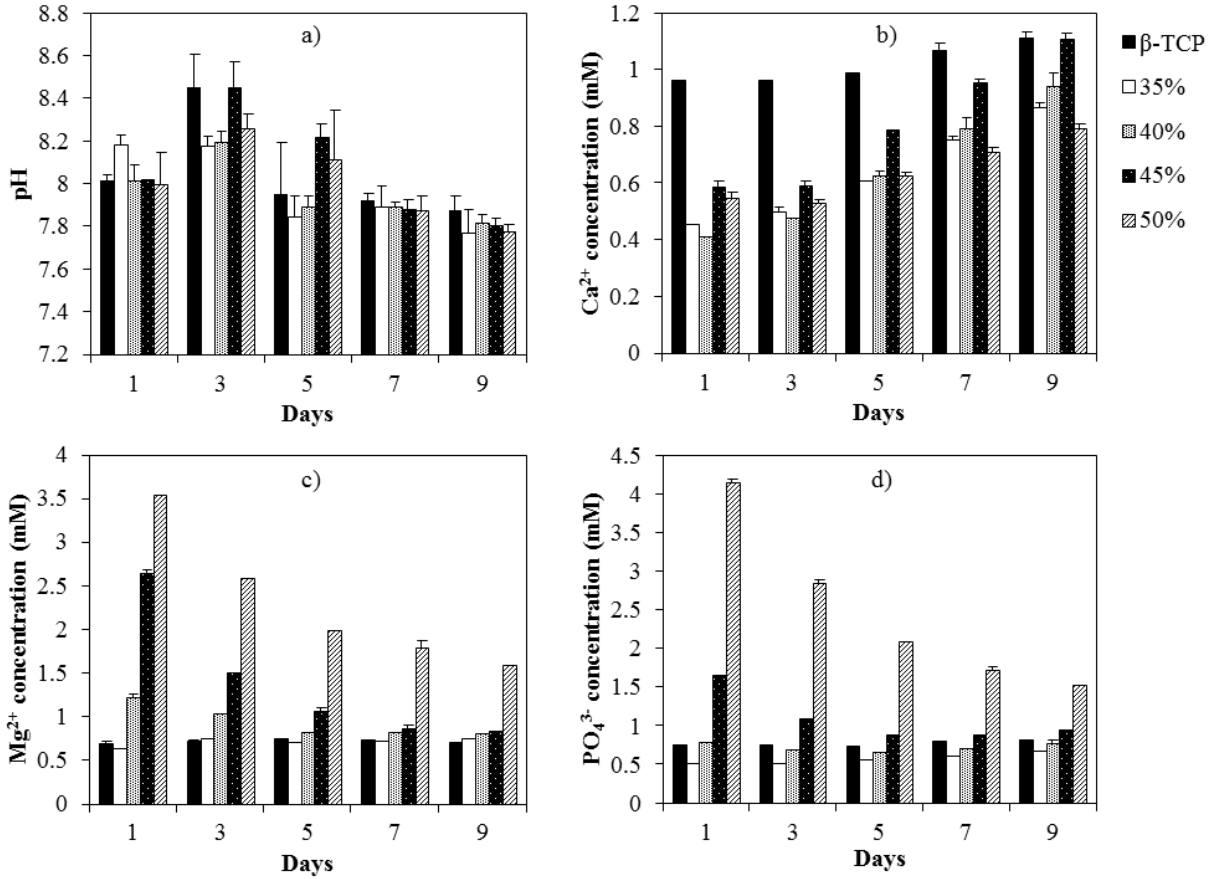


Figure 3.14 The a) pH and b) Ca²⁺, c) Mg²⁺, and d) PO₄³⁻ concentrations in cell culture media during the MC3T3-E1 proliferation experiments.

3.3.2.5 Alkaline Phosphatase Activity

β-TCP scaffolds prepared with 35-50% Mg were all shown to support at least similar levels of MC3T3-E1 proliferation in comparison to commercially available β-TCP. However, their capability to support the differentiation of MC3T3-E1 cells towards mature osteoblasts is yet to be determined. ALP is an enzyme secreted by cells during differentiation which hydrolyzes pyrophosphates, resulting in increased local PO₄³⁻ concentrations, thus promoting mineralization [95]. ALP is expressed at early stages of mineralization and can be observed both on the cell surface and matrix vesicles [156]. ALP activity was determined after 7, 14, and 21 days of

culture in osteogenic media for all conditions (Figure 3.15). After 7 days, significantly increased ALP activity was measured from cells cultured on scaffolds prepared with 50% Mg in comparison to all other groups. After 14 days, ALP activity increased for all conditions and cells cultured on samples prepared with 50% Mg once again had an elevated ALP activity. After 21 days, a slight reduction in ALP activity was observed in comparison to 14 days. However, cells cultured on scaffolds prepared with 50% Mg once again had an elevated ALP activity and a significant increase in comparison to β -TCP was observed.

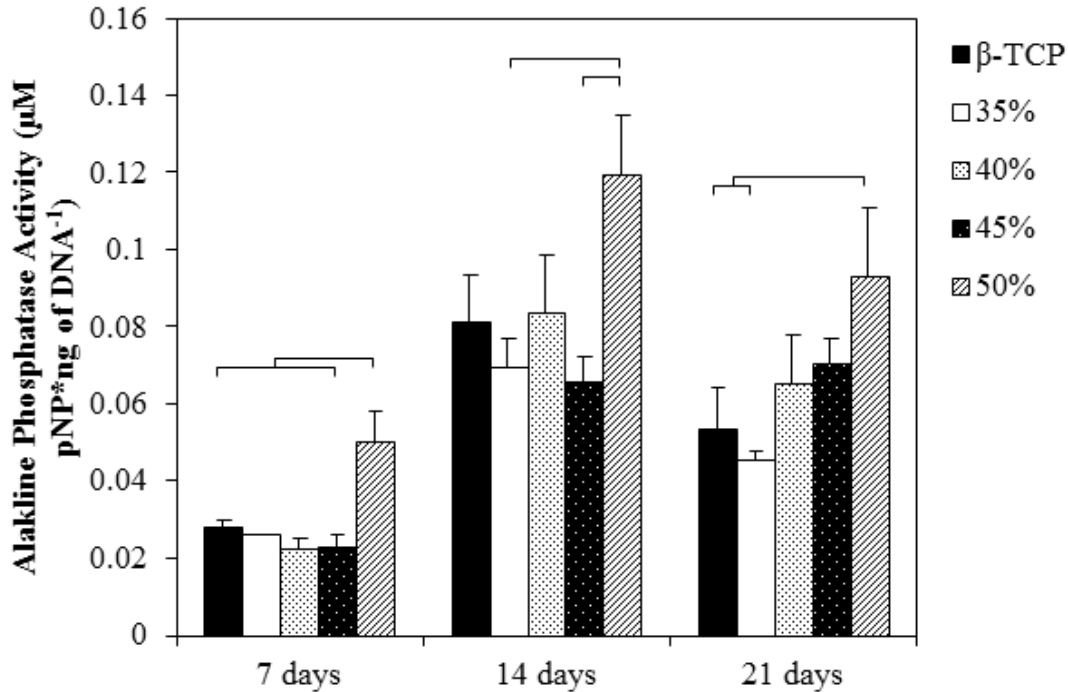


Figure 3.15 Alkaline phosphatase activity measured after 7, 14, and 21 days in osteogenic media normalized with respect to DNA concentration. A p value of < 0.05 was considered significant.

As a result of the elevated ALP activity, it appears that cells cultured on samples prepared with 50% Mg are more mature and prone to mineralize in comparison to those cultured on other β -TCMP and β -TCP substrates. However, in some cases it has been reported that Mg^{2+} ions are

capable of enhancing ALP activity and several mechanisms by which Mg^{2+} may influence ALP activity have been proposed [119]. In the current study, Mg^{2+} concentration continuously decreased throughout the culture period (Figure 3.14 c)). Therefore, if the ALP assay was indeed influenced by Mg^{2+} concentration, it was most likely to occur at earlier rather than later time points for samples prepared with 50% Mg during the dissolution of Mg^{2+} rich amorphous phases. Nonetheless, ALP activity alone cannot be used to conclude that increased osteogenic differentiation has occurred on β -TCMPs prepared with 50% in comparison to all other groups and further experiments are required.

3.3.2.6 Osteogenic Gene Expression

qRT-PCR was used to further assess the effect of Mg^{2+} substitution, phase composition, and physicochemical properties on the osteogenic differentiation of mouse preosteoblast cells. Collagen type 1 (Col-1), osteocalcin (OCN), and Runt related transcription factor 2 (Runx2) were chosen as osteoblast differentiation markers. Differentiating osteoblasts have been shown to produce Col-1 during bone formation and OCN is a mature osteoblast marker typically expressed at the end of matrix maturation [7, 18]. In contrast, Runx2 is an earlier marker for osteogenic differentiation which is down regulated during the latter stages of differentiation to support mature bone growth [141].

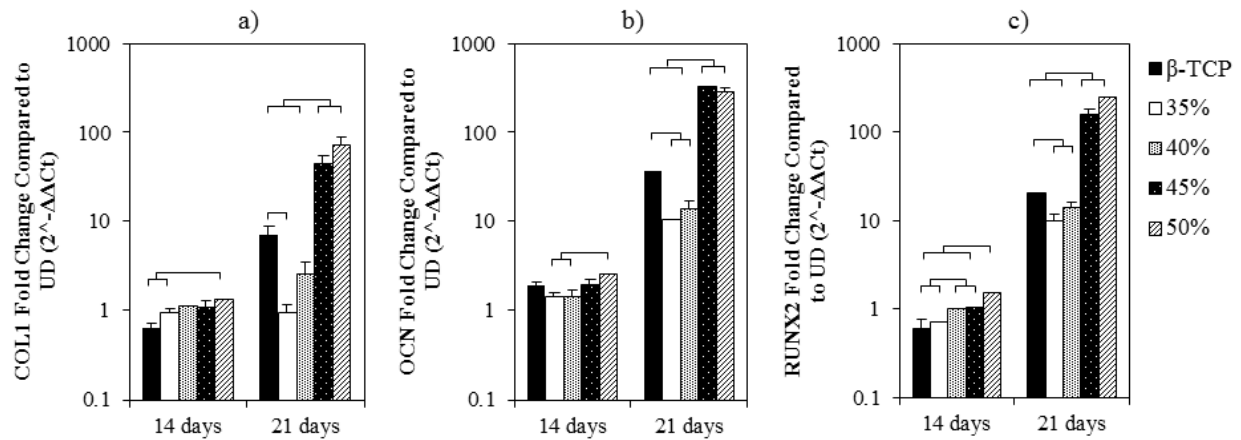


Figure 3.16 qRT-PCR gene expression of a) collagen 1, b) osteocalcin, and c) runx2 for MC3T3-E1 cells cultured on commercially available β -TCP and β -TCMP scaffolds after 14 and 21 days in osteogenic media. All conditions were normalized to undifferentiated cells. A p value of < 0.05 was considered significant.

After 14 days, cells cultured on scaffolds prepared with increased Mg^{2+} concentrations had a slightly increased expression of Col-1, OCN, and Runx2 in comparison to other groups (Figure 3.16 a-c)). After 21 days, an up regulation of all of the selected markers was observed. Similar to the observations made after 14 days, cells cultured on samples prepared with increased Mg^{2+} concentrations also had an increased expression of Col-1, OCN, and Runx2 in comparison to the other β -TCMPs. In comparison to β -TCP, cells cultured on scaffolds prepared with 35-40% Mg had a decreased expression of osteogenic genes while those cultured on scaffolds prepared with 45-50% Mg had as much as a tenfold greater expression of all three genes of interest. Based on the results obtained from qRT-PCR and the ALP assay, it can be concluded that increased osteogenic differentiation was observed for cells cultured on β -TCMP scaffolds prepared with 50% Mg in comparison to all other groups, including commercially available β -TCP.

The capability of these scaffolds prepared with increased Mg^{2+} concentrations to support the enhanced differentiation may be due to either the increased ionic concentrations in culture

media or the interaction of MC3T3-E1 cells with the scaffold surface. Differentiation was induced after 7 days using growth media supplemented with β -glycerophosphate, ascorbic acid, and dexamethasone. Although the release of Mg^{2+} and PO_4^{3-} ions constantly decreased up to 9 days, a near two fold increase in Mg^{2+} and PO_4^{3-} concentration was measured after 9 days from scaffolds prepared with 50% Mg in comparison to all other groups (Figure 3.14 c) and d)). High Mg^{2+} concentrations have previously been reported to inhibit human osteoblast differentiation *in vitro* while increased PO_4^{3-} concentrations have been reported to reduce human mesenchymal stem cell differentiation [68, 90]. However, conflicting reports on the role of Mg^{2+} on differentiation have been reported [157]. The previously mentioned variations in ionic concentrations did not seem to influence cell proliferation since increased proliferation was observed on samples prepared with 50% Mg prior to inducing differentiation (Figure 3.13). Therefore it appears that the further reduction of Mg^{2+} and PO_4^{3-} concentrations, below 1.5 mM, for samples prepared with 50% Mg after 9 days did not inhibit differentiation.

In a previous study where cationic substituted β -TCP was synthesized using a solid state approach and no amorphous content was formed, undoped β -TCP was observed to support increased Runx2 expression in comparison to β -TCMP for human osteoblasts cultured directly on scaffolds [141]. However, the opposite trend was observed in the current study. The observed differences in the current study are most likely due to the presence of amorphous phases which may influence both the ionic concentrations in culture media and the biomimetic precipitation of mineral on scaffold surfaces. In another study where MC3T3-E1 differentiation in the presence of the extracts of β -TCMP was compared to β -TCP and a biphasic mixture of β -TCMP and HA, cells cultured in β -TCP extracts were observed to express increased ALP, OCN, and TGF- β 1 in comparison to β -TCMP [86]. Although the ionic concentrations in the extracts were not reported,

the absence of amorphous content in this study suggests that Mg^{2+} and PO_4^{3-} concentrations were most likely lower than the values obtained in the current study due to the capability of Mg^{2+} to reduce the solubility of β -TCP [137]. In addition, the absence of physical contact between cells and the scaffold may also influence differentiation and further study is warranted to identify the underlying mechanisms driving osteoblast differentiation when cultured on biphasic β -TCMP scaffolds.

3.4 CONCLUSIONS

Biphasic mixtures of β -TCMP with 11-13% Mg^{2+} substitution in β -TCP and a secondary amorphous calcium magnesium phosphate phase were synthesized. Protein adsorption, cell attachment, and cell spreading on scaffolds prepared with β -TCMP were observed to increase on samples prepared with increased Mg^{2+} concentrations and were at least comparable to commercially available β -TCP. Osteogenic differentiation studies indicated that the expression of both early and mature osteogenic markers were as much as ten-fold up-regulated on scaffolds prepared with increased Mg^{2+} concentrations in comparison to scaffolds prepared using commercially available β -TCP. These results suggest that low temperature synthesis methods can be a useful technique to prepare Mg^{2+} substituted β -TCP which may more closely mimic the native structure of mineralized tissues resulting in enhanced osteogenic differentiation. However, further work is required to more accurately determine whether the chemical cues, such as the release of bioactive Mg^{2+} , Ca^{2+} , and PO_4^{3-} ions, or the physical cues, such as the ceramic microstructure, provided by the scaffolds prepared using these materials support the enhanced osteogenic differentiation observed. In addition, little is known on the signaling pathways

involved in regulating osteogenic differentiation upon exposure to β -TCP scaffolds prepared with increased Mg^{2+} concentrations. As a result, further work to understand the cellular mechanisms involved in regulating this process is required.

4.0 SYNTHESIS AND CHARACTERIZATION OF MAGNESIUM-STRONTIUM CO-SUBSTITUTED B-TRICALCIUM PHOSPHATE

4.1 INTRODUCTION

In the results presented in Chapter 3, it was observed that β -TCP prepared with 50% Mg supported enhanced differentiation in comparison to scaffolds prepared using commercially available β -TCP. In addition to Mg^{2+} , Sr^{2+} substituted CaPs have also gained significant interest, as discussed in earlier Chapters, due to the capability of Sr^{2+} to support osteoblastic differentiation while simultaneously inhibiting osteoclastogenesis [158]. Work by Yang et al. showed that enhanced *in-vitro* osteogenic differentiation was observed in human mesenchymal stem cells (hMSCs) cultured in the presence of increased Sr^{2+} concentrations through Wnt/ β -catenin signaling. Sr^{2+} substituted HA-collagen composites were also implanted into rat calvarial defects and Sr^{2+} substituted HA was shown to significantly enhance *in-vivo* bone regeneration in comparison to HA [159]. However, the release of increased amounts of Sr^{2+} may lead to rickets and renal failure [119]. Mg^{2+} - Sr^{2+} co-substituted CaPs have also been explored to further mimic native mineralized tissues [82]. Nevertheless, the majority of studies performed to date have focused only on the synthesis and characterization of these materials rather than evaluating either their *in-vitro* or *in-vivo* biocompatibility.

Although cationic substituted CaPs have been demonstrated to support osteogenic differentiation, little is known on the signaling pathways involved in regulating this process (Figure 4.1), particularly with respect to hMSCs, which are capable of differentiating to form myoblasts, adipocytes, fibroblasts, and chondrocytes, in addition to osteoblasts [160]. In order to study the role of individual ions on cell proliferation and osteogenic differentiation while avoiding the influence of scaffold surface or physical properties, several studies have been performed using culture media supplemented with various concentrations of Ca^{2+} , Mg^{2+} , Sr^{2+} , and PO_4^{3-} [124, 126, 161]. In Chapter 3, the scaffolds which supported increased differentiation also released increased concentrations of Mg^{2+} and PO_4^{3-} into the surrounding culture media. However, it is yet to be determined whether either the physical or the chemical cues provided by the scaffold supported enhanced differentiation.

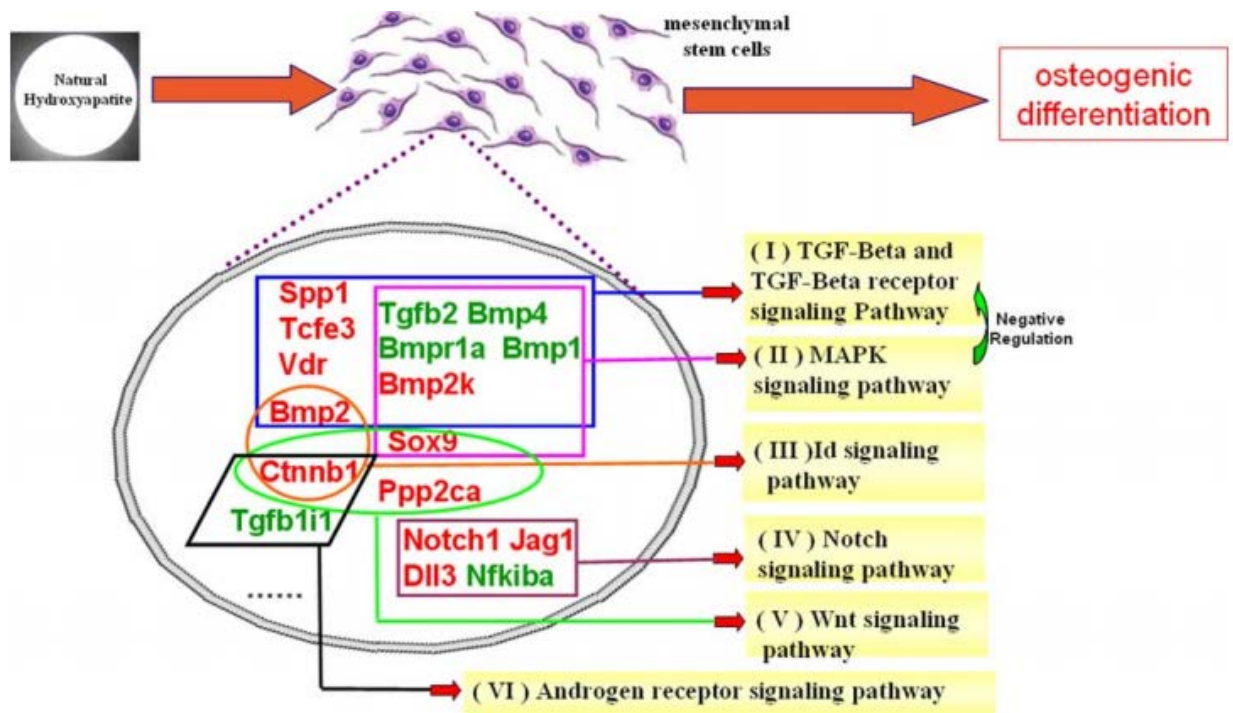


Figure 4.1 The signaling pathways involved in regulating MSC differentiation on natural hydroxyapatite scaffolds [160].

In the current Chapter, the co-substitution of Mg^{2+} and Sr^{2+} in β -TCP was studied using the simple low temperature chemical synthesis approach applied in Chapter 3 to synthesize β -TCMP of varying levels of divalent cation substitution. It was previously observed that upon increasing the Mg^{2+} concentration, increased amounts of amorphous content were formed in addition to β -TCMP. The β -TCMP prepared with a 50% $Mg/(Ca+Mg)$ ratio using this low temperature approach also supported significantly increased levels of osteogenic differentiation in a mouse preosteoblast cell line in comparison to scaffolds prepared using commercially available β -TCP. However, the roles of the chemical and physical cues provided by the scaffold were not determined and the mechanisms through which these scaffolds supported differentiation were also not studied. Therefore, in the current Chapter the influence of Mg^{2+} and Mg^{2+} - Sr^{2+} co-substitution on the phase composition, physicochemical properties, proliferation, and mechanisms through which these scaffolds support hMSC osteogenic differentiation are reported. The influence of varying scaffold composition on TGF- β and BMP signaling was also investigated.

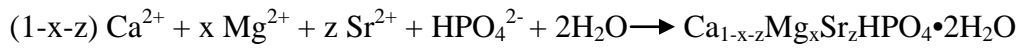
4.2 MATERIALS AND METHODS

4.2.1 Synthesis of Mg and Mg-Sr Co-Substituted β -Tricalcium Phosphate

$CaCl_2 \cdot 2H_2O$ (ACS Reagent $\geq 99.0\%$, Acros Organics), $MgCl_2 \cdot 6H_2O$ (ACS Reagent, $\geq 99.0\%$, Acros Organics), and $SrCl_2 \cdot 6H_2O$ (ACS Reagent, $\geq 99.0\%$, Sigma Aldrich) were dissolved in 100 ml of deionized water (Table 4.1). This solution was then slowly added under constant stirring to 100 ml of 0.5 M of disodium hydrogen phosphate (Na_2HPO_4 , $\geq 99.0\%$ Sigma-Aldrich) at room

temperature, during which the reaction illustrated in Equation 4.1 is believed to proceed. The mixture was stirred for 15 minutes prior to centrifuging and washing the precipitate formed with deionized water. In all cases, the (Ca+Mg+Sr)/P mole ratio was kept constant at a value of 1. The washed precipitate was then dispersed in 200 ml of deionized water and was refluxed for 2 hours. After refluxing, the powders were once again collected by centrifugation and washed with deionized water prior to drying overnight at 60°C.

Equation 4.1



Where $0.35 \leq x \leq 0.50$ and $0 \leq z \leq 0.15$

Table 4.1 Amounts of Ca^{2+} , Mg^{2+} , and Sr^{2+} containing precursors used in the precipitation of Mg and Mg-Sr doped $\text{CaHPO}_4 \cdot 2\text{H}_2\text{O}$.

Mg-Sr	CaCl₂•2H₂O (g)	MgCl₂•6H₂O (g)	SrCl₂•6H₂O (g)
35-15%	3.68	3.56	2.00
40-10%	3.68	4.07	1.33
45-5%	3.68	4.57	0.67
50%	3.68	5.08	-

4.2.2 Powder Characterization

X-ray diffraction (XRD) was performed using a Philips X-Pert PRO diffractometer employing Cu K α radiation ($\lambda=1.5406 \text{ \AA}$) with a Si-detector (X'celerator). The X-ray generator was operated at 45 kV and 40 mA at a 2θ range of 10-70° with a step size of 0.0167° and a time per step of 3s. Specific surface area was determined using multi point Brunauer Emmett Teller (BET, ASAP 2020, Micromeritics). True density was measured using helium pycnometry

(Accupyc II 1340, Micromeritics). Thermogravimetric and differential thermal analyses were performed using a Netzsch STA 409 PC DTA/TGA. Measurements were performed by heating samples in air to 1000°C at a rate of 10°C min⁻¹. Heat treatments of the as synthesized powder and pressed pellets were performed using a Lindberg box furnace (Lindberg/blue, Riverside MI). Elemental analysis was performed using inductively coupled plasma optical emission spectrometry (ICP-OES, iCAP duo 6500, Thermo Scientific). Scanning electron microscopy (SEM, Philips, XL30) and high resolution transmission electron microscopy (HRTEM, JEOL JEM-2100F with Gatan GIF-Tridiem) were used to observe particle morphology and crystallinity.

4.2.3 Scaffold Preparation

13 mm diameter β -TCMP pellets were formed by uniaxially pressing (Carver, Wabash, IN) 0.35 g of powder with an applied load of 2,500 psi. All β -TCMP pellets were heat treated to 600°C for 4 hours prior to use in any further experiments. Commercially available β -TCP (HIMED, Old Bethpage, NY, $\geq 53 \mu\text{m}$) was similarly uniaxially pressed and heat treated to 1000°C for 4 hours to be used as a control. Heat treated pellets were used for all of the subsequent experiments described.

4.2.4 Cell Culture and Maintenance

Human mesenchymal stem cells (hMSCs) obtained from the normal human bone marrow were purchased from Lonza (Lonza, Allendale, NJ) and were cultured under 37 °C, 5% CO₂, and 95% relative humidity. Cells after the third passage were used in all experiments and were cultured in

growth media containing minimum essential media α (MEM α) supplemented with 20% FBS and 1% P/S. Osteogenic differentiation was induced after 7 days of culture in growth media supplemented with 100 nM dexamethasone, 50 μ M ascorbic acid, and 10 mM β -glycerophosphate.

4.2.5 Cell Proliferation

Cell viability was assessed using the MTT assay (Vybrant MTT Cell Proliferation Assay Kit, Invitrogen, Carlsbad, CA) and live/dead staining (Invitrogen, Carlsbad, CA). Water soluble MTT is reduced to insoluble formazan crystals in living cells. Formazan is then solubilized and its concentration can be determined by measuring optical density at 570 nm. Growth media containing 12 mM MTT was added to each well and incubated for 4 hours. A 0.1 g/ml solution of sodium dodecyl sulfate in 0.01 M hydrochloric acid was then added and the samples were incubated for an additional 15 hours. Absorbance was then measured at 570 nm. For live/dead staining, at the time points of interest samples were washed with PBS and were then incubated for 30 minutes with calcein and ethidium homodimer-1 diluted in PBS. After incubation, samples were once again gently washed with PBS prior to imaging using fluorescence (Olympus CKX41).

4.2.6 Live/dead Staining

At the time points of interest samples were washed with PBS and were then incubated for 30 minutes with calcein AM and ethidium homodimer-1 diluted in PBS (Invitrogen, Live/dead

Staining Kit) at room temperature. After incubation, samples were once again gently washed with PBS prior to imaging using fluorescence (Olympus CKX41).

4.2.7 Chemical Analysis of Culture Media

The concentration of Ca^{2+} , Sr^{2+} , Mg^{2+} , and PO_4^{3-} in the culture media during the viability experiment was determined using ICP-OES. Culture media samples were collected every other day and diluted in pH 7.4 tris buffer for analysis using ICP-OES using known standards.

4.2.8 Alkaline Phosphatase Activity

hMSCs were lysed using a lysis buffer following the manufacturer's protocol (CellLytic M, Sigma Aldrich). 170 μL of 1 g L^{-1} p-nitrophenyl phosphate (pNPP) dissolved in 0.2 M tris buffer (SIGMAFAST™ p-Nitrophenyl phosphate tablets, Sigma Aldrich) was then added to 30 μL of lysate. Samples were then incubated at 37°C for one hour. The reaction was terminated by the addition of 20 μL of 0.3 N NaOH. The concentration of p-nitrophenyl (pNP) in solution after incubation was determined by measuring the absorbance at 405 nm. pNP standards were prepared by diluting pNP in 0.02 N NaOH. Alkaline phosphatase (ALP) activity was normalized with respect to total protein concentration.

4.2.9 Indirect Cell Culture

hMSCs were cultured in the presence of Mg^{2+} and Sr^{2+} substituted β -TCP pellet extracts using transwell membrane inserts. The membranes used in the study had a pore size of 0.4 μm and a

nominal pore density of 4,000,000 pores cm^{-2} (Transwell PET, Corning). Sintered dense pellets were placed on transwell inserts and hMSCs were cultured below on tissue culture plastic. The influence of extracts containing various Ca^{2+} , Mg^{2+} , Sr^{2+} , and PO_4^{3-} concentrations on the proliferation and osteogenic differentiation of hMSCs in the absence of physical contact with dense cationic substituted β -TCP pellets was also studied.

4.2.10 Osteogenic Protein Expression

Osteogenic protein expression was quantified using a MAGPIX instrument (Luminex, Austin, TX). A Human Bone Magnetic Bead Panel kit (EMD Millipore, Billerica, Ma) was used according to the manufacturer's protocols. Cell lysates were incubated overnight at 4°C with antibody conjugated magnetic beads. After incubation, the well contents were washed prior to measuring protein concentration using known standards. The intracellular expression of osteoprotegrin (OPG) and osteopontin (OPN) were determined. Measurements were conducted in triplicate for each sample and were normalized with respect to total protein concentration.

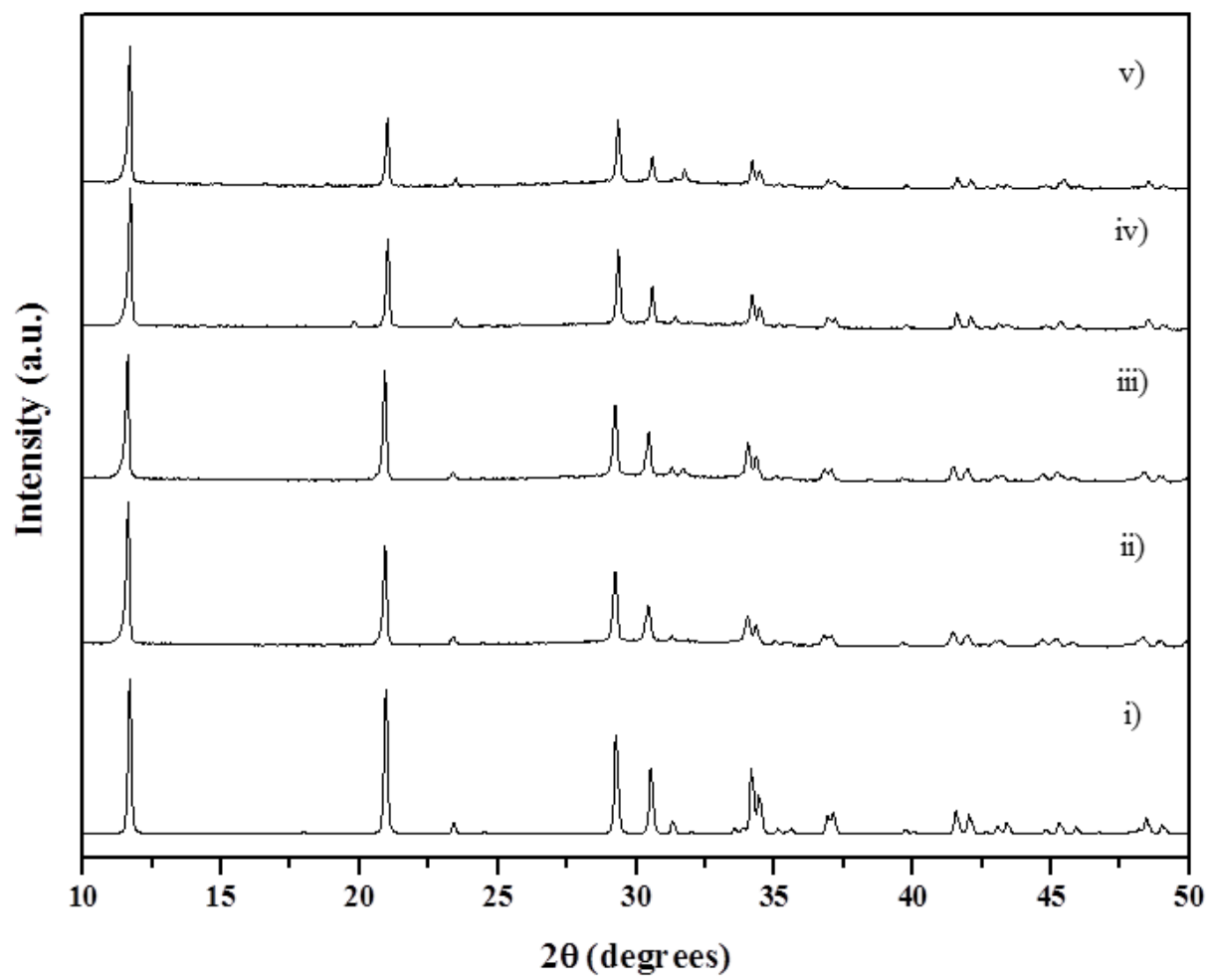


Figure 4.2 X-ray diffraction data collected from as prepared i) DCPD (JCPDS 09-0077), ii) 35-15%, iii) 40-10%, iv) 45-5%, and 50% Mg and Mg-Sr doped DCPD.

4.2.11 Transforming Growth Factor- β Signaling PCR Array

After 21 days of culture in osteogenic media directly on scaffolds prepared with varying Mg^{2+} and Sr^{2+} content, RNA was collected using a NucleoSpin RNA II kit (Macherey Nagel, Bethlehem, Pa) according to the manufacturer's protocol. RNA concentration was determined by measuring absorbance at 260 and 280 nm, respectively, using a BioRad SmartSpec spectrophotometer. Reverse transcription was performed using the RT² First Strand Kit (Qiagen, Germantown, MD). cDNA was then combined with SYBR Green (RT² SYBR Green qPCR Mastermix, Qiagen) and added to 96 well plates preloaded with primers relevant to TGF- β and BMP signaling (TGF- β /BMP Signaling Pathway PCR Array, Qiagen). The markers with cycle threshold (C_t) values of less than 30 were reported. The data collected was analyzed using software provided by the PCR Array manufacturer.

4.2.12 Statistical Analysis

All experiments were performed with a minimum of three repeats for each condition. The mean and standard error were reported. One way analysis of variance (ANOVA) was used to determine statistical significance. The Tukey-Kramer test was used for all pairwise comparisons. A p value < 0.05 was considered significant.

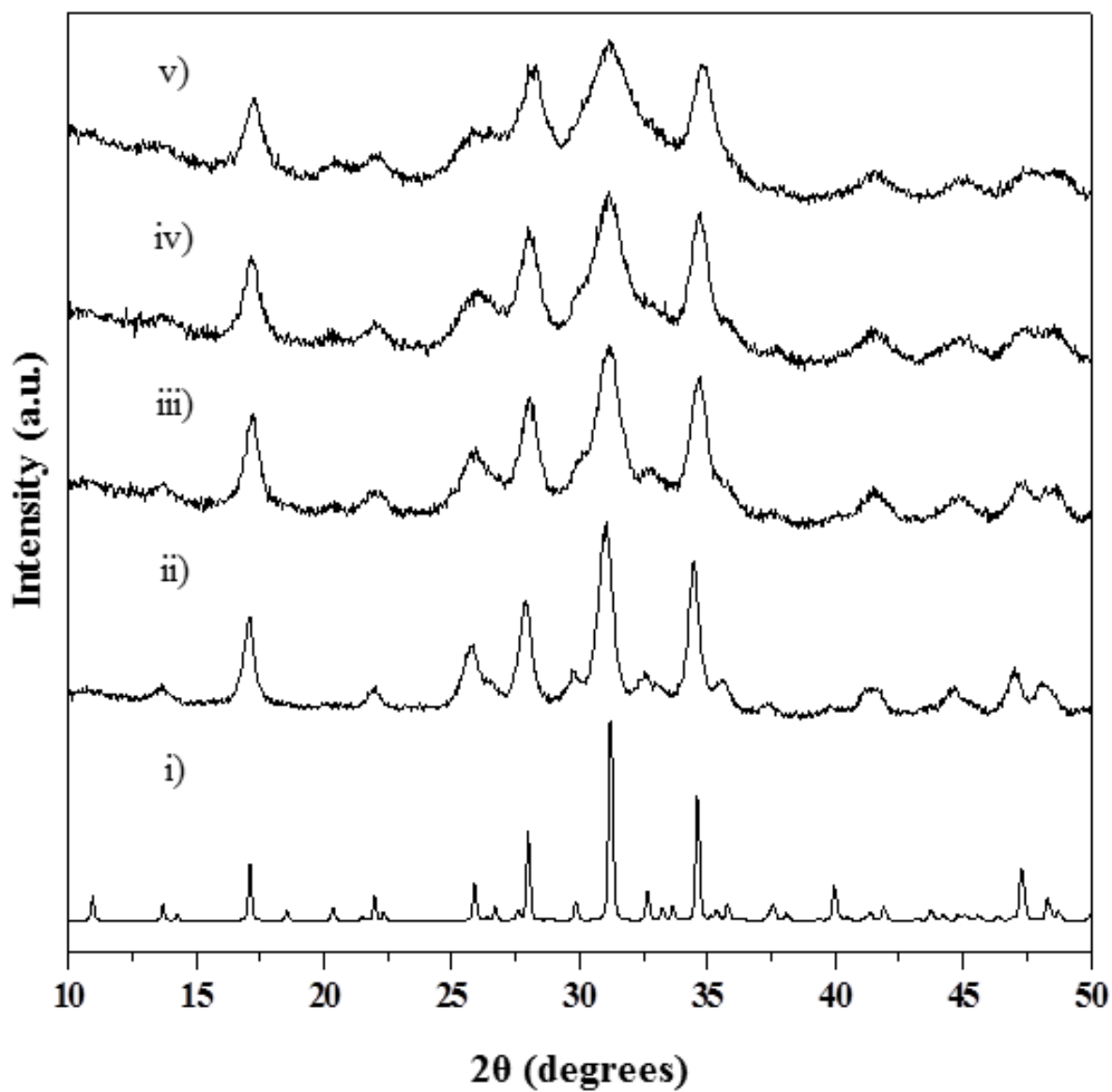


Figure 4.3 X-ray diffraction data collected from as prepared i) β -TCP (JCPDS 09-0169), ii) 35-15%, iii) 40-10%, iv) 45-5%, and 50% Mg and Mg-Sr doped β -TCP.

4.3 RESULTS AND DISCUSSION

4.3.1 Powder Characterization

4.3.1.1 Phase Composition

X-ray diffraction was used to determine the crystallinity and phase composition of the powders precipitated with varying Mg^{2+} and Sr^{2+} concentrations both after precipitating and after refluxing. After precipitating, the data collected for all of the conditions described in Table 4.1 closely resembled that of DCPD (JCPDS 09-0077) and no other crystalline phases were detected (Figure 4.2). After refluxing (Figure 4.3), the patterns observed for all compositions closely resembled that of β -TCP (JCPDS 09-0169). A slight peak shift to lower 2θ values was observed for samples prepared with increased Sr^{2+} concentrations in comparison to β -TCP (Figure 4.3 i) and ii)). The observed peak shift is likely due to an increase in lattice parameter as a result of the ionic substitution of Ca^{2+} by larger Sr^{2+} ions [82]. An increase in full width half maxima (FWHM) was also observed upon increasing Mg^{2+} concentration and reducing Sr^{2+} concentration.

Previous work has shown that the maximum amount of Mg^{2+} that can be substituted into the β -TCP crystal structure is roughly 14 mol. % [122, 134]. This is primarily due to the large difference in ionic radii between Mg^{2+} and Ca^{2+} ions [118, 162]. In contrast, although larger than Ca^{2+} , Sr^{2+} is known to have an increased solubility in β -TCP due to less of a discrepancy in ionic radii with Ca^{2+} . Previous reports have found that up to 80 atomic % Sr^{2+} can be substituted for Ca^{2+} in the β -TCP structure thereby resulting in a linear enlargement of the unit cell [163, 164]. As a result of the increase in FWHM, the presence of amorphous phases could not be confirmed

for compositions prepared with increased Mg^{2+} concentrations. However, for all conditions β -TCP was the only crystalline phase detected.

4.3.1.2 Elemental Composition

Elemental analysis was performed on the refluxed powders using ICP to determine the mol. % of Mg^{2+} and Sr^{2+} retained after precipitating, refluxing, and washing steps (Table 4.2). For all of the conditions synthesized with Sr^{2+} , the mol. % of Sr^{2+} measured after refluxing was similar to the mol. % of Sr^{2+} used in the initial precipitation step. However, the mol. % of Mg^{2+} measured using ICP was much lower than the mol. % of Mg^{2+} used during synthesis for all conditions. Interestingly, although β -TCP was the only crystalline phase detected using X-ray diffraction (Figure 4.3), the mol. % of Mg^{2+} measured in some cases exceeded the maximum amount of Mg^{2+} that can be substituted for Ca^{2+} in the β -TCP crystal structure [122, 134]. In addition, the $(Ca+Mg+Sr)/P$ ratio measured using ICP was much lower than 1.5, that of β -TCP, for all conditions.

Table 4.2 Elemental analysis of as prepared Mg and Mg-Sr doped β -TCP.

	Sr/(Ca+Mg+Sr)	Mg/(Ca+Mg+Sr)	(Ca+Mg+Sr)/P
35-15%	$19.0 \pm 0.1\%$	$12.9 \pm 0.2\%$	1.36 ± 0.01
40-10%	$13.4 \pm 0.2\%$	$17.2 \pm 0.2\%$	1.34 ± 0.01
45-5%	$7.0 \pm 0.3\%$	$22.4 \pm 2.4\%$	1.33 ± 0.01
50%	-	$27.9 \pm 1.3\%$	1.33 ± 0.02

4.3.1.3 Thermal Stability

The presence of excess Mg^{2+} and the lower than expected $(\text{Ca}+\text{Mg}+\text{Sr})/\text{P}$ ratio suggests that in addition to cationic substituted β -TCP, amorphous phases may also be formed. Therefore, thermal analysis was performed on the refluxed powders to further study the phase composition and thermal stability (Figure 4.4). A weight loss was observed for samples prepared with 50% Mg and 35-15% Mg-Sr while heating to 1000°C in air. A greater than 10% weight loss was observed for samples prepared with 50% Mg while those prepared with 35-15% Mg-Sr experienced a near 5% weight loss. In both cases, an endothermic peak near 150°C was also observed. Similar to the observed weight loss, samples prepared with 50% Mg had a more intense endothermic peak in comparison to those prepared with 35-15% Mg-Sr. The endothermic peak near 150°C is believed to correspond to the evaporation of moisture adsorbed to the surface of powder samples. The observed change in weight is also believed to be due to the evaporation of adsorbed moisture since the majority of weight loss occurred at temperatures below 200°C for both of the compositions shown.

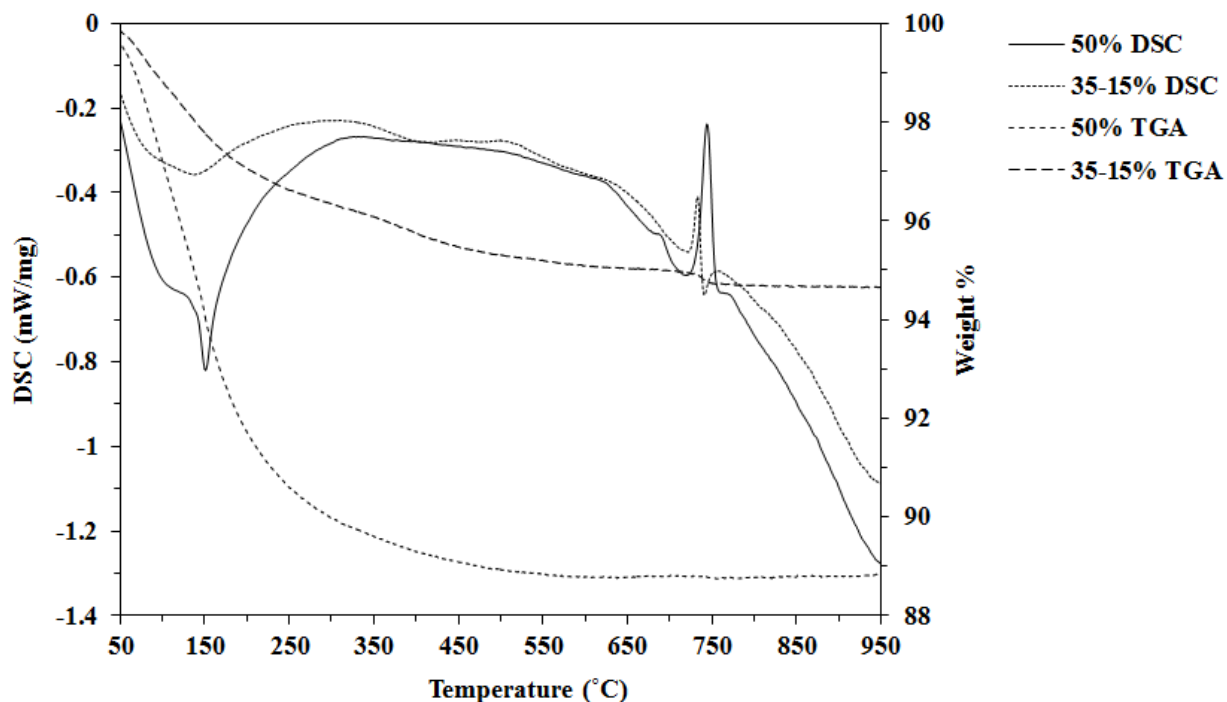


Figure 4.4 DTA-TGA data collected from samples prepared with 50% Mg and 35-15% Mg-Sr doped β -TCP while heating in air at a rate of $10^{\circ}\text{C min}^{-1}$ up to 1000°C .

At elevated temperatures, a sharp exothermic peak was observed between $700\text{-}750^{\circ}\text{C}$ in the DSC curves collected from samples prepared with 50% Mg and 35-15% Mg-Sr. Similar to the trends observed in weight loss and the intensity of the endothermic peak due to the evaporation of moisture, the intensity of the exothermic peak observed was much greater for samples prepared with 50% Mg. This exothermic peak is believed to correspond to the crystallization of an amorphous phase which was not previously detected using X-ray diffraction. The increased peak intensity for samples prepared with 50% Mg also suggests that increased amorphous content may be formed in comparison to samples prepared with 35-15% Mg-Sr. Further analysis using X-ray diffraction confirmed the formation of pyrophosphates after heat treating refluxed powders to temperatures greater than 750°C . Unconverted DCPD is known to

form calcium pyrophosphate upon heat treatment to elevated temperatures [143, 145]. However, after heat treatment to 600°C, β -TCP remained the only crystalline phase detected (Figure 4.5).

4.3.1.4 Particle Size and Density

Thermal analysis confirmed that in addition to poorly crystalline cationic substituted β -TCP, a secondary amorphous phase was formed for all of the conditions described in Table 4.1. Therefore, the presence of Sr^{2+} in addition to Mg^{2+} did not result in the formation for single phase cationic substituted β -TCP. High resolution transmission electron microscopy (HRTEM) was used to further study the crystallinity and to observe the particle size after heat treatment to 600°C (Figure 4.6). The representative low magnification image shown in Figure 4.6 a) of samples prepared using 35-15% Mg-Sr illustrates the formation of 40-50 nm particles after heat treatment. A higher magnification image with a Fast Fourier Transform Diffraction Pattern (FFT-DP) inset collected from the region marked 'X' indicates the formation of primarily crystalline material (Figure 4.6 b)). Figure 4.6 c) illustrates a similar representative low magnification image of samples prepared with 50% Mg. A slight increase in particle size after heat treatment in comparison to samples prepared with 35-15% Mg-Sr was observed. In contrast to samples prepared with 35-15% Mg-Sr, high magnification images of samples prepared using 50% Mg indicated the formation of both crystalline and amorphous material, indicated using the symbols 'X' and 'A', respectively (Figure 4.6 d)). This data confirms the formation of increased amorphous content for samples prepared with 50% Mg and suggests that these samples may have been sintered to a higher degree after heat treatment to 600°C.

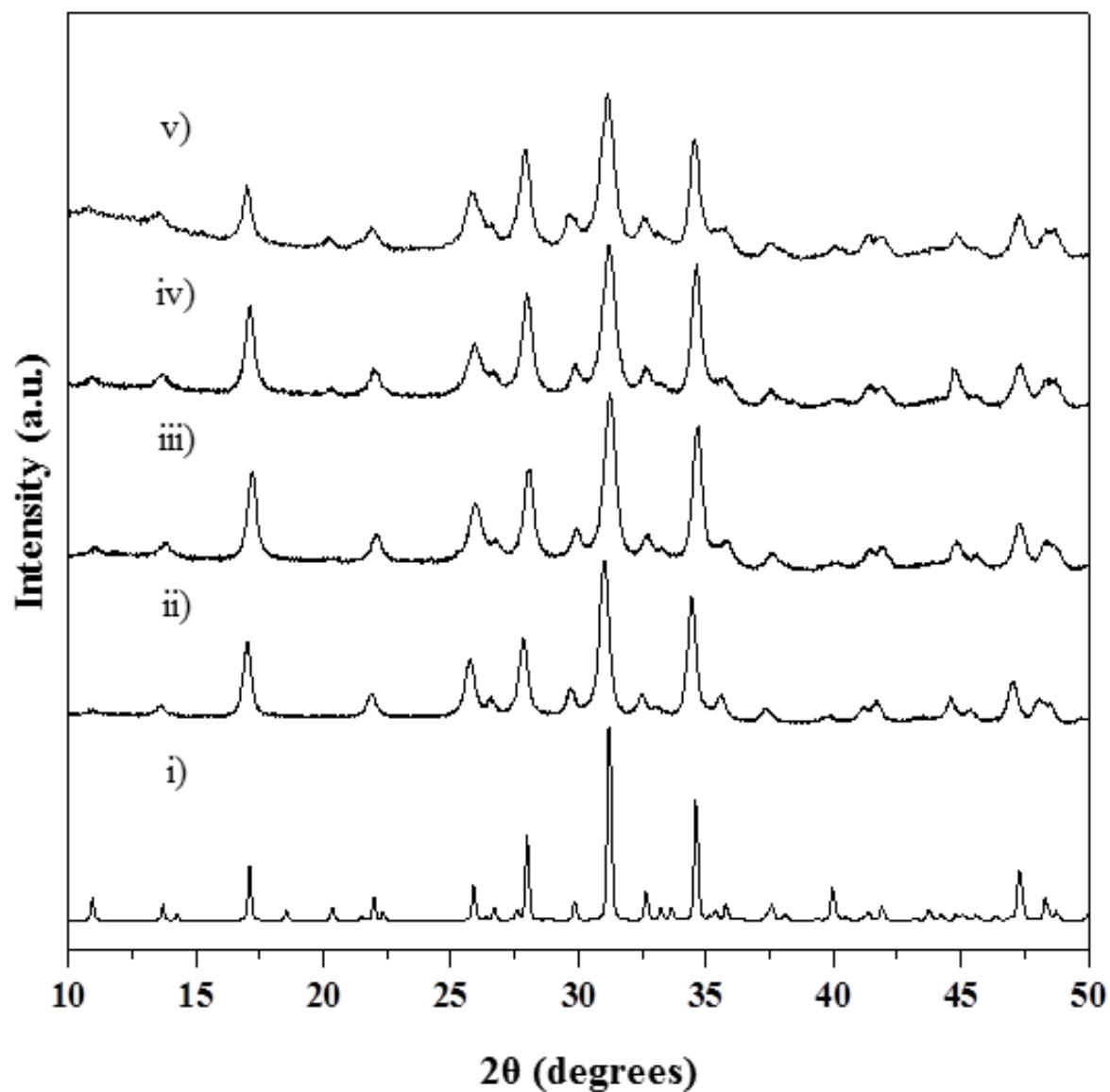


Figure 4.5 X-ray diffraction data collected from i) β -TCP (JCPDS 09-0169), ii) 35-15%, iii) 40-10%, iv) 45-5%, and v) 50% Mg and Mg-Sr β -TCP heat treated to 600°C.

BET and helium pycnometry were used to further study the influence of composition on particle size and density after precipitating, refluxing, and heat treatment (Table 4.3). After precipitating, samples prepared with increased Sr^{2+} concentrations had increased surface area. Upon refluxing, surface area further increased at least five-fold for all conditions. Samples

prepared with 50% Mg had the largest surface area after refluxing. As expected, surface area decreased after heat treatment to 600°C due to an increase in particle size. Similar to HRTEM images, BET results also indicate an increased particle size for samples prepared with 50% Mg in comparison to 35-15% Mg-Sr after sintering. The true density after heat treatment to 600°C was also measured. Increasing Sr²⁺ concentration resulted in an increase in true density while the opposite trend was observed upon increasing Mg²⁺ concentration. The reduced density observed upon increasing Mg²⁺ concentration may be due to a reduction in mass and lattice parameters as a result of smaller Mg²⁺ ions substituting for larger Ca²⁺ ions in the β-TCP crystal structure or the formation of increased amounts of an amorphous phase, previously confirmed using DSC and HRTEM (Figure 4.4 and Figure 4.6).

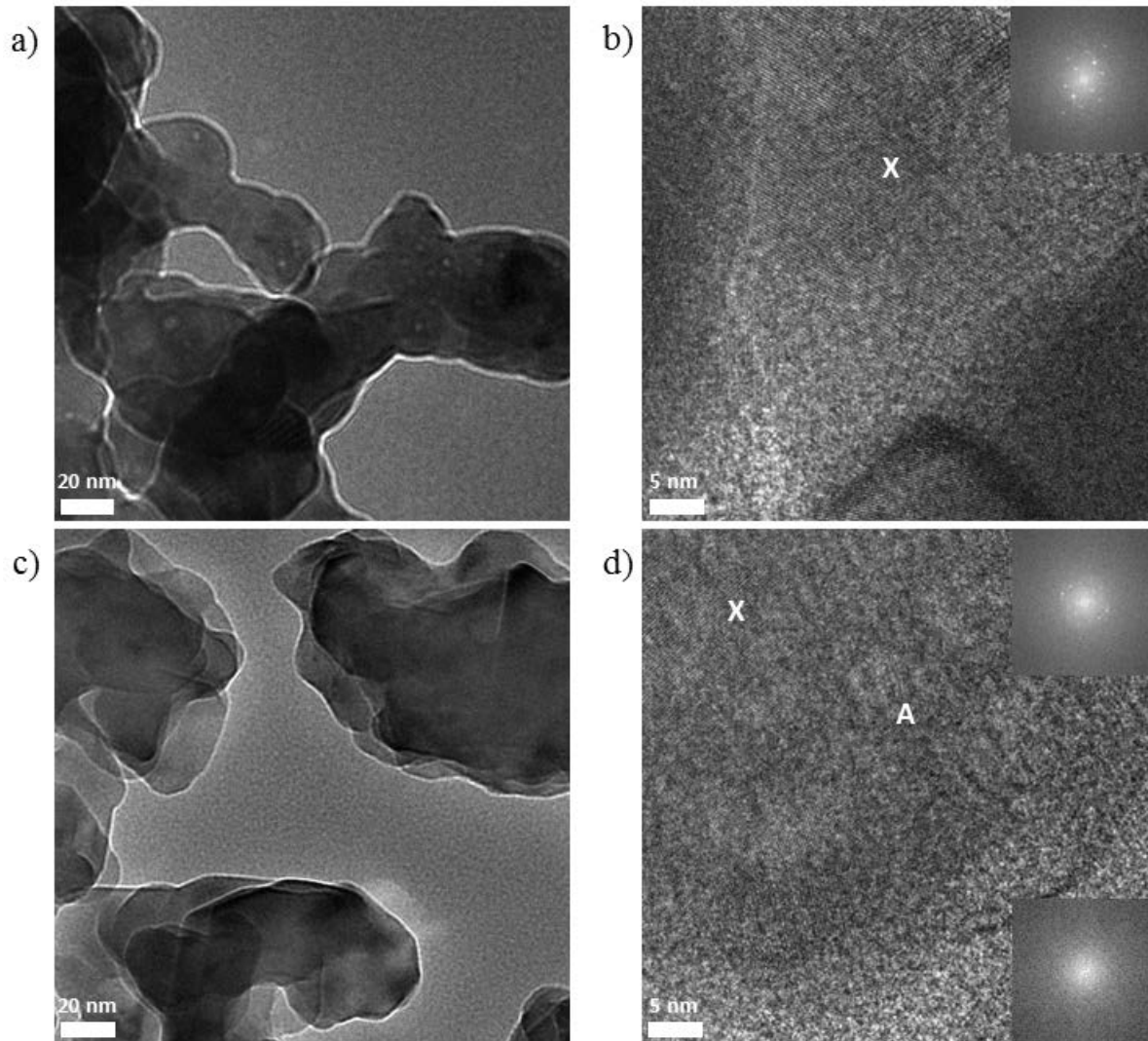


Figure 4.6 TEM images of 35-15% Mg-Sr doped β -TCP after heat treatment to 600°C at a magnification a) 6,000X and b) 40,000X and 50% Mg doped β -TCP after heat treatment to 600°C at a magnification of c) 6,000X and d) 40,000X. The crystalline and amorphous regions observed in the areas from which the Fast Fourier Transform Diffraction Patterns (FFT-DPs) were collected are illustrated using the symbols 'X' and 'A', respectively.

Table 4.3 Surface area and true density of Mg and Mg-Sr doped β -TCP after precipitating, refluxing, and heat treatment to 600°C.

	BET Surface Area after precipitating (m²/g)	BET Surface Area after Refluxing (m²/g)	BET Surface Area after Heat Treatment (m²/g)	True Density after Heat Treatment (g/cm³)
35-15%	43.37	115.20	17.98	3.28 ± 0.01
40-10%	34.68	185.09	14.12	3.21 ± 0.02
45-5%	24.29	184.11	15.96	3.14 ± 0.01
50%	28.84	207.96	9.21	3.00 ± 0.01

From this experimental data it can be concluded that biphasic mixtures of cationic substituted β -TCP and amorphous calcium phosphates were formed for all conditions. The majority of the Sr²⁺ added during synthesis was retained in the product formed after refluxing while large amounts of Mg²⁺ were lost. X-ray diffraction indicated that β -TCP remained the only crystalline phase formed after heat treatment at temperatures of up to 600°C. The differences in composition were also observed to vary the particle size and the degree of sintering. Due to the varying crystallinity and particle size, the surface properties and rate at which Ca²⁺, Mg²⁺, Sr²⁺, and PO₄³⁻ ions are released due to dissolution from cationic substituted β -TCP will vary upon exposure to physiological solutions [64, 75]. Interestingly both surface properties and ionic concentrations are known to influence cell proliferation and differentiation [124, 165]. Therefore, by varying the composition used in synthesis, β -TCP with tailored properties for improved cytocompatibility can be synthesized.

4.3.2 In-Vitro Cytocompatibility

4.3.2.1 Cell Proliferation

To evaluate the cytocompatibility of cationic substituted β -TCP, the powders formed after heat refluxing were uniaxially pressed and heat treated to 600°C in air forming dense pellets of crystalline cationic substituted β -TCP and amorphous cationic substituted calcium phosphate. The heat treated scaffolds were rinsed with ethanol and dried under ultraviolet light prior to seeding human mesenchymal stem cells (hMSCs) cells directly on their surface. hMSC proliferation on Mg^{2+} and Sr^{2+} containing scaffolds in comparison to commercially available β -TCP was assessed after 3 and 9 days using the MTT assay (Figure 4.7). After 3 days of culture, the scaffolds prepared with 35-15% Mg-Sr supported increased hMSC proliferation in comparison to other cationic substituted β -TCPs. In addition, a similar level of proliferation was observed in comparison to commercially available β -TCP. However, after 9 days similar levels of proliferation were obtained for all conditions in comparison to β -TCP.

Live/dead staining and SEM were used to observe cell morphology after 3 days of culture in growth media (Figure 4.8). hMSCs cultured on pellets prepared with 35-15% Mg-Sr had a similar live cell density in comparison to hMSCs cultured on commercially available β -TCP (Figure 4.8 a) and b)). However, a slightly increased number of dead cells were also observed on scaffolds prepared using 35-15% Mg-Sr in comparison to those cultured on β -TCP. The samples were then fixed using 2.5% glutaraldehyde and were subjected to alcohol dehydration prior to imaging using SEM (Figure 4.8 c) and d)). In both cases, hMSC morphology was broad rather than elongated and the cells were evenly dispersed throughout the surface of the substrate.

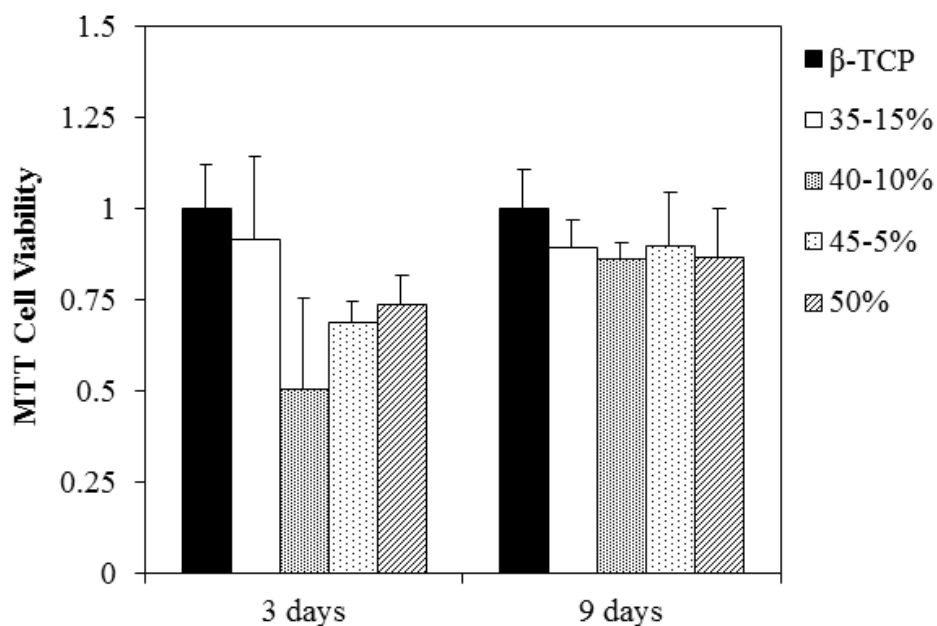


Figure 4.7 Cell viability was assessed after 3 and 9 days in growth media using the MTT assay. The data collected for all conditions was normalized to that of commercially available β -TCP.

The results obtained suggest that at earlier time points the increased Sr^{2+} and reduced Mg^{2+} content in samples prepared with 35-15% Mg-Sr β -TCP supports increased proliferation in comparison to all other conditions. In previous work studying Sr^{2+} substituted CaP cements, a similar level of hMSC proliferation was observed for cells cultured in growth media without osteogenic supplementation containing no Sr^{2+} and media containing up to 1 mM Sr^{2+} [124]. With respect to Mg^{2+} , the addition of up to 10 mM MgSO_4 resulted in a similar level of human bone marrow stromal cell (hBMSC) proliferation in both growth media and osteogenic media [126]. Therefore, hMSCs are capable of tolerating much greater Mg^{2+} rather than Sr^{2+} concentrations. However, the concentration of these ions in culture media is yet to be determined. Nonetheless, after longer periods of culture, the scaffolds prepared with both increased Mg^{2+} and Sr^{2+} concentrations were at least equally capable of supporting hMSC proliferation in comparison to commercially available β -TCP.

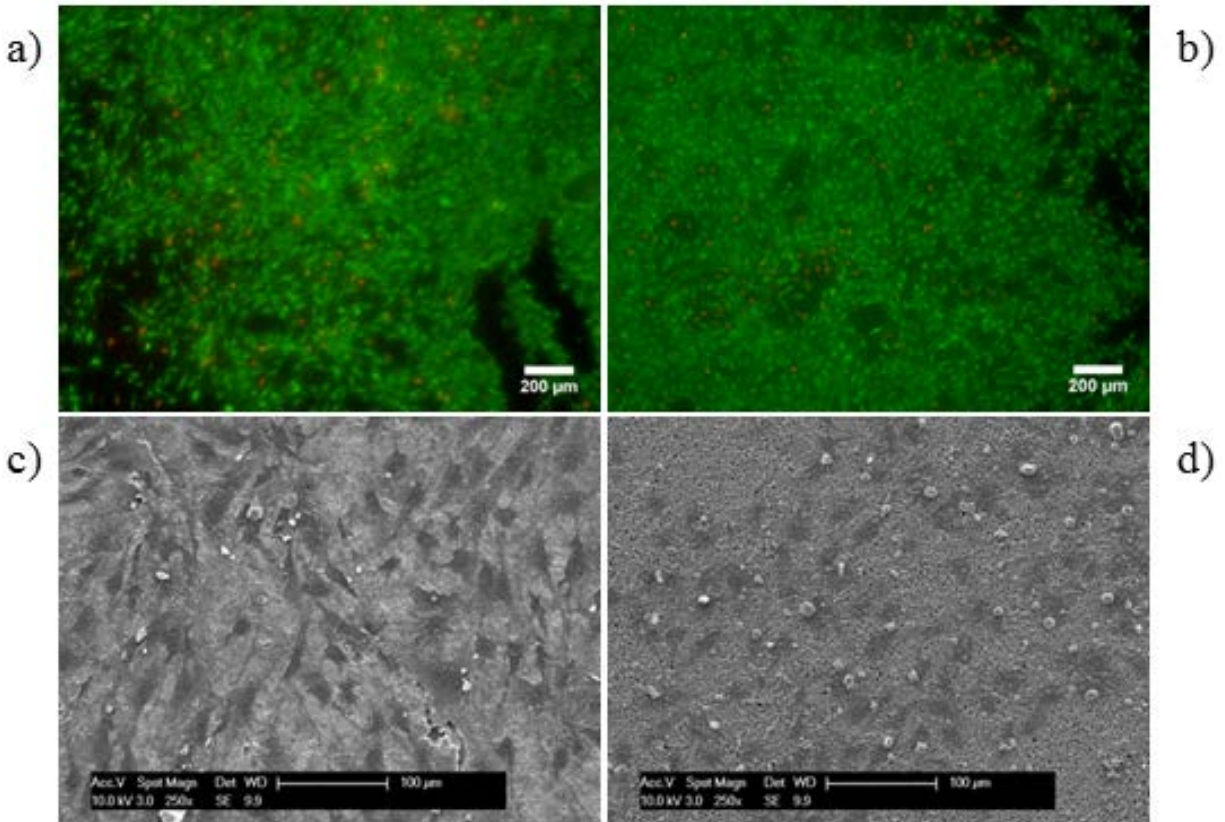


Figure 4.8 Live/dead staining of hMSCs seeded on scaffolds prepared with a) 35-15% Mg-Sr β -TCP and b) β -TCP after 3 days and SEM images of hMSCs after 3 days on samples prepared using c) 35-15% Mg-Sr β -TCP and d) β -TCP.

4.3.2.2 Chemical Analysis of Culture Media

To evaluate the role of ionic concentrations on cell proliferation, the concentrations of Sr^{2+} , Mg^{2+} , Ca^{2+} , and PO_4^{3-} in culture media were measured throughout the experiment using ICP (Figure 4.9). The culture media was collected on the days it was changed and diluted in a pH 7.4 tris-HCl buffer solution. Known standards were similarly diluted and used to generate a standard curve. The Ca^{2+} concentration measured from β -TCP scaffolds was initially increased in comparison to all other groups and remained relatively constant at approximately 1.2 mM throughout the 9 day period (Figure 4.9 a)). The Ca^{2+} concentration for all other groups gradually

increased throughout the proliferation experiment and was comparable to that of β -TCP after approximately 7 days. The measured basal concentration of Ca^{2+} in the culture media was 1.7 mM. This data suggests that a greater amount of mineral from the media was therefore deposited on cationic substituted β -TCP scaffolds at earlier time points in comparison to β -TCP. The increased surface modification at earlier time points may explain the reduced proliferation observed for most of the cationic substituted β -TCP conditions (Figure 4.7).

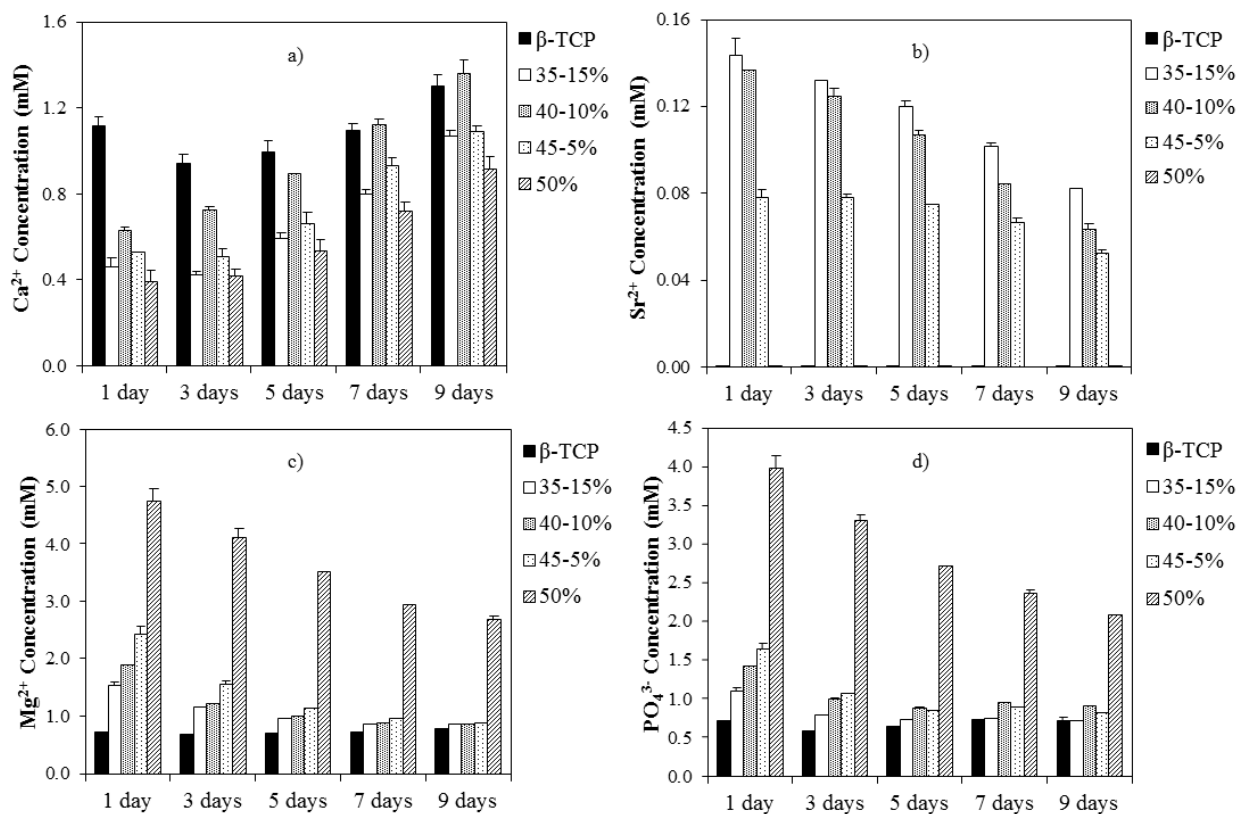


Figure 4.9 The ionic concentrations of a) Ca^{2+} , b) Sr^{2+} , c) Mg^{2+} , and d) PO_4^{3-} in culture media throughout the experiment.

Sr^{2+} concentration was observed to constantly decrease throughout the experiment (Figure 4.9 b)). Scaffolds prepared with increased amounts of Sr^{2+} also released increased

amounts of Sr^{2+} into the surrounding culture media. Based on previous reports, it can be concluded that the amount of Sr^{2+} released into the culture is non-toxic to hMSCs [124]. Similar trends in the ionic concentrations of both Mg^{2+} and PO_4^{3-} were observed throughout the experiment (Figure 4.9 c) and d)). The basal concentrations of Mg^{2+} and PO_4^{3-} in culture media were measured to be 0.8 and 0.9 mM, respectively. Increased Mg^{2+} and PO_4^{3-} concentrations were measured for samples prepared with increased Mg^{2+} concentrations. This is most likely due to the formation of increased amounts of a highly soluble Mg^{2+} rich amorphous calcium phosphate phase upon increasing the Mg^{2+} concentration during synthesis, previously confirmed using thermal analysis (Figure 4.4).

It can be concluded that the concentrations of the ions released into the culture media are non-toxic to hMSCs. However, their role of supporting the differentiation of hMSCs towards mature osteoblasts, or bone forming cells, is yet to be determined. In previous work, Sr^{2+} concentrations between 0.01 and 0.1 mM were found to support increased hMSC alkaline phosphatase expression [124]. Concentrations of Mg^{2+} between 5 and 10 mM were found support the increased formation of mineral in comparison to hMSCs cultured in basal concentrations of Mg^{2+} [126]. In addition to the increased Sr^{2+} and Mg^{2+} concentrations compared to β -TCP, increased PO_4^{3-} concentrations were also detected. Recent work studying the role of PO_4^{3-} ions on osteogenic differentiation found that growth media containing 5 mM PO_4^{3-} and no osteogenic supplementation was able to support comparable levels of OCN, a mature osteoblast marker, expression in comparison to hMSCs cultured in growth media containing osteogenic supplementation [161]. Therefore, it can be concluded that based on the reported literature the amounts of these ions released into the culture media are within the range required to support enhanced osteogenic differentiation.

4.3.2.3 Osteogenic Protein Expression

After demonstrating that CaP scaffolds prepared with varying concentrations of Mg^{2+} and Sr^{2+} were capable of supporting hMSC proliferation and showed minimal cytotoxicity in comparison to commercially available β -TCP, their capability to also support the differentiation of hMSCs towards an osteogenic lineage was studied. hMSCs were cultured for up to 7 days in growth media, allowing them to become near fully confluent. Osteogenic differentiation was then induced by culturing in media supplemented with glycerophosphate, ascorbic acid, and dexamethasone for up to 21 days. Alkaline phosphatase (ALP) activity and the intracellular expression of osteogenic proteins, such as osteopontin (OPN) and osteoprotegrin (OPG) were used to study hMSC differentiation towards mature osteoblasts.

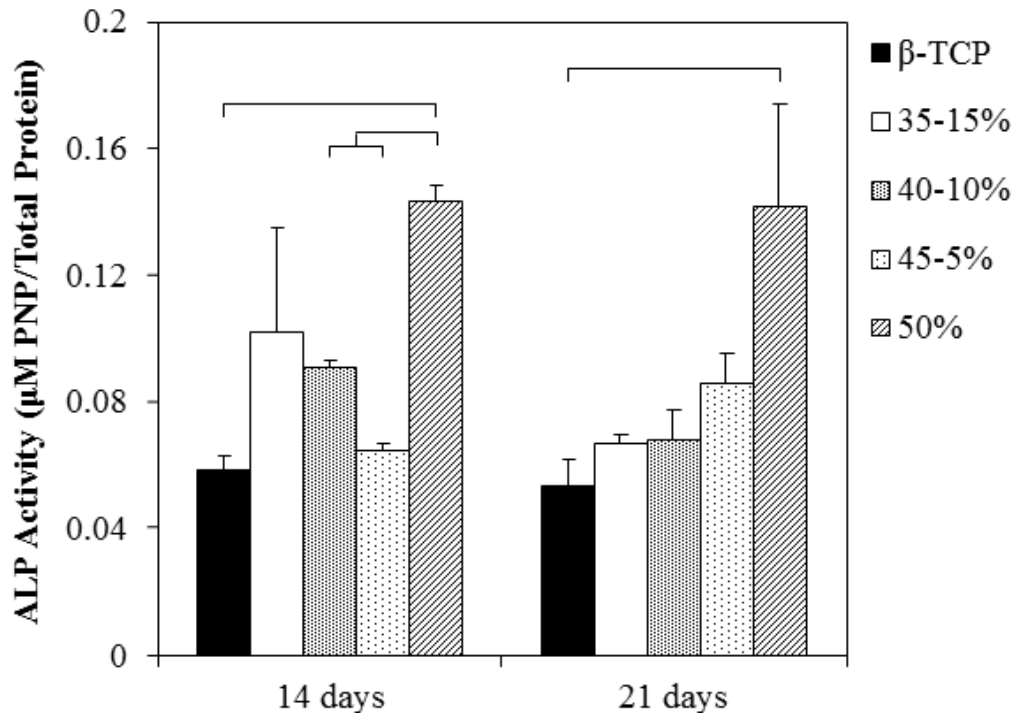


Figure 4.10 Alkaline phosphatase (ALP) activity measured from hMSCs after culturing for 14 and 21 days in osteogenic media on β -TCP prepared with various amounts of Mg and Mg-Sr. A p value of < 0.05 was considered significant.

ALP is an enzyme secreted during osteogenic differentiation which cleaves PO_4^{3-} from surrounding molecules providing the increased PO_4^{3-} concentrations necessary for osteoblast progenitor cells to mineralize their extracellular matrix [166]. ALP activity was determined after 14 and 21 days of culture in osteogenic media and was normalized with respect to total protein concentration (Figure 4.10). At both time points, hMSCs cultured on scaffolds prepared with 50% Mg and no Sr^{2+} expressed increased ALP activity in comparison to cells cultured on all Mg-Sr containing compositions. Between time points, a slight decrease in ALP activity was observed for most conditions. Interestingly, a near three-fold increase in ALP activity was observed for hMSCs cultured on samples prepared with 50% Mg in comparison to those cultured on commercially available β -TCP at both time points.

The intracellular expression of two osteogenic proteins, OPN and OPG, were also analyzed after 21 days of culture in osteogenic media using a magnetic bead kit. OPN is a secreted protein which regulates attachment to extracellular matrix thus modulating the resorption of mineralized tissues [167]. OPN is considered to be a potent inhibitor of mineralization and is expressed at the initial stages of differentiation [18]. In addition to its role in bone remodeling, elevated OPN levels have been observed during wound healing and inflammation [168]. OPG is a RANKL antagonist secreted by osteoblasts and other cell types which has been shown to inhibit the formation of osteoclasts through the RANK-RANKL-OPG signaling pathway [169]. OPG deficient knockout mice have been shown to develop osteoporosis due an increased number of osteoclasts [170]. The expression of OPN and OPG in hMSCs cultured on scaffolds prepared using β -TCP and the two conditions synthesized with the maximum concentrations of Mg^{2+} and Sr^{2+} were reported (Figure 4.11 a)).

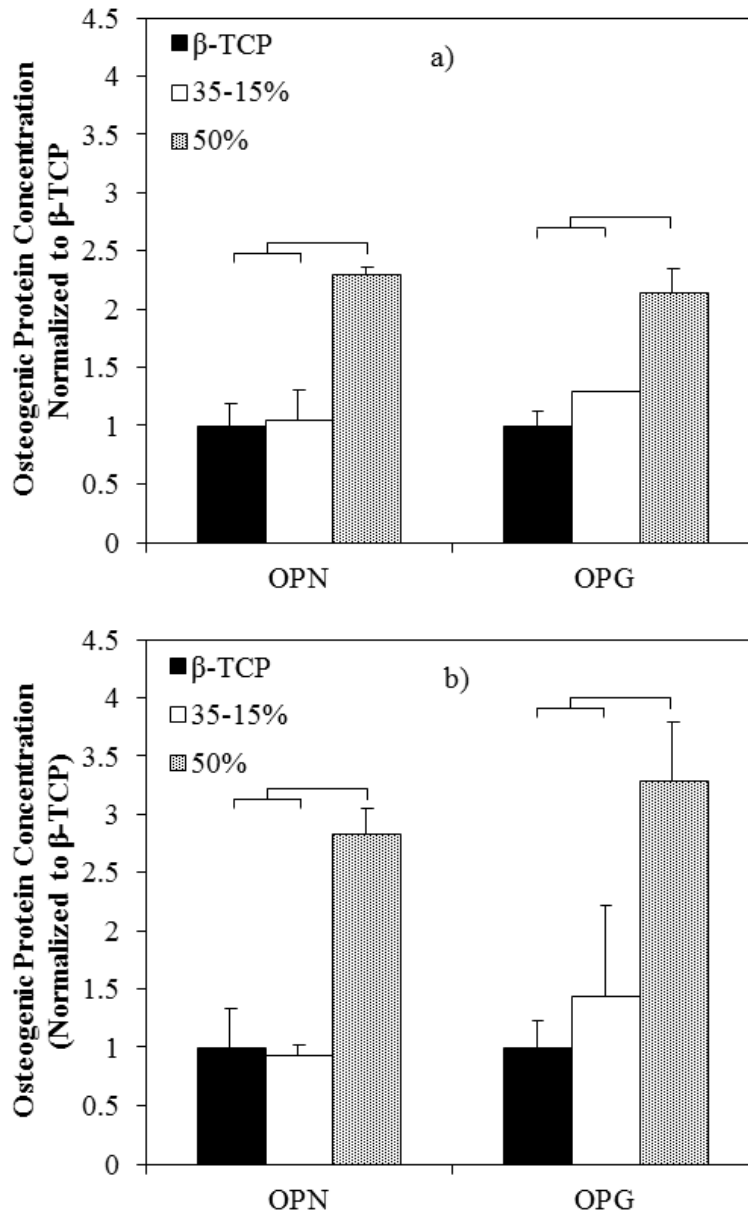


Figure 4.11 The intracellular expression of osteopontin (OPN) and osteoprotegrin (OPG) of hMSCs cultured for 21 days in osteogenic media a) directly and b) indirectly on β -TCP prepared with various amounts of Mg and Mg-Sr. A p value of < 0.05 was considered significant.

After 21 days, similar to ALP activity, the OPN and OPG expression of hMSCs cultured on samples prepared with 50% Mg was elevated in comparison to all other groups (Figure 4.11 a)). In summary, samples prepared with 50% Mg and no Sr supported increased levels of osteogenic markers in comparison to all other Mg and Mg-Sr containing compositions as well as commercially available β -TCP. Interestingly, although increased Sr^{2+} concentrations have been shown to enhance osteogenic differentiation, in the current study the incorporation of Sr^{2+} did not facilitate increased hMSC differentiation in comparison to samples prepared with 50% Mg. It has been previously shown that increasing the Mg^{2+} concentration in synthesis results in the formation of increased amorphous content [171]. While amorphous CaP phases are generally considered to be more reactive and more soluble than their crystalline counterparts, the influence of the amorphous phase on the physical and chemical cues provided by the scaffold to support osteogenic differentiation remains largely unknown.

4.3.2.4 Indirect Cell Culture

In order to study the role of the physical and chemical cues provided by cationic substituted β -TCP scaffolds prepared with varying Mg^{2+} and Sr^{2+} concentrations on supporting hMSC osteogenic differentiation independently, transwell membrane inserts were used. hMSCs were cultured on tissue culture plastic for the duration of the experiment while cationic substituted β -TCP scaffolds were suspended on permeable membranes supports. The use of transwell membranes enabled hMSCs to be exposed to Ca^{2+} , Mg^{2+} , Sr^{2+} , and PO_4^{3-} concentration profiles identical to the previous experiments while eliminating the physical contact with sintered dense CaP substrates. The intracellular expression of OPG and OPN were once again used to study hMSC differentiation after 21 days (Figure 4.11 b)). In the absence of physical contact with scaffold surfaces, similar trends in the expression of OPN and OPG were observed. Therefore,

this data suggests that the release of Mg^{2+} , Sr^{2+} , and PO_4^{3-} ions from these scaffolds plays a more influential role in providing the signaling necessary to support differentiation rather than the exposure of hMSCs to the scaffold surface.

4.3.2.5 Transforming Growth Factor- β Signaling PCR Array

In the data reported, scaffolds prepared with Mg^{2+} and no Sr^{2+} supported increased differentiation in comparison to all other conditions, including commercially available β -TCP. The capability of these scaffolds to support increased differentiation in comparison to β -TCP was determined to be due to the release of sufficient amounts of Mg^{2+} and PO_4^{3-} ions resulting in concentrations within the desired range for both ions previously reported to stimulate hMSC differentiation. To study the influence of Mg^{2+} and PO_4^{3-} on the mechanisms involved in regulating osteogenic differentiation, a TGF- β and BMP signaling PCR array was used. All three forms of TGF- β are found in bone tissue and both osteoblasts and osteoclasts are capable of synthesizing TGF- β [172]. In contrast to TGF- β s, BMPs are capable of stimulating ectopic bone formation and are expressed in multiple mineralized tissues at various stages throughout development [173]. Through the activation of TGF- β and BMP receptors, the regulatory SMADs are phosphorylated and together with SMAD4, a co-SMAD, the complex formed then translocates to the nucleus [174]. SMAD4 serves to stabilize the SMAD complex and interacts with several critical transcription factors. In addition to SMAD dependent TGF- β and BMP signaling, TGF- β and BMP proteins can also enhance differentiation through SMAD independent signaling using the mitogen activated protein kinase (MAPK) pathway [175, 176].

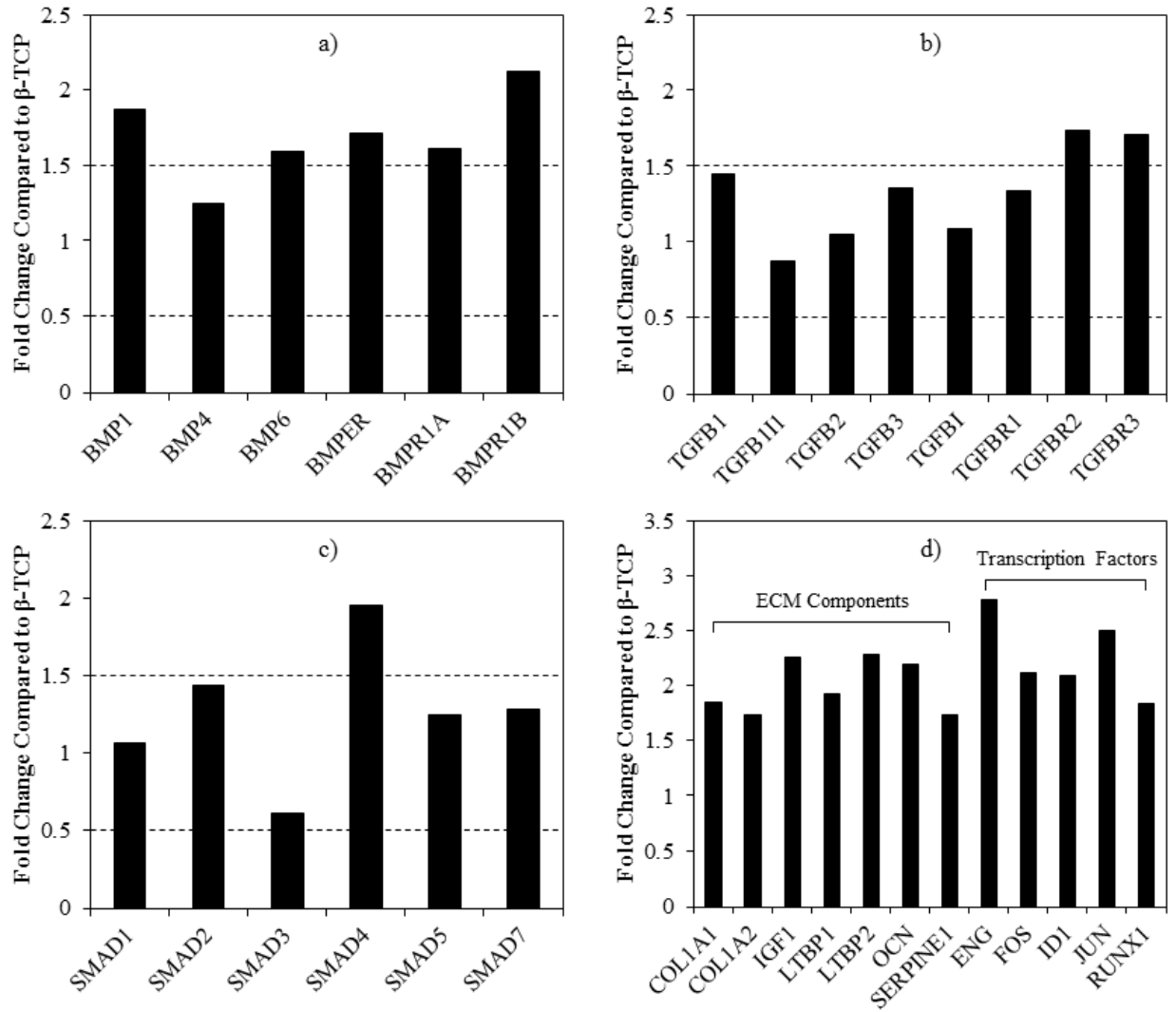


Figure 4.12 The gene expression of a) BMP and its receptors b) TGF- β and its receptors, c) SMAD proteins, and d) the ECM components and transcription factors either up or downregulated by more than 50% cultured on 50% Mg β -TCP in comparison to commercially available β -TCP. The markers with C_t values of less than 30 were reported.

RNA was collected from hMSCs cultured directly on scaffolds prepared with β -TCP and 50% Mg β -TCP after 21 days in osteogenic media. The gene expression of cells cultured on scaffolds prepared with 50% Mg β -TCP was normalized with respect to those cultured on scaffolds prepared with β -TCP. Therefore, the data was reported as fold change with respect to β -TCP. The markers with C_t values of less than 30 for both β -TCP and 50% Mg β -TCP were reported. In Figure 4.12 a) the gene expression of several BMPs and BMP receptors is illustrated. The gene expression of two of the three BMP proteins was upregulated by greater than 1.5 fold in comparison to hMSCs cultured on β -TCP while all three of the BMP receptors illustrated were upregulated by greater than 1.5 fold. The gene expression of TGF- β and its receptors is reported in Figure 4.12 b). None of the TGF- β family proteins had a gene expression greater than 1.5 fold in comparison to β -TCP while the gene expression for two of the three receptors exceeded a 1.5 fold increase. The gene expression of the SMAD proteins is illustrated in Figure 4.12 c). SMAD4, the co-SMAD, which is critical for SMAD dependent TGF- β and BMP signaling, was upregulated by greater than 1.5 fold. In Figure 4.12 d) the gene expression of the ECM components and transcription factors included in the PCR array with C_t values of less than 30 and either up or downregulated by greater than 50% are illustrated. The upregulation of several key ECM components, such as COL1A1 and OCN, once again suggests that hMSCs cultured on scaffolds prepared with 50% Mg β -TCP undergo increased levels of differentiation in comparison to those cultured on β -TCP.

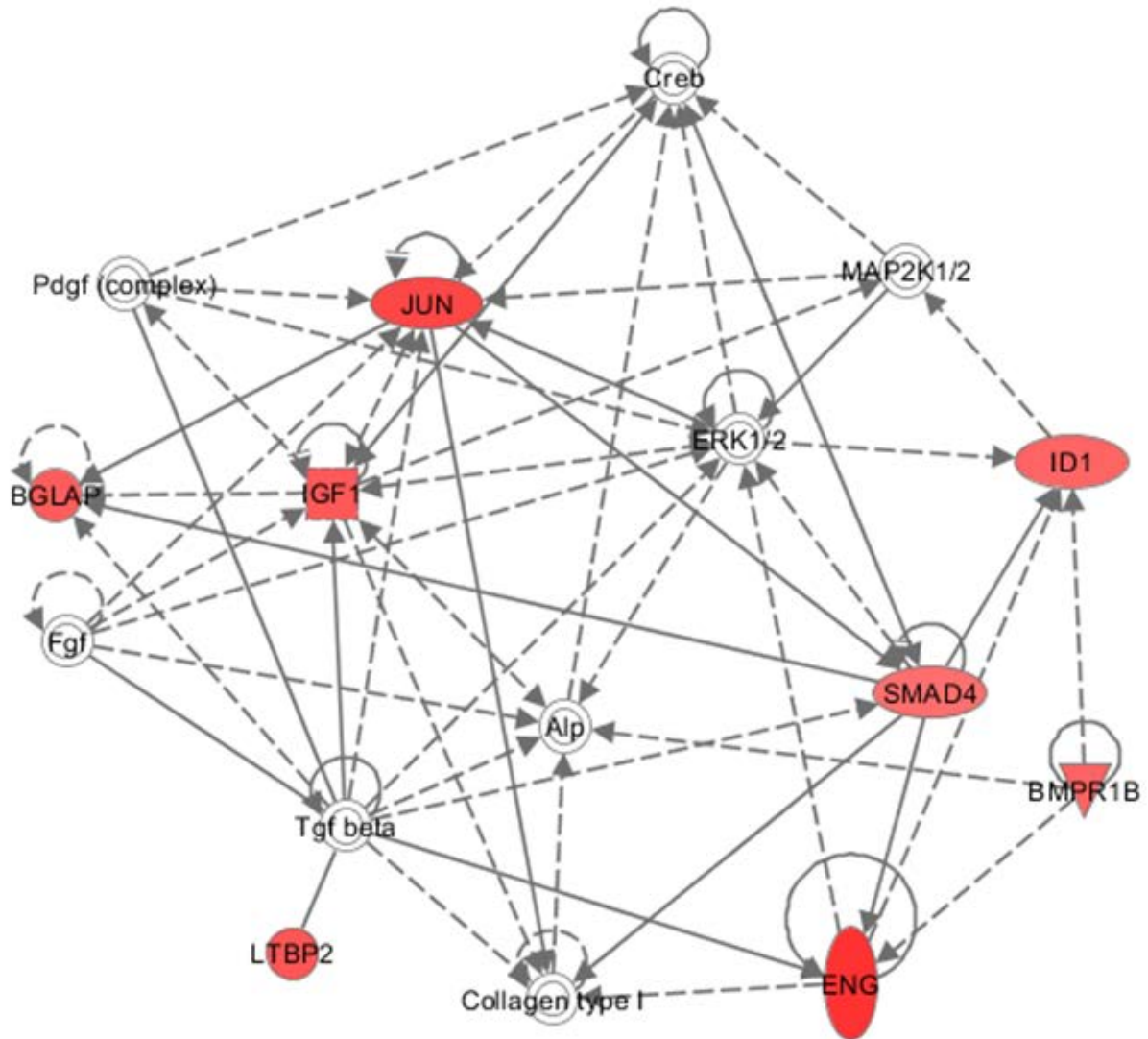


Figure 4.13 The interaction of genes in the Cellular Development network analyzed using Ingenuity Pathway Analysis. The red filled shapes correspond to the up-regulated genes while the blank ones were not found in the input list. The genes with a fold change greater than or equal to 2 in comparison to β -TCP were included in the analysis.

The greater than 50% increase in the gene expression of both TGF- β and BMP receptors and near two fold upregulation of SMAD4 suggests that hMSCs cultured on scaffolds prepared with 50% Mg β -TCP undergo osteogenic differentiation through SMAD dependent TGF- β and BMP signaling. Commercially available β -TCP, which is known for its excellent biocompatibility and has been demonstrated to possess osteoinductive properties, was used as a control [29]. Therefore, very few markers were greater than two fold upregulated in comparison to β -TCP.

A further analysis of the interaction network between the markers which were upregulated by greater than two fold in comparison to β -TCP was performed using Ingenuity Pathway Analysis (Figure 4.13). From the data illustrated, several interactions were observed between the markers upregulated by greater than two fold in comparison to β -TCP and both CREB and ERK1/2. Interestingly, in previous work studying the differentiation of human adipose derived stem cells in the presence of the extracts of a Ca, Mg, and Si containing ceramic, it was observed that ERK signaling could facilitate the enhanced differentiation observed [177]. Similar to the current work, this effect was also observed to be concentration dependent. In the current study, the increased Mg²⁺ and PO₄³⁻ ion concentrations stimulated increased levels of osteogenic differentiation. With respect to PO₄³⁻ ions, the mechanisms by which the cellular uptake of PO₄³⁻ ions are regulated and their roles in supporting osteogenic differentiation have only recently been reported [161]. However, the role of Mg²⁺ in regulating this process in the presence of PO₄³⁻ ions is yet to be determined. Therefore, further work is required to evaluate the role of the individual ions released in the current system on supporting osteogenic differentiation and to determine which of the two is more influential.

4.4 CONCLUSIONS

Biphasic mixtures of Mg^{2+} and Mg^{2+} - Sr^{2+} co-substituted β -TCP and an amorphous phase were formed using a low temperature synthesis approach for all of the conditions synthesized. All of the compositions prepared supported similar levels of hMSC proliferation in comparison to commercially available β -TCP. A significantly increased expression of osteogenic proteins, such as ALP, OPN, and OPG, was measured from hMSCs cultured directly on samples prepared with 50% Mg and no Sr^{2+} in comparison to all other groups, including those prepared with increased Sr^{2+} concentrations. In the absence of physical contact with scaffold surfaces while maintaining similar ionic concentrations to direct cell culture experiments, similar trends in the expression of osteogenic markers were also observed. Therefore, it was concluded that the release of increased amounts of Mg^{2+} and PO_4^{3-} ions from scaffolds prepared with 50% β -TCMP supported increased hMSC osteogenic differentiation rather than physical contact between hMSCs and the scaffold surface due to the material microstructure and grain boundary effects. The influence of these scaffolds, capable of releasing increased Mg^{2+} and PO_4^{3-} ions, on hMSC TGF- β and BMP signaling was evaluated using a TGF- β and BMP signaling qRT-PCR array kit. From the data collected, it was concluded that scaffolds prepared with 50% β -TCMP supported increased differentiation in comparison to commercially available β -TCP through the SMAD dependent TGF- β and BMP signaling. Further work is required to determine whether either Mg^{2+} or PO_4^{3-} ions independently or together to provide the chemical cues necessary to support enhanced differentiation and to determine whether or not the stimulation provided by these ions is a synergistic effect. In addition, the blocking of SMAD signaling may be a useful approach to determine whether or not other pathways, such as MAPK, are involved in the signaling which regulates the enhanced differentiation observed with hMSCs cultured on 50% β -TCMP.

5.0 SYNTHESIS AND CHARACTERIZATION OF AMORPHOUS CALCIUM MAGNESIUM PHOSPHATES

5.1 INTRODUCTION

The ideal concentration ranges of both Mg^{2+} and PO_4^{3-} ions to support the osteogenic differentiation of hMSCs and osteoblast progenitor cells under *in vitro* conditions have previously been determined [90, 126, 161]. In Chapter 4, it was concluded that 50% β -TCMP containing scaffolds supported increased hMSC differentiation through the release of increased amounts of bioactive ions rather than their surface characteristics. In comparing the concentration profiles obtained for the various ions of interest, increased Mg^{2+} and PO_4^{3-} ion concentrations in the culture media were observed for samples prepared using 50% β -TCMP. These increased ionic concentrations were likely due to the formation of increased amounts of a highly soluble magnesium rich amorphous calcium phosphate phase that was formed upon increasing the Mg^{2+} concentration used during the synthesis of Mg substituted β -TCP. As outlined in Chapters 3 and 4, it is clear that a large amount of amorphous content is generated when the nominal concentration of Mg is 50%. However, it was difficult to examine the amount of amorphous content present. Therefore, an attempt was made to isolate the amorphous phase formed in the biphasic system.

Amorphous calcium phosphates (ACPs) have been synthesized using a wide range of techniques in the presence of several ions, including Mg^{2+} [150]. ACPs have also been prepared with a wide range of Ca/P ratios, ranging from 1.2-2.2, under both acidic and basic conditions [104, 178]. This variation in the stoichiometric composition of ACPs also results in a wide range of solubility for the metastable phase formed. Ionic substitutions for Ca^{2+} and PO_4^{3-} ions, such as Mg^{2+} , F^- , CO_3^{2-} , and $\text{P}_2\text{O}_7^{4-}$, have also been shown to stabilize the ACP phase which readily converts to poorly crystalline HA over extended periods of time even while stored under dry conditions [179, 180]. During the aqueous synthesis of ACP, the careful control of the solution pH is often required to stabilize the amorphous phase [171]. However, simplified chemical precipitation approaches which do not require pH control have also been explored. For example, work by Lee et al. demonstrated the synthesis of ACP using multiple (Ca+Mg)/P ratios at room temperature and under a physiological pH without the need for the external control of the pH [151]. In the absence of pH control, relatively high Mg/(Ca+Mg) ratios of 20% and 30% for (Mg+Ca)/P ratios of 1.5 and 1.67, respectively, were required to stabilize the disordered amorphous phase. The biological response of the Mg substituted ACP formed was however not explored.

In the current Chapter, the synthesis of either fully amorphous or fully crystalline β -TCMP using a similar synthesis approach to that which was studied in Chapters 3 and 4 was utilized. The formation of fully amorphous 50% β -TCMP, rather than a biphasic mixture of crystalline β -TCMP and amorphous content, is hypothesized to result in an increased release rate of Mg^{2+} and PO_4^{3-} ions into the surrounding culture media upon exposure to aqueous environments. The influence of the modified release profile of these bioactive ions on the proliferation and differentiation of hMSCs towards mature osteoblasts cultured with and without

osteogenic supplementation was systematically characterized. Additionally, although previous studies have explored the capability of Mg^{2+} and PO_4^{3-} ions to support hMSC osteogenic differentiation separately, their roles when delivered simultaneously is yet to be reported. Understanding the role of Mg^{2+} and PO_4^{3-} ions when delivered simultaneously to hMSCs is of particular importance in determining the mechanisms through which magnesium and phosphate containing ceramics, bioactive glasses, and magnesium based alloys support cell proliferation and differentiation. Therefore, in the current Chapter the goal was to study the influence of the supplementation of cell culture media with a combination of Mg^{2+} and PO_4^{3-} ions particularly on hMSC cell proliferation and osteogenic differentiation was also studied.

5.2 MATERIALS AND METHODS

5.2.1 Synthesis of pH Modified β -TCMP

DCPD was precipitated with 50% Mg, as described in Chapters 3 and 4 and Equation 3.1. After precipitating and washing 50% Mg DCPD, the powders collected were dispersed in 200 ml of deionized water and boiled with reflux. While refluxing, the pH of the solution was continuously monitored throughout the two hour period using a pH meter (Beckman Coulter, Φ 350). Throughout the refluxing process, the pH was adjusted to either 4 or 8 every 15 minutes using solutions of either 1 M HCl or 1 M NaOH, as required. At the end of the two hour period, the powders formed were collected by centrifugation and washed with deionized water. After washing, they were dried overnight at 60°C prior to further use.

5.2.2 Characterization of Amorphous β -TCMP Powder

The phase composition of the powders formed after refluxing was characterized by X-ray diffraction using a Philips X-Pert PRO diffractometer employing Cu K α radiation ($\lambda=1.5406 \text{ \AA}$) with a Si-detector (X'celerator). The parameters used were similar to those described in section 4.2.2. Fourier transform infrared spectroscopy (FT-IR, Nicolet 6700 Thermo Fisher) was used to study the chemical structure of the powders formed. An average of 32 scans was reported using a spectral resolution of 4 cm^{-1} . The elemental composition of the powders formed was analyzed using inductively coupled plasma optical emission spectroscopy (ICP-OES, iCAP duo 6500 Thermo Fisher). The powder samples were dissolved in a 3% HNO₃ solution and the concentrations of Ca²⁺, Mg²⁺, and PO₄³⁻ ions in solution were determined using known standards (Sigma-Aldrich, St. Louis MO) for the ions of interest.

5.2.3 The Formation of β -TCP and β -TCMP Scaffolds

13 mm diameter pellets of amorphous β -TCMP were formed by uniaxial compression using an applied load of 2,500 psi, as previously described. The constructs formed were sintered at the appropriate temperatures for 4 h, rinsed in ethanol, and dried under UV prior to seeding cells directly on their surfaces.

5.2.4 Human Mesenchymal Stem Cell Culture and Maintenance

hMSCs isolated from human bone marrow were used in all experiments (Lonza, Allendale NJ). The cells collected after passaging twice were used. They were cultured under 37°C in 5% CO₂

and 97% humidity. The culture media consisted of MEM α containing 20% FBS and 1% P/S. For differentiation experiments, the growth media was supplemented with 100 nM dexamethasone, 50 μ M ascorbic acid, and 10 mM β -glycerophosphate. The cells were seeded directly on scaffolds using a seeding density of 30,000 cells per well.

5.2.5 Cell Proliferation

Cell proliferation was assessed using the alamarblue assay (Life Technologies, Grand Island NY). At the time points of interest, the cells were incubated in 500 μ L of the alamarblue reagent diluted in growth media, according to the manufacturer's protocol. Growth media was used to ensure that the assay was not influenced by the presence of increased Mg²⁺ and PO₄³⁻ ions or the osteogenic supplements used. After 4 hours, 100 μ L aliquots of media were removed from each well and fluorescence was measured at an excitation wavelength of 540 nm and an emission wavelength of 590 nm using a microplate reader (Synergy 2 Multi-Mode Microplate Reader, Biotek). Four repeats were performed for each condition at each time point.

5.2.6 Alkaline Phosphatase Activity

hMSC osteogenic differentiation was assessed using the ALP assay. Cell lysates were collected after 14, and 21 days in either growth media or osteogenic media. The samples were first rinsed in PBS prior to incubation on a platform shaker using the CellLytic M lysis buffer (Sigma Aldrich, St. Louis MO) at room temperature, according to the manufacturer's protocol. ALP activity was determined using the protocol described previously. Briefly, 30 μ L of cell lysate was added to 170 μ L a tris buffered solution containing pNPP. The concentration of pNP in solution

after 1 hour of incubation at 37°C was determined. The data collected was normalized with respect to the total protein concentration in the cell lysate solution, determined using the BCA assay.

5.2.7 qRT-PCR

RNA isolation was performed using a Nucleospin RNA Extraction Kit (Macherey Nagel, Bethlehem PA) according to the manufacturer’s protocol at the time points of interest. RNA concentration was measured using a spectrophotometer (BioRad, SmartSpec) by measuring the absorbance at wavelengths of 260 and 280 nm. Reverse transcription was performed using the Improm-II Reverse Transcription Kit (Promega, Madison WI). Approximately 100 ng of RNA was loaded for each reaction. The PCR reactions were then performed using the primer sequences described in Table 5.1. A SYBR green mastermix (Brilliant II, Agilent) was also used in the PCR reactions. The data collected was presented as the fold change with respect to the cells cultured on commercially available β -TCP under the same conditions.

Table 5.1 The qRT-PCR primer sequences used to determine the gene expression of GAPDH, RUNX2, collagen-1, and osteocalcin.

	Forward Primer (5'-3')	Reverse Primer (5'-3')
GAPDH	TTGTCTCCTGCGACTTCAACA	GTGGTCCAGGGTTTCTTACTCC
RUNX2	CGGCCCTCCCTGAACTCT	TGCCTGCCTGGGATCTGTA
COL-1	CAGCCGCTTCACCTACAGC	TTTTGTATTCAATCACTGTCTTGCC
OCN	CCGGGAGCAGTGTGAGCTTA	TAGATGCGTTTGTAGGCGGTC

5.2.8 Media Supplementation with Mg^{2+} and PO_4^{3-} Ions

hMSC growth media was supplemented with 5 mM Mg^{2+} , 5 mM PO_4^{3-} , or a combination of 5 mM Mg^{2+} and 5 mM PO_4^{3-} . The cells were cultured in media containing increased ionic concentrations of Mg^{2+} and PO_4^{3-} to determine the role of these ions on hMSC proliferation and osteogenic differentiation. In these experiments, the cells were seeded on tissue culture plastic. $\text{MgCl}_2 \cdot 6\text{H}_2\text{O}$ was used to supplement culture media with additional Mg^{2+} ions. A combination of Na_2HPO_4 and NaH_2PO_4 was used to supplement cell culture media with additional inorganic PO_4^{3-} ions. These salts were combined using a 4:1 ratio of Na_2HPO_4 : NaH_2PO_4 by weight to ensure the maintenance of a physiological pH. Growth media and differentiation media without additional ionic supplementation were used as controls during this experiment.

5.2.9 MTT Assay

The MTT assay (Vybrant MTT Cell Proliferation Assay Kit, Invitrogen, Carlsbad, CA) was used to analyze cell proliferation in media supplemented with various amounts of Mg^{2+} and PO_4^{3-} ions. A protocol similar to that described in Sections 3.2.8 and 4.2.5 was followed. Briefly, at the time points of interest, a 12 mM MTT solution in PBS was diluted in growth media. 110 μl of this solution was added to each well and incubated for 4 hours. After 4 hours, 100 μl of 0.1 g ml^{-1} SDS dissolved in 0.01 M HCl was added to each well. The samples were incubated overnight and absorbance was measured using a microplate reader at a wavelength of 570 nm.

5.2.10 Osteoimage Mineralization Assay

The Osteoimage Mineralization Assay (Lonza, Allendale NJ) was used to stain and quantify the amount of mineral formed by the hMSCs seeded on tissue culture plastic in the presence of various concentrations of Mg^{2+} and PO_4^{3-} ions. The cells cultured in differentiation, or osteogenic, media were used as a positive control and those cultured in growth media were used as a negative control. At the time points of interest, the cells were fixed by incubation for 10 minutes in a solution of 95% ethanol and 5% acetic acid. They were then washed with PBS and incubated in the Osteoimage staining solution for 30 minutes at room temperature, according to the manufacturer's protocol, while protected from light. After removing the staining solution and washing several times using the reagents provided, the samples were imaged using fluorescence to detect the hydroxyapatite mineral formed due to osteogenic differentiation. The amount of hydroxyapatite formed was quantified by measuring the intensity of the fluorescent signal using a microplate reader. The data was collected at an excitation wavelength of 490 nm and an emission wavelength of 520 nm.

5.2.11 Statistical Analysis

All experiments were performed with a minimum of three repeats for each condition. The mean and standard error were reported. One way analysis of variance (ANOVA) was used to determine statistical significance. The Tukey-Kramer test was used for all pairwise comparisons. A p value < 0.05 was considered significant.

5.3 RESULTS AND DISCUSSION

5.3.1 Characterization of Amorphous β -TCMP

Based on the reaction illustrated in Equation 2.3, resulting in the formation of β -TCP through the moderate temperature induced hydrolysis of DCPD without providing additional Ca^{2+} ions, H_3PO_4 is formed as a by-product. Therefore, as the reaction proceeds a reduction in pH is expected. In Figure 5.1, the pH as a function of time while refluxing is illustrated for samples prepared with 35 and 50% Mg. In both cases, as expected, a reduction in pH is observed over the two hour period. However, a substantially greater reduction in pH was observed for samples prepared with 35% Mg. This result confirms the limited conversion of Mg^{2+} containing DCPD to β -TCMP as the Mg^{2+} concentration used in the synthesis of DCPD is increased from 35% to 50% thereby resulting in the formation of increased amounts of an amorphous phase.

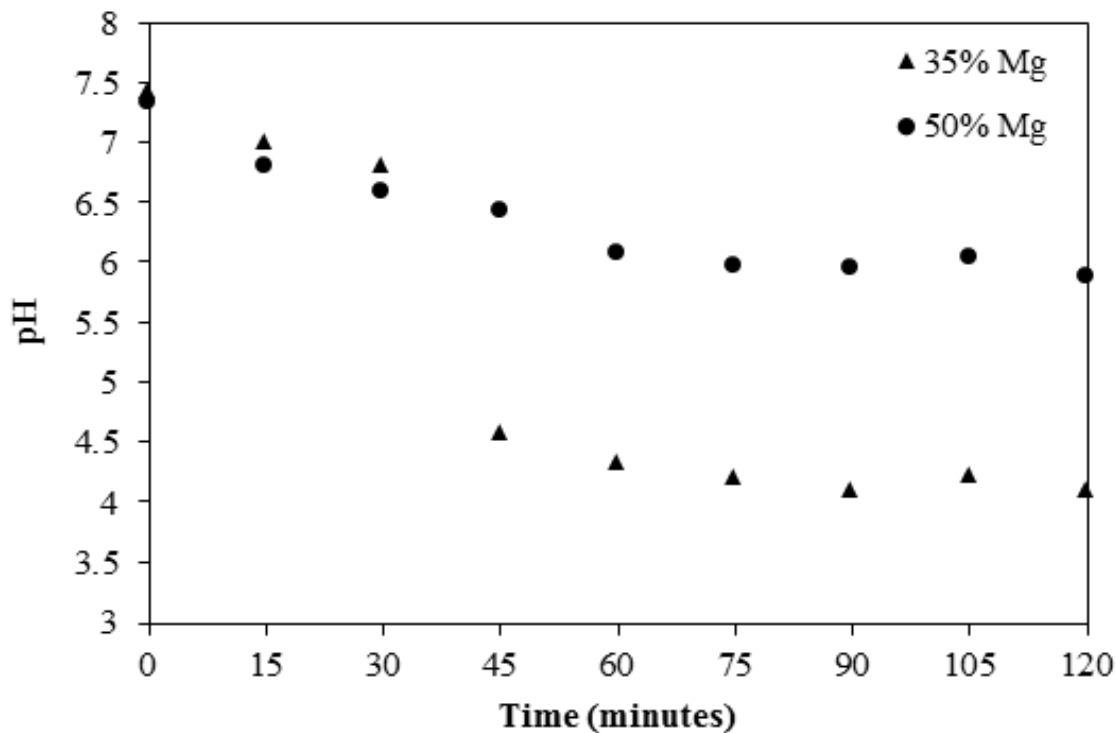


Figure 5.1 The pH with respect to time while refluxing DCPD precipitated with 35 and 50% Mg.

In an attempt to form fully amorphous or fully crystalline β -TCMP, rather than biphasic mixtures, the pH while refluxing 50% Mg DCPD was adjusted. It was hypothesized that the consumption of the H_3PO_4 , formed as an undesired by-product, would result in the formation of increased amounts of crystalline β -TCMP rather than mixtures of β -TCMP and an amorphous phase. The X-ray diffraction spectra collected from 50% Mg DCPD refluxed under both acidic and basic conditions are illustrated in Figure 5.2. The reference X-ray diffraction reference spectra for β -TCP (JCPDS 09-0169) is illustrated in Figure 5.2 i). In Figure 5.2 ii), the X-ray diffraction data collected after refluxing DCPD prepared with 50% Mg at a pH of 4 is illustrated. In comparison to the data collected without pH modification (Figure 5.2 iii)), a reduction in FWHM is observed upon reducing the pH while refluxing. Upon maintaining the pH at a value

of 8 while refluxing, the crystalline peaks indicative of the formation of β -TCP were no longer detected and a fully amorphous material was formed (Figure 5.2 iv)).

The reduction in FWHM upon reducing the pH while refluxing suggests that more crystalline β -TCP has been formed in comparison to when the pH is not modified or when a basic pH is maintained. Due to the capability of Mg^{2+} ions to reduce the crystallinity of calcium phosphates, this data may also suggest that less Mg^{2+} is retained in the β -TCP crystals formed under acidic conditions [181, 182]. Interestingly, upon increasing the pH to a value of 8 a fully amorphous product is formed. This data suggests that, although the excess H_3PO_4 formed as a result of the hydrolysis of DCPD was consumed by the NaOH added to maintain the pH, such basic conditions may also disrupt the stability of the crystalline β -TCMP formed [137]. In addition, increased amounts of Mg^{2+} ions may be retained in the structure while refluxing at a basic pH resulting in the stabilization of the amorphous phase.

ICP-OES was used to analyze the influence of pH modification on the elemental composition of the powders formed before and after refluxing (Table 5.2). Despite synthesizing DCPD with a 50% $\text{Mg}/(\text{Ca}+\text{Mg})$ ratio, a substantial loss of Mg^{2+} ions was observed as a value of approximately 34% was measured. In addition, the $(\text{Ca}+\text{Mg})/\text{P}$ ratio used during synthesis was maintained at a value of 1, corresponding to that of pure DCPD. However, a value of 1.23 was measured. The increased $(\text{Ca}+\text{Mg})/\text{P}$ ratio suggests that in addition to the crystalline DCPD formed during precipitation with 50% Mg, illustrated in Figure 3.1 and Figure 4.2, HPO_4^{2-} ions are lost and an amorphous phase is also formed. The increased $(\text{Ca}+\text{Mg})/\text{P}$ ratio in comparison to that expected for DCPD also suggests that the amorphous phase is composed of PO_4^{3-} ions rather than HPO_4^{2-} ions.

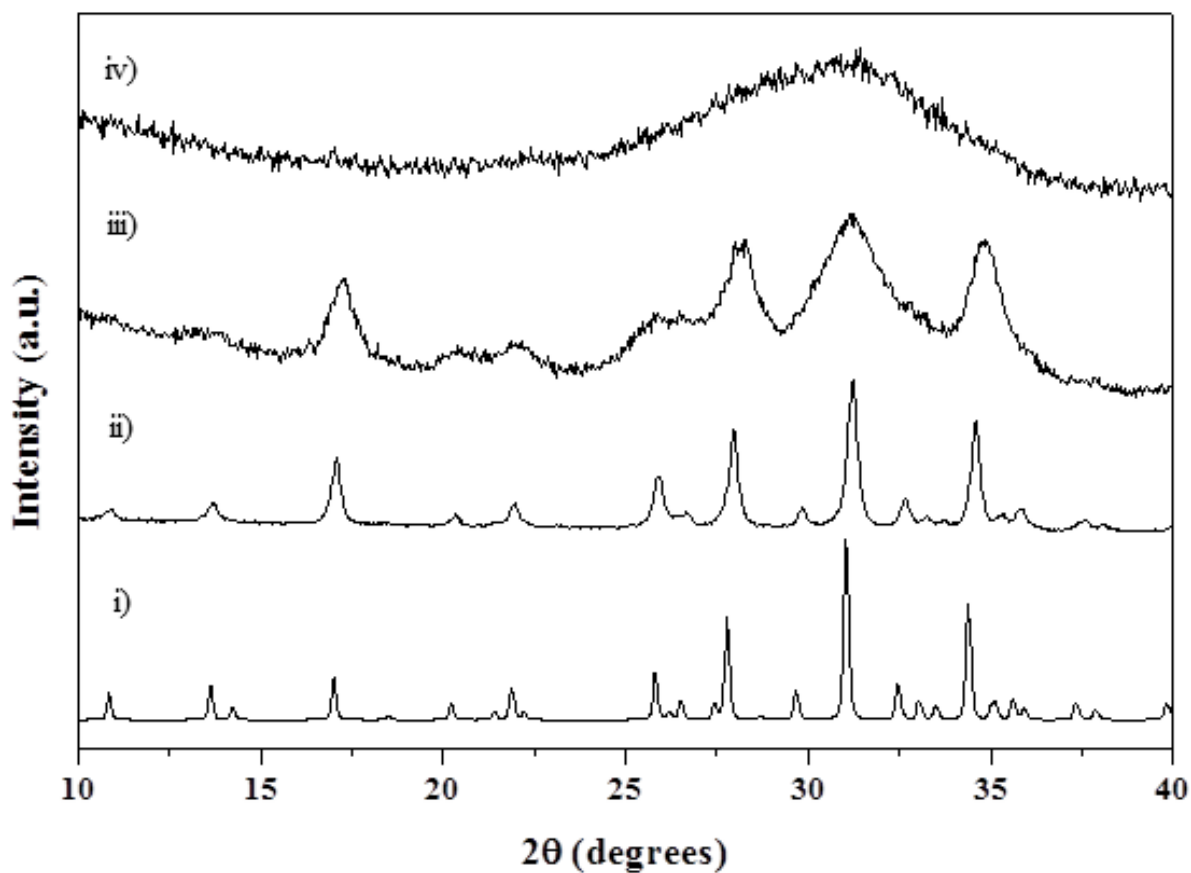


Figure 5.2 X-ray diffraction data collected from i) β -TCP (JCPDS 09-0169), 50% Mg DCPD refluxed at ii) a pH of 4, iii) with no pH modification, and iv) a pH of 8.

Table 5.2 The elemental composition of 50% Mg DCPD and the powders collected after refluxing 50% Mg DCPD at a pH of 4, without pH modification, and at a pH of 8.

	Mol. % Ca	Mol. % Mg	Mol. % P	Mg/(Ca+Mg)	(Ca+Mg)/P
50% Mg DCPD	43.9	22.9	54.2	34.3	1.23
pH 4	51.2	6.6	42.2	11.3	1.37
No Modification	41.2	16.0	42.8	27.9	1.34
pH 8	37.5	20.3	42.2	35.1	1.37

Upon refluxing the Mg^{2+} containing amorphous-crystalline DCPD mixture and increasing the solution pH, the mol. % of Ca steadily decreased while that of Mg increased. Despite the variations in cationic composition, the mol. % of P and the (Ca+Mg)/P ratio remained relatively constant for all three conditions after refluxing with or without pH modification. These results suggest that the amorphous PO_4^{3-} phase formed prior to refluxing is Mg^{2+} rich and is lost due to dissolution upon reducing the solution pH while refluxing. Upon increasing the solution pH, this magnesium rich amorphous phase is retained in the powders formed and provides the increased Mg^{2+} concentration necessary to stabilize a fully amorphous product under basic conditions.

FT-IR was performed to analyze the chemical composition of the biphasic mixtures of crystalline and Mg^{2+} rich amorphous content, determined using ICP, formed after refluxing since X-ray diffraction could not be used to characterize the amorphous phase. The spectra collected for commercially available β -TCP and 50% Mg DCPD refluxed either without pH modification or at a pH of 8 are illustrated in Figure 5.3. In general, the spectra collected for 50% β -TCMP, prepared either without pH modification or under basic conditions, closely resembled that of commercially available β -TCP. The characteristic PO_4^{3-} vibrational modes at approximately 500 and 1000 cm^{-1} were observed for all samples [81, 151]. However, in comparison to commercially available β -TCP, these peaks were relatively diffuse. The reduced resolution of these peaks is

most likely due to the distortion of the Ca^{2+} and PO_4^{3-} vibrations upon increasing the Mg^{2+} content, previously confirmed using ICP.

In addition to the similar peaks observed in comparison to β -TCP, several additional peaks were also detected. For both 50% β -TCMP conditions, a broad peak between 3500-3000 cm^{-1} was observed. This peak is due to the presence of H_2O , either bound to the surface of the powder particles or incorporated into the structure of the phosphate phases formed after refluxing [183]. Additional peaks near 850 and 1700 cm^{-1} were also observed for both 50% β -TCMP conditions and were not detected for commercially available β -TCP. These peaks are characteristic of the presence of HPO_4^{2-} in addition to PO_4^{3-} groups [184, 185]. Based on the $(\text{Ca}+\text{Mg})/\text{P}$ ratios measured after refluxing, it is not surprising that HPO_4^{2-} was detected in addition to PO_4^{3-} . Despite the quite different X-ray diffraction spectra obtained for samples refluxed with no pH modification and those refluxed at a pH of 8, similar FT-IR patterns were observed for both of these conditions. Therefore, it can be concluded that the amorphous phase formed after refluxing 50% Mg DCPD at a pH of 8 closely resembles the structure of β -TCP rather than DCPD.

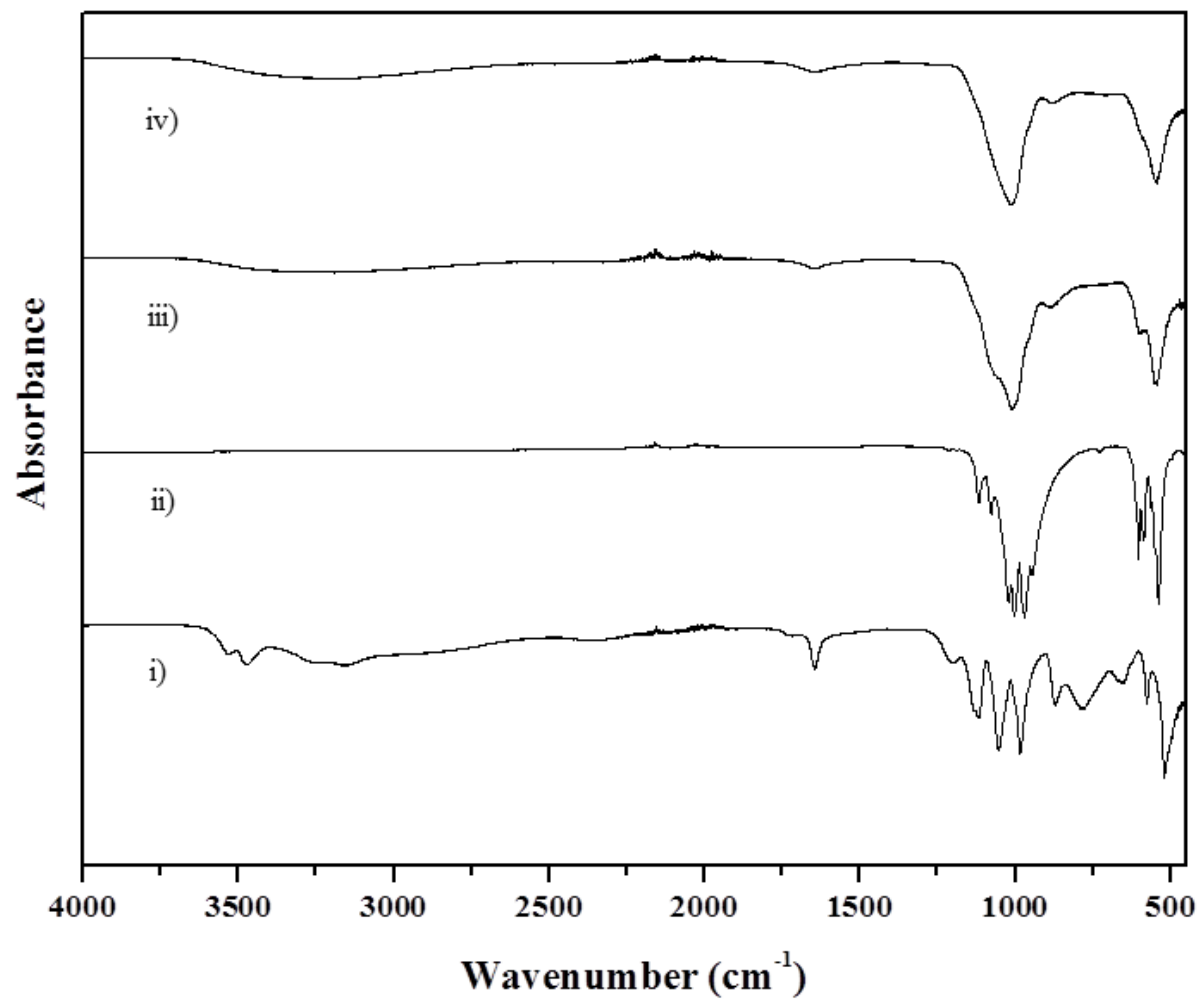


Figure 5.3 FT-IR spectra collected from commercially available i) DCPD, ii) β -TCP, iii) 50% β -TCMP, and iv) 50% β -TCMP refluxed at a pH of 8.

The incorporation of increased amounts of Mg^{2+} , determined using ICP-OES, resulted in the formation of increased amorphous content. In Chapters 3 and 4, the amorphous content formed along with crystalline Mg and Mg-Sr containing β -TCP was observed to crystallize at temperatures of approximately $750^{\circ}C$ forming pyrophosphates. Thus the scaffolds were prepared by sintering at temperatures of $600^{\circ}C$ thereby avoiding the crystallization of the amorphous content. The thermal stability of the amorphous β -TCMP formed after refluxing at a pH of 8 was assessed to determine the temperature at which the amorphous powders could be processed without inducing their crystallization. In Figure 5.4, the phase composition of the amorphous powders refluxed at a pH of 8 after heat treatment to various temperatures is illustrated. The β -TCP reference spectra (JCPDS 09-0169) and the data collected after refluxing are illustrated in Figure 5.4 i) and ii), respectively. After heat treatment to both 200 and $400^{\circ}C$, the amorphous phase was retained and either very little or no crystalline content was detected (Figure 5.4 iii) and iv)). However, after heat treatment to $600^{\circ}C$ several crystalline peaks, which closely matched that of β -TCP, were observed. This data confirms that the amorphous β -TCMP formed while refluxing at a pH of 8 crystallizes at a temperature between 400 and $600^{\circ}C$ and suggests that this material can be processed at temperatures of up to $400^{\circ}C$ while maintaining the amorphous state.

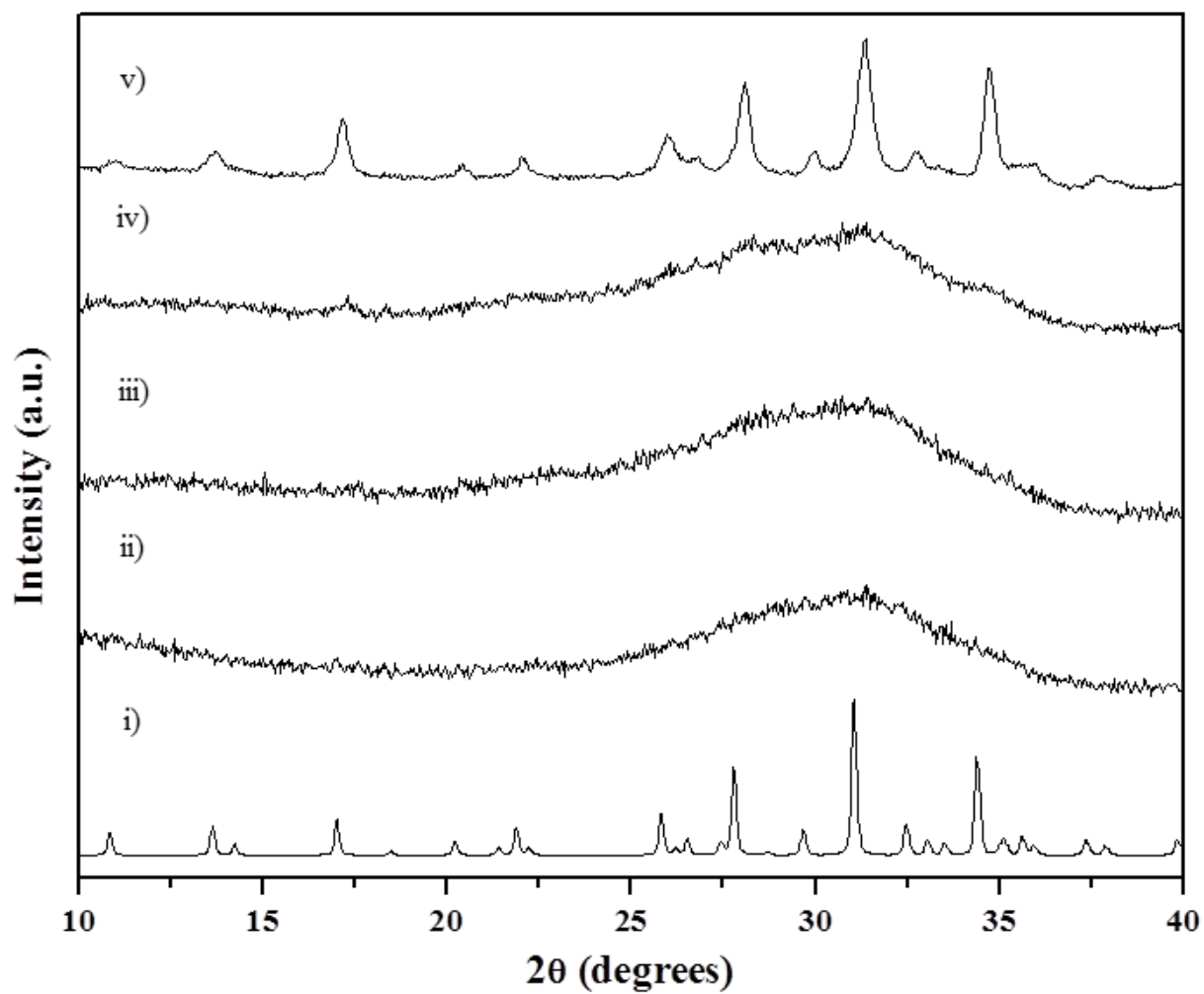


Figure 5.4 Powder X-ray diffraction of i) β -TCP (JCPDS 09-0169), ii) as prepared amorphous β -TCMP, amorphous β -TCMP heat treated to iii) 200°C, iv) 400°C, and v) 600°C.

5.3.2 Cell Proliferation on Amorphous β -TCMP

Dense 13 mm diameter scaffolds were prepared using commercially available β -TCP, 50% β -TCMP, prepared without pH modification, and fully amorphous 50% β -TCMP prepared using a pH of 8. The fully amorphous 50% β -TCMP scaffolds were sintered at 400°C to maintain the amorphous state while those prepared with 50% β -TCMP and commercially available β -TCP were sintered at temperatures of 600 and 1000°C, respectively. After sterilization and overnight immersion in cell culture media, hMSCs were seeded directly on these scaffolds, as previously described. The alamarblue assay was used to evaluate cell proliferation on these dense scaffolds after 4 and 7 days of culture in hMSC growth media. Substrates without cells were used as negative controls to ensure that subtle variations in both the ionic concentration and pH of the culture media during incubation with the alamarblue reagent did not influence the measurement.

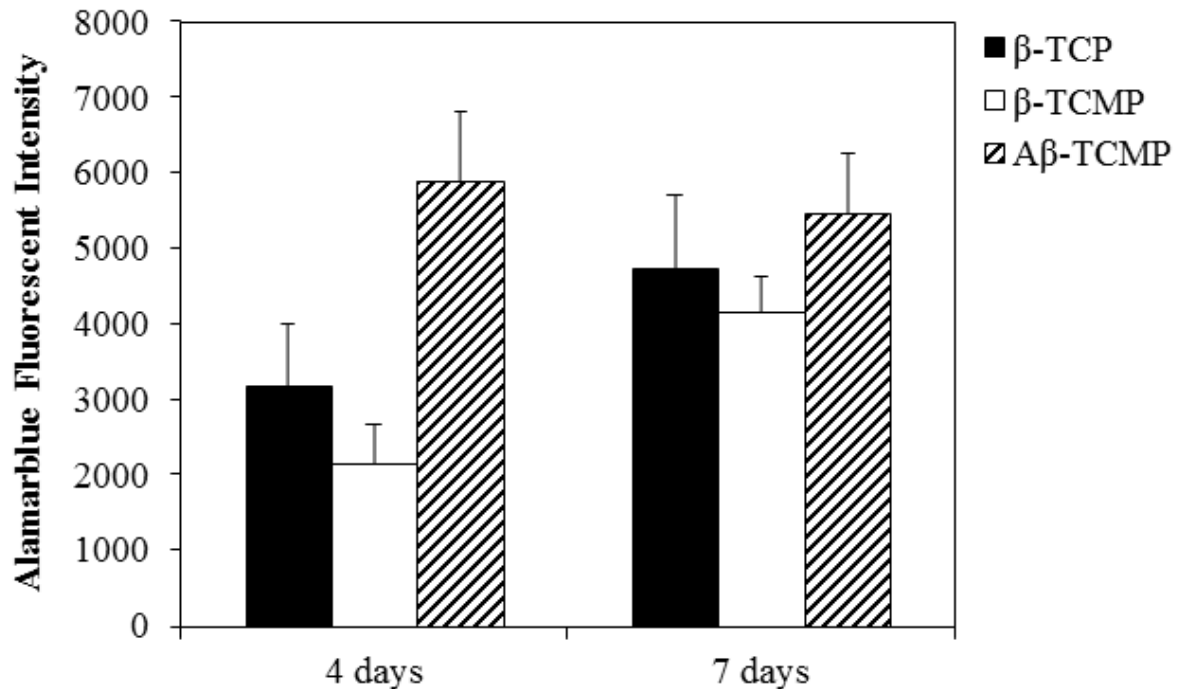


Figure 5.5 hMSC proliferation on scaffolds prepared using commercially available β -TCP, 50% β -TCMP, and fully amorphous 50% β -TCMP refluxed at a pH of 8.

After 4 days, increased proliferation was observed on scaffolds prepared with fully amorphous β -TCMP in comparison to both 50% β -TCMP and commercially available β -TCP (Figure 5.6). After 7 days, an increase in proliferation was observed for cells cultured on samples prepared with both 50% β -TCMP and commercially available β -TCP while a comparable value was obtained for cells cultured on fully amorphous 50% β -TCMP at both time points. The increased alamarblue fluorescence value obtained at earlier time points on fully amorphous 50% β -TCMP suggests that the cells cultured on these substrates proliferate more rapidly in comparison to those cultured on both 50% β -TCMP and commercially available β -TCP. The similar value obtained at the later time point suggests that the cells have become confluent by 4 days while the increase observed for the other two conditions between the two time points indicates that the cells seeded on these samples become confluent between 4 and 7 days. From

this data, it can be concluded that the expected increase in the release of Mg^{2+} and PO_4^{3-} ions from fully amorphous 50% β -TCMP in comparison to 50% β -TCMP does not inhibit cell proliferation. In contrast, the release of increased amounts of Mg^{2+} and PO_4^{3-} ions may actually support the enhanced proliferation of hMSCs. This is not surprising since Mg^{2+} was previously demonstrated to be a mitogenic factor capable of supporting proliferation [141]. It can also be concluded that the amount of ions released from the fully amorphous scaffolds does not result in a concentration of Mg^{2+} and PO_4^{3-} ions which is toxic and incompatible with hMSCs.

5.3.3 Ionic Concentrations in Culture Media

Similar to the data collected in Chapters 3 and 4, the media was once again collected on the days it was changed and the concentrations of the ions of interest were measured using ICP-OES for the duration of the experiment to correlate these values with that observed for cell proliferation. As previously observed, the concentration of Ca^{2+} for all conditions gradually increased (Figure 5.6 a)). Initially, an increased Ca^{2+} concentration was observed in the media collected from commercially available β -TCP. However, after approximately 13 days in growth media, similar Ca^{2+} concentrations were measured for all groups.

Increased Mg^{2+} and PO_4^{3-} concentrations in comparison to β -TCP were once again observed (Figure 5.6 b) and c)). Interestingly, although fully amorphous, only a slight increase in Mg^{2+} concentration was observed at earlier time points in comparison to β -TCMP (Figure 5.6 b)). At later time points, a steeper reduction in Mg^{2+} concentration was observed for β -TCMP while a sustained release of Mg^{2+} was observed for the amorphous β -TCMP and a value slightly greater than 4 mM was measured after 21 days. In contrast to the Mg^{2+} release profile, a sharp increase in PO_4^{3-} concentration was observed for amorphous β -TCMP in comparison to β -TCMP

(Figure 5.6 c)). Despite the sharper reduction in PO_4^{3-} concentration throughout the 21 day period, for amorphous β -TCMP, as expected, an increased release of PO_4^{3-} in comparison to β -TCMP was observed. Similar to Mg^{2+} concentration, after 21 days a value of approximately 4 mM was measured.

The reduced Ca^{2+} concentration at earlier time points is due to increased formation of mineral on the surface of both β -TCMP and amorphous β -TCMP in comparison to commercially available β -TCP [153]. However, it appears that the deposition of mineral nears completion on both β -TCMP conditions prior to β -TCP due to the sharper increase in Ca^{2+} concentration as it approaches the basal value of 1.8 mM. Based on previously published work, values of approximately 5-10 mM Mg^{2+} and 5 mM PO_4^{3-} were both found to support enhanced differentiation [126, 161]. Despite the formation of a fully amorphous scaffold, the bulk concentration in the media collected after 21 days was approximately 4 mM for both of these ions of interest. Therefore, it is possible that the amorphous scaffold may provide a more ideal microenvironment to support differentiation in comparison to the other two conditions.

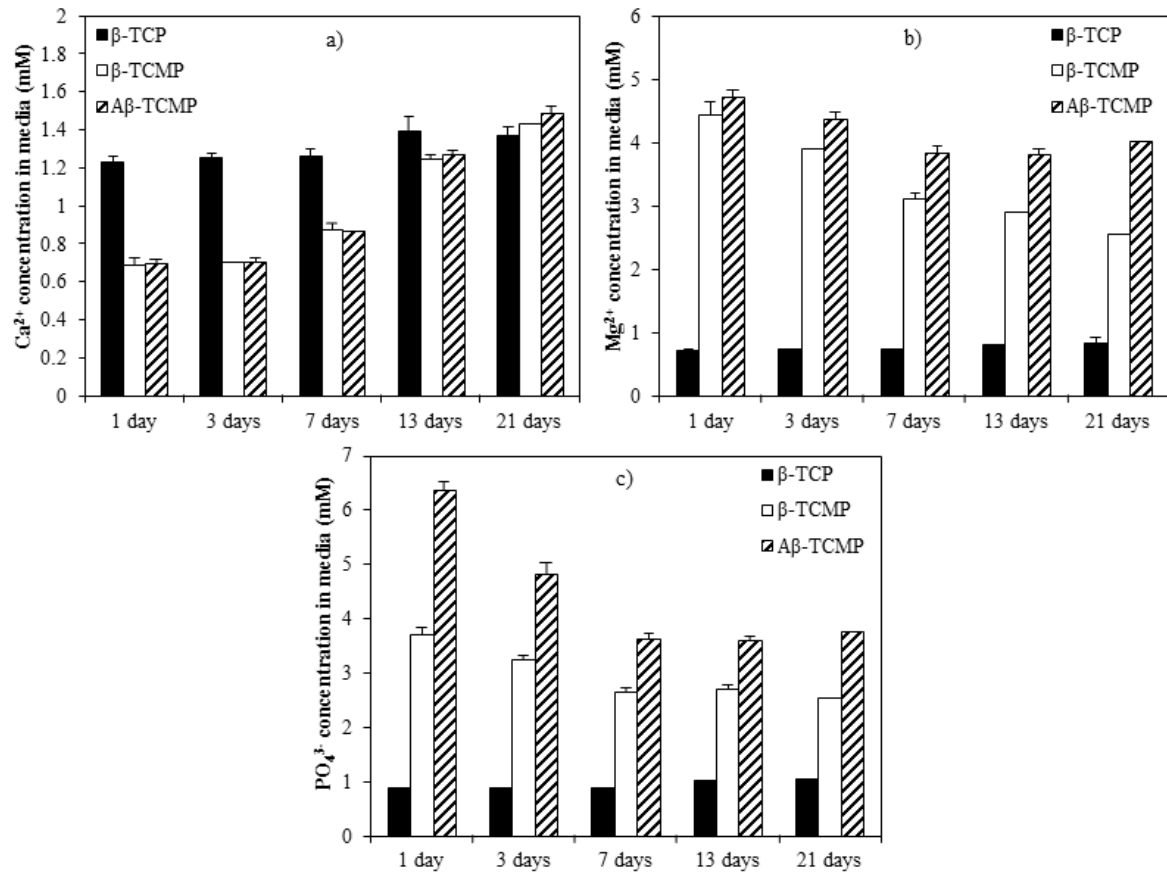


Figure 5.6 The ionic concentrations of a) Ca^{2+} , b) Mg^{2+} , and c) PO_4^{3-} in culture media after up to 21 days in growth media released from β -TCP, β -TCMP, and A β -TCMP scaffolds.

5.3.4 Osteogenic Differentiation on Amorphous β -TCMP

In previous work studying hMSC proliferation and differentiation on 50% β -TCMP containing scaffolds, similar levels of proliferation were observed on 50% β -TCMP in comparison to commercially available β -TCP while the increased expression of osteogenic markers, such as ALP, OPG, and OPN, was observed on 50% β -TCMP. However, the capability of fully amorphous 50% β -TCMP containing scaffolds to support hMSC osteogenic differentiation is yet to be determined, which is the basis of the work conducted in the current Chapter. ALP activity was once again used to evaluate osteogenic differentiation on 50% β -TCMP scaffolds prepared with and without pH modification in comparison to commercially available β -TCP (Figure 5.7). The capability of the material to support osteogenic differentiation in the absence of osteogenic supplements was also determined.

After 14 days, a comparable level of ALP activity was observed for cells cultured in growth media in comparison to those cultured on β -TCP in differentiation media. However, for both β -TCMP and amorphous β -TCMP, an increase in ALP activity was observed on samples cultured in differentiation, or osteogenic, media in comparison to the other conditions. A statistically significant increase was observed for the cells cultured on amorphous β -TCMP in comparison to all other conditions. After 21 days, a similar trend was observed. A slight reduction in ALP activity was observed on scaffolds prepared with fully amorphous 50% β -TCMP between 14 and 21 days. However, the value obtained was once again greater than that measured for β -TCMP and β -TCP. Based on this data it can also be concluded that osteogenic supplementation is required to support osteogenic differentiation on these materials.

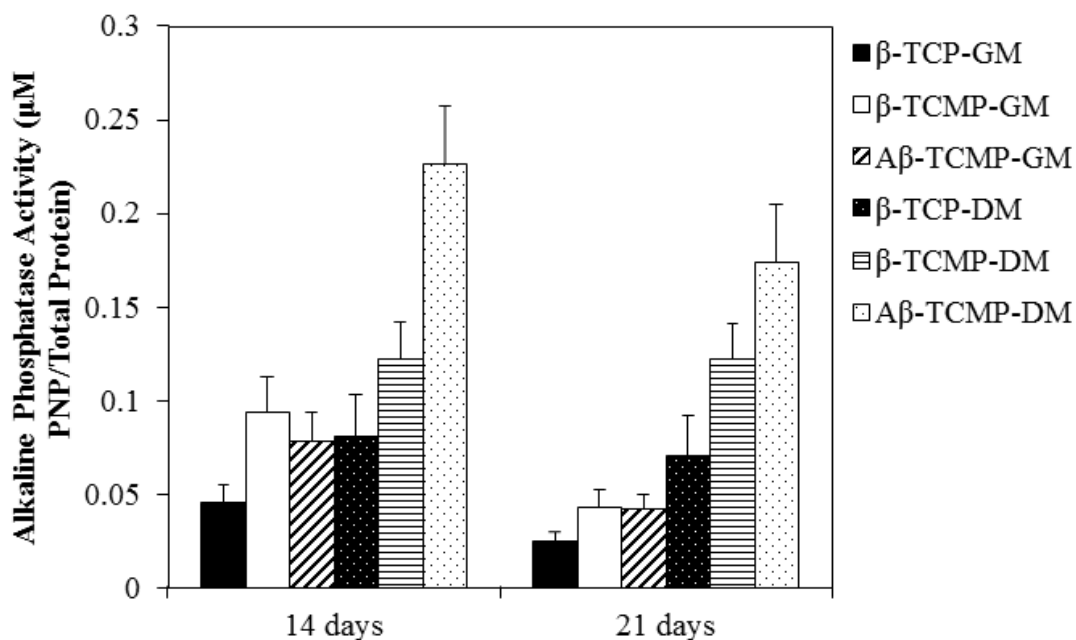


Figure 5.7 The alkaline phosphatase activity of hMSCs cultured directly on β -TCP, β -TCMP, and A β -TCMP containing scaffolds with growth media (GM) and differentiation media (DM) after 14 and 21 days.

qRT-PCR was performed to further analyze the expression of additional osteogenic markers to determine the capability of amorphous β -TCMP to support enhanced osteogenic differentiation (Figure 5.8). The data presented for β -TCMP and amorphous β -TCMP are normalized with respect to cells cultured on β -TCP. The samples cultured for 14 days in osteogenic media were analyzed. A similar expression of RUNX2, a marker expressed relatively early in the osteogenic differentiation process, was observed for all three systems of β -TCP, β -TCMP, and amorphous β -TCMP [18, 141]. The expression of two mature osteoblast markers, COL-1, the most abundant organic component of native mineralized tissues, and OCN, a protein produced solely by mature osteoblasts, were also analyzed [18, 44]. In comparison to β -TCP, a two to three fold increase in the expression of both mature osteoblast markers were observed for β -TCMP and amorphous β -TCMP. In contrast to the results observed from the ALP assay where

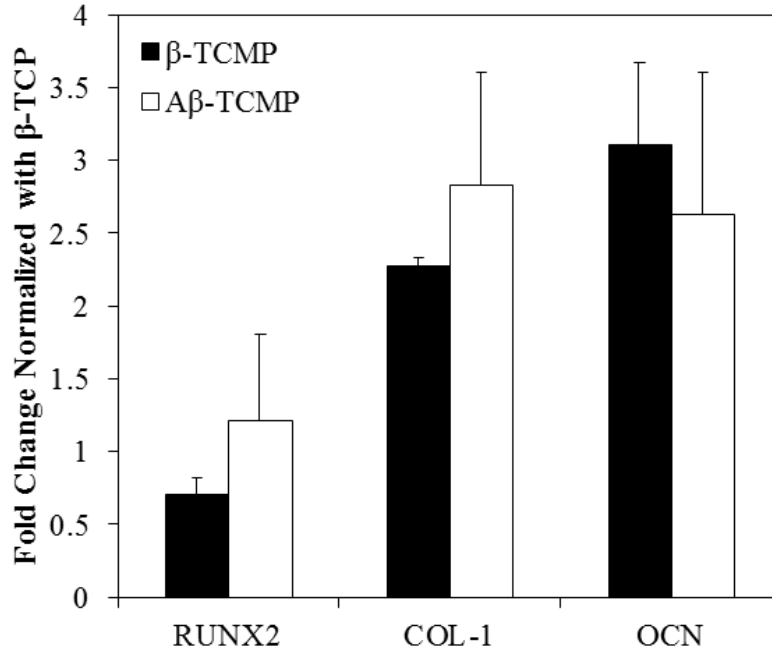


Figure 5.8 qRT-PCR results collected from hMSCs cultured on β-TCMP and amorphous β-TCMP constructs after 14 days in osteogenic media. The data presented is normalized to that determined for hMSCs cultured on scaffolds prepared using commercially available β-TCP.

a statistically significant increase in ALP activity was observed for amorphous β-TCMP in comparison to β-TCMP, a comparable gene expression of COL-1 and OCN were observed for both the amorphous and biphasic β-TCMP conditions.

The increased ALP activity observed suggests that the cells cultured on fully amorphous β-TCMP undergo enhanced differentiation in comparison all other conditions. However, the similar OCN and COL-1 expression for both amorphous β-TCMP and biphasic β-TCMP in comparison to β-TCP after 14 days suggests that the formation of a fully amorphous scaffold does not enhance the differentiation of hMSCs in comparison to the biphasic mixture. Nonetheless, a substantial increase in the expression of osteogenic markers for both experiments was observed in comparison to β-TCP. However, although the concentrations of Mg^{2+} and PO_4^{3-}

released into the culture media are near the desired range after extended periods of culture, it remains to be confirmed which of these ions released are more influential in supporting differentiation.

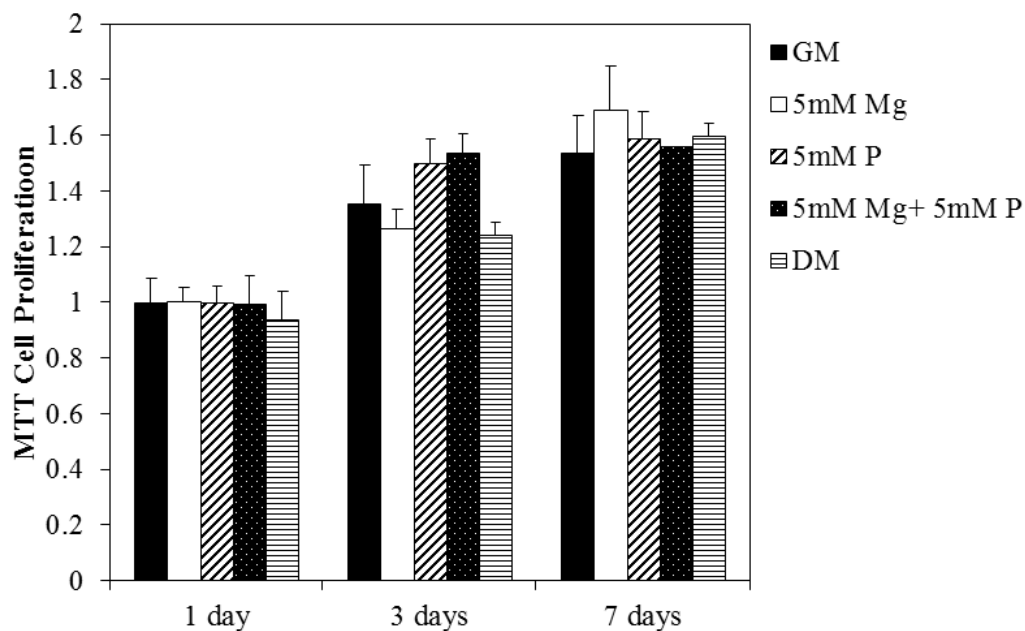


Figure 5.9 MTT cell viability data collected from hMSCs cultured in growth media (GM) supplemented with 5 mM Mg, 5 mM PO₄, 5 mM Mg and 5 mM PO₄, and differentiation, or osteogenic, media (DM). The data presented is normalized with respect to that collected for the cells cultured in growth media after 1 day. hMSCs cultured in GM with 10% DMSO was used as a negative control.

5.3.5 Influence of Mg²⁺ and PO₄³⁻ Concentration on Proliferation

To assess the roles of Mg²⁺ and PO₄³⁻ ions both individually and when delivered simultaneously on hMSC proliferation, growth media was supplemented with 5 mM Mg²⁺, 5 mM PO₄³⁻, and a combination of the two. The MTT assay was used to evaluate proliferation after up to one week of culture (Figure 5.9). After one day, a similar level of proliferation was observed for all

conditions, including the cells cultured in hMSC growth media containing osteogenic supplements. After 3 days, an increase in proliferation was observed for all conditions in comparison to day 1. A slight increase in comparison to the other conditions was observed for the cells cultured in media prepared with 5 mM PO_4^{3-} and the combination of 5 mM Mg^{2+} and 5 mM PO_4^{3-} . However, no statistically significant differences were observed. After 7 days, a slight increase in comparison to the data collected after 3 days was observed. Once again, no statistically significant differences were detected between groups. In summary, this data confirms that the supplementation of hMSC growth media with these concentrations of Mg^{2+} and PO_4^{3-} ions is non-toxic to cells. However, the role of culturing hMSCs in the presence of these ions on their capability to differentiate towards an osteoblastic lineage is yet to be determined.

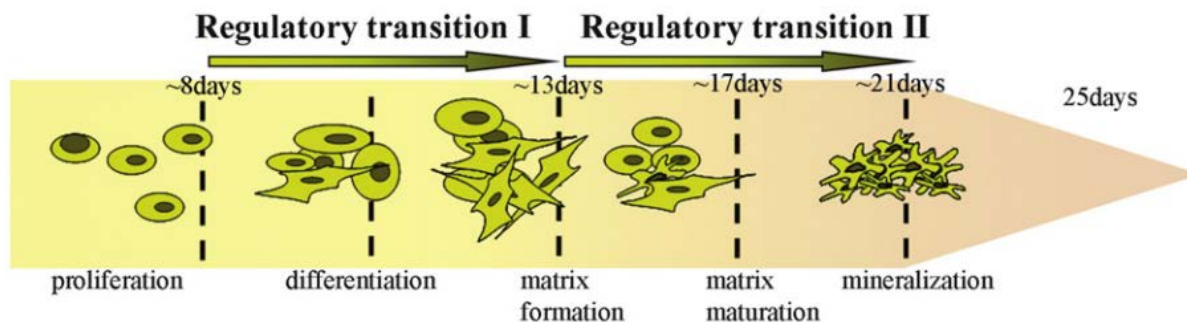


Figure 5.10 A proposed scheme for the stages of osteogenic differentiation. Active proliferation typically occurs for up to one week. The first regulatory transition during the differentiation process result in matrix formation which the second concludes with matrix maturation and mineralization [18].

5.3.6 Influence of Mg^{2+} and PO_4^{3-} Concentration on Mineralization

After confirming that cell proliferation was not influenced by ionic supplementation, the influence of these ions on osteogenic differentiation was studied. In Figure 5.10, the stages of osteogenic differentiation are illustrated. At the end of the proliferative stage, differentiation begins resulting in the formation of the extracellular matrix. As this process progresses, the matrix formed is eventually mineralized. The amount of mineral formed at various stages throughout this process is often measured to assess the stage of differentiation. In the current study, the mineral formed at various time points was stained and imaged using fluorescence. The amount of mineral formed was also quantified using a microplate reader.

The staining of the mineral formed after culturing for 14 days in media supplemented with additional Mg^{2+} and PO_4^{3-} ions is illustrated in Figure 5.11. Very little or no mineral was detected while culturing in media containing 5 mM Mg^{2+} while the formation of mineral was observed for hMSCs cultured in media supplemented with 5 mM PO_4^{3-} (Figure 5.11 a) and b)). Interestingly, mineral was not observed with cells cultured the combination of 5 mM Mg^{2+} and 5 mM PO_4^{3-} (Figure 5.11 c)). Mineral staining was performed once again after 21 days. A similar trend in mineral formation was observed in comparison to the data collected after 14 days (Figure 5.12). The cells cultured in PO_4^{3-} containing media underwent a similar amount of mineral formation in comparison to the cells cultured in differentiation media while either very little or no mineral was detected by the cells cultured in media containing Mg^{2+} and a combination of Mg^{2+} and PO_4^{3-} .

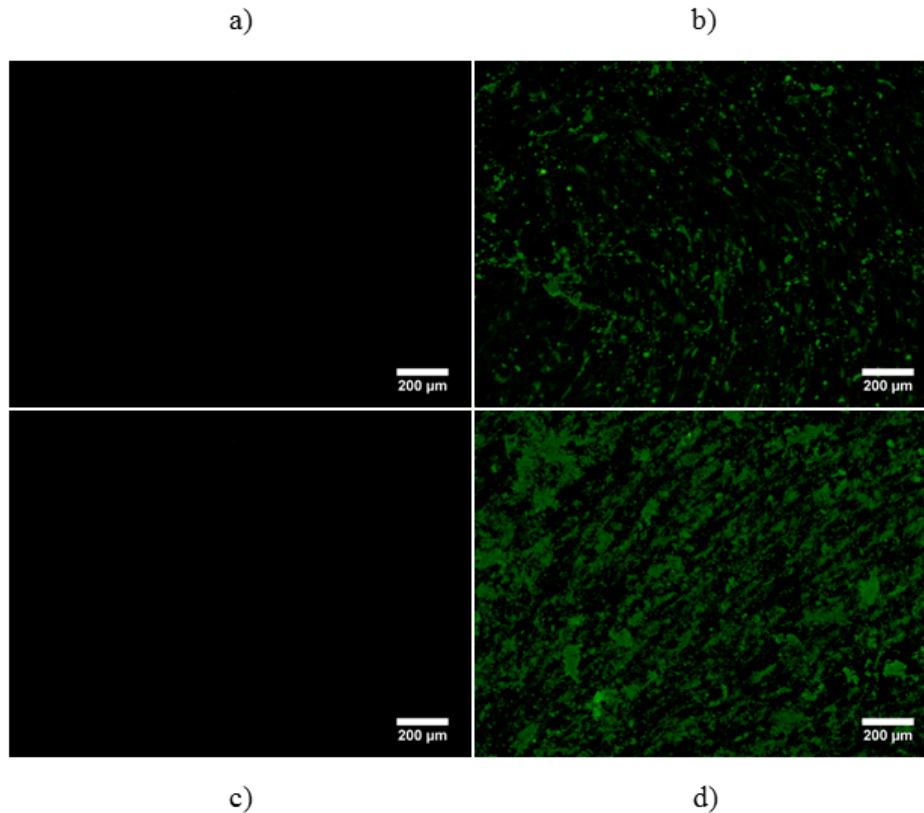


Figure 5.11 The staining of the mineral formed by hMSCs cultured in media supplemented with a) 5 mM Mg, b) 5 mM PO₄, c) 5 mM Mg and 5 mM PO₄, and d) osteogenic or differentiation media after 14 days.

The amount of mineral formed was also quantified using a microplate reader after 14 and 21 days (Figure 5.13). After 14 days, only a slight increase in mineral formation was observed in the cells cultured in 5 mM PO₄³⁻ in comparison to the cells cultured in 5 mM Mg²⁺ and a combination of PO₄³⁻ and Mg²⁺. However, after 21 days the amount of mineral formed in 5 mM PO₄³⁻ was similar to that which was measured in differentiation media. From this data, it can be concluded that PO₄³⁻ ions support mineralization and the addition of Mg²⁺ ions appears to inhibit the mineralization of hMSCs which was induced by PO₄³⁻ ions.

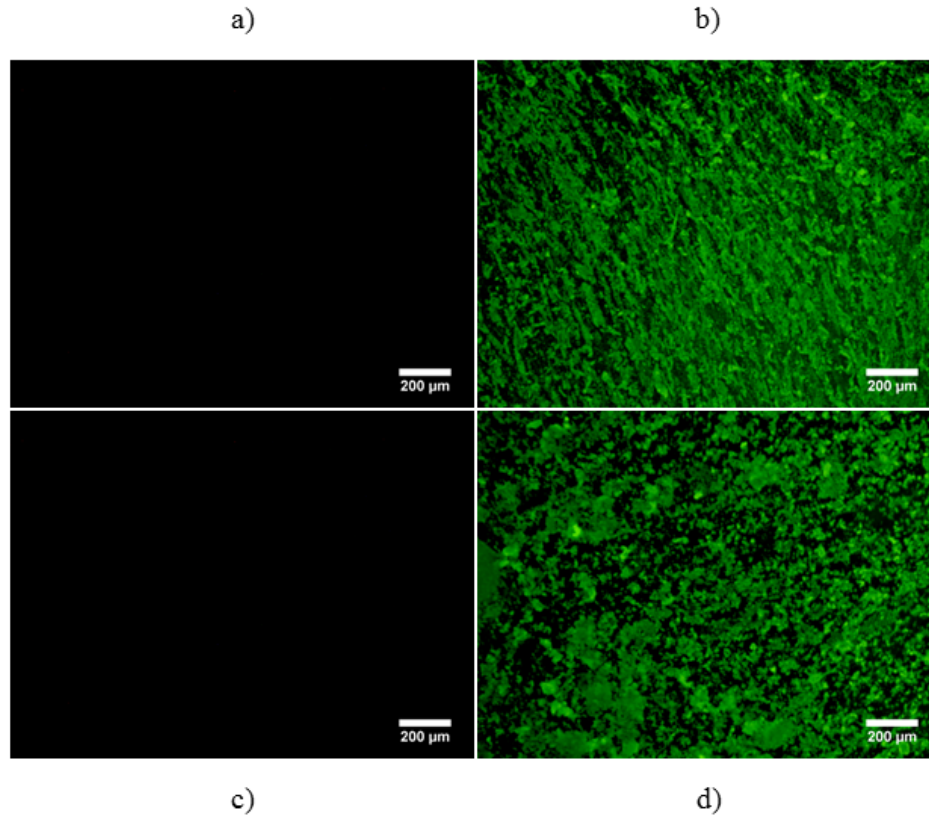


Figure 5.12 The staining of the mineral formed by hMSCs cultured in media supplemented with a) 5 mM Mg, b) 5 mM PO₄, c) 5 mM Mg and 5 mM PO₄, and d) osteogenic or differentiation media after 21 days.

Interestingly, the scaffolds prepared using β -TCMP which released increased amounts of both PO₄³⁻ and Mg²⁺ ions in comparison to β -TCP supported increased osteogenic differentiation. This result contradicts that observed in the experiments where media was supplemented with PO₄³⁻ and Mg²⁺ ions. Based on this observation, it appears that either the interaction between Mg²⁺ ions and the other components of osteogenic media, such as dexamethasone and ascorbic acid, may reduce the inhibition of mineralization by Mg²⁺ ions or the increased Ca²⁺ concentration at later time points may enhance differentiation. Further work is required to determine which of these mechanisms acts to support osteogenic differentiation in the presence of β -TCMP scaffolds.

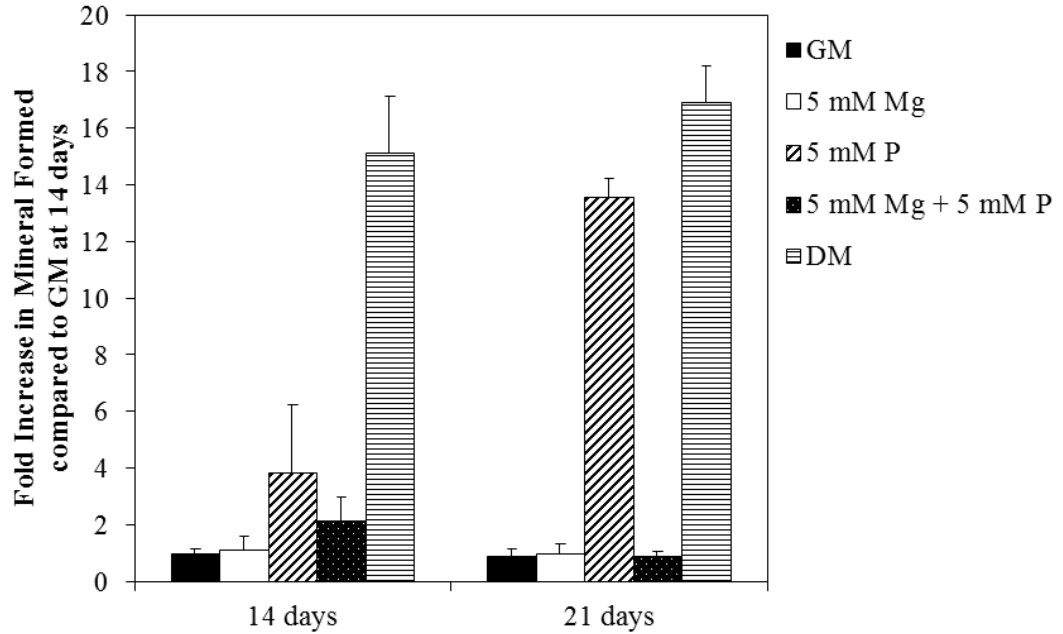


Figure 5.13 The quantification of the mineral formed in the presence of growth media supplemented with various amounts of Mg and PO₄ ions. The data collected was normalized with respect to that collected for cells cultured in growth media after 14 days.

5.4 CONCLUSIONS

The maintenance of basic conditions while refluxing was observed to result in the formation of a fully amorphous calcium magnesium phosphate phase. Upon increasing the solution pH, an increased retention of Mg²⁺ was observed in the amorphous powders formed. The increased Mg²⁺ content is believed to result in a reduction in crystallinity. Scaffolds prepared using these fully amorphous β-TCMPs were observed to support the enhanced proliferation of hMSCs in comparison to both commercially available β-TCP and 50% β-TCMP, composed of a biphasic mixture of crystalline β-TCMP and an amorphous phase. These amorphous scaffolds also supported increased ALP activity, a marker for early stage osteogenic differentiation. However, a

similar level of osteogenic gene expression was observed between amorphous β -TCMP and β -TCMP based on the expression of two mature osteoblast markers, OCN and COL-1.

The influence of Mg^{2+} and PO_4^{3-} ion concentration on hMSC proliferation and differentiation was also studied. Similar to previously reported work, the addition of Mg, either on its own or in combination with PO_4^{3-} was observed to support cell proliferation. The supplementation of growth media with 5 mM PO_4^{3-} was found to support a similar level of mineralization in comparison to the cells cultured in differentiation, or osteogenic, media. However, the addition of 5 mM Mg^{2+} to the media containing 5 mM PO_4^{3-} was observed to completely suppress mineral formation. Therefore, the enhanced concentration of Ca^{2+} at the later stages of cell culture with both β -TCMP and amorphous β -TCMP is most likely also playing a role in supporting enhanced differentiation.

Cationic substitutions have been demonstrated in Chapters 3-5 to be a useful tool to enhance the properties of β -TCP. However, thus far they have been studied in the form of granules or a preformed scaffold. Based on the discussion provided on the clinically relevant forms of calcium phosphate in Chapter 1, there are many other more useful forms of these materials that can be potentially used for clinical application. Therefore, in Chapters 6 and 7 cationic substitutions in β -TCP and HA will be explored in alternative forms, namely bioactive coatings and injectable self-setting calcium phosphate based cements to observe whether or not a similar improvement in cytocompatibility can be achieved through ionic substitutions for Ca^{2+} using Mg^{2+} and Sr^{2+} .

6.0 CATIONIC SUBSTITUTED CALCIUM PHOSPHATE COATINGS ON BIODEGRADABLE MAGNESIUM ALLOYS

6.1 INTRODUCTION

Biodegradable Mg based alloys have become widely studied in the development of degradable implants, particularly cardiovascular stents and both orthopedic and craniofacial bone fixation devices [109]. The human body is known to contain as much as 30g of Mg, the majority of which is found in mineralized tissues [127]. As a result, Mg is believed to play a critical role in bone biology. Previous studies have demonstrated the influence of Mg on both osteoblast and osteoclast differentiation, rendering Mg based alloys an attractive material for bone tissue engineering applications [118]. Nonetheless, the exact role of Mg^{2+} in the regeneration of mineralized tissues remains poorly understood, warranting further research.

While degradable metallic implants hold great promise, the uncontrolled non-uniform corrosion, typical of the majority of Mg alloys developed to date, remains a primary concern [186]. In order to control the corrosion of Mg alloys, coatings have been widely studied. Unfortunately, the relatively low melting points of Mg alloys preclude the use of high temperature coating processes which are routinely employed for refractory metals, such as titanium and stainless steel. Alternative approaches to control corrosion behavior, including alloying with rare earths and the development of Mg based bulk metallic glasses, have also been

explored to date [187, 188]. Unfortunately, the unknown long term toxicity of the varying alloying elements, reduced mechanical stability, and the challenges of large scale production of these metallic systems with reproducible microstructural, mechanical, and corrosion properties limit the wider acceptance of these approaches [189, 190].

As a result, coating strategies remain one of the more promising approaches to tailor the corrosion of Mg alloys. For bone tissue engineering applications in particular, CaP coatings are of interest since CaPs are a major component of native mineralized tissues [7]. Several CaP phases have therefore been studied as coatings on Mg alloys and have been shown to provide corrosion control while also enhancing bioactivity [108]. Low temperature processes such as electrodeposition and various aqueous immersion techniques, including biomimetic approaches, are a few of the more commonly studied techniques. Immersion techniques are also of considerable interest since they are relatively simple, cost effective, and can be used to coat a variety of complex porous structures in a controlled manner.

To date, the CaP coatings formed on Mg alloys by immersion techniques are typically non-uniform and porous, limiting their ability to provide corrosion control [108]. Pretreatment is thus a critical step with immersion techniques in order to form a passivation layer on which CaP coatings are subsequently grown or deposited. Both acidic and alkaline conditions have been studied to form pretreatment layers [191, 192]. Surprisingly, very few reports have explored the influence of pretreatment conditions on the coating performance, although the microstructure and mechanical stability of CaP coatings are highly dependent upon the properties of the underlying pretreated layer [112].

Ionic substitutions to stabilize the phase composition are an alternative approach to optimize the physicochemical properties of CaP coatings. In this regard, the doping of CaP

coatings with Sr^{2+} is of much interest since it is known to cause an imbalance in bone turnover, favoring the formation rather than the resorption of bone [193]. For example, previous work by Bracci et al. has explored the use of a biomimetic approach to deposit Sr^{2+} doped CaP coatings on Ti and their results concluded that doped coatings promoted osteogenic differentiation due to an upregulation of collagen type 1 [162]. Interestingly, to the best of our knowledge Sr^{2+} doped CaP coatings deposited on Mg alloys using immersion approaches are yet to be studied leaving much to be explored in the coating space for these systems. However, strontium phosphate coatings have only recently been explored [194].

In the current work, the influence of pretreatment conditions and the role of Sr^{2+} doping into the CaP structure on providing corrosion protection and cytocompatibility were explored. Substrates were accordingly pretreated by immersion in Na_2HPO_4 followed by heat treatment to various temperatures. The effect of substrate pretreatment on CaP coating structure was also studied. It was hypothesized that Sr^{2+} doped CaP coatings could improve the ability of CaP coatings to support the osteogenic differentiation of a mouse preosteoblast cell line and human mesenchymal stem cells (hMSCs) in comparison to undoped CaPs.

6.2 MATERIALS AND METHODS

6.2.1 Substrate Preparation, Pretreatment, and Coating Formation

A 0.81 mm thick sheet of AZ31 was acquired from Alfa Aesar (Ward Hill, MA) and was subjected to acid etching followed by polishing with SiC paper, as previously described [128]. Cleaned substrates were then immersed in an $80 \text{ g l}^{-1} \text{ Na}_2\text{HPO}_4$ solution at 40°C for 3 h before

rinsing in DI water and drying in air. Na₂HPO₄ treated substrates were heat treated in argon to either 350 or 400°C for 10 h. After heat treatment, the substrates were immersed in solutions prepared with 0, 5, and 10% Sr/(Ca+Sr) ratios and a fixed (Ca+Sr)/P ratio, illustrated in Table 6.1, at 70°C for 48 h. Upon completion of the coating process, substrates were once again rinsed in DI water and dried at 60°C prior to further experiments. Throughout the manuscript, the substrates subjected to the above pretreatments will be represented as wherein the numbers following Sr refer to % Sr/(Ca+Sr) and the numbers following the hyphen refer to the pretreatment temperature (Sr0-350, Sr0-400, Sr5-350, Sr5-400, Sr10-350, and Sr10-400).

Table 6.1 The molar concentrations of the salts used to prepare coating solutions. A (Ca+Sr)/P of 1.67 was maintained for all conditions and the Sr/(Ca+Sr) ratio was varied between 0, 5, and 10%.

	CaCl ₂ •2H ₂ O Conc. (mM)	SrCl ₂ •6H ₂ O Conc. (mM)	Na ₂ HPO ₄ Conc. (mM)
Sr0	100	-	60
Sr5	95	5	60
Sr10	90	10	60

6.2.2 Coating Characterization

X-ray diffraction (X-Pert PRO Cu K α $\lambda=1.5418\text{\AA}$, with X'celerator detector, Philips) was performed to determine the phase composition and crystallinity of CaP coated substrates. Diffraction patterns were collected between 2θ values of 10-90° with the X-ray generator operated at 45 kV and 40 mA. Further analysis of the phase composition of pretreated and coated substrates was performed using the attenuated total reflectance Fourier transform infra-red spectroscopy (ATR-FTIR, Nicolet 6700, Thermo Scientific). A spectral resolution of 2 cm⁻¹

between 400-4000 cm^{-1} was used and the average of 64 scans was recorded. Coating microstructure and elemental composition were then analyzed using scanning electron microscopy (Philips, XL30 FEG ESEM) and inductively coupled plasma optical emission spectroscopy (ICP-OES, iCAP duo 6500 Thermo Fisher).

6.2.3 Corrosion Experiments

6.2.3.1 Hydrogen Evolution

Three samples for each condition were placed in individual sample holders made of a non-degradable polymer mesh, ensuring that the complete surface area of each sample was fully exposed. The samples were then suspended in a 9.7 g/l Hank's balanced salt solution (HBSS, Sigma Aldrich, Catalog # H1387) supplemented with 0.35 g/l sodium bicarbonate (NaHCO_3 , Sigma Aldrich), maintaining an initial pH of 7.4. The ratio of substrate surface area to HBSS volume was kept constant at $10 \text{ cm}^2 \text{ l}^{-1}$ to ensure that sufficient hydrogen would be generated for both coated and bare substrates. Additionally, the temperature was maintained at 37°C throughout the experiment. The hydrogen generated was collected in an inverted burette and measurements of the volume of HBSS displaced were correspondingly recorded during a one week period.

6.2.3.2 Immersion Test

Coated and bare substrates were immersed in 2 ml of Dulbecco's modification of eagle medium (DMEM, Mediatech Inc., Manassas, VA) supplemented with 10% fetal bovine serum (FBS, Atlanta Biologicals, Lawrenceville, GA) and 1% P/S (penicillin streptomycin, Gibco, Grand Island, NY). The samples were stored in an incubator at 37°C and 5% CO_2 for up to 3 weeks.

The media was refreshed every 48 h and collected for further analysis by measuring the pH (Φ 350 pH meter, Beckman Coulter) and elemental composition using ICP.

6.2.3.3 Electrochemical Corrosion Testing

Electrochemical corrosion experiments were performed at 37°C in DMEM supplemented with 10% FBS and 1% P/S using a CH604a electrochemical workstation (CH Instruments, Austin TX). A three electrode cell comprised of platinum as a counter electrode and a Ag/AgCl reference electrode was used. Open circuit potential (OCP) was first established for all the samples after at least 1 h of stabilization in 125 ml of DMEM. Potentiodynamic polarization tests were then performed at a scan rate of 1 mV s⁻¹. The corrosion current and potential were determined using a Tafel extrapolation added into the OriginPro 8 data analysis and graphing software.

6.2.4 In-Vitro Cytocompatibility

6.2.4.1 Cell Culture and Maintenance

MC3T3-E1 cell line (ATCC, Manassas, VA) was cultured in minimum essential medium α (MEM α , Gibco) containing 10% FBS and 1% P/S under 37 °C, 5% CO₂, and 95% relative humidity. Cells after fourth passage were used in all experiments at a seeding density of 50,000 cells ml⁻¹. For osteogenic differentiation studies, MC3T3-E1 growth media was accordingly supplemented with 100 nM dexamethasone, 50 μ M ascorbic acid, and 10 mM β -glycerophosphate. The cells were cultured on samples for 7 days prior to inducing differentiation.

The hMSCs obtained from the normal human bone marrow were purchased from Lonza (Lonza, Allendale, NJ) and were cultured under 37 °C, 5% CO₂, and 95% relative humidity. Cells after the third passage were used in all experiments and were cultured in MEM α containing 20% FBS and 1% P/S. Similar to MC3T3-E1 cells, for osteogenic differentiation studies, hMSC growth media was accordingly supplemented with 100 nM dexamethasone, 50 μ M ascorbic acid, and 10 mM β -glycerophosphate.

6.2.4.2 Cell Proliferation

Live/dead staining (Invitrogen, Live/Dead staining kit) was used to observe live cell attachment on coated and bare substrates after 3 and 7 days of culture. Samples were rinsed with PBS followed by incubation for 40 minutes with the live/dead stain diluted in PBS. Imaging was performed using a fluorescent microscope (Olympus, CKX41) prior to fixing samples with 2.5% glutaraldehyde. Once fixed, samples were dehydrated by washing with ethanol and were subsequently sputter coated with palladium before imaging using SEM.

The DNA concentration on coated and bare substrates was assessed using the Quant-iT PicoGreen dsDNA Kit (Invitrogen, Carlsbad, Ca). Culture media was removed and samples were rinsed with PBS. The cells were then lysed (CellLytic M Cell Lysis Reagent, Sigma Aldrich) and the supernatants were collected after centrifuging. DNA concentration in the supernatant was determined by measuring the fluorescence at an excitation wavelength of 480 nm and an emission wavelength of 520 nm (Synergy 2 Multi-Mode Microplate Reader, Biotek).

Table 6.2 The qRT-PCR primer sequences used for mouse preosteoblast cell line MC3T3-E1.

	Forward Primer (5'-3')	Reverse Primer (5'-3')
GAPDH	AGGAGTATATGCCCGACGTG	TCGTCCACATCCACACTGTT
Osteocalcin	GGGAGACAACAGGGAGGAAAC	CAGGCTTCCTGCCAGTACCT
Osteopontin	CTTTCACTCCAATCGTCCCTAC	CCTTAGACTCACCGCTCTTCAT

Table 6.3 The qRT-PCR primer sequences used for human mesenchymal stem cells.

	Forward Primer (5'-3')	Reverse Primer (5'-3')
GAPDH	TTGTCTCCTGCGACTTCAACA	GTGGTCCAGGGTTTCTTACTCC
Osteocalcin	CCGGGAGCAGTGTGAGCTTA	TAGATGCGTTTGTAGGCGGTC
Osteopontin	CTTTCACTCCAATCGTCCCTAC	CCTTAGACTCACCGCTCTTCAT

6.2.4.3 Osteogenic Gene Expression

After culturing in osteogenic media, RNA extraction was performed using the NucleoSpin RNA II kit (Macherey Nagel, Bethlehem, Pa) according to the manufacturer's protocol. The RNA concentration and purity was determined by measuring the absorbance at 260 and 280 nm using a microplate reader. Reverse transcription was then performed using the ImProm II Promega reverse transcription kit (Promega, Madison, WI) according to the manufacturer's protocol. Primers for mouse and human GAPDH, osteocalcin, and osteopontin were used in the qRT-PCR experiments (Table 6.2 and Table 6.3). Measurements were then conducted in triplicate for each sample.

6.2.4.4 Osteogenic Protein Expression

Protein expression was quantified using a MAGPIX instrument (Luminex, Austin, TX). A Human Bone Magnetic Bead Panel kit (EMD Millipore, Billerica, Ma) was purchased and used

according to the manufacturer's protocols. The expression of osteocalcin (OCN) was studied after 18 days of culture in osteogenic media.

6.2.4.5 Statistical Analysis

All of the experiments were performed also with a minimum of three repeats for each condition. Measurements for each repeat were performed in triplicate. The mean and standard error were accordingly reported. Unless otherwise mentioned, analyses were performed independently. Two way analysis of variance (ANOVA) was used to determine the statistical significance. The Tukey-Kramer test was used for all pairwise comparisons. A p value < 0.05 was considered significant for the data collected.

6.3 RESULTS AND DISCUSSION

6.3.1 Pretreatment Characterization

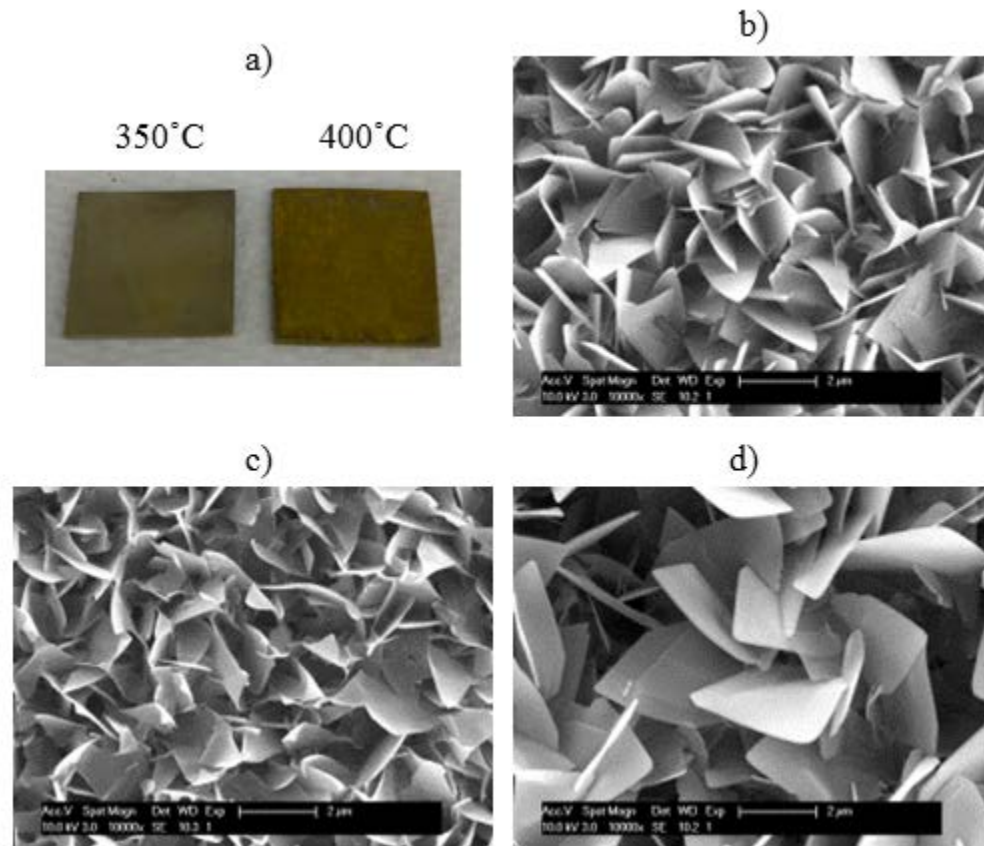


Figure 6.1 a) Optical images of AZ31 after immersion in Na_2HPO_4 and heat treatments as well as SEM images of the substrate surface after b) immersion in Na_2HPO_4 , c) heat treatment to 350°C , and d) heat treatment to 400°C (Scale bars are $2\ \mu\text{m}$).

All substrates were pretreated by immersion in Na_2HPO_4 forming a passivation layer on the substrate surface prior to depositing the CaP coating. Basic phosphate solutions were used for pretreatment to enhance the local PO_4^{3-} concentration during the precipitation of CaP coatings and to reduce the formation of more soluble acidic CaP phases, such as dicalcium phosphate dihydrate. After immersion in Na_2HPO_4 , the AZ31 substrates were heat treated to either 350 or 400°C in argon for 10 h. Heat treatment to either temperature resulted in the formation of a dull yellow film. Samples heat treated to 400°C formed a film with a more intense yellow color in comparison to those heat treated to 350°C (Figure 6.1 a)). The microstructure of the layer formed as a result of Na_2HPO_4 treatment was highly porous and comprised of lamellar shaped plate-like particles approximately 2 μm wide (Figure 6.1 b)), determined using SEM. After heat treatment to 350°C (Figure 6.1 c)), minimal change in microstructure was observed by SEM. After heat treatment to 400°C (Figure 6.1 d)), an estimated two to three fold increase in the width of the lamellar plates formed after immersion in Na_2HPO_4 and heat treatment to 350°C was observed.

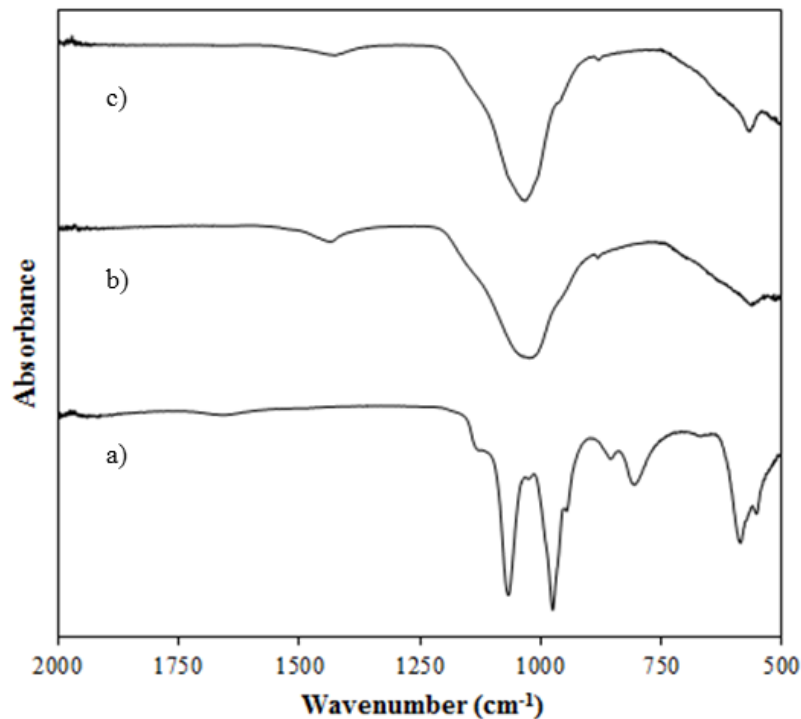


Figure 6.2 ATR-FTIR spectra collected from samples after a) Na_2HPO_4 treatment, b) heat treatment to 350°C , and c) heat treatment to 400°C .

FT-IR was used to characterize variations in the chemical structure of the coatings formed prior to and after heat treatment. The FT-IR spectra collected after Na_2HPO_4 treatment (Figure 6.2 a)) closely resembled that of HPO_4^{2-} with characteristic bands observed at 1069, 804, 595, and 555 cm^{-1} [195]. After heat treatment to 350°C , the FTIR spectra collected contained relatively broad peaks in comparison to the spectra collected prior to heat treatment (Figure 6.2 b)). The FT-IR spectra of samples heat treated to 400°C (Figure 6.2 c)) closely resembled that of samples heat treated to 350°C . After both heat treatments similar characteristic peaks of HPO_4^{2-} were observed at 1039 and 569 cm^{-1} while the peaks observed prior to heat treatment near 853 and 804 cm^{-1} were no longer detected. It is believed that the peak broadening after heat treatment

may be due to the distortion of bond vibrations as a result of the incorporation of the alloying elements, Mg, Al, and Zn, into the pretreated layer.

XRD was used to further characterize the Na_2HPO_4 pretreated layer before and after heat treatments. Prior to heat treatment, the predominant crystalline phase detected was Na_2HPO_4 despite thorough washing after removing the substrates from the Na_2HPO_4 solutions (Figure 6.3 i)). In addition, peaks from the AZ31 substrate, $\text{Mg}_3(\text{PO}_4)_2 \cdot 8\text{H}_2\text{O}$, and an amorphous background were also observed. Previous work studying magnesium phosphate cements has shown that after reacting MgO with Na_2HPO_4 an amorphous material is formed while the reaction of MgO with $(\text{NH}_4)_2\text{HPO}_4$ results in the formation of crystalline $\text{MgNH}_4\text{PO}_4 \cdot 6\text{H}_2\text{O}$ [196].

In addition, the immersion of AZ31 in $(\text{NH}_4)_2\text{HPO}_4$ followed by steam curing was previously observed to result in the formation $\text{NH}_4\text{MgPO}_4 \cdot 6\text{H}_2\text{O}$ at elevated $(\text{NH}_4)_2\text{HPO}_4$ concentrations, confirmed using XRD [197, 198]. Therefore, it appears that an amorphous magnesium sodium phosphate phase may also be formed after immersion in Na_2HPO_4 . Interestingly, the XRD spectra of pretreated samples after heat treatment to 350°C showed mostly AZ31 peaks while after heat treatment to 400°C only MgO could be detected (Figure 6.3 ii) and iii)). Thus, it appears that after heat treatment to 350°C an amorphous magnesium sodium phosphate phase and poorly crystalline MgO is formed while the heat treatment to 400°C enhances the crystallization of MgO.

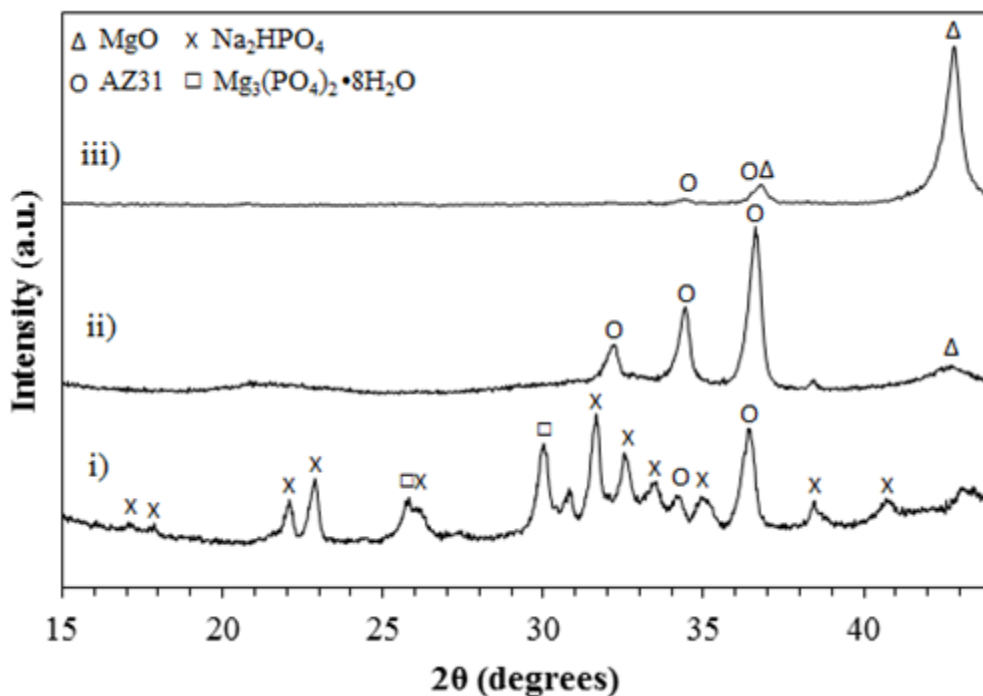


Figure 6.3 XRD collected from coatings formed on AZ31 after i) Na_2HPO_4 treatment, ii) heat treatment to 350°C , and iii) heat treatment to 400°C . (Na_2HPO_4 (JCPDS 01-0997), $\text{Mg}_3\text{PO}_4\cdot 8\text{H}_2\text{O}$ (JCPDS 33-0877), and MgO (JCPDS 04-0829)).

Elemental analysis was performed using ICP in order to confirm the diffusion of alloying elements, Mg, Al, and Zn, into the Na_2HPO_4 pretreated layer after heat treatments (Table 6.4). The coatings formed after pretreatments were collected, after carefully removing from the surface of the substrate, and dissolved in dilute HNO_3 solutions prior to determining their elemental composition using ICP. After immersion in Na_2HPO_4 , relatively large amounts of Na and P were detected despite thorough washing of the substrates after Na_2HPO_4 treatment, similar to XRD observations. After heat treatment to 350°C , the mol. % of Na and P sharply decreased while that of Mg and Zn expectedly increased. Upon heat treatment to 400°C , Na and P content further decreased, while Mg and Zn content once again was observed to increase. The increase in Zn content after heat treatment is most likely due to either the relatively low melting point of Zn

in comparison to Mg and Al or the formation of an intermetallic. The increasing Mg content after heat treatment is due to the formation of greater amounts of MgO with increasing temperature, also confirmed by XRD.

Table 6.4 ICP elemental analysis of pretreated coatings formed after immersion in Na₂HPO₄. Coatings from 9 samples were collected and analyzed.

	Mol. %				
	Mg	Al	Zn	Na	P
Na ₂ HPO ₄	34.8	0.5	0.04	35.6	29.1
Na ₂ HPO ₄ - 350°C	61.0	0.7	0.09	19.7	18.6
Na ₂ HPO ₄ - 400°C	83.5	0.3	0.13	3.4	12.7

6.3.2 Coating Structural Characterization

To develop coatings of undoped CaP and Sr doped CaPs, pretreated substrates were then immersed in solutions containing Ca²⁺, Sr²⁺, and HPO₄⁻ ions kept at 70°C with a fixed (Ca+Sr)/P ratio and varying Sr/(Ca+Sr) ratios (Table 6.1). XRD was used to determine the crystallinity and phase composition of CaP coatings formed in the presence of varying Sr²⁺ concentrations (Figure 6.4). Biphasic mixtures of hydroxyapatite (HA) and β-tricalcium phosphate (β-TCP) were observed to form on substrates pretreated to 350°C (Figure 6.4 a)). Similar to the CaP coatings formed on substrates pretreated to 350°C, the CaP films deposited on substrates pretreated to 400°C also consisted of biphasic mixtures of HA and β-TCP (Figure 6.4 b)). β-TCP is known to be unstable under aqueous conditions, however, increased Mg²⁺ concentrations have been reported to stabilize β-TCP [81]. Moreover, the formation of increased amounts of MgO after heat treatment to 400°C, previously confirmed using ICP and XRD, may lead to increased local

Mg²⁺ concentrations during the precipitation of CaP coatings thus promoting the formation of β -TCP rather than HA.

The elemental composition of CaP coatings was evaluated using ICP (Table 6.5). Once again, coatings were gently removed from the substrate and solubilized in dilute HNO₃ solutions. Despite the use of different pretreatment temperatures, the amount of Sr²⁺ incorporated into CaP coatings was similar between both groups. Similar to the elemental analysis of pretreated layers, increased amounts of Mg were also detected in CaP coatings formed on substrates pretreated to 400°C. This suggests that increased levels of ionic substitution of Ca²⁺ by Mg²⁺ occurred in the CaP coatings formed on substrates pretreated to 400°C, since neither magnesium phosphate nor excess MgO were detected using XRD. The (Ca+Mg+Sr)/P ratio of CaP coatings formed on substrates pretreated to 400°C was also slightly increased. However, the Ca/P ratios were similar between both groups.

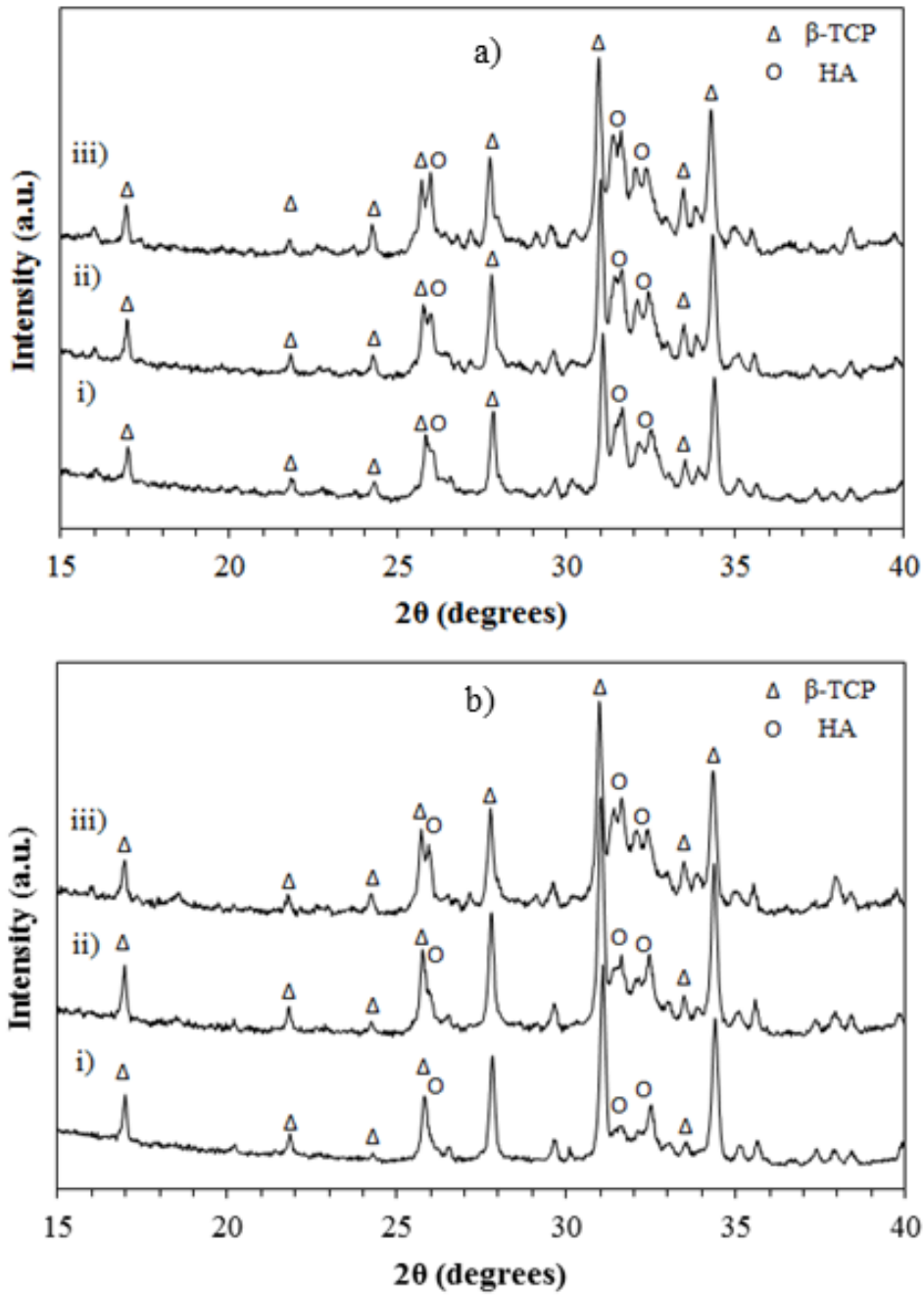


Figure 6.4 XRD collected from CaP coatings formed on pretreated AZ31 after heat treatment to a) 350°C and b) 400°C and immersion in solutions prepared with i) 0, ii) 5, and iii) 10% Sr/(Ca+Sr) ratios (β -TCP (JCPDS 09-0169) and HA (JCPDS 09-0432)).

Table 6.5 ICP elemental analysis of CaP coatings formed after immersion in solutions containing various amounts of Ca²⁺, Sr²⁺, and PO₄³⁻. Coatings from 9 samples were collected and analyzed.

	Mol. % Ca	Mol. % Mg	Mol. % Sr	Mol. % P	Mol. % Na	(Ca+Mg+Sr)/P
Sr0-350	52.4	4.6	-	40.5	2.3	1.41
Sr5-350	49.8	5.1	2.4	40.3	2.2	1.42
Sr10-350	47.8	5.4	4.3	40.5	1.7	1.42
Sr0-400	50.9	7.5	-	39.7	1.7	1.47
Sr5-400	47.9	7.6	2.6	39.7	1.9	1.46
Sr10-400	44.6	9.9	4.6	38.4	2.2	1.54

The influence of pretreatment and Sr²⁺ concentration on as deposited coating microstructure was observed using SEM (Figure 6.5). Coatings formed on substrates pretreated to 350°C without Sr²⁺ consisted mostly of rod shaped particles. In addition, fiber like structures and rosette shaped particles were also observed (Figure 6.5 a)). Upon increasing Sr²⁺ concentration, fewer rod shaped particles were detected and primarily rosette and fiber like particles were observed (Figure 6.5 b)). In contrast, CaP coatings formed on substrates pretreated to 400°C without Sr²⁺ consisted of mostly round 10 µm or greater particles (Figure 6.5 c)). Upon increasing Sr²⁺ concentration, particle size greatly decreased (Figure 6.5 d)). Coating thickness on substrates pretreated to either temperature without Sr²⁺ was also determined using SEM (Figure 6.6). Despite the formation of increased MgO after heat treatment to 400°C, coating thickness was similar for both conditions prepared without Sr²⁺. Similar trends in coating thickness were observed for coatings prepared with 5 and 10% Sr.

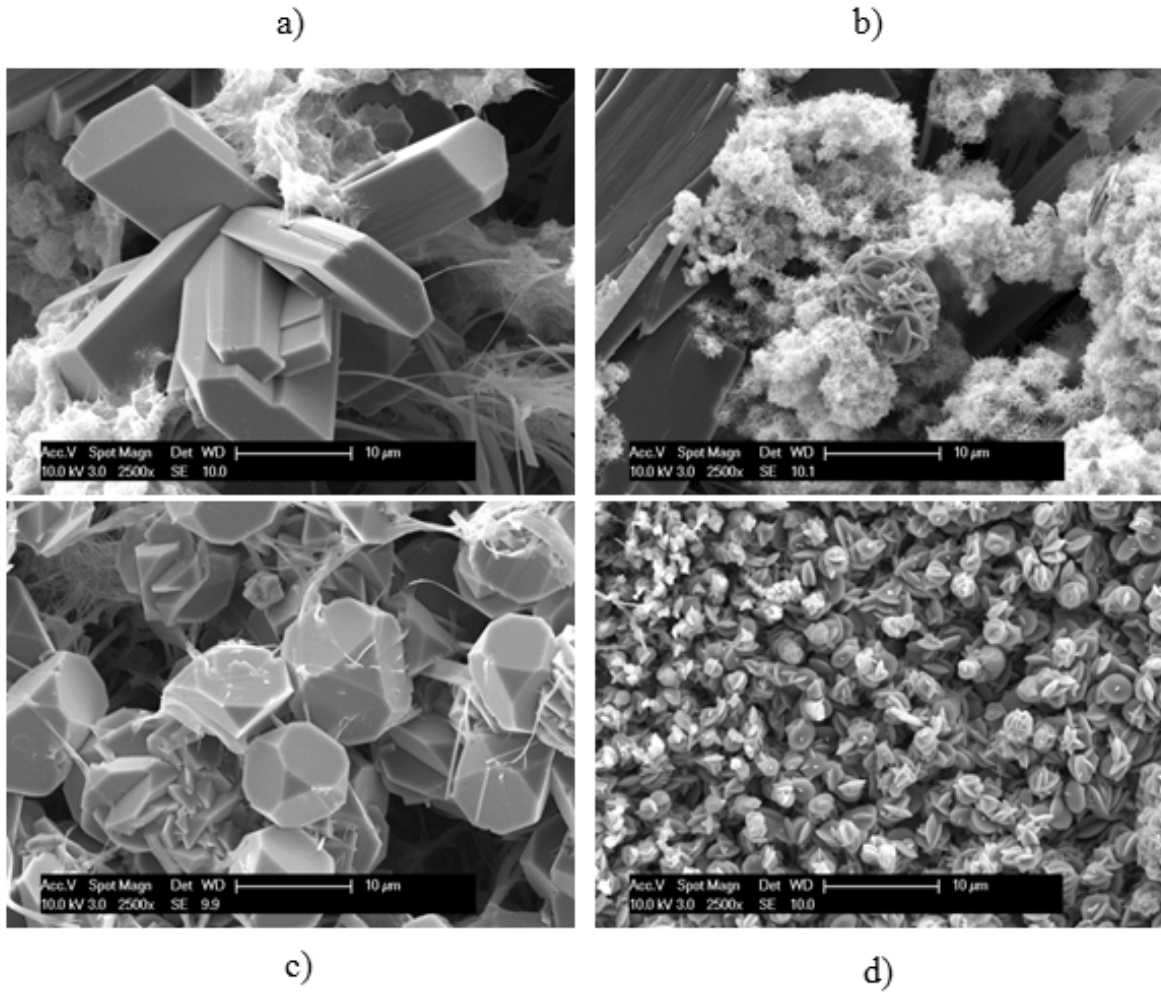


Figure 6.5 The morphology of CaP coatings formed on substrates pretreated to 350°C prepared with a) no Sr and b) 10% Sr; substrates pretreated at 400°C with c) no Sr and d) 10% Sr.

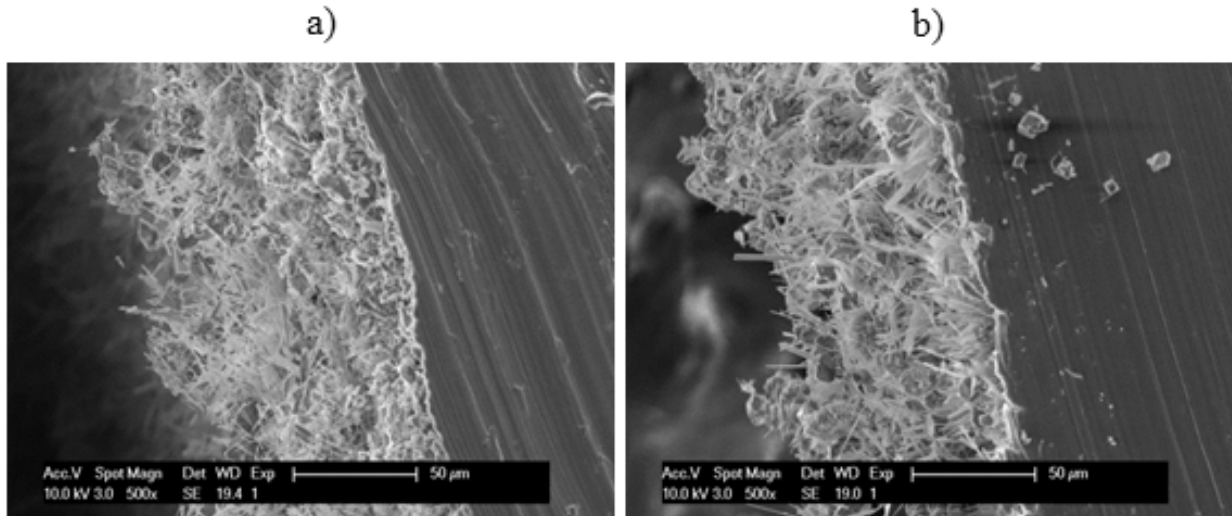


Figure 6.6 The thickness of CaP coatings formed on substrates pretreated to a) 350 and b) 400°C with no Sr.

6.3.3 Corrosion Protection

6.3.3.1 Hydrogen Evolution and Immersion Test

Upon exposure to aqueous environments, Mg alloys are known to corrode rapidly forming $\text{Mg}(\text{OH})_2$ and releasing H_2 gas as corrosion products. As a result, the rate at which H_2 is released and the total amount of H_2 generated are commonly used to study the corrosion behavior of Mg alloys [199]. HBSS without serum proteins was used for H_2 evolution experiments in order to study coated samples in an environment where corrosion occurs rapidly. A relatively large volume of HBSS to substrate surface area of 0.1 l cm^{-2} was used in order to minimize the risk of saturation of Mg^{2+} . In comparison to bare AZ31, all coated samples generated much less hydrogen over a one week period (Table 6.6). Unfortunately, the difference in the amount of H_2 generated between coated samples varied by less than 0.2 ml, despite the use of HBSS without serum proteins. As a result, based on the amount of H_2 generated alone, the role of either

pretreatment or Sr²⁺ doping on the capability of CaP coatings to act as a protective layer cannot be determined. However, it can be concluded that CaP coated samples corroded much less than bare AZ31 substrates.

Table 6.6 Corrosion data collected from hydrogen evolution experiments and potentiodynamic polarization tests. Three repeats for each condition were performed for electrochemical corrosion experiments.

	H₂ Generated (mL)	E_{corr}(V)	I_{corr}(μA/cm²)
AZ31	2.70	-1.50 ± 0.04	3.02 ± 1.69
Sr0-350	0.60	-1.49 ± 0.01	0.48 ± 0.06
Sr5-350	0.60	-1.48 ± 0.06	0.54 ± 0.10
Sr10-350	0.70	-1.44 ± 0.05	0.23 ± 0.19
Sr0-400	0.80	-1.44 ± 0.03	0.26 ± 0.02
Sr5-400	0.85	-1.48 ± 0.06	0.34 ± 0.05
Sr10-400	0.60	-1.50 ± 0.01	0.46 ± 0.09

The amount of Mg²⁺ released and the pH for both coated and bare substrates were measured after immersion in DMEM containing serum proteins. Media was collected and refreshed every 48 h. As mentioned previously, Mg alloys are known to form a Mg(OH)₂ passivation layer as a result of Mg²⁺ ions reacting with H₂O during corrosion. The subsequent dissolution of Mg(OH)₂ results in an increase in pH. For both coated and bare substrates, pH was initially high and decreased throughout the 21 day immersion period (Figure 6.7 a)). After 4 days, the pH of media collected from coated samples stabilized at a pH of 8 while that of AZ31 remained slightly elevated. Similar to H₂ evolution experiments, the difference in pH between CaP coated groups remained relatively small. This may be due to the buffering capacity of culture media and the frequent changing of media. Further analysis of the collected culture media

by ICP showed that throughout the 21 day incubation period Mg^{2+} concentration from bare AZ31 substrates was much greater than that of coated samples (Figure 6.7 b)). Similar to pH measurements, the amount of Mg^{2+} measured decreased throughout the experiment.

The Mg^{2+} released into solution and measured by elemental analysis is due to the dissolution of the $Mg(OH)_2$ passivation layer formed in the presence of chloride containing solutions. Therefore, the measurement of Mg^{2+} in solution does not directly correlate with corrosion since the rate at which the passivation layer dissolves is much slower than the rate at which it is formed and is dependent upon the chemical stability of the resulting hydroxide. As a result, a decrease in Mg^{2+} concentration for coated samples in comparison to the bare substrate is observed for all conditions throughout the incubation period. Nonetheless, the concentration of Mg^{2+} in media is critical in determining the cytotoxicity of coated and bare substrates. The high initial Mg^{2+} concentration measured for CaP coated samples is most likely due to the exposure of the underlying bare AZ31 substrate to the surrounding culture media due to the porosity of CaP coatings and the underlying pretreated layer.

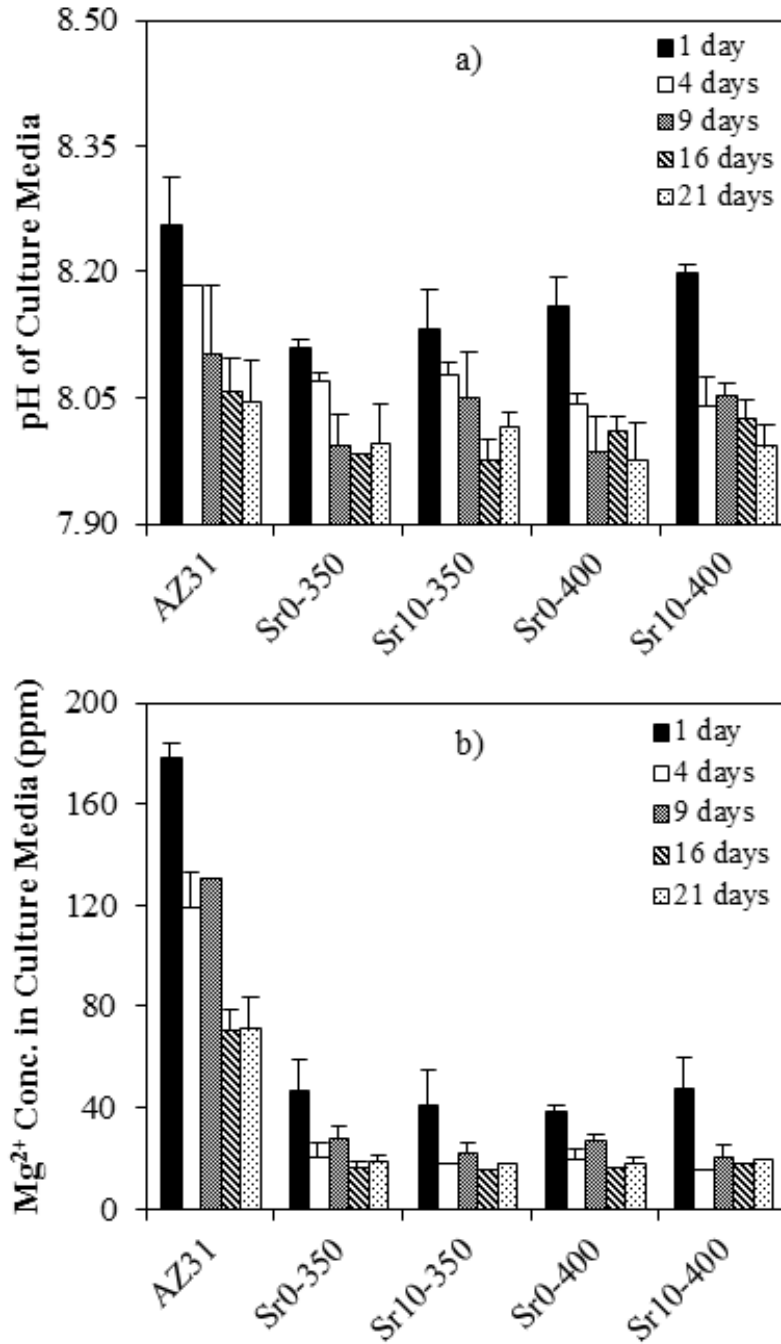


Figure 6.7 a) pH measurements and b) elemental analysis of culture media after incubation with coated and uncoated samples for up to 21 days.

6.3.3.2 Electrochemical Corrosion Testing

The H₂ evolution experiments and immersion tests both fail to provide definitive conclusions relating to the role of various pretreatments or the film composition on corrosion protection. Therefore, potentiodynamic polarization (PDP) tests were also performed in order to further assess the effect of Sr²⁺ doping and pretreatment conditions on the corrosion control. After at least 1h of stabilization in order to establish the open circuit potential (OCP), substrates were subjected to PDP testing over a range of 200 mV lower than OCP and 500 mV greater than OCP at a scan rate of 1 mV s⁻¹. It can be seen that similar to non-polarized current and voltage induced corrosion experiments, such as H₂ evolution and immersion tests, coated samples were determined to be more stable than bare AZ31 samples due to a higher anodic corrosion potential (E_{corr}) and lower corrosion current densities (I_{corr}), determined by Tafel extrapolation (Table 6.6). Interestingly, between the various Sr doped CaP coated AZ31 substrates pretreated to 350°C, corrosion resistance increased upon increasing Sr²⁺ concentration. The observed increase in corrosion protection may be due to variations in phase composition of CaP coatings upon varying Sr²⁺ concentration or the increased doping of Sr²⁺ resulting in decreased coating solubility (Table 6.5). In contrast, the corrosion resistance of CaP coated substrates deposited on AZ31 pretreated at 400°C decreased with increasing Sr²⁺ concentration. Elemental analysis by ICP (Table 6.5) indicated that the mol. % of Mg in CaP coatings formed on substrates pretreated to 400°C increased upon increasing Sr²⁺ content, while it was much lower and remained relatively constant on substrates pretreated to 350°C. Therefore, it appears that pretreatment has a greater influence on coating stability for substrates pretreated to higher temperatures. Nonetheless, in comparing the two groups, the optimum E_{corr} and I_{corr} values achieved were similar for Sr10-350 and Sr0-400.

6.3.4 In-Vitro Cytocompatibility

6.3.4.1 Live/Dead Staining

CaP coatings with similar levels of Sr^{2+} doping were prepared, despite varying pretreatment conditions. The CaP coatings formed on substrates pretreated at increased temperatures consisted of increased amounts of Mg and Zn as a result of the diffusion of alloying elements into the pretreated layer at elevated temperatures. Both pretreatment conditions and Sr^{2+} concentration were observed to influence the capability of CaP coatings to protect against corrosion of the underlying substrate in culture media containing serum proteins. To study the capability of CaP coatings to support the proliferation of MC3T3-E1 cells, live/dead staining after 3 and 7 days on both coated and uncoated substrates was performed (Figure 6.8).

Initial cell attachment and spreading on coated substrates was relatively low in comparison to MC3T3-E1 cells seeded on tissue culture plastic (Figure 6.8 a-d)). A slightly increased number of live cells were observed on samples prepared with increased Sr^{2+} concentrations. After 7 days, a substantial increase in the number of live cells was observed for all conditions (Figure 6.8 e-h)). Interestingly, slightly fewer cells were observed on samples prepared with increased Sr^{2+} concentrations. Cell morphology was observed on coated samples using SEM (Figure 6.9). The cells observed appeared broad rather than elongated and were evenly spread throughout the surface of the coated substrate after 7 days.

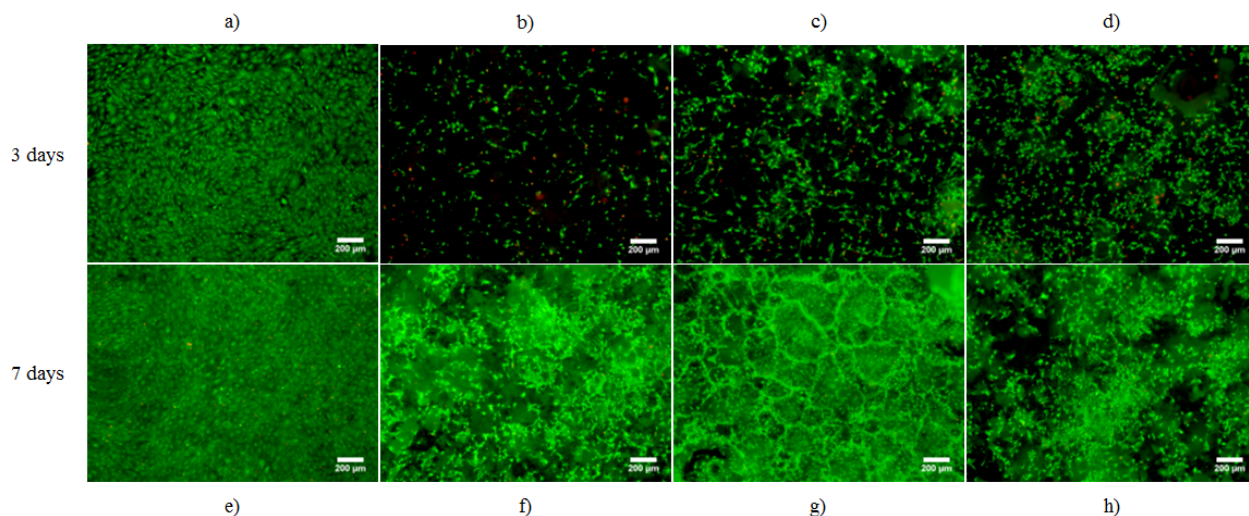


Figure 6.8 Live/dead staining on culture plastic, Sr0-350, Sr5-350, and Sr10-350 after 3 (a-d) and 7 (e-h) days of culture with MC3T3-E1 cells.

The initial low live cell attachment on coated samples, in comparison to tissue culture plastic, suggests that many of the seeded cells did not attach. For bare AZ31 this is expected due to the rapid corrosion resulting in increased Mg^{2+} concentration and the release of hydrogen upon initial contact with cell culture media prior to passivation. For coated samples, initial attachment also remained low despite the fact that a passivation and coating layer had been formed prior to exposure to cell culture media. Nonetheless, cells which attached to coated substrates proliferated rapidly between 3 and 7 days.

6.3.4.2 DNA Concentration

To further study the capability of CaP and Sr^{2+} doped CaP coatings to support the proliferation of osteoblast-like cells in comparison to bare substrates, MC3T3-E1 mouse preosteoblasts were cultured on coated and bare substrates for 3 and 7 days prior to measuring DNA concentration (Figure 6.10 a)). After 3 days of culture, coatings prepared with no Sr^{2+} on substrates pretreated

to 350°C supported significantly enhanced cell proliferation in comparison to uncoated AZ31 and coatings prepared with 5 and 10% Sr on substrates pretreated to 400°C. After 7 days, a substantial increase in DNA concentration was observed for all conditions. Once again, elevated DNA concentrations were measured on CaP coated substrates prepared without Sr²⁺ and significant increases in DNA concentration in comparison to uncoated AZ31 were observed for CaP coated substrates.

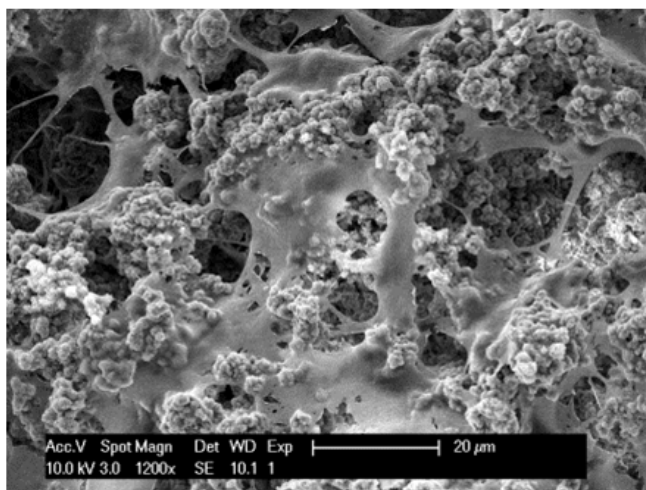


Figure 6.9 An SEM image of MC3T3-E1 cells after 3 days of culture on Sr10-350.

hMSCs were also cultured on CaP coated and bare AZ31 substrates for 3 and 7 days prior to measuring DNA concentration (Figure 6.10 b)). Similar trends in comparison to MC3T3-E1 cells after 3 days were observed. Once again, cells cultured on coatings prepared with less Sr²⁺ had elevated DNA concentrations which were near double that of bare AZ31. After 7 days of culture, DNA concentration once again substantially increased and elevated DNA concentrations were again observed on Sr0-350 coatings. In summary, minimal toxicity was observed for both cell types on CaP coated AZ31 substrates. At both time points for both cell

types, coatings prepared with reduced Sr^{2+} concentrations supported increased proliferation. Although statistically significant differences were not observed between groups pretreated to 350 and 400°C, cell proliferation on Sr0-350 coatings was increased in comparison to all other groups for all time points of interest.

6.3.4.3 Osteogenic Gene and Protein Expression

CaP and Sr doped CaP coatings are both capable of supporting MC3T3-E1 cell and hMSC proliferation with minimal toxicity. In order to study the capability of CaP and Sr doped CaP coatings to facilitate the differentiation of MC3T3-E1 cells to mature osteoblasts, the expression of osteogenic genes, osteocalcin (OCN) and osteopontin (OPN), were studied on coated and bare AZ31 substrates. OPN is a non-collagenous protein known to influence wound healing, tumorigenesis, and the mineralization of bones and teeth [168]. With respect to its role in mineralization, OPN has also been shown to regulate cell attachment to extracellular matrix including the growth of hydroxyapatite crystals within the interfibrillar spaces of the bone matrix [167]. As a result, OPN is considered a relatively early marker for osteogenic differentiation since lower levels of OPN are required for matrix mineralization to occur [18]. In contrast, OCN is a late stage marker for osteogenic differentiation and is the most abundant non-collagenous protein found in bone [200].

qRT-PCR was performed with MC3T3-E1 cells after 18 days of culture in osteogenic media (Figure 6.11 a)). Gene expression was normalized to that of cells cultured on AZ31. Among coated samples, greater levels of OPN were expressed on CaP coatings deposited on substrates pretreated to 350°C. For CaP coatings on substrates pretreated to either temperature, a slight increase in OPN expression was observed upon increasing Sr^{2+} concentration.

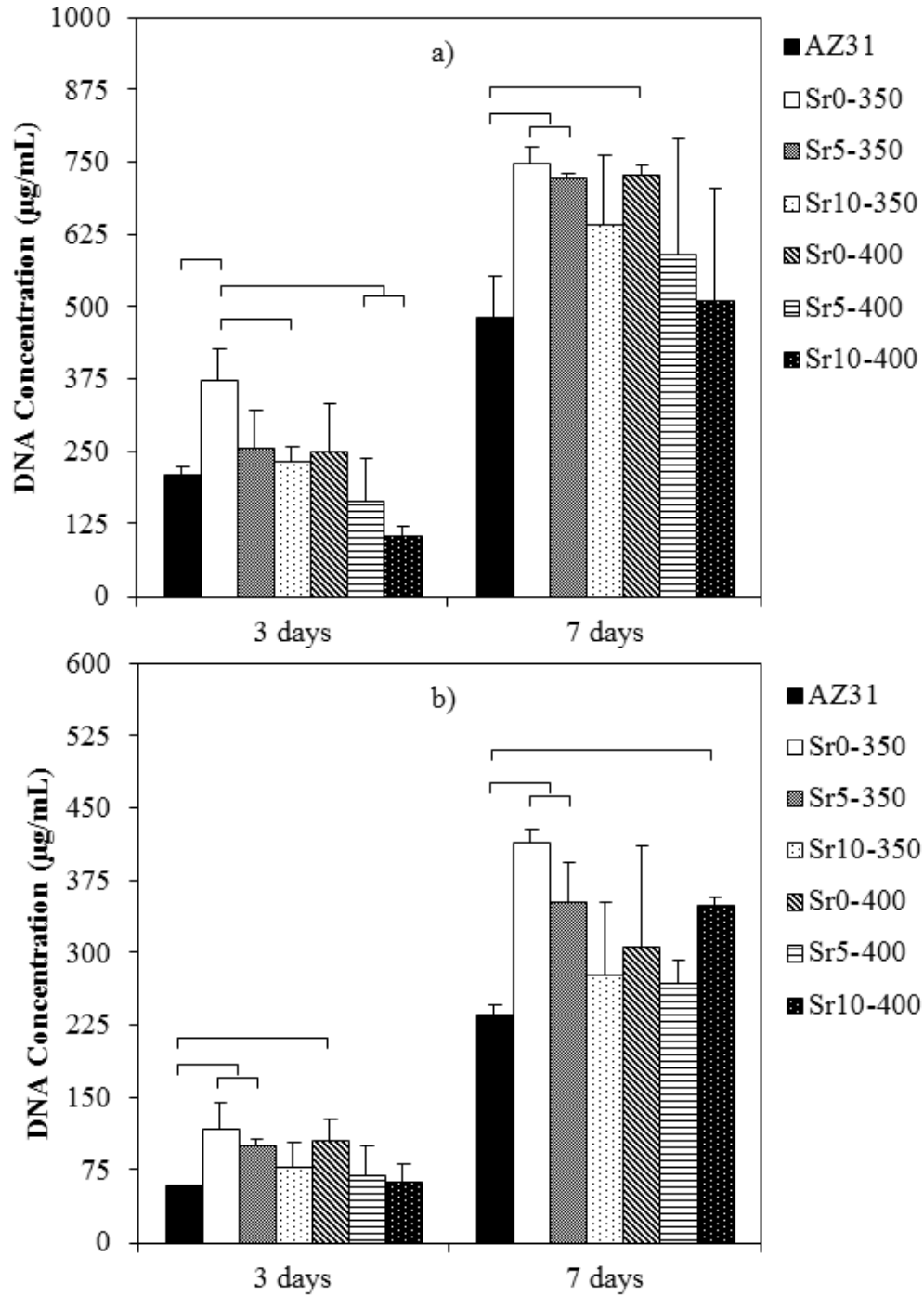


Figure 6.10 DNA concentration measured from a) MC3T3-E1 preosteoblast cells and b) hMSCs after 3 and 7 days of culture in growth media on AZ31 coated and uncoated substrates.

OPN expression on CaP coatings deposited on substrates pretreated to 400°C was similar to that of bare AZ31.

Similar to OPN, OCN expression was also slightly increased for both pretreatment conditions upon increasing Sr²⁺ concentration. Interestingly, a near tenfold greater expression of OCN was observed for samples prepared on Sr10-400 coated substrates in comparison to bare AZ31. The combination of the decreased expression of OPN, an early differentiation marker, and the elevated expression of OCN, a mature osteoblast marker, on samples prepared with 10% Sr pretreated to 400°C suggests that MC3T3-E1 cells cultured on these coatings are more mature osteoblasts in comparison to other conditions.

Osteogenic gene expression was also studied on AZ31 coated substrates using hMSCs to further analyze the capability of coatings deposited on substrates pretreated to 400°C to support enhanced differentiation (Figure 6.11 b)). In contrast to the trends observed with MC3T3-E1 cells, elevated OPN expression was observed for cells cultured on coatings prepared on substrates pretreated to 400°C rather than 350°C. A comparable OPN expression was measured for hMSCs cultured on Sr10-350 coatings in comparison to those formed on substrates pretreated to 400°C while much lower values were obtained on Sr0-350 and Sr5-350. In addition, no distinct trend upon increasing Sr²⁺ concentration was observed for OPN expression. However, a subtle increase in hMSC OCN expression was observed upon increasing Sr²⁺ concentration for both pretreatment conditions. In general, similar levels of OCN expression were measured for both groups.

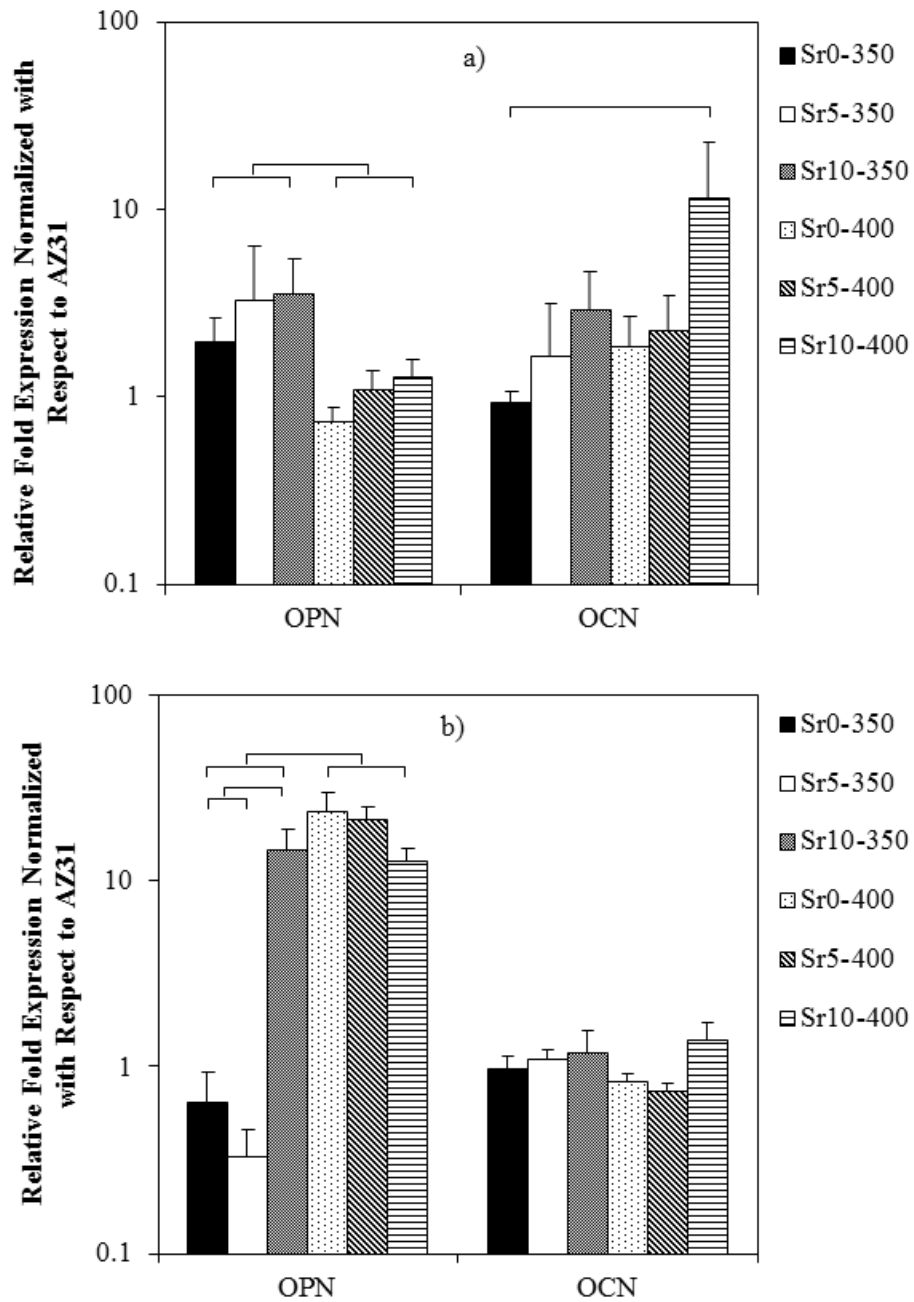


Figure 6.11 qRT-PCR gene expression data showing the expression of osteopontin (OPN) and osteocalcin (OCN) of a) MC3T3-E1 cells and b) hMSCs cultured on coated samples normalized with respect to cells cultured on bare AZ31.

The relatively low expression of OCN, a mature osteoblast marker, for hMSCs cultured on CaP coated AZ31 substrates in comparison to bare AZ31 suggests that hMSCs cultured on these coated samples have not differentiated into mature osteoblast and are yet to mineralize their extracellular matrix [18]. Therefore, the enhanced expression of OPN, an earlier marker for osteoblastic differentiation, on coatings deposited on substrates pretreated to 400°C suggests that these coatings may promote the osteogenic differentiation of hMSCs rather than those prepared with similar Sr²⁺ concentrations on substrates pretreated to 350°C. While this was more obvious for hMSCs cultured on samples prepared with 0 and 5% Sr, similar OPN and OCN values were obtained for both pretreatment conditions for hMSCs cultured on coatings prepared with 10% Sr.

The intracellular concentration of OCN in hMSCs cultured on coated samples after 18 days in osteogenic media was determined using a Luminex instrument (Figure 6.12). Similar to the trends observed in hMSC gene expression, comparable levels of OCN were measured for most conditions. Interestingly, a distinct trend with increasing OCN expression upon increasing Sr²⁺ concentration was also observed regardless of the pretreatment temperature and a statistically significant increase in OCN concentration was observed between hMSCs cultured on Sr0-400 and Sr10-400 coatings.

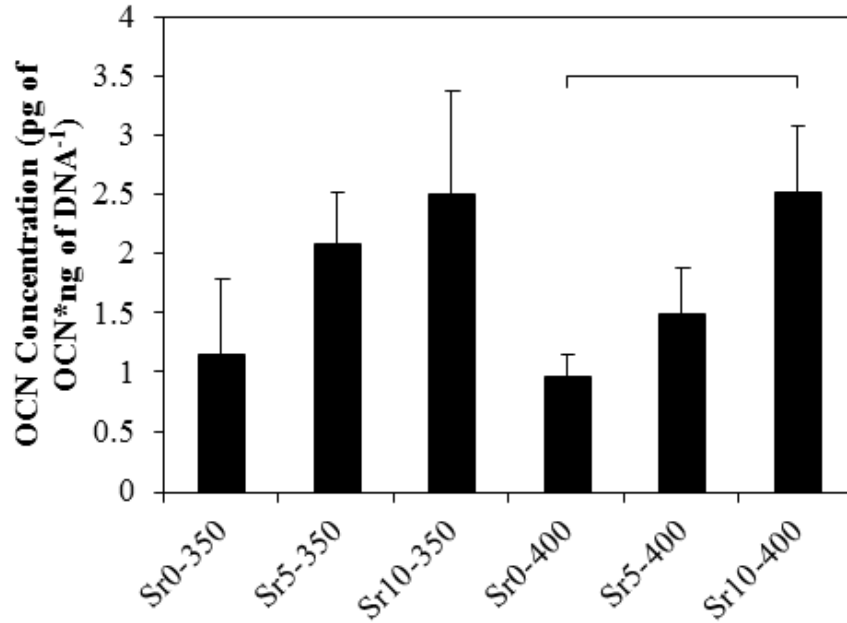


Figure 6.12 Osteocalcin (OCN) concentration measured from lysed hMSCs after 18 days of culture in osteogenic media.

Coatings prepared with reduced Sr²⁺ concentrations were observed to support increased cell proliferation for both cell types. In contrast, increased Sr²⁺ concentrations supported the increased expression of osteogenic markers for both cell types. MC3T3-E1 cells and hMSCs are both known to possess Ca²⁺ sensing receptors (CaSRs) and recent publications have shown that Sr²⁺ is capable of increasing the expression of bone morphogenic protein 2 (BMP-2) and OCN through Wnt and MAPK signaling pathways by activating CaSRs [123, 159, 201]. Although coatings deposited on substrates pretreated to both temperatures retained similar amounts of Sr²⁺ (Table 6.5), increased levels of differentiation were observed for MC3T3-E1 cells cultured on coatings deposited on substrates pretreated to 400°C rather than 350°C. A similar trend was also observed for hMSCs, except for samples prepared with 10% Sr. Therefore, this data suggests that, in addition to Sr²⁺ doping, pretreatment conditions of AZ31 substrates also influence osteogenic differentiation. As a result, further work is needed to optimize pretreatment

conditions prior to depositing CaP coatings to enhance not only coating stability and corrosion protection, but also cytocompatibility.

6.4 CONCLUSIONS

In the current Chapter, CaP coatings with various levels of Sr^{2+} doping were formed on Na_2HPO_4 pretreated AZ31 heat treated to either 350°C or 400°C . Heat treatment to 400°C resulted in the formation of greater amounts of MgO and increased diffusion of Zn into the pretreated layers prior to the deposition of CaP coatings. The CaP coatings formed consisted of biphasic mixtures of HA and β -TCP with increased HA formed upon increasing Sr^{2+} concentration. The corrosion protection offered by CaP coatings was influenced by both the Sr^{2+} concentration and the pretreatment conditions.

Sr^{2+} doping was observed to reduce the proliferation of both MC3T3-E1 cells and hMSCs on coated substrates but increased the level of osteogenic differentiation due to the upregulation of OCN gene and protein expression in MC3T3-E1 cells and hMSCs, respectively. The coatings formed on substrates pretreated to 400°C also supported increased differentiation in comparison to those formed on substrates pretreated to 350°C . As a result, it can be concluded that both Sr^{2+} doping and pretreatment conditions influence the capability of CaP coatings to provide corrosion protection and further to also support osteogenic differentiation on biodegradable Mg alloys. It can also be concluded that Mg^{2+} ions did not influence the variation in osteogenic differentiation, in contrast to the trends observed in Chapters 3, 4, and 5 since similar amounts of Mg^{2+} were measured in the culture media surrounding the coated substrates. The favorable response of osteoblast progenitor cells to CaP coatings prepared with Sr^{2+} on AZ31 substrates suggests that

Sr^{2+} substitution may also be useful in various other clinically relevant forms of calcium phosphate for bone used for tissue regeneration. As previously discussed, CaP systems have been explored in various forms for clinical application in addition to bulk scaffolds and coatings. Therefore, the capability of Sr^{2+} to enhance the properties of a HA forming self-setting cement will be discussed in detail in Chapter 7.

7.0 MURINE OSTEOBLASTIC AND OSTEOCLASTIC DIFFERENTIATION ON STRONTIUM RELEASING HYDROXYAPATITE FORMING BONE CEMENTS

7.1 INTRODUCTION

Sr^{2+} substituted CaPs have shown promise in the development of synthetic bone graft substitutes [159, 202]. This is primarily due to the capability of Sr^{2+} ions to stimulate the differentiation of osteoblast progenitor cells, limit osteoclastic resorption, and enhance the radiopacity of CaPs [119]. To improve the clinical application of Sr^{2+} substituted CaP based scaffolds, self-setting Sr^{2+} substituted HA and DCPD forming cements have been developed [203]. HA forming CaP cements are traditionally of greater interest due to their less acidic setting reaction and improved mechanical properties in comparison to DCPD forming cements. HA forming cements have also been prepared using a wide range of CaP precursors. However, they are most commonly prepared either by the hydrolysis of α -TCP or by an acid-base reaction between TTCP and either DCPA or DCPD [72, 101].

To date, the majority of work reported on Sr^{2+} substituted HA forming cements has been with formulations prepared using α -TCP rather than TTCP and either DCPA or DCPD. Schumacher et. al prepared Sr^{2+} releasing HA forming cements using α -TCP and DCPA with mixtures of CaCO_3 and SrCO_3 forming either Sr^{2+} substituted HA or clusters of SrCO_3 within a HA matrix [124, 133]. The capability of these cements to support the proliferation and

differentiation of human mesenchymal stem cells was also demonstrated. $\text{SrCl}_2 \cdot 6\text{H}_2\text{O}$ has also been used to introduce Sr^{2+} ions to HA forming cements prepared using α -TCP [204, 205]. In both cases, the incorporation of Sr^{2+} into the HA crystal structure, which is necessary for the sustained release of Sr^{2+} ions, is dependent upon the relative solubility of Sr^{2+} containing precursors with respect to α -TCP and the participation of Sr^{2+} in the reprecipitation process occurring during cement formation. Therefore, the use of Sr^{2+} directly substituted into CaP precursors, which are directly involved in the cements setting reaction, may be a more efficient and promising route to incorporate Sr^{2+} ions into the HA crystal structure during the cement setting reaction in comparison to using Sr^{2+} containing salts. This approach has previously been explored using Sr^{2+} substituted α -TCP [206].

In one of the few reports where Sr^{2+} substituted HA forming cements were prepared using TTCP and either DCPA or DCPD rather than α -TCP, Guo et. al prepared SrHPO_4 (DSP) by precipitation and studied the cements formed using ternary mixtures of TTCP, DCPA, and DSP [203]. As a result of the varying solubility and particle sizes of DSP and DCPA, unreacted DSP was detected in the cements formed after up to one week in 100% humidity. Further work studying these cements indicated improved *in vitro* cytocompatibility and *in vivo* degradation when implanted intramuscularly and in a femoral defect in rabbits with increasing Sr^{2+} content [207]. However, the incorporation of Sr^{2+} ions into the HA crystal structure is once again dependent upon the relative solubility of the two acidic precursors, DCPA and DSP.

Therefore, in the current study, Sr^{2+} substituted DCPD (SrDCPD) of varying levels of substitution were prepared by precipitation reaction conducted under aqueous conditions and further reacted with TTCP to form Sr^{2+} directly substituted into HA (SrHA) forming cements. It was hypothesized that the use of SrDCPD would lead to not only the incorporation of Sr^{2+}

directly into the HA formed during the cement setting reaction, but more importantly, introduce Sr^{2+} in a very controlled manner during the acid-base reaction between TTCP and DCPD. The influence of varying the Sr^{2+} content in cement scaffolds on the setting kinetics, phase composition, and compressive strength was characterized. In addition, the capability of Sr^{2+} containing cements to support the *in vitro* osteoblastic and osteoclastic differentiation of mouse preosteoblasts and monocytes was also studied and discussed in detail in this Chapter.

7.2 MATERIALS AND METHODS

7.2.1 Synthesis of Strontium Substituted Dicalcium Phosphate Dihydrate

All reagents were acquired from Sigma-Aldrich and used in the form in which they were received. DCPD was precipitated under aqueous conditions using a method previously described [81]. Briefly, a mixture of calcium and strontium salts dissolved in DI water was added dropwise to a phosphate containing solution under constant stirring at room temperature. The mixture was then stirred for ten minutes. The precipitate formed was then centrifuged and washed using DI water. The final washing step was performed with ethanol and the precipitate was dried at room temperature under vacuum to avoid the formation of DCPA.

7.2.2 Powder Characterization

The phase composition of the powders formed after precipitation was determined using X-ray diffraction. X-ray diffraction patterns were collected using a Philips X-Pert PRO diffractometer

employing Cu K α radiation ($\lambda=1.5406 \text{ \AA}$) with a Si-detector (X'celerator). The X-ray generator was operated at 45 kV and 40 mA at a 2θ range of $10\text{-}70^\circ$ with a step size of 0.0167° and a time per step of 3s. Elemental analysis of the precipitated powders was performed using inductively coupled plasma optical emission spectrometry (ICP-OES, iCAP duo 6500, Thermo Scientific). Briefly, 10 mg of powder samples were dissolved in 3.5% HNO₃. These solutions were further diluted and analyzed using ICP-OES with known standards for Ca²⁺, Sr²⁺, and PO₄³⁻, also prepared using a 3.5% HNO₃ stock solution. Scanning electron microscopy (SEM, Philips XL30 FEG ESEM) was used to analyze the particle size and microstructure of the powders formed after precipitation. Samples were sputter coated with palladium (Cressington, 108) prior to analysis using SEM.

7.2.3 Cement Scaffold Characterization

Powder mixtures of DCPD and TTCP ($< 53 \mu\text{m}$, HIMED, Old Bethpage, NY), by weight, were prepared using a mortar and pestle. Cement pastes were formed by combining TTCP-DCPD powder mixtures with either DI water or a 1.25% Na₂HPO₄ solution using a powder to liquid ratio of 2.2 g ml^{-1} . The resulting pastes were filled into 10 mm diameter cylindrical molds and allowed to fully set at 37°C . The cement reaction between TTCP and DCPD resulting in the formation of HA is illustrated in Equation 7.1.

Equation 7.1



The initial and final setting times were determined using a Gillmore Needle Apparatus (ASTM C-266). After setting, the cements were immersed in phosphate buffered saline (PBS, Lonza, Allendale, NJ) and incubated at 37°C for up to one week. At various time points during

the one week period, samples were collected and analyzed using X-ray diffraction. Rietveld refinement was used to quantitatively analyze the phase composition (HighScore Plus, Version 3.0e) using the ICSD reference patterns for HA (22060), DCPD (16132), and TTCP (2631). The wet compressive strength of cement scaffolds after immersion in PBS was analyzed using a 2 kN load cell (Instron, Norwood, MA) and a cross head speed of 1.3 mm min⁻¹. A minimum of six repeats were performed for each condition at each time point using 6 mm diameter cylindrical scaffolds which were 12 mm long. The % porosity of cement scaffolds after immersion in PBS was determined using the formula illustrated in Equation 7.2.

Equation 7.2

$$\% \text{ porosity} = 1 - \rho_A / \rho_T$$

The true density (ρ_T) was determined using helium pycnometry (AccuPyc II 1340, Micromeritics, Norcross, GA) and the apparent density (ρ_A) was determined using an envelope density analyzer (GeoPyc, Micromeritics, Norcross, GA). A minimum of four independent repeats were analyzed for each condition.

7.2.4 Cell Culture and Maintenance

7.2.4.1 MC3T3-E1 Cell Culture

MC3T3-E1 murine preosteoblast cell line was obtained from ATCC (Manassas, VA). Cells were cultured at 37°C in 5% CO₂ and 95% relative humidity in minimum essential medium alpha (MEM α , Gibco, Grand Island, NY) containing 10% fetal bovine serum (FBS, Atlanta Biologicals, Lawrenceville, GA) and 1% penicillin streptomycin (P/S, Gibco, Grand Island, NY). During direct culture experiments, cells were seeded at a density of 50,000 cells per well directly on cement scaffolds. For indirect culture, cells were seeded on tissue culture plastic and cement

scaffolds were placed on transwell permeable supports with a pore size of 0.4 μm and a nominal pore density of 4×10^6 pores cm^{-2} (Corning, Tewksbury, MA). In both cases, samples were sterilized using ethanol and ultraviolet light. Osteogenic differentiation was induced by culturing in growth media supplemented with 0.05 mM ascorbic acid, 10 mM β -glycerophosphate, and 100 nM dexamethasone.

7.2.4.2 RAW 264.7 Cell Culture

RAW 264.7 murine monocyte cell line was also obtained from ATCC. The cells were cultured in Dulbecco's Minimum Essential Medium (DMEM, ATCC, Manassas, VA) supplemented with 10% FBS and 1% P/S at 37°C in 5% CO_2 and 95% relative humidity. Cells were seeded directly on cement scaffolds at a density of 10,000 cells per well. After 1 day of culture, the culture media was supplemented with 50 ng ml^{-1} of receptor activator of nuclear factor kappa-B ligand (RANKL, BioLegend, San Diego, CA) and was refreshed daily for the duration of the experiment.

7.2.5 MC3T3-E1 Cell Proliferation

The alamarblue cell viability assay (Invitrogen, Grand Island, NY) was used to evaluate MC3T3-E1 proliferation on cements prepared with varying elemental compositions. At the time points of interest, the growth media was replaced by 1 ml of alamarblue diluted in growth media, according to the manufacturer's protocol. Samples were then incubated with the alamarblue reagent for 6 hours. 50 μl aliquots of media were collected at the end of the incubation period and fluorescence was measured at an excitation wavelength of 540 nm and an emission wavelength of 590 nm. The cement scaffolds without cells were used as negative controls to

ensure that the release of Ca^{2+} , Sr^{2+} , and PO_4^{3-} ions into the surrounding culture media did not influence the reduction of alamarblue. The concentration of Ca^{2+} , Sr^{2+} , and PO_4^{3-} in the culture media during the viability experiment was determined using ICP-OES. Culture media samples were collected every other day and diluted in pH 7.4 tris buffer for analysis using ICP-OES using known standards.

7.2.6 Alkaline Phosphatase Activity

MC3T3-E1 cells were lysed using a commercially available lysis buffer according to the manufacturer's protocol (CellLytic M, Sigma Aldrich). 170 μl of 1 g l^{-1} p-nitrophenyl phosphate (pNPP) dissolved in 0.2 M tris buffer (SIGMAFAST™ p-Nitrophenyl phosphate tablets, Sigma Aldrich) was added to 30 μl of cell lysate. Samples were incubated at 37°C for one hour prior to stopping the reaction by adding 20 μl of 0.3 M NaOH. The concentration of p-nitrophenyl in solution after 1 hour of incubation was determined by measuring the absorbance at 405 nm. ALP activity was normalized with respect to the total protein concentration in the collected cell lysate.

7.2.7 Osteogenic Protein Expression

The intracellular expression of osteopontin (OPN) and osteocalcin (OCN) of MC3T3-E1 cells cultured on the CaP cements was quantified using a MAGPIX instrument (Luminex, Austin, TX). Cell lysates were incubated overnight at 4°C with antibody conjugated magnetic beads (EMD Millipore, Billerica, MA) according to the manufacturer's protocol. After incubation, the well contents were washed and exposed to a biotinylated detection antibody followed by streptavidin-phycoerythrin to complete the surface reaction. Protein concentrations were

determined by using known standards. Measurements were conducted in triplicate for each sample and were normalized with respect to the total protein concentration.

7.2.8 Tartarate Resistant Acidic Phosphatase (TRAP) Activity

Cell lysates were collected as previously described. 100 μ l of RAW 264.7 cell lysate, collected after 5 and 10 days of culture on cement scaffolds in the presence of RANKL, were added to 50 μ l of 5 mM pNPP in 25 mM sodium acetate/20 mM sodium tartarate at pH 4.9. Samples were incubated at 37°C for one hour prior to stopping the reaction by adding 200 μ l of 0.5 M NaOH. The concentration of p-nitrophenyl in solution after 1 hour of incubation was determined by measuring absorbance at 405 nm.

7.2.9 RAW264.7 Morphology

After 10 days of culture on the cements with varying Sr^{2+} content in the presence of RANKL, RAW264.7 cells were fixed using 4% paraformaldehyde and washed with PBS. Prior to staining, the cell membranes were permeabilized using 0.1% Triton-X diluted in PBS for ten minutes. Actin staining was performed by incubating the samples in phalloidin (Phalloidin tetramethylrhodamine B isothiocyanate, Sigma Aldrich) diluted in PBS for forty minutes. DAPI (4',6-Diamidino-2-phenylindole dihydrochloride, Sigma Aldrich) was similarly diluted in PBS and used to stain the cell nuclei according to the manufacturer's protocol. Samples were then imaged using fluorescence (Olympus CXK41).

7.2.10 Statistical Analysis

A one way analysis of variance (ANOVA) was used to determine statistical significance. The mean and standard deviation were reported. The Tukey-Kramer test was used for all pairwise comparisons and a p value < 0.05 was considered significant.

7.3 RESULTS AND DISCUSSION

7.3.1 Dicalcium Phosphate Dihydrate Characterization

X-ray diffraction was used to study the phase composition and crystallinity of the powders formed by the chemical precipitation reaction at room temperature after drying under vacuum (Figure 7.1). For all of the compositions, DCPD (JCPDS 09-0077) was the only crystalline phase detected. The increased intensity of the peak near $12^\circ 2\theta$ for all of the conditions employed in the synthesis in comparison to the reference spectra is indicative of a preferred orientation along the (020) direction. A similar preferred orientation has previously been reported when DCPD was precipitated under aqueous conditions [81, 208]. Based on these results, it appears that up to 10% Sr could be incorporated into the lattice without inducing any phase separation.

Elemental analysis of the precipitated powders was performed to more accurately determine the amount of Sr^{2+} incorporated into the DCPD crystal structure. Powder samples were dissolved in dilute acidic solutions and analyzed using ICP-OES with known standards for Ca^{2+} , Sr^{2+} , and PO_4^{3-} . Four batches for each condition were analyzed independently (Table 7.1). As expected, Sr^{2+} was not detected in undoped DCPD. However, 4.30 and 8.84% $\text{Sr}/(\text{Ca}+\text{Sr})$

values were obtained for samples precipitated with 5 and 10% Sr/(Ca+Sr), respectively. In all cases, the measured (Ca+Sr)/P ratio was also close to 1, that of DCPD, further confirming the formation of single phase DCPD.

Due to the similar ionic radii of Sr^{2+} (0.12 nm) in comparison to Ca^{2+} (0.099 nm), a relatively high retention of Sr^{2+} in the various CaP phases has been reported in comparison to other elements [118, 209]. Despite the fact that Sr^{2+} can occupy all of the Ca^{2+} sites in the DCPD crystal lattice, the majority of work reported on the ionic substitution of Sr^{2+} in CaPs has focused on HA [210]. The influence of Sr^{2+} substitution on the microstructure of DCPD particles was also analyzed since the reactant particle size and shape are known to influence the cement properties (Figure 7.2). For undoped DCPD, the characteristic broad plate like morphology of DCPD was observed (Figure 7.2 a)) [211]. The particles imaged were approximately 10-15 μm in width. A similar morphology was also observed for DCPD prepared with both 5 and 10% Sr (Figure 7.2 b) and c)). However, a slight reduction in the particle size was observed for DCPD particles prepared with 10% Sr in comparison to those precipitated either without Sr or with 5% Sr.

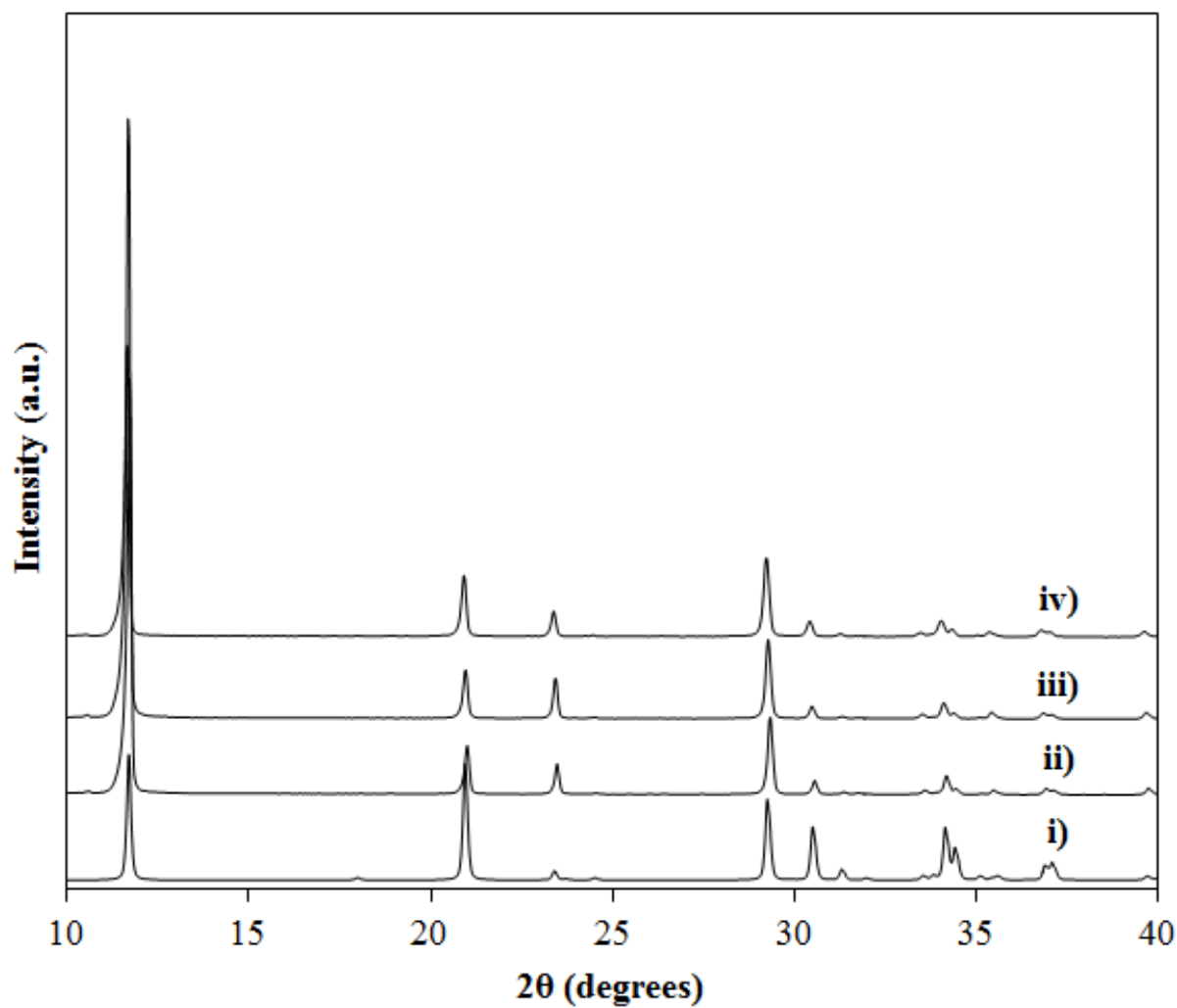


Figure 7.1 The X-ray diffraction patterns of i) DCPD (JCPDS 09-0077), ii) undoped DCPD, iii) 5% Sr DCPD, and iv) 10% Sr DCPD after drying under vacuum.

Table 7.1 The elemental compositions of DCPD precipitated with and without Sr, determined using ICP.

	Mol. % Ca	Mol. % Sr	Mol. % P	Sr/(Ca+Sr)	(Ca+Sr)/P
Undoped	50.6 ± 0.2	-	49.4 ± 0.2	-	1.02 ± 0.01
5% Sr	48.9 ± 0.3	2.2 ± 0.1	48.9 ± 0.4	4.3 ± 0.1	1.05 ± 0.02
10% Sr	45.9 ± 0.1	4.4 ± 0.0	49.7 ± 0.7	8.8 ± 0.0	1.01 ± 0.00

7.3.2 Cement Scaffold Characterization

7.3.2.1 Setting Time

Single phase DCPD with varying levels of Sr²⁺ substitution were combined with commercially available TTCP powder in a 45:55 DCPD:TTCP mixture by weight. The powder mixtures were thoroughly mixed by hand using a mortar and pestle and combined with either DI water or a Na₂HPO₄ solution using a P/L ratio of 2.2 g ml⁻¹. The resulting pastes were allowed to fully set at 37°C during which setting times were determined using a Gillmore Needle Apparatus (Table 7.2). The cements prepared using undoped DCPD set after approximately 26 minutes when using water as the liquid component. The final setting times for the undoped cements were however reduced to 6 minutes when using 1.25% Na₂HPO₄. The final setting times with both water and Na₂HPO₄ increased in comparison to undoped cements when the cements were prepared using either 5 or 10% SrDCPD. Furthermore, a similar decrease in setting time was also observed when using Na₂HPO₄ rather than water for both Sr²⁺ containing cement compositions.

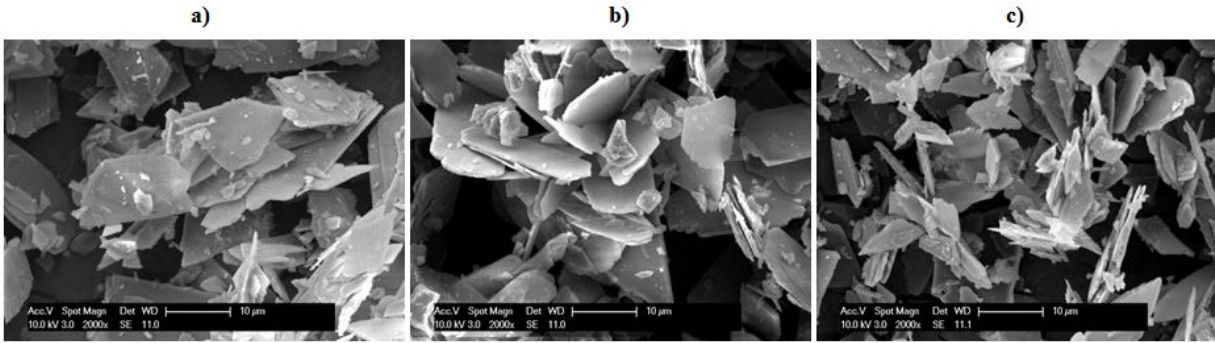


Figure 7.2 The microstructure of DCPD particles precipitated a) without Sr, b) with 5% Sr, and c) with 10% Sr.

The TTCP-DCPD setting reaction is initiated by the dissolution of DCPD particles [212]. Therefore, the use of Na_2HPO_4 rather than water accelerates the cement setting due to the enhanced solubility of DCPD under slightly basic conditions and provides the increased PO_4^{3-} concentration necessary to support the formation of apatite [84, 213]. In studying the TTCP-DCPA cement setting reaction, Greish et. al concluded that DCPA was first completely consumed while TTCP was only partially consumed, resulting in the formation of calcium deficient HA (CDHA) [214]. The subsequent further consumption of TTCP and the increasing pH then resulted in the formation of stoichiometric HA from CDHA. Therefore, the increased setting time observed upon increasing Sr^{2+} content may be due to either the reduced solubility of SrDCPD or the inhibition of CDHA formation in the presence of Sr^{2+} ions. A similar increase in setting time was observed by Guo et. al upon increasing Sr^{2+} content in the TTCP-DCPA-DSPA system using various concentrations of phosphoric acid as the liquid component [203]. The increased setting time was attributed to the inhibition of the deposition of HA by Sr^{2+} ions. However, the influence of Sr^{2+} on the solubility of DCPD is largely unexplored and the present study appears to be the first to the best of our knowledge.

Table 7.2 The setting times at 37°C for cements prepared with a 55:45 TTCP:DCPD ratio by weight and a P/L ratio of 2.2 g ml⁻¹.

	First Setting time with H ₂ O (mins)	Final Setting time with H ₂ O (mins)	First Setting time with 1.25% Na ₂ HPO ₄ (mins)	Final Setting time with 1.25% Na ₂ HPO ₄ (mins)
Undoped	18.5 ± 0.5	26.2 ± 1.8	4.0 ± 0.5	6.3 ± 0.1
5% Sr	20.3 ± 1.1	36.3 ± 3.1	6.4 ± 0.4	9.9 ± 0.8
10% Sr	33.8 ± 2.1	> 60	6.9 ± 0.3	12.0 ± 1.4

7.3.2.2 Phase Composition

To further analyze the consumption of the cement precursors and formation of HA, X-ray diffraction of the cement scaffolds after setting and after immersion in PBS, kept at 37°C, for up to one week was performed. Figure 7.3 illustrates the diffraction data collected from the samples after the final setting was reached and for all of the compositions studied. After setting, peaks indicative of the presence of unreacted DCPD (JCPDS 09-0077) and TTCP (25-1137) were clearly identified. The XRD data collected after 3 days in PBS is illustrated in Figure 7.4. After immersion in PBS for 3 days, a reduction in the intensity of DCPD peaks was clearly observed while poorly crystalline peaks indicative of the formation of increased amounts of HA (JCPDS 09-0432) were also detected. Similar peaks corresponding to unreacted TTCP were also observed.

To more quantitatively study the phase composition of the cement scaffolds both after setting and after immersion in PBS, Rietveld refinement was employed (Figure 7.5). After setting, a reduced amount of HA was detected in the cements prepared with increasing Sr²⁺ content in comparison to undoped cements (Figure 7.5 a)), which would also suggest an increase in setting time for Sr²⁺ containing cements, as was previously observed (Table 7.2). However,

after immersion in PBS a similar amount of HA was detected for all of the compositions at later time points. After setting, the wt. % of both DCPD and TTCP in Sr^{2+} containing cements increased upon increasing Sr^{2+} content due to the reduced consumption of the reactants during the initial setting reaction (Figure 7.5 b) and c)). After immersion in PBS, SrDCPD was consumed more rapidly in comparison to undoped DCPD, particularly within the first 24 hours, and little or no DCPD remained after 7 days while greater than 25 wt. % TTCP remained after 7 days for all of the compositions studied.

In the current study, a non-stoichiometric ratio of the reactants was used to enhance the influence of Sr^{2+} substitution in DCPD on the cement properties. Despite the use of excess DCPD, the complete consumption of DCPD and remaining TTCP after 7 days in PBS at 37°C suggests that large amounts of DCPD may be lost due to dissolution and do not react with TTCP. A possible explanation may be that an initial layer of HA is formed on the surface of TTCP particles which limits the diffusion of the DCPD dissolution products and retards the consumption of TTCP [215]. Increased TTCP reactivity may be achieved either by using a smaller particle size or by mechanical milling to form a thin layer of highly reactive amorphous calcium phosphate [80].

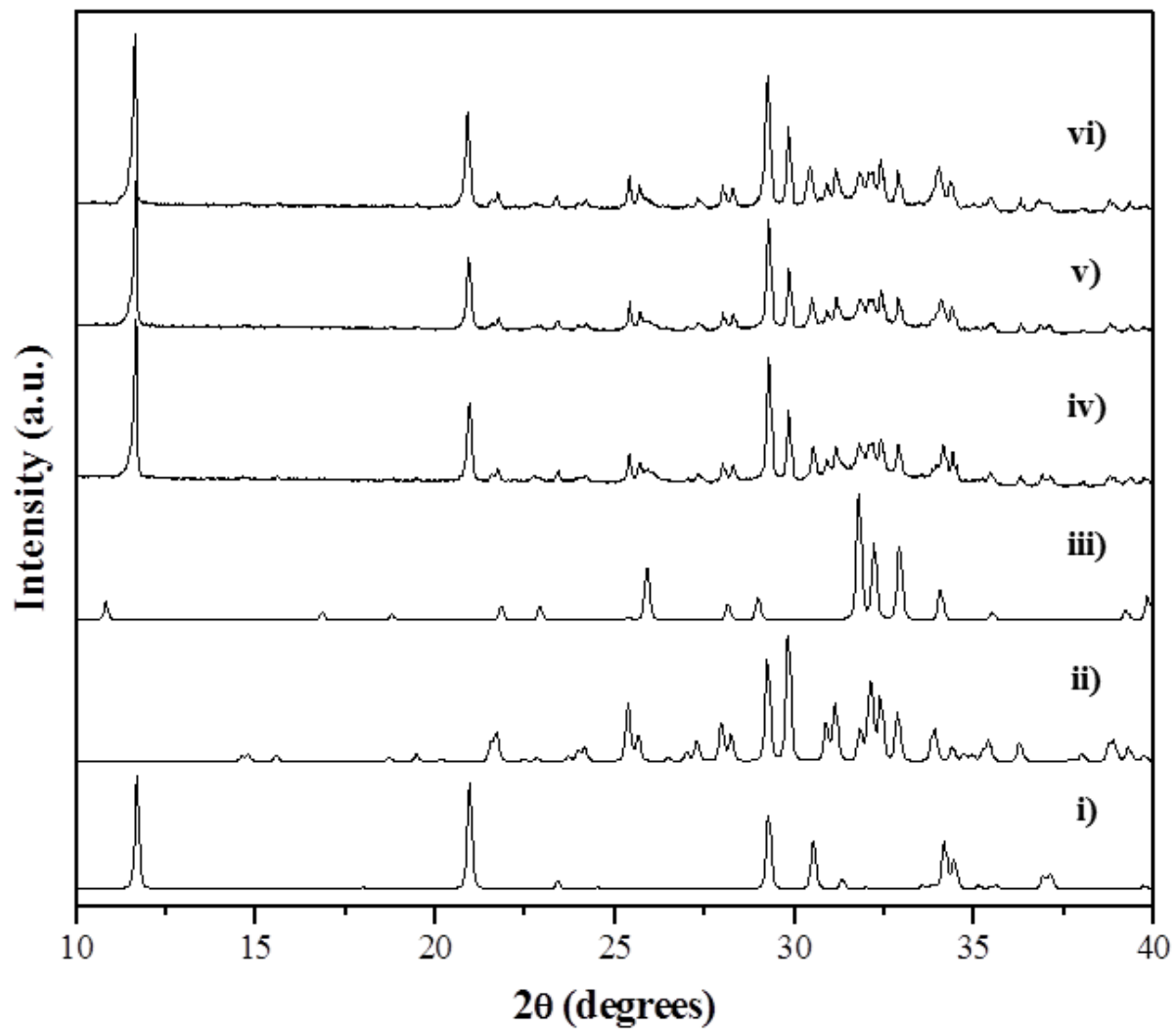


Figure 7.3 X-ray diffraction patterns of i) DCPD (JCPDS 09-0077), ii) TTCP (JCPDS 25-1137), iii) HA (JCPDS 09-0432), and cement samples after setting prepared with iv) undoped DCPD, v) 5% Sr DCPD, and vi) 10% Sr DCPD.

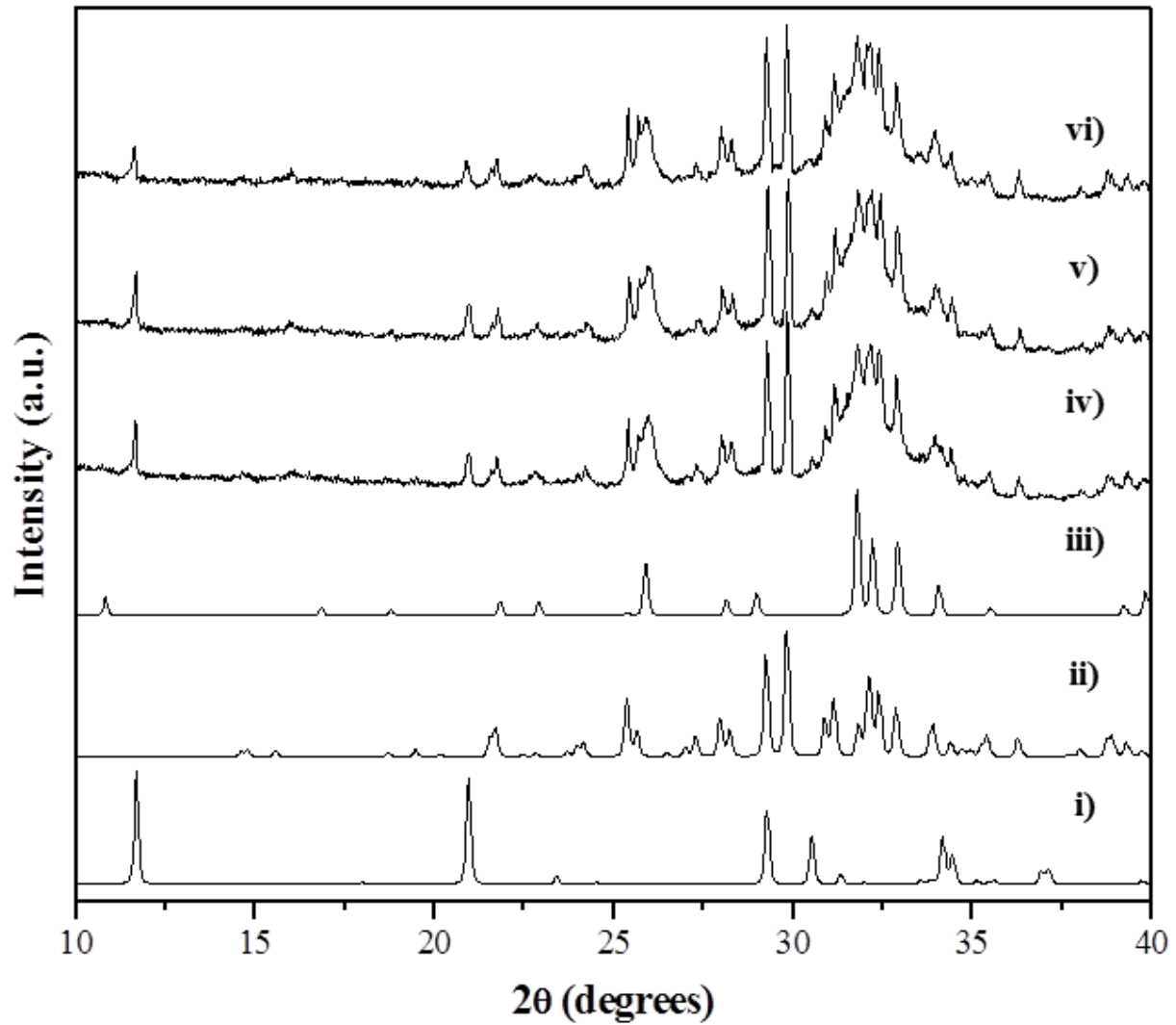


Figure 7.4 X-ray diffraction patterns of i) DCPD (JCPDS 09-0077), ii) TTCP (JCPDS 25-1137), iii) HA (JCPDS 09-0432), and cement samples after 3 days in PBS prepared with iv) undoped DCPD, v) 5% Sr DCPD, and vi) 10% Sr DCPD.

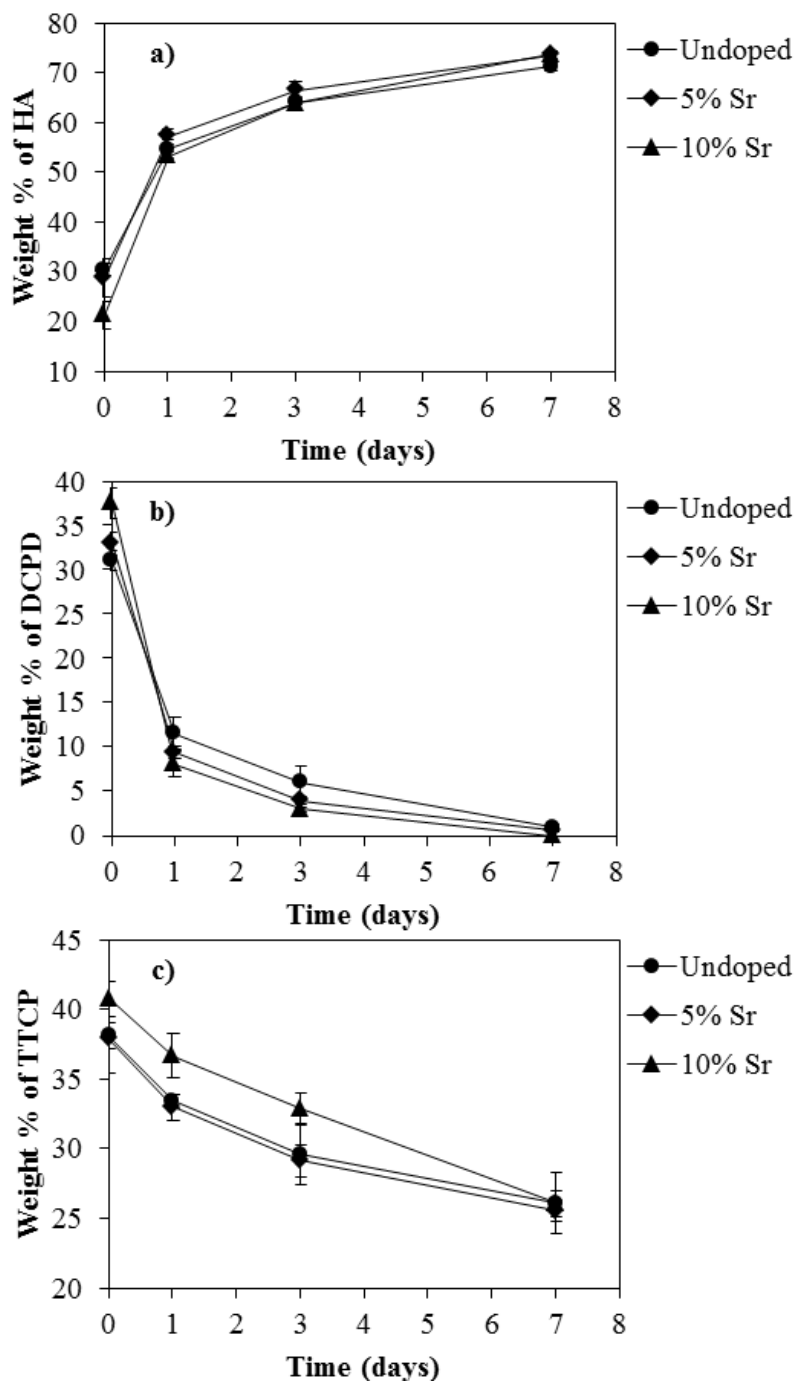


Figure 7.5 The weight % of a) HA, b) DCPD, and c) TTCP in cement samples after setting and after immersion in PBS at 37°C for 1, 3, and 7 days determined using Rietveld refinement.

7.3.2.3 Elemental Composition of Cement Scaffolds

Due to concerns of large amounts of DCPD, the Sr^{2+} containing precursor, dissolving and not reacting with TTCP to form Sr^{2+} substituted HA, an elemental analysis of the cement scaffolds following setting and after immersion in PBS for 7 days was performed (Table 7.3). After the setting reaction and after 7 days in PBS, a slight reduction in the $(\text{Ca}+\text{Sr})/\text{P}$ ratio for all the conditions was observed. With respect to the $\text{Sr}/(\text{Ca}+\text{Sr})$ value, very similar amounts of Sr^{2+} were measured for both Sr^{2+} containing compositions at either time point. After 7 days, either very little or no DCPD remained in the cement scaffolds (Figure 7.5 b)). Therefore, the similar Sr^{2+} concentration measured prior to immersion in PBS and after 7 days in PBS confirms that most of the Sr^{2+} added is retained in the scaffold despite the near complete consumption of DCPD. Based on the phase composition after 7 days (Figure 7.5), it can therefore be concluded that the Sr^{2+} retained has indeed formed SrHA. This result confirms that the use Sr^{2+} substituted CaP precursors rather than Sr^{2+} containing salts may be a useful approach to efficiently incorporate Sr^{2+} ions into HA forming cements.

Table 7.3 The elemental composition of cement powders after setting and after immersion in PBS at 37°C for 7 days.

	(Ca+Sr)/P after setting	(Ca+Sr)/P after 7 days in PBS	Sr/(Ca+Sr) after setting	Sr/(Ca+Sr) after 7 days in PBS
Undoped	1.50 ± 0.01	1.46 ± 0.01	-	-
5% Sr	1.50 ± 0.01	1.46 ± 0.01	1.30 ± 0.01%	1.34 ± 0.01%
10% Sr	1.49 ± 0.01	1.45 ± 0.01	2.68 ± 0.02%	2.65 ± 0.03%

7.3.2.4 Wet Compressive Strength and % Porosity

The compressive strength and % porosity of cement scaffolds after immersion in PBS for 24 hours and 7 days was also determined to correlate the phase composition with mechanical properties (Table 7.4). Preformed cylindrical samples were tested immediately following removal from PBS. After 24 hours of immersion in PBS, a compressive strength of 6.51 MPa was measured for the undoped cements while values of 5.74 and 4.73 MPa were obtained for cements prepared with 5 and 10% SrDCPD, respectively. After 7 days however, the compressive strength for all the conditions increased due to the enhanced formation of HA (Figure 7.5). Comparable values were obtained for the cements prepared with both undoped and 5% SrDCPD while a slightly increased compressive strength was measured for samples prepared using 10% SrDCPD although the amount of HA formed appeared to be quite similar (Figure 7.5).

Table 7.4 The wet compressive strength and % porosity of cement samples after incubation in PBS at 37°C for 1 and 7 days. The % porosity was calculated using the formula $1-(\rho_A/\rho_T)$, where ρ_A is the apparent density and ρ_T is the true density.

	CS After 1 day in PBS (MPa)	CS After 7 days in PBS (MPa)	% Porosity After 1 day in PBS	% Porosity After 7 days in PBS
Undoped	6.51 ± 0.96	8.84 ± 0.82	49.1 ± 1.6	50.8 ± 0.9
5% Sr	5.74 ± 1.23	8.55 ± 1.12	49.6 ± 0.4	51.9 ± 1.0
10% Sr	4.73 ± 0.36	10.94 ± 2.33	40.8 ± 1.3	40.4 ± 0.1

The typical range of compressive strength values obtained for CaP cements is known to be within 10-100 MPa. That of trabecular bone, which cement scaffolds are in direct contact with when implanted *in vivo*, is also approximately 10 MPa [83]. In many studies, cement pastes are

compressed prior to setting which is known to reduce the inherent porosity, thus increasing the compressive strength [216]. In the current study, cement pastes were not compressed prior to setting and despite that, compressive strength values similar to trabecular bone were achieved. To further analyze the cement scaffolds, the % porosity was determined by measuring ρ_T and ρ_A after 24 hours and 7 days in PBS (Table 7.4). As expected from the compressive strength results, the cements prepared with undoped and 5% SrDCPD had an increased porosity at both time points in comparison to those prepared with 10% SrDCPD.

The reduced porosity and increased compressive strength for cements prepared with 10% SrDCPD may be due to the slightly reduced DCPD particle size with increasing Sr^{2+} content (Figure 7.2). In the TTCP-DCPA cement system, a 10:1 TTCP:DCPA ratio in particle size was found to form cements with the best mechanical stability [80]. While the optimum particle size ratio for the TTCP-DCPD system is not known, the reduced particle size of 10% SrDCPD may be closer to the optimum particle size ratio to obtain increased mechanical stability. Nevertheless, similar compressive strength values to trabecular bone were obtained for the cements formed. Despite the near 50% total porosity, the scaffolds formed for all conditions were stable under aqueous conditions. The relatively high porosity may lead to increased protein adsorption upon exposure to physiological fluids which may support increased cell attachment and proliferation.

7.3.2.5 MC3T3-E1 Proliferation

MC3T3-E1 cells were seeded directly on the pre-formed cement scaffolds and cultured for up to two weeks in growth media to determine whether or not the cement scaffolds would support proliferation. Cell proliferation was quantified using the alamarblue assay at various time points (Figure 7.6). After 1 day, similar levels of proliferation were measured for all the conditions.

After 3 days, an increase in proliferation was clearly measured in comparison to 1 day for all of the groups and a slight increase in fluorescence intensity was measured on cements prepared with increasing Sr^{2+} content. At later time points, a statistically significant increase in proliferation was measured on cements prepared with 10% SrDCPD in comparison to all other groups. This data thus suggests that the cements prepared with up to 10% SrDCPD support greater proliferation in comparison to the undoped cements while similar levels of proliferation were observed for cements prepared with 5% SrDCPD and undoped DCPD.

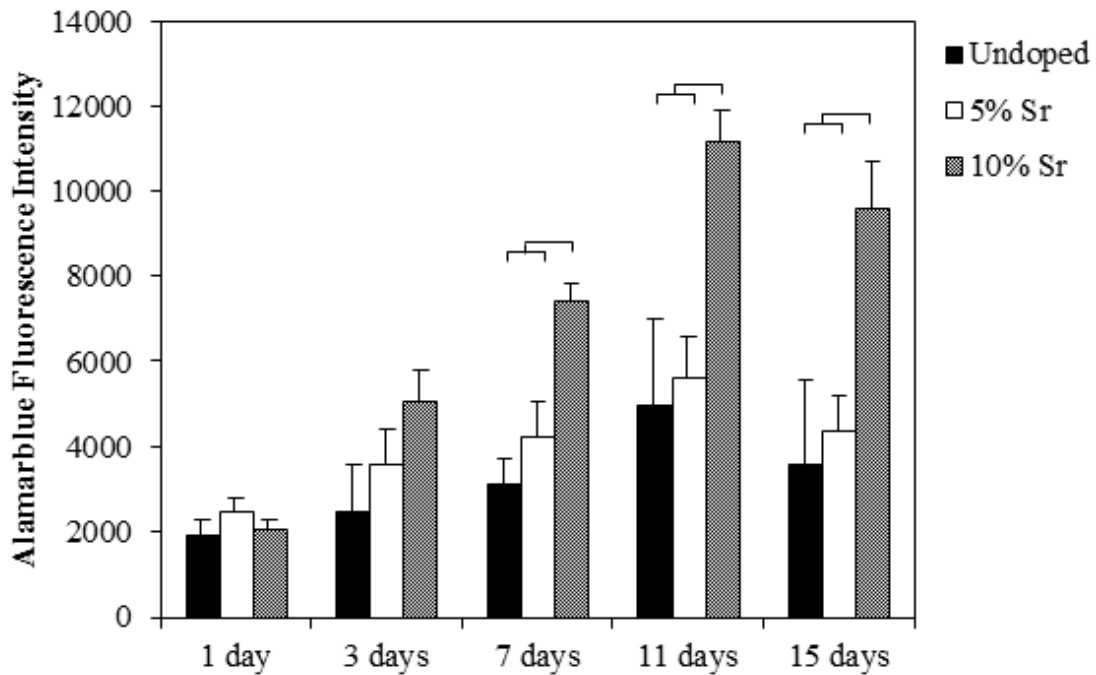


Figure 7.6 MC3T3-E1 cell proliferation determined using the alamarblue assay after culturing on cements prepared using undoped, 5, and 10% Sr DCPD for up to 15 days in growth media.

Sr^{2+} has previously been reported to stimulate the proliferation of both osteoblasts and mesenchymal stem cells [119, 158]. It has also been demonstrated to influence the cellular processes through interactions with the calcium sensing receptor (CaSR) resulting in an

increased gene expression of *c-fos* and *egr1*, which are both involved in the regulation of osteoblast proliferation [217]. Therefore, it is not surprising that cements prepared with increased Sr^{2+} stimulated the increased proliferation of mouse preosteoblast cells. However, Sr^{2+} concentrations greater than 1 mM have been shown to suppress the proliferation of mesenchymal stem cells drastically [124]. Therefore, based on these results it can be concluded that amounts of Ca^{2+} , Sr^{2+} , and PO_4^{3-} released into the culture media from these HA forming cements prepared using a non-stoichiometric ratio of TTCP and SrDCPD are non-toxic to MC3T3-E1 cells.

7.3.2.6 Ionic Concentrations in Media

During the cell proliferation experiments, the culture media was collected on the days it was changed and analyzed. The pH and concentrations of Ca^{2+} , Sr^{2+} , and PO_4^{3-} in the culture media were measured (Figure 7.7). Despite the use of excess DCPD, it is important to note that the pH remained slightly basic and similar to physiological conditions throughout the experiment for all the conditions studied (Figure 7.7 a)). The basal concentrations of Ca^{2+} and PO_4^{3-} in the MC3T3-E1 growth media were approximately 1.7 and 0.9 mM, respectively. After 1 day of incubation with cement samples, Ca^{2+} concentration was approximately 1 mM for all the conditions and gradually decreased throughout the 15 day culture period (Figure 7.7 b)). A sustained release of Sr^{2+} ranging from 0.02-0.05 mM during the culture period was observed for cements prepared with SrDCPD (Figure 7.7 c)). In contrast to Ca^{2+} concentration, a gradual increase in PO_4^{3-} concentration was also observed throughout the culture period (Figure 7.7 d)).

The reduced Ca^{2+} concentration from basal levels suggests that mineral was deposited from the culture media onto the surface of the cement samples throughout the two week experiment. Although PO_4^{3-} was also consumed during mineral formation, the increase in PO_4^{3-} concentration from basal levels is most likely due to dissolution of excess DCPD since a non-

stoichiometric amount of DCPD was used and little or no DCPD was detected after 7 days during immersion in PBS (Figure 7.5 b)). Although either very little or no DCPD remained after 7 days in PBS, a sustained release of Sr^{2+} was detected at time points greater than 7 days in culture media. This result is most likely due to different rates of dissolution of the various calcium phosphate phases in the presence of culture media containing Ca^{2+} and serum proteins in comparison to PBS, which did not contain either Ca^{2+} or serum proteins [218].

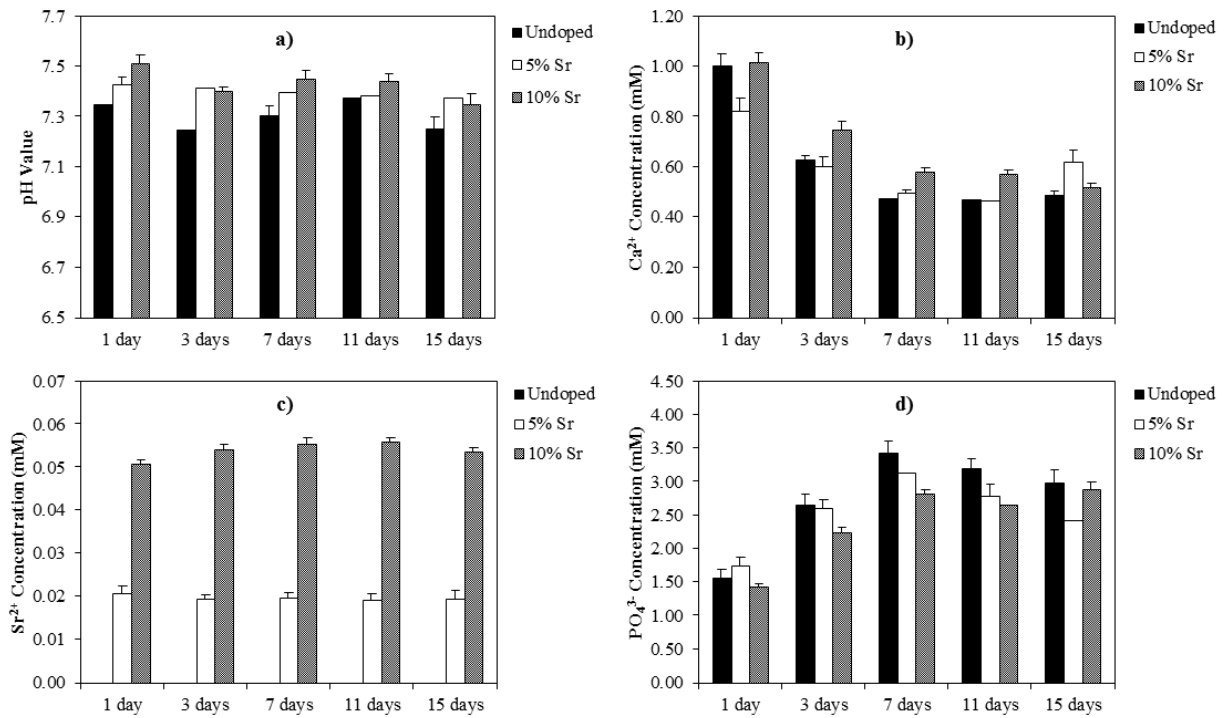


Figure 7.7 The a) pH and concentrations of b) Ca^{2+} , c) Sr^{2+} , and d) PO_4^{3-} in culture media during MC3T3-E1 viability experiments on cements prepared with undoped, 5% Sr, and 10% Sr DCPD.

In a study where postmenopausal women were treated with strontium ranelate, the baseline concentration of Sr^{2+} in serum was $0.3 \mu\text{M}$ and after three months of treatment it had risen to $117.9 \mu\text{M}$ [219]. Previous work by Schumacher et. al has also shown that with human mesenchymal stem cells a slight increase in proliferation was observed when cells were cultured

in media containing up to 0.1 mM of Sr^{2+} [124]. In the same study, with respect to osteogenic differentiation, increased ALP activity was observed at earlier time points for mesenchymal stem cells cultured in osteogenic media containing between 0.01-0.1 mM Sr^{2+} , which is similar to the serum concentration observed during strontium ranelate treatment. Although MC3T3-E1 cells were used in the current study, the amount of Sr^{2+} released into culture media throughout the experiment from cement scaffolds is well within the optimum range of Sr^{2+} concentration to support likely both mesenchymal stem cell proliferation and differentiation based on the previously published data.

7.3.2.7 MC3T3-E1 Osteogenic Differentiation

After confirming that Sr^{2+} containing cements were capable of supporting MC3T3-E1 proliferation and released sufficient amounts of Sr^{2+} that may also support osteogenic differentiation, MC3T3-E1 differentiation was evaluated by measuring ALP activity and the intracellular concentrations of OPG and OCN. The ALP activity of cells cultured for 10 and 21 days in osteogenic media seeded directly on pre-formed cement scaffolds is illustrated in Figure 7.8 a). Similar to the results observed from the alamarblue proliferation assay, comparable levels of ALP activity were observed between all groups at earlier time points. However, after 21 days increased levels of ALP activity were measured from cells cultured on cements prepared with both 5 and 10% SrDCPD in comparison to undoped cements. A near 50% increase in comparison to undoped cements was observed for the cells cultured on cement scaffolds prepared with 10% SrDCPD.

The expression of two osteogenic proteins, OPG and OCN, was measured after 21 days to further assess osteogenic differentiation on cements prepared with varying amounts of Sr^{2+} (Figure 7.8 b)). For cells cultured directly on cement substrates, significantly increased levels of

OPG were measured on cements prepared with both 5 and 10% SrDCPD in comparison to undoped cements. A similar trend was also observed in OCN expression after 21 days. Elevated levels of OCN were measured on cements prepared with 5 and 10% SrDCPD while much lower concentrations of OCN were measured on undoped cements.

The capability of Sr²⁺ containing cements to support osteogenic differentiation may be due to either the chemical or physical cues provided by the scaffold during direct culture. Therefore, to study osteogenic differentiation in the absence of physical contact with cement substrates while maintaining similar ionic concentrations to direct cell culture experiments, permeable transwell inserts were used. ALP activity and the expression of OPG and OCN after 21 days in osteogenic media were once again determined. In contrast to the results observed during direct culture experiments, similar levels of ALP activity were measured for cells cultured indirectly with all cement compositions after both 10 and 21 days (Figure 7.8 c)). OPG and OCN concentration after 21 days also exhibited similar trends to those observed for ALP activity where a comparable expression of both osteogenic proteins was observed for all the conditions (Figure 7.8 d)).

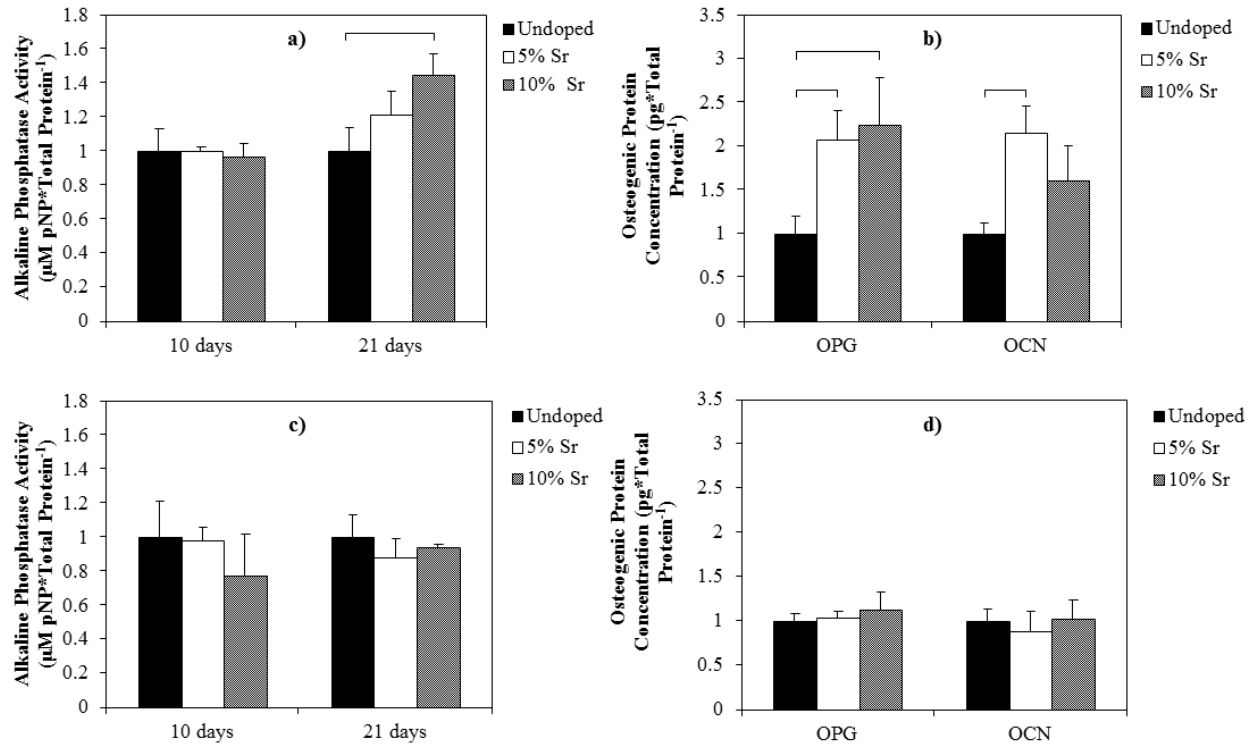


Figure 7.8 Alkaline phosphatase activity and osteogenic protein expression after 21 days of MC3T3-E1 cells cultured a)-b) directly on cement scaffolds and c)-d) indirectly with cement scaffolds in osteogenic media.

This data suggests that cells cultured directly on cement scaffolds prepared with Sr^{2+} experience increased levels of differentiation either due to the microstructure of Sr^{2+} containing cement scaffolds or the increased local Sr^{2+} concentration cells are exposed to near the scaffold surface. Sr^{2+} ions are known to interact with cells through either the CaSRs or non-selective Ca^{2+} channels which may initiate Wnt and other signaling pathways that regulate osteogenic differentiation [141]. However, in addition to Ca^{2+} , PO_4^{3-} , and Sr^{2+} concentration, CaP microstructure has also been demonstrated to influence cell proliferation and differentiation [220]. Therefore, to further assess the role of Sr^{2+} release and scaffold microstructure in supporting osteogenic differentiation, the blocking of either CaSRs or the signaling pathways

known to be activated upon exposure to Sr^{2+} ions is required and will be performed in future studies.

7.3.2.8 RAW 264.7 TRAP Activity and Morphology

In addition to osteoblasts, osteoclasts also play a key role in bone remodeling. In the current study RAW264.7 cells, a murine monocyte cell line, were seeded directly on cement samples. The cells were cultured for up to 10 days in media supplemented with 50 ng ml^{-1} of RANKL, a key growth factor in osteoclast development [22]. TRAP activity and cell morphology were analyzed to study the influence of varying Sr^{2+} content in HA forming CaP cements on the osteoclastic differentiation of RAW264.7 cells. With respect to TRAP activity, after 5 days similar values were observed between the three conditions (Figure 7.9). After 10 days a two to three fold increase in TRAP activity was observed. At both time points, no statistically significant differences were observed upon varying Sr^{2+} content.

In addition to increased TRAP activity, the formation of multinucleated cells is characteristic of the differentiation of monocytes towards mature osteoclasts. Therefore, after 10 days of culture in RANKL, the cells cultured on cement scaffolds were fixed using paraformaldehyde and cytoskeletal staining was performed (Figure 7.10). On tissue culture plastic several $200 \mu\text{m}$ or greater multinucleated cells were observed (Figure 7.10 a)). However, on cement samples similar cell aggregates were observed but the large well defined actin rings observed for the cells cultured on tissue culture plastic were not detected (Figure 7.10 b-d)). In comparing the cement samples, slightly larger cell aggregates were observed on cements prepared with 10% SrDCPD. However, no substantial differences were observed.

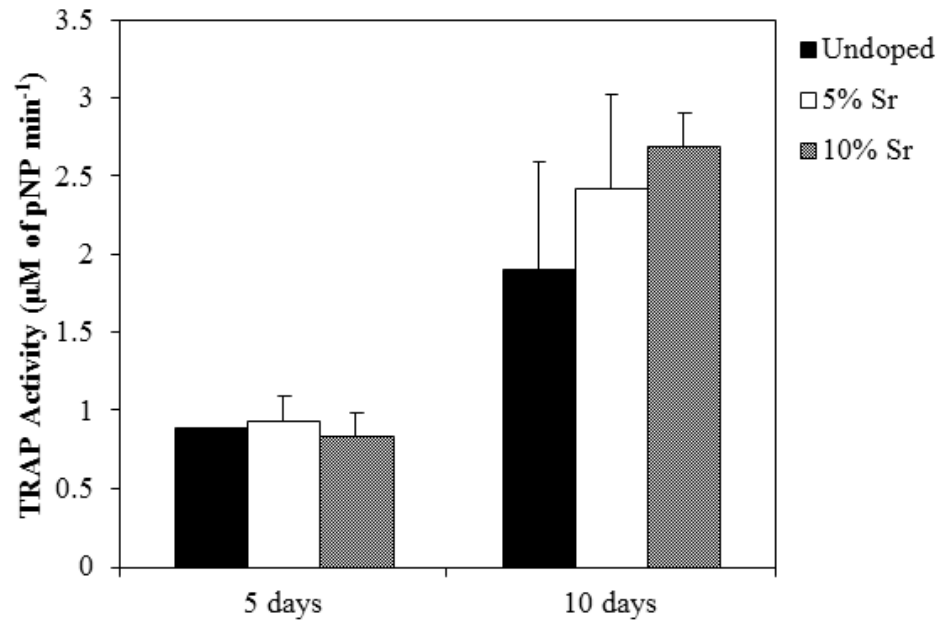


Figure 7.9 Tartarate resistant acidic phosphatase (TRAP) activity of RAW 264.7 cells cultured directly on cement scaffolds in media supplemented with 50 ng*ml⁻¹ of RANKL.

Similar to osteoblasts, osteoclasts can also be stimulated by many ions through CaSRs [119]. Interestingly, Sr²⁺ has been reported to inhibit the differentiation of monocytes towards mature osteoclasts. However, in the current study no statistically significant differences TRAP activity or multinuclear cell formation was observed. This result suggests that the amount of Sr²⁺ released into the culture media may be too low to inhibit osteoclastic differentiation in comparison to cells cultured on undoped HA forming cements.

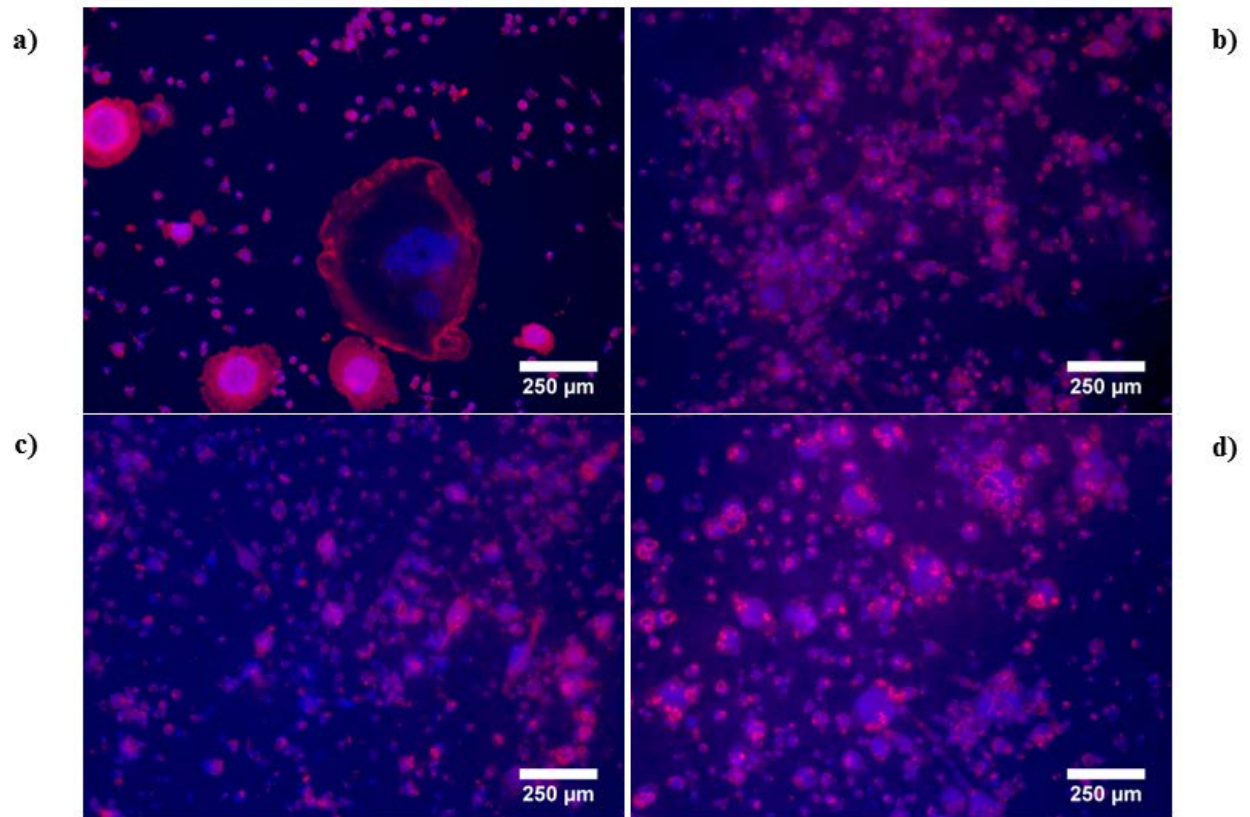


Figure 7.10 Cytoskeletal staining of RAW 264.7 cells cultured a) on culture plastic, and directly on cement scaffolds prepared with b) undoped DCPD, c) 5% Sr DCPD, and d) 10% Sr DCPD in media supplemented with $50 \text{ ng} \cdot \text{ml}^{-1}$ of RANKL for 10 days.

7.4 CONCLUSIONS

Sr^{2+} substituted HA forming cements were prepared using TTCP and chemical synthesized Sr incorporated DCPD as cement precursors. The setting time increased with increasing Sr^{2+} content which may be due to the inhibition of HA formation in the presence of Sr^{2+} . Similar amounts of Sr^{2+} were measured in the cements formed both after setting and after immersion in PBS for up to one week suggesting that most of the Sr^{2+} introduced was incorporated into the HA formed. An increase in compressive strength was also measured for cements prepared with increasing Sr^{2+} content after immersion in PBS for 7 days. Sr^{2+} substituted cements supported increased MC3T3-E1 proliferation and differentiation in comparison to undoped cements. Interestingly, both the release of Sr^{2+} ions and cement microstructure appeared to support osteogenic differentiation. Despite the differences in the amount of Sr^{2+} incorporated into and released from cement scaffolds, no statistically significant difference in the osteoclastic differentiation of RAW264.7 cells was observed. These results indicate that the use of chemical introduced Sr^{2+} substituted calcium phosphate precursors rather than Sr^{2+} containing salts may be a simplified approach to preparing Sr^{2+} substituted HA forming cements. The favorable setting characteristics, mechanical properties, and *in vitro* cytocompatibility indicate that these self-setting cements could serve well for further *in vivo* applications. These studies will be conducted in the near future.

8.0 GENERAL CONCLUSIONS AND FUTURE WORK

Biphasic mixtures of amorphous calcium magnesium phosphate and Mg^{2+} substituted β -TCP were prepared using a low temperature chemical synthesis technique for a wide range of substitution levels for Ca^{2+} . The compositions prepared with increasing Mg^{2+} concentrations resulted in the formation of increased amorphous content. Interestingly, the scaffolds prepared with increased amorphous content were also observed to enhance MC3T3-E1 mouse preosteoblast osteogenic differentiation in comparison to those prepared with commercially available β -TCP. The presence of increased amorphous content is most likely to also result in the greater dissolution of β -TCMP thereby resulting in the increased release of Mg^{2+} and PO_4^{3-} ions into the culture media, which are known to play an important role in the osteogenic differentiation of osteoblast progenitor cells. It was concluded that the enhanced differentiation observed may be due to either the physical cues provides by the scaffold surface or the release of increased Mg^{2+} and PO_4^{3-} ions after immersion in culture media.

The composition prepared with 50% β -TCMP, which facilitated increased MC3T3-E1 proliferation and differentiation in comparison to commercially available β -TCP and all other β -TCMPs, was then compared to Mg^{2+} - Sr^{2+} co-substituted β -TCP scaffolds prepared using the same low temperature synthesis approach. Interestingly, the addition of Sr^{2+} ions to the system did not stimulate enhanced hMSC differentiation in comparison to 50% β -TCMP, as was expected. However, a slight increase in the expression of osteogenic markers was observed for

samples synthesized with the same Mg^{2+} concentration upon adding Sr^{2+} . Using permeable transwell inserts, it was also concluded that the release of increased amounts of bioactive ions rather than the physical contact between hMSCs and the scaffold surfaces rather than the surface microstructure supported enhance osteogenic differentiation. Due to similar Ca^{2+} concentrations among all conditions, it was concluded that the enhanced Mg^{2+} and PO_4^{3-} ions released from the scaffolds prepared using 50% β -TCMP were acting to support the enhanced osteogenic differentiation observed. However, it was not determined which of these two ions were more influential in supporting differentiation or whether or not the release of these two ions provides a synergistic effect.

A qRT-PCR array was also used to study the influence of Mg^{2+} substitution in β -TCP on TGF- β and BMP signaling to gain further insight on the mechanisms through which β -TCMP supported enhanced osteogenic differentiation. It was concluded that the scaffolds prepared with 50% β -TCMP supported enhanced differentiation through increased hMSC SMAD dependent TGF- β and BMP signaling in comparison to scaffolds prepared using commercially available β -TCP. Therefore, in future studies the blocking of SMAD signaling may be a useful approach to determine whether or not β -TCMP scaffolds are still capable of supporting differentiation.

Since experiments with transwell inserts indicated that the release of bioactive ions supported enhanced differentiation on β -TCMPs rather than the contact with scaffold surfaces, approaches to alter the release of bioactive ions from β -TCMPs were explored. The modification of the pH during the synthesis of β -TCMP to a value of 8 was observed to result in the formation of completely amorphous β -TCMP. hMSCs seeded on the scaffolds prepared using these fully amorphous powders exhibited improved proliferation and the expression of ALP, an early osteogenic differentiation marker, in comparison to both β -TCP and β -TCMP prepared using

50% Mg. However, a similar gene expression of mature osteoblast markers between amorphous β -TCMP and β -TCMP was also observed. Therefore, it was concluded that the enhanced release of bioactive ions from fully amorphous β -TCMP supported enhanced proliferation but was incapable of further enhancing differentiation in comparison to β -TCMP.

To determine whether or not the increased release of Mg^{2+} and PO_4^{3-} ions had a synergistic effect on osteogenic differentiation, hMSC growth media was supplemented with 5 mM Mg^{2+} , 5 mM PO_4^{3-} , or a combination of both ions. The influence of varying ionic concentration on both hMSC proliferation and osteogenic differentiation was characterized. As previously reported, the addition of Mg^{2+} resulted in an increase in cell proliferation. Interestingly, the addition of 5 mM PO_4^{3-} to growth media also resulted in a similar level of mineral formation in comparison to hMSCs cultured in osteogenic media while little or no mineral was observed for all other conditions, including the cells cultured in the combination of 5 mM Mg^{2+} and 5 mM PO_4^{3-} . As a result, it appears that Mg^{2+} inhibits the osteogenic differentiation observed upon exposure to PO_4^{3-} ions. Therefore, it was concluded that the presence of increased Ca^{2+} concentrations at later time points in the media collected from β -TCMP may also be playing a role to support differentiation in the presence of Mg^{2+} and PO_4^{3-} which was previously overlooked.

Cationic substitutions in β -TCP were also observed to enhance its cytocompatibility. Therefore, the strategies employed to improve the performance of bulk β -TCP scaffolds were also applied to other clinically relevant forms of β -TCP. Accordingly, cationic substituted β -TCPs were studied as bioactive coatings on biodegradable Mg based metallic substrates to provide improved osseointegration and temporary corrosion resistance under physiological conditions. Despite the use of varying pretreatment conditions, the coatings prepared with

increased Sr^{2+} concentrations also supported increased MC3T3-E1 and hMSC osteogenic differentiation. The Mg^{2+} concentration measured in the culture media was similar among all groups. Therefore, in this system Mg^{2+} ions did not contribute to the differences observed between groups as was observed for the systems described in Chapters 3, 4, and 5. Interestingly, both pretreatment conditions and coating composition were observed to influence the capability of the coating to provide corrosion protection. In summary, cationic substituted CaP coatings were successfully deposited on degradable substrates and were demonstrated to be capable of providing corrosion protection and enhancing cytocompatibility.

Finally, cationic substituted HA forming self-setting cements were also studied. Due to the inhibition of HA crystal formation in the presence of Mg^{2+} ions, Sr^{2+} and not Mg^{2+} substituted HA forming cements were studied. Sr^{2+} substituted DCPD was prepared using the same chemical technique described in Chapters 3 and 4 prior to refluxing and forming β -TCP. The cements prepared with 10% Sr DCPD had a slightly increased compressive strength in comparison to those prepared without Sr^{2+} and supported increased MC3T3-E1 proliferation and differentiation. Interestingly, when using permeable transwell inserts to determine the roles of the physical and chemical cues in supporting differentiation, a comparable expression of osteogenic markers was observed for all conditions, despite the release of increased amounts of Sr^{2+} from Sr^{2+} containing cements. It was therefore concluded that both the chemical and physical cues provided by the scaffold supported increased osteogenic differentiation since previous reports have demonstrated that culture media supplemented with Sr^{2+} supports enhanced differentiation. Thus from these results the influence of the scaffold surface properties could not be eliminated. The differentiation of RAW264.7 murine monocyte like cells to mature osteoclasts, or bone resorbing cells, on these cement scaffolds was also studied. No statistically

significant differences in TRAP activity or cell morphology were observed between any of the conditions studied. Therefore, it was concluded that increased Sr^{2+} concentrations in these self-setting cements is required to influence both osteoblastic and osteoclastic differentiation.

Despite the improvement in the expression of osteogenic markers in comparison to commercially available gold standards, the use of relevant animal models is required to confirm the efficacy of treatments using cationic doped CaPs. Although *in vivo* work with the systems described in Chapters 3-7 was not performed, several publications have attempted to correlate *in vitro* differentiation of hMSC with *in vivo* bone formation in the presence of ceramic scaffolds and coatings [221, 222]. For example, hMSC *in vitro* differentiation on a calcium magnesium silicate ceramic and *in vivo* bone regeneration in a rabbit femoral defect model, both in comparison to β -TCP, have been reported [223]. In this work, a lesser fold increase in hMSC ALP and OPN expression (Figure 8.1) was observed in comparison to β -TCP with that reported in the data illustrated in Figure 4.10, Figure 4.11, and Figure 5.7. However, a significant improvement in the *in vivo* bone regeneration in comparison to β -TCP was observed. Therefore, based on this data it could be concluded that scaffolds fabricated with the materials developed in the current work may also support possibly enhanced *in vivo* bone regeneration in comparison to β -TCP. These are studies to be planned in the future.

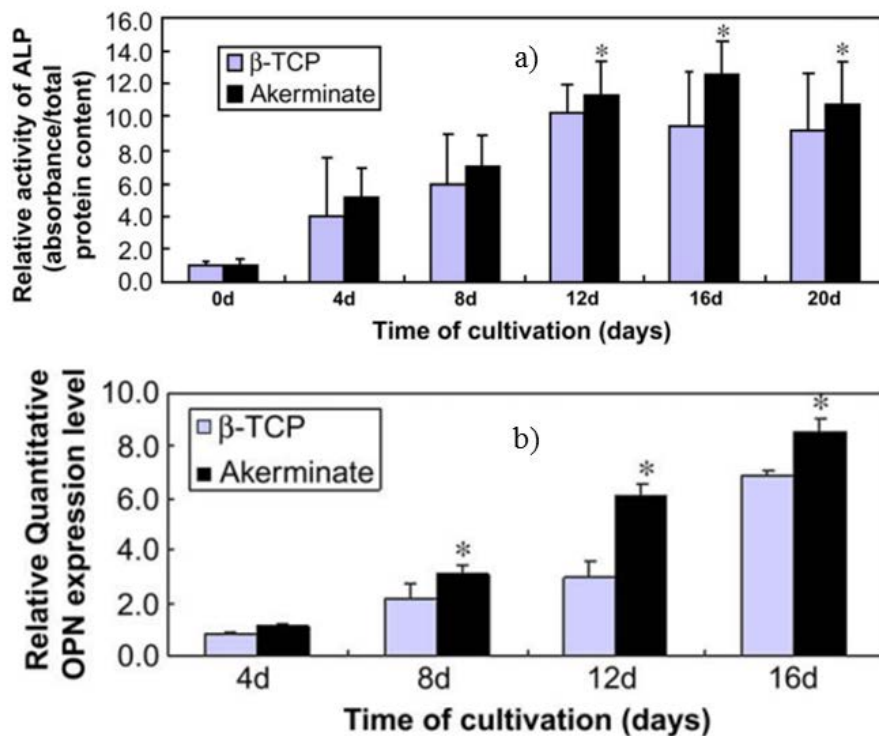


Figure 8.1 The a) alkaline phosphatase activity and b) OPN expression of hMSCs cultured with scaffolds prepared using β -TCP and a calcium magnesium silicate bioceramic (akerminate) [223].

In summary, the efficacy of Mg^{2+} and Sr^{2+} containing CaPs as bulk scaffolds, bioactive coatings, and self-setting cements was demonstrated. It was concluded that amorphous rather than crystalline magnesium phosphate compounds may be more useful in tissue engineering applications due to the capability to release sufficient Mg^{2+} and PO_4^{3-} ions to provide a microenvironment necessary to support osteogenic differentiation. Sr^{2+} containing scaffolds were also demonstrated to support osteogenic differentiation. However, the concentrations of Sr^{2+} required to support differentiation are much lower than that of either Mg^{2+} or PO_4^{3-} . Therefore, Sr^{2+} containing crystalline CaPs, which dissolve at a much slower rate, are capable of delivering sufficient amounts of Sr^{2+} . However, due to the dilute concentrations of Sr^{2+} in the bulk solutions when performing indirect culture experiments, it is difficult to confirm whether the physical or

chemical cues provided by these scaffolds support enhanced osteogenic differentiation. The exact roles of cationic substitutions in all of the materials studied are worth further exploring to determine the mechanisms through which they support enhanced differentiation. These mechanisms will be explored in future studies.

APPENDIX A

DICALCIUM PHOSPHATE DIHYDRATE CEMENTS FROM MAGNESIUM SUBSTITUTED B-TRICALCIUM PHOSPHATE

A.1 INTRODUCTION

In addition to the hydroxyapatite forming cements described in Chapter 7, calcium phosphate cements are also capable of forming DCPD upon setting under acidic conditions. DCPD cements, although less mechanically stable and more acidic, are much more resorbable than HA forming cements under physiological environments. Mg^{2+} substitution in HA forming cements was not studied in Chapter 7 due to the inhibition of HA crystal formation in the presence of Mg^{2+} ions. However, Sr^{2+} ions are a much less potent inhibitor of HA crystal formation. Mg^{2+} substitution in DCPD forming cements has previously been studied using Mg^{2+} substituted β -TCP prepared by high temperature approaches. In the current work, Mg^{2+} substituted DCPD forming cements were also studied. Biphasic mixtures of β -TCMP and amorphous calcium magnesium phosphates were prepared using the low temperature approach described in Chapters 3-5 was employed as a source of Mg^{2+} ions.

A.2 MATERIALS AND METHODS

A.2.1 Cement Preparation and Characterization

An equimolar mixture of either commercially available β -TCP or low temperature synthesized β -TCMP and monocalcium phosphate monohydrate (MCPM) was combined and mixed thoroughly by hand using a mortar and pestle. The powder mixture was then combined with water deionized using a powder to liquid ratio of 2 g ml^{-1} and allowed to set at 37°C using Teflon molds. The cement paste setting time was determined using a Gilmore Needle Apparatus. The specific surface area of the β -TCMP precursor and the powder samples once the cements had fully set was determined using a BET surface area analyzer (Micromeritics, Norcross GA).

A.3 RESULTS AND DISCUSSION

DCPD cements are known to set relatively quickly due to the use of highly soluble acidic calcium phosphate precursors. The dissolution of these precursors and precipitation of DCPD crystals, which become entangled, results in the setting of the paste formed upon exposure to aqueous environments. As expected, the cements prepared using commercially available β -TCP fully set in less than 10 minutes (Figure A.1). Due to the rapid setting times, additives such as sodium citrate, and pyrophosphate salts are added to the liquid component to retard the setting reaction. Interestingly, the cements prepared with 35% β -TCMP took much longer to fully set, requiring almost 50 minutes utilizing the same powder to liquid ratio as commercially available β -TCP. Upon increasing the Mg content in β -TCMP, the setting time significantly reduced.

Cement scaffolds prepared with 50% β -TCMP fully set in less than 5 minutes, much quicker than even those prepared with commercially available β -TCP.

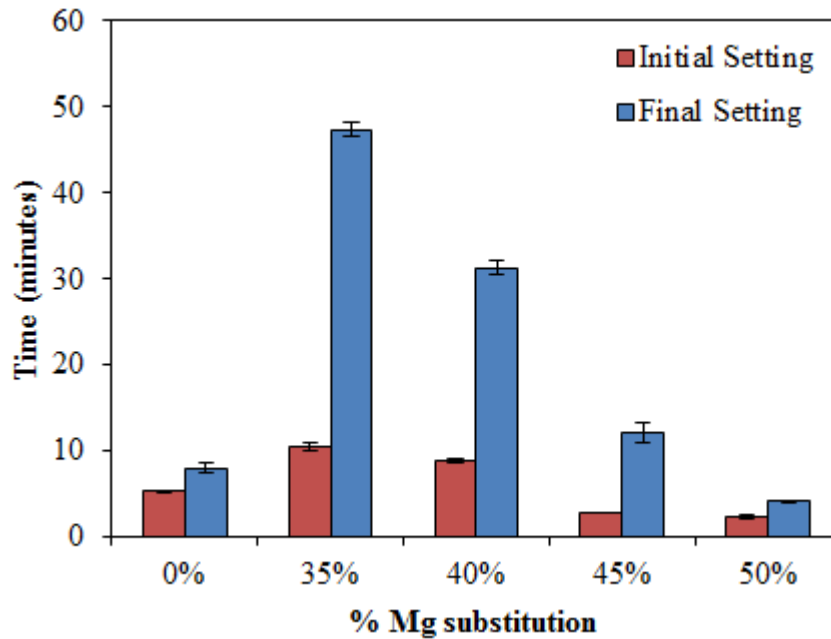


Figure A.1 The setting times of DCPD forming cements prepared using deionized water and a powder to liquid ratio of 2 g ml^{-1} at 37°C .

In addition to the dissolution rate of calcium phosphate cement precursors, the particle size of the powders used is also known to influence the setting kinetics. To determine the variation in particle size of the precursors used, their specific surface areas were determined using BET (Table A.1). The commercially available β -TCP powders have an extremely low surface area, less than $1 \text{ m}^2/\text{g}$, due to the high temperature processing required in preparing these materials and the high degree of sintering which subsequently occurs. For β -TCMP, the surface area increased upon increasing Mg^{2+} content. As a result of this increasing surface area for the same mass of β -TCMP, a much larger amount of liquid is required to sufficiently hydrate the surface of β -TCMP particles prepared with increasing Mg^{2+} content. Therefore, the cement

pastes prepared with β -TCMP containing increased amounts of Mg^{2+} are much more viscous in comparison to those prepared with less Mg^{2+} . As a result, a reduced setting time was observed at 37°C.

Table A.1 BET surface areas of β -TCMP prior to forming DCPD cements and the surface area of the cement powders after setting.

% Mg	β-TCMP SSA (m²/g)	Cement SSA (m²/g)
0%	0.57	2.38
35%	77.69	2.71
40%	158.83	4.41
45%	180.01	3.99
50%	207.96	4.53

A.4 CONCLUSIONS AND FUTURE WORK

Cements with varying Mg^{2+} content were formed by reacting β -TCMP, prepared with varying amounts of Mg^{2+} and monocalcium phosphate monohydrate. The cement scaffold initial and final setting times varied depending on the amount of Mg^{2+} incorporated. The variation in setting time observed may be due to the varying particle size of β -TCMP upon varying Mg^{2+} content. Future studies will focus on determining the *in vitro* cytocompatibility of these cements using osteoblast progenitor cells. Particularly of interest will be the pH upon incubation in cell culture media due to the acidic degradation products of DCPD cements. In the event that cement

scaffolds are too acidic for static culture experiments. The stoichiometry of the cement reaction will be varied to ensure that unreacted β -TCMP, which is less acidic than DCPD, remains to facilitate enhanced cell proliferation and differentiation, as was observed in Chapters 3-5 when studying the either the biphasic mixtures of crystalline β -TCMP and amorphous calcium magnesium phosphate formed or fully amorphous β -TCMP scaffolds.

APPENDIX B

AQUEOUS DEPOSITION OF CALCIUM PHOSPHATES AND SILICATE SUBSTITUTED CALCIUM PHOSPHATES ON MAGNESIUM ALLOYS

B.1 INTRODUCTION

CaP coatings deposited through phosphating solutions were investigated on two alloy systems, AZ31 (96% Mg, 3% Al, and 1% Zn by wt.) and Mg-4Y (96% Mg and 4% Y by wt.). Previous work has explored the use of phosphating bath approaches to deposit CaPs onto AZ31, however, they are yet to be reported on Mg-Y alloy systems [224, 225]. Mg-Y and rare earth alloys, such as WE43 (93% Mg, 4% Y, and 3% rare earths), have shown improved degradation and mechanical strength in comparison to other Mg-alloy systems, specifically for degradable stent applications [226]. The deposition of silicon substituted CaPs on Mg alloys through the phosphating bath approach was also investigated, which to the best of our knowledge has not yet been reported. *In vivo* studies have shown that silicon substituted CaPs were more capable of recruiting osteoclasts over short periods of time and possessed a greater bone contact percent compared to undoped CaPs [227]. It has also been hypothesized that Si is a trace element essential for bone regeneration, however, there is indeed a great paucity of information on the mechanisms and the true effect of Si on bone metabolism [228]. The present study was

conducted as a preliminary attempt to shed light on the generation of CaP coatings by phosphating bath and also its effect on osteoblast cell viability.

B.2 MATERIALS AND METHODS

B.2.1 Material Preparation and Coating Protocol

A sheet of hot rolled AZ31 was acquired from Alfa Aesar (Ward Hill, MA) and was used as received. An ingot of Mg-4Y was cast and acquired from the GKSS Research Institute (Geesthacht, Germany) kindly provided by Dr. Norbert Hort, and was further homogenized by heat treatment to 525°C in an inert atmosphere prior to cleaning and coating. ACS reagent grade calcium chloride dihydrate, sodium dihydrogen phosphate, and sodium hydroxide pellets were acquired from Acros Organics (Morris Plains, NJ). Sodium metasilicate was acquired from Fisher Scientific (Fair Lawn, NJ). Substrates were cut into 1.25 x 1.25 x 0.08 cm samples and were cleaned by first acid etching in a 3% nitric acid solution in ethanol. They were then rinsed in acetone and polished with up to 4000 grit SiC paper followed by sonication in acetone. Cleaned substrates were then subjected to an alkaline treatment by immersion in 50 g/L NaOH solution kept at 65°C for 1h followed by drying at 60°C in air. The pre-treated samples were immersed in phosphating bath solutions modified to those described by Gray-Munro et al. [225] with 3.0 mM CaCl₂ and 1.8 mM NaH₂PO₄ maintaining a Ca/P ratio of 1.67, identical to that of hydroxyapatite (HA). Silicon was incorporated as silicates by substituting corresponding amounts of Na₂SiO₃ for NaH₂PO₄ maintaining the Ca/(P+Si) ratio of 1.67 identical to HA, as is further illustrated in detail in Table B.1. The pH of all the phosphating bath solutions was

decreased to 4.5 with hydrochloric acid. The samples were stored in phosphating solutions for up to 72 h at 37°C and were finally dried at 60°C prior to further experiments and characterization.

Table B.1 **The phosphating bath ionic concentrations**

	Ca ²⁺	PO ₄ ³⁻	SiO ₃ ²⁻
PB1	3.0 mM	1.8 mM	-
PB2	3.0 mM	1.5 mM	0.3 mM
PB3	3.0 mM	1.2 mM	0.6 mM

B.2.2 Characterization Methods

Coated substrates were rinsed and dried overnight at 60°C and were then evaluated by attenuated total reflectance Fourier transform infrared spectroscopy (ATR-FTIR, Nicolet 6700 Thermo Scientific) using a diamond ATR smart orbit with a spectral resolution of 2 cm⁻¹. An average of 64 scans was recorded for each sample in the frequency range of 400 to 4000 cm⁻¹. X-ray diffraction (XRD) was performed using a Philips X-Pert PRO diffractometer employing Cu K α radiation with a Si-detector (X'celerator). The X-ray generator operated at 45 kV and 40 mA at a 2 θ range of 10-90 utilizing a step size of 0.016 and 20.9 sec time step. Samples were sputter coated with palladium (Cressington sputter coater 108A) prior to performing scanning electron microscopy (Philips XL30 FEG ESEM) to analyze the coating microstructure and morphology along with energy dispersive X-ray (EDX, EDAX Genesis) which was used to perform elemental analysis of the coated substrates. Elemental analysis of the media collected after immersion of the coated samples in the medium was performed by inductively coupled plasma optical emission spectroscopy (ICP-OES, iCAP duo 6500 Thermo Fisher).

B.2.3 *In-Vitro* Degradation

Coated and control samples were immersed in 2 ml of Dulbecco's modified eagle medium (DMEM), which was refreshed daily, and kept at 37°C in a 5% CO₂ atmosphere for up to 2 weeks. Collected media was then analyzed by measuring pH (Φ 350 pH Meter, Beckman Coulter) as well as ionic concentrations of magnesium, yttrium, aluminum, and zinc by ICP-OES. The surfaces of coated and control substrates were also analyzed by FT-IR after incubation in DMEM in order to determine the degradation products formed for various conditions.

B.2.4 Cell Culture

Murine osteoblast cell line, MC3T3-E1, was obtained from ATCC (Manassas, VA). Cells were cultured under 37°C, 5% CO₂, and 95% relative humidity in Dulbecco's modified eagle medium (DMEM, Cellgro, Manassas, VA) containing 10% fetal bovine serum (FBS, Atlanta Biologicals, Lawrenceville, GA) and 1% penicillin streptomycin (P/S, Gibco, Grand Island, NY). Cells after fourth passage were used in experiments. After initial seeding of 60,000 cells/ml, cells were then cultured in minimum essential medium alpha (MEM α , Gibco, Grand Island, NY) containing ascorbic acid, 10% FBS, and 1% P/S.

B.2.5 Live/dead Staining

Cell viability was assessed using live/dead staining (Invitrogen, Live/Dead Staining Kit). After 3 days of culture, during which media was changed daily, samples were washed with phosphate buffered saline (PBS) and then incubated for 40 minutes with the live/dead stain diluted in PBS.

After incubation, samples were once again gently washed with PBS prior to imaging using fluorescence (Olympus CKX41). Cells were then fixed by using 4% paraformaldehyde followed by incubation for 20 minutes. After fixing, samples were subjected to alcohol dehydration and coated with palladium in order to observe the cell morphology by SEM.

B.3 RESULTS AND DISCUSSION

B.3.1 Coating Characterization

Upon drying and visual inspection, the substrates appeared to be coated inhomogeneously with a white precipitate which was deposited either due to the further corrosion or the precipitation of Ca, P, and Si from the phosphating bath due to the local increase in pH during incubation. There was also an accumulation of precipitates at the bottom of the flasks in which the substrates were immersed, which probably suggests that not all of the Ca, P, and Si that precipitated from the phosphating bath solutions were deposited on the surface of the substrates. The pH of the coating bath solutions was monitored throughout the coating process and it was observed to stabilize at approximately 8.3 for all conditions after 24 h for both alloy systems. X-ray diffraction was used to analyze the crystallinity and phase composition of the coated substrates, however, due to either the inhomogeneity or incomplete coverage of the substrate surface or the amorphous nature of the deposited coatings, there were no extra peaks observed in the XRD spectra besides those of the substrate itself.

While XRD results were inconclusive, FT-IR was used in order to confirm the presence of phosphates on the coated substrates and to observe whether or not the incorporation of silicate

ions in the phosphating bath solutions affected the bonding between calcium and phosphate on the coated substrates. Due to the visual inhomogeneity of the coating, for each condition a minimum of 4 spectra, each from different samples, were collected and averaged. Figure B.1 a) and b) illustrate the FT-IR spectra for all three coating conditions on AZ31 and Mg-4Y in comparison to β -TCP. While the Ca/P or Ca/(P+Si) ratio of the phosphating bath solutions was kept constant at 1.67, characteristic of HA, in the FT-IR spectra of the coated samples it was difficult to detect the weak band at $\sim 3600\text{ cm}^{-1}$, indicative of the hydroxyl bending band of HA, for all of the coated samples suggesting that the coated phase were not identical to HA but structurally closer to tri-calcium phosphate (β -TCP) and the formation of mixed HA and β -TCP phases as a valid possibility. However, in some cases the broad band between 2500 and 3500 cm^{-1} , due to absorbed moisture, may be overlapping with the weak hydroxyl bending band. This structural inhomogeneity also suggests the possible formation of β -TCP since Mg ions are well known to stabilize its structure and the major peaks indicative of PO_4^{3-} can indeed be detected [81]. Of the other possible CaP phases that could be formed, brushite ($\text{CaHPO}_4 \cdot 2\text{H}_2\text{O}$) was probably not deposited due to its instability at elevated pH, and the fact that this basic pH was achieved after only 24 hours in phosphating bath solutions. Peaks in the range 570 and 605 cm^{-1} are due to O-P-O bending mode and the intense band in the range 960 - 1088 can be attributed to P-O stretching vibration modes.

While the crystallinity of the coatings remained unknown and FT-IR confirmed the presence of PO_4^{3-} , in order to estimate the phase composition of the deposited coatings, elemental analysis by EDX was utilized to determine the Ca/P and Ca/(P+Si) ratios. SEM confirmed the formation of inhomogeneous coatings for all conditions, as is illustrated in Figure B.2 a) and b) with a thickness ranging from 10 - $20\text{ }\mu\text{m}$ obtained by observing the cross sections

of the coated substrates. EDX results on AZ31 coated samples for all three conditions showed that the Ca/P ratios were between 1.3-1.5, and the (Ca+Mg)/(P+Si) ratios ranged from 1.4-1.6 indicating that the chemical composition was closer to β -TCP. Similar to the observations made from the FT-IR spectra, this may suggest that mixed Mg and Si doped CaP phases of HA and β -TCP are being deposited on the surface of the alloy. Work by Gray-Munro et. al on AZ31 using a similar method suggested that Mg doped HA was being formed, however, upon including silicates this does not appear to yield purely HA [225].

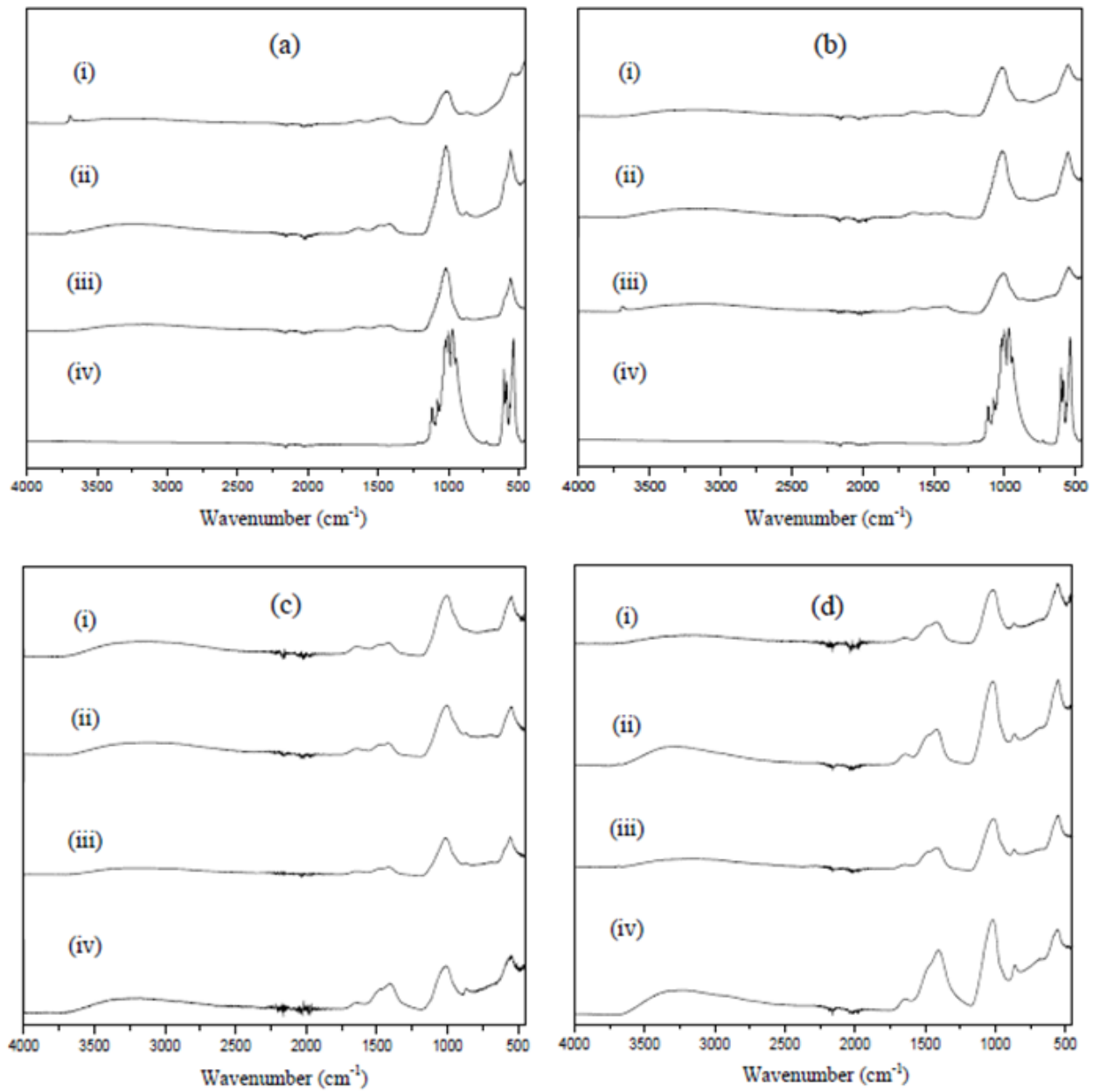


Figure B.1 FT-IR spectra of iv) β -TCP, iii) PB1, ii) PB2, and i) PB3 coated samples as prepared on a) AZ31 and b) Mg-4Y. Also included are the FT-IR spectra of iv) uncoated, iii) PB1, ii) PB2, and i) PB3 samples after incubation for one week in DMEM on c) AZ31 and d) Mg-4Y are also shown.

On Mg-4Y the Ca/P ratios were again between 1.3 and 1.5, however, on PB1 and PB2 the $(\text{Ca}+\text{Mg})/(\text{P}+\text{Si})$ ratios were between 1.5 and 1.6, while on PB3 they were much closer to 1.3. This is due to a much larger amount of Si being deposited on Mg-4Y compared to AZ31, as is illustrated in Figure B.2 e) and f). The $\text{Si}/(\text{P}+\text{Si})$ ratios on PB2 and PB3 for AZ31 were close to 0.02 whereas on Mg-4Y they were closer to 0.07 and 0.2, respectively. Figure B.2 c) and d) illustrates representative EDX plots for data obtained from PB1 and PB3 coated Mg-4Y samples, where the Si peak can be observed at approximately 1.75 KeV and is correspondingly absent for the PB1 coated samples. Therefore, by FT-IR and EDX it can be confirmed that Ca, P, and Si have been deposited on the surface of both alloys.

Such large amounts of Si probably indicate that magnesium and calcium silicates are also being deposited. This is not of concern with respect to bioactivity as calcium and magnesium silicates have also been shown to have favorable bioactive properties [78, 229]. The increased amounts of silicon may be due to the varying stabilities of the hydroxide layers formed on the two alloys. Yttrium is known to increase the protectiveness of the surface layer of Mg alloys due to the formation of the tenacious Y_2O_3 coating, however, Y intermetallics may accelerate corrosion [230]. Perhaps once the hydroxide layer reacted with acidic environment in the phosphating bath, the surface of the pristine Mg-4Y substrate becomes more corrosive. This enhancement in the corrosion of the substrates will increase the local pH of the solution and will accelerate the deposition of Ca, P, and Si by nucleation and precipitation. Thus the presence of Y intermetallics possibly explains the increased presence of Si on the CaPs coating on Mg-4Y compared to AZ31.

B.3.2 *In-Vitro* Degradation

Coated and uncoated substrates were then immersed in DMEM, which was refreshed daily, and kept in *in vitro* conditions in order to determine the effect of the various coating conditions on stability. Interestingly, the coatings did not appear to have a significant impact on corrosion protection based on pH measurements alone. For both alloys at all conditions, the pH remains approximately 8.4-8.7 over the two week period. Therefore, one hypothesis may be that the formation of a $\text{Mg}(\text{OH})_2$ layer on the uncoated samples occurs rapidly enough that after 24 hours, for which the first measurement was taken, there is not a measurable difference observed between coated and uncoated groups. Also based on pH measurements, it appears that it is the presence of this protective layer that governs degradation as well as the interactions of cells and biological fluids with Mg alloy substrates.

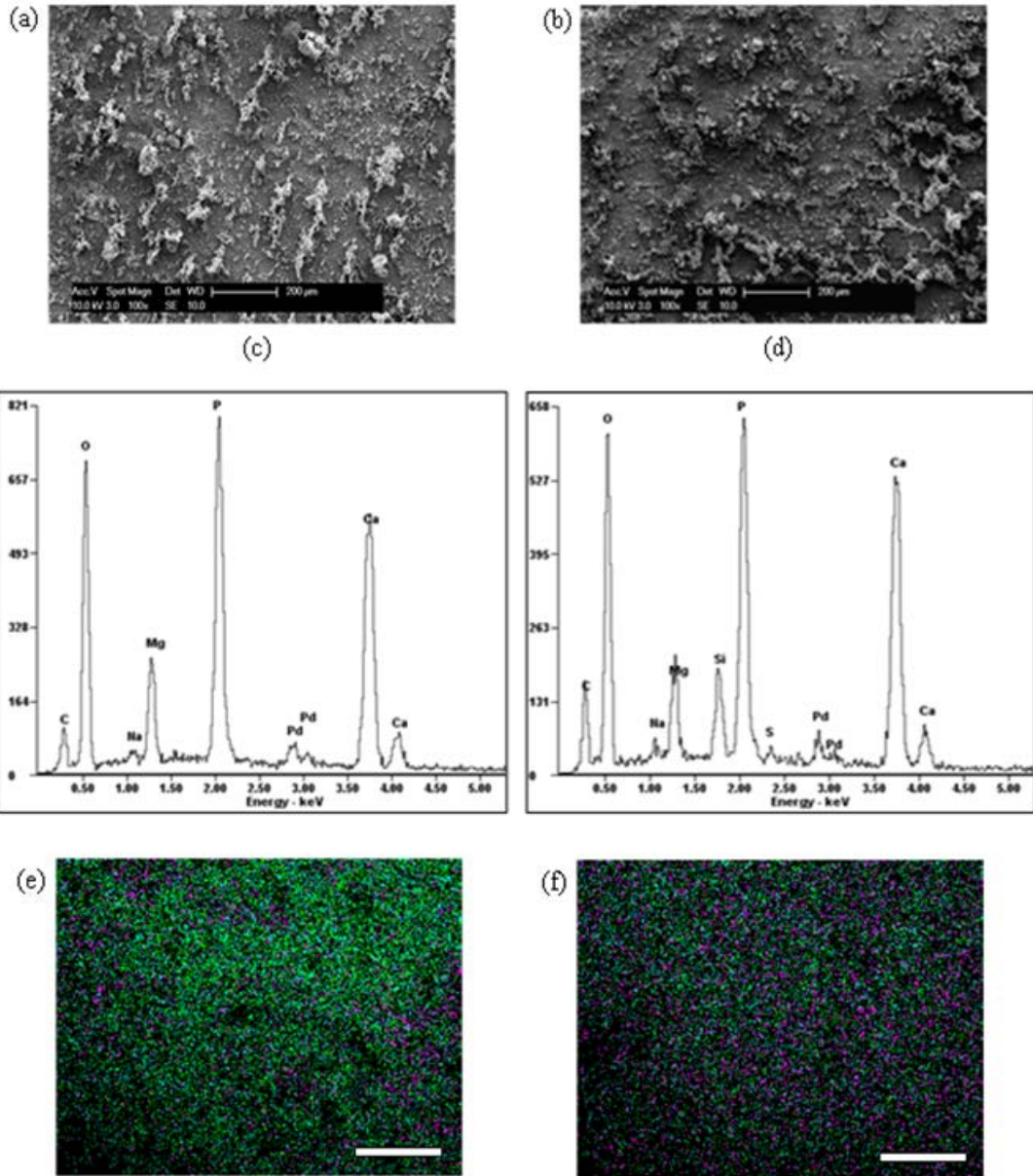


Figure B.2 SEM images of Mg4Y samples coated in a) PB1 and b) PB3 as well as EDX plots taken from Mg4Y samples coated in c) PB1 and d) PB3. EDX mapping was also performed illustrating the distribution of Ca (blue), P (green), and Si (pink) for (e) AZ31 coated in PB3 and (f) Mg-4Y coated in PB3. Scale bars are 500 μm.

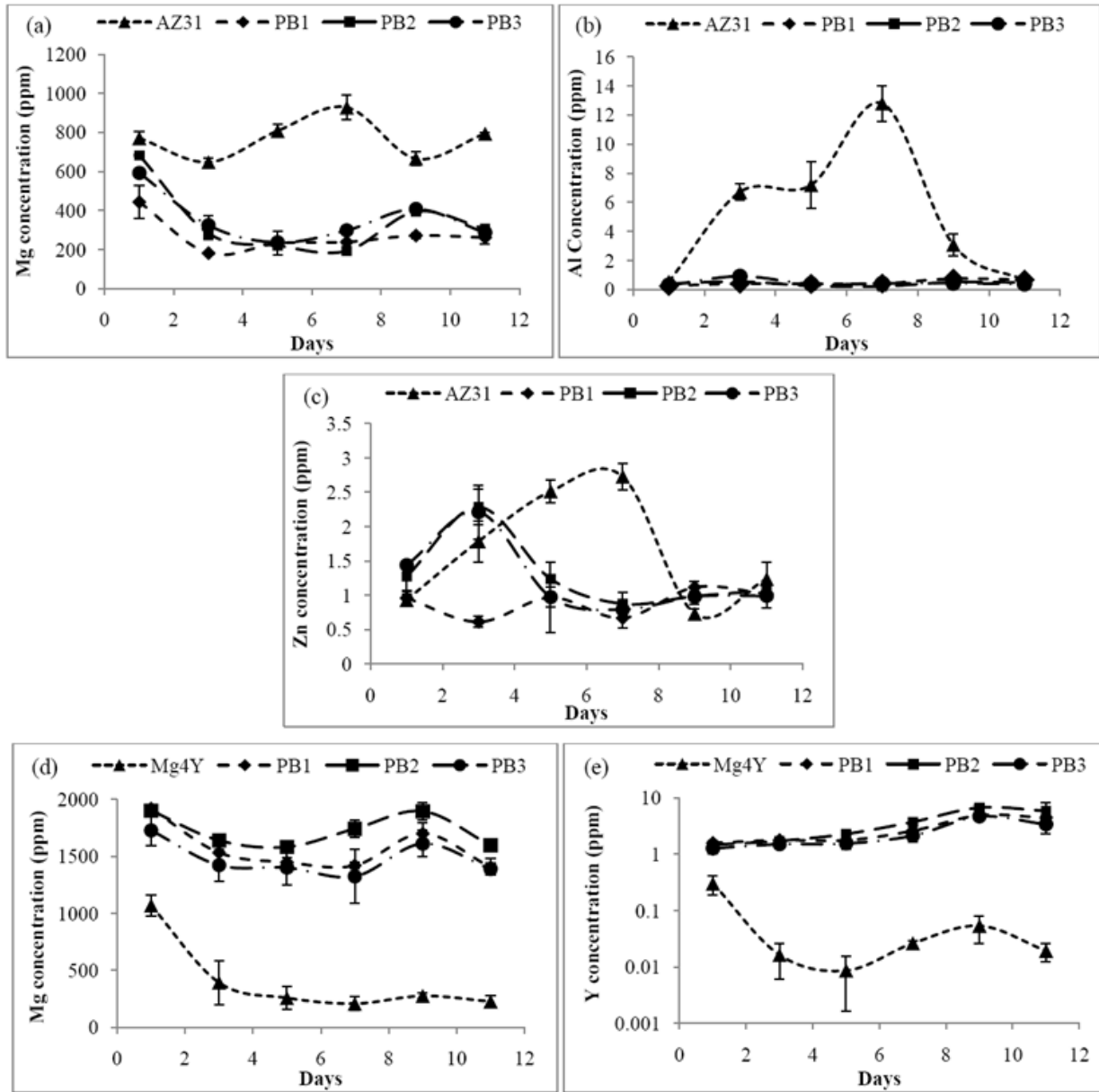


Figure B.3 The ICP-OES measurements of a) Mg, b) Zn, and c) Al in collected DMEM from AZ31 coated and uncoated samples as well as d) Mg and e) Y from MgY coated and uncoated samples.

ICP was used to determine ionic concentrations of collected DMEM in order to further evaluate the effect of coatings on the degradation of both substrates. Measurements of the ionic concentrations by ICP not only gives the degradation characteristics of the substrate, but also can be used to assist in the evaluation of toxicity. Ionic toxicity *in vivo* is of great concern as studies have shown that aluminum may accelerate brain aging and may be neurotoxic in larger concentrations. Excess aluminum can lead to increased levels of inflammatory cytokines and eventually the onset of Alzheimer's disease [231]. In the case of Zn, the adult body naturally consists of 2-3 g and Zn is an essential dietary supplement, however, excess amounts of Zn can also be toxic [232]. There have been fewer reports on the long term toxicity of yttrium, but its more frequent use as an alloying element in magnesium based implant devices increases the necessity for such studies.

For AZ31 coated samples (Figure B.3: a, b, and c), ICP-OES measurements show that the pristine alloy released larger amounts of Mg, Al, and Zn compared to the coated samples over the period of interest. Also for the pristine uncoated alloy, the release profiles of Mg, Al, and Zn do not show similar trends, which may indicate that intermetallics exist and alter the rate of release of individual ions due to varying composition and solubility. For Mg, the coated samples show a similar release profile and appear to have stabilized at approximately 300 ppm, however, the uncoated samples appear to stabilize between 600-800 ppm. Al showed a very interesting release profile with the uncoated samples reaching a maximum of 14 ppm and then decreasing to similar concentrations of the coated samples, which were consistently less than 1 ppm for the entire period of interest. This extremely high release of Al from uncoated AZ31 is alarming due to the fact that Al is a well-known neurotoxin, as mentioned previously. This may perhaps indicate that AZ31 is not the best choice of alloy for the repair of craniofacial defects,

considering the large amounts of Al that will be released in close proximity to neural tissues during degradation. For Zn, there is an initial burst release for the uncoated alloy that appears to decrease upon application of the CaP coatings since the coated samples appear to stabilize at approximately 1 ppm much sooner than the uncoated sample. Interestingly, PB2 and PB3, both Si containing coatings, also have a slight initial burst release, whereas no initial burst was detected for PB1. This may suggest that PB1 is the coating condition on AZ31 that is most stable and likely desirable.

ICP-OES measurements on Mg-4Y (Figure B.3: d and e) coated samples showed the opposite trend compared to AZ31 with the coated samples releasing almost four times Mg and an order of magnitude more Y in comparison to the uncoated samples for the time period of interest. A similar release profile is observed for both Mg and Y for the uncoated samples where the concentrations are initially high and then decrease and become stable. This period between 1 and 3 days is perhaps when a passivation layer of $\text{Mg}(\text{OH})_2$ is formed on Mg-4Y, limiting the degradation of the alloy and reducing the transport of Mg ions into the surrounding DMEM. ICP measurements for Mg concentration for both alloys were not corrected for the Mg already present in media in order to show the total amount of Mg cells may potentially be exposed to during experiments although serum proteins are known to inhibit corrosion.

It is interesting in both cases that although the coated and uncoated samples have such different concentration values and profiles in DMEM, there is no great difference between pH for the coated and uncoated samples as well as between the two different alloy systems. In both cases the pH is slightly basic, 8.4-8.7, which can only be due to the dissolution of $\text{Mg}(\text{OH})_2$ as a corrosion product. The coated samples are subjected to an alkaline treatment and are coated in aqueous environments, therefore there will be $\text{Mg}(\text{OH})_2$ present on the surface of these alloys

prior to observing their behavior in DMEM. For AZ31, the difference in Mg concentration between coated and uncoated groups is much smaller than that for Mg-4Y, for which the coated samples appear to release almost 4 times as much Mg and approximately 10 times more Y. Therefore, the trends in behavior must be due to the presence of intermetallics of the alloying elements as well as the stability of the corrosion products.

The fact that Mg concentrations for the AZ31 uncoated samples are only slightly higher than the coated samples suggests that the corrosion products of AZ31 are fairly stable. The opposite is true for Mg-4Y since for the coated samples, which already contain $\text{Mg}(\text{OH})_2$ on their surface, the Mg concentrations were much higher than the uncoated samples. Although evident from the ICP-OES results, this change is probably too small to be shown by pH measurements alone, perhaps if DMEM was not refreshed daily this change would be more noticeable by pH measurements as well.

The drastic difference in the dissolution behavior of Mg-4Y coated samples irrespective of the coating containing Si in comparison to the pristine Mg-4Y sample could be attributed to several factors such as film thickness, instability of the corrosion products, poor adhesion on the film, and compositional inhomogeneity of the Mg-4Y alloy. The exact reason for the variation in the dissolution behavior in the two alloy systems used is unclear at the moment warranting more work which is currently on-going.

The surfaces of both uncoated and coated substrates were analyzed by FT-IR after incubating in DMEM for one week and are illustrated in Figure B.1 c) and d). For CaP coated AZ31 samples (Figure B.1, a: i), ii), and iii) and c: i), ii), and iii)), there is not a significant difference in the FT-IR spectra prior to and after immersion in DMEM. For uncoated AZ31 (Figure B.1, c: iv)), the broad peak due to moisture adsorbed to the surface of the samples made

it difficult to detect the presence of the hydroxyl bending band at 3600 cm^{-1} , however, the presence of PO_4^{3-} stretching and bending modes, as seen with coated samples, were detected along with those of CO_3^{2-} at 1500 cm^{-1} and 900 cm^{-1} , as were previously reported on pure Mg kept in HBSS with and without FBS [233]. For CaP coated Mg-4Y samples (Figure B.1, b: i), ii), and iii) and d: i), ii), and iii)), after immersion in DMEM increased amounts of CO_3^{2-} appeared to form on the coated substrates. Similarly to uncoated AZ31, for uncoated Mg-4Y (Figure B.1 d: iv)) CO_3^{2-} and PO_4^{3-} were once again confirmed to have formed and the presence of OH^- was difficult to confirm by the FT-IR spectra alone. These results confirm those observed by ICP where CaP coatings appear to protect AZ31 to a greater extent in comparison to Mg-4Y.

Standard solutions to be used to study the *in vitro* degradation of Mg alloys, closely mimicking *in vivo* conditions, are yet to be generally accepted. Significantly slower corrosion rates have been observed during *in vivo* experiments in comparison to those performed under *in vitro* conditions, which is believed to be due to the interactions of proteins with the degrading alloy [187]. Furthermore, for *in vitro* experiments there is a strong dependence on the composition of the solution being used, more specifically, the concentrations of chloride ions and serum proteins [234]. In the current study, the major goal was to compare the capability of various coating conditions to protect the underlying substrate. As a result, a physiologically relevant solution which didn't slow down corrosion to the point where it may be difficult to observe differences between groups was required. In order to meet these criteria DMEM without FBS was used, however, further studies are required to evaluate the interaction of proteins with the alloy surface and the capability CaP coatings to adsorb specific proteins which may influence cell adhesion and degradation characteristics.

B.3.3 *In-Vitro* Cytocompatibility

MC3T3-E1 murine osteoblasts were then used in order to study cell attachment on coated and uncoated alloys. After 3 days of culture for AZ31 coated and uncoated samples in osteogenic media, PB1 and PB3 were the conditions that showed the best cell attachment (Figure B.4: a), b), c), and d)). This result was confirmed by SEM as there were quite a few cells on PB1 and PB3 which appeared to be attached and well spread, however, on the uncoated AZ31 there were fewer attached cells (Figure B.5: a), b), c), and d)). In contrast, after 3 days of culture in osteogenic media, for Mg-4Y coated and uncoated samples, the uncoated substrate and PB3 were the conditions that showed the best cell attachment (Figure B.4: e), f), g), and h)). From SEM this result was also confirmed as it is clearly evident that cells are well attached to the uncoated substrate and much fewer were observed on the coated substrates for which PB3 was the best condition (Figure B.5: e), f), g), and h)).

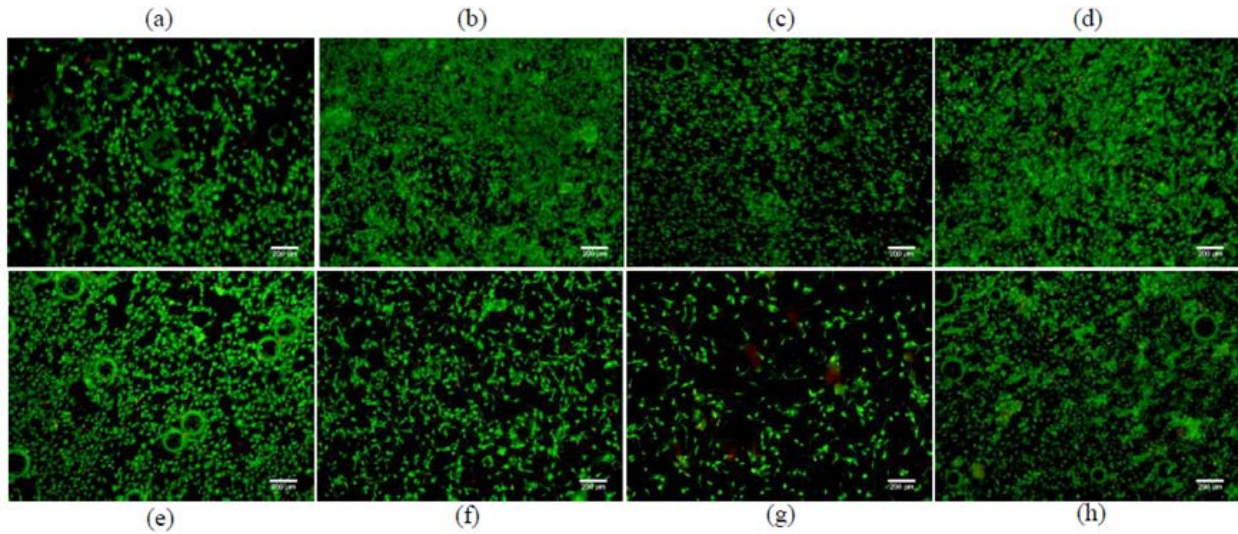


Figure B.4 Live/dead imaging at a magnification of 10X of a) uncoated AZ31 and AZ31 immersed in b) PB1, c) PB2, and d) PB3 as well as uncoated e) Mg4Y and Mg4Y immersed in f) PB1, g) PB2, and h) PB3 after 3 days of culture.

ICP-OES results confirmed that the uncoated Mg-4Y substrates released the lowest amounts of Mg and Y for the period of interest. The much lower yttrium amounts released perhaps contribute to the increased cell attachment over the 3 day period since yttrium may be toxic in higher concentrations. Previous studies have shown that the physical properties of the surfaces of biomaterials, such as surface roughness, and not just its chemical functionality can greatly influence cell attachment and proliferation [165, 235, 236]. Uncoated samples were polished with a relatively high grit SiC polishing paper, up to 4000. Surface roughness is not something that has been taken into account between conditions and may be influencing cell attachment since there is potentially a large discrepancy in roughness between the uncoated and coated samples. This may explain the relatively high attachment seen on uncoated Mg-4Y in comparison to the uncoated AZ31 samples wherein the larger amounts of Zn and especially Al

released from AZ31 in comparison to the coated samples may explain the discrepancy between coated and uncoated samples for that system.

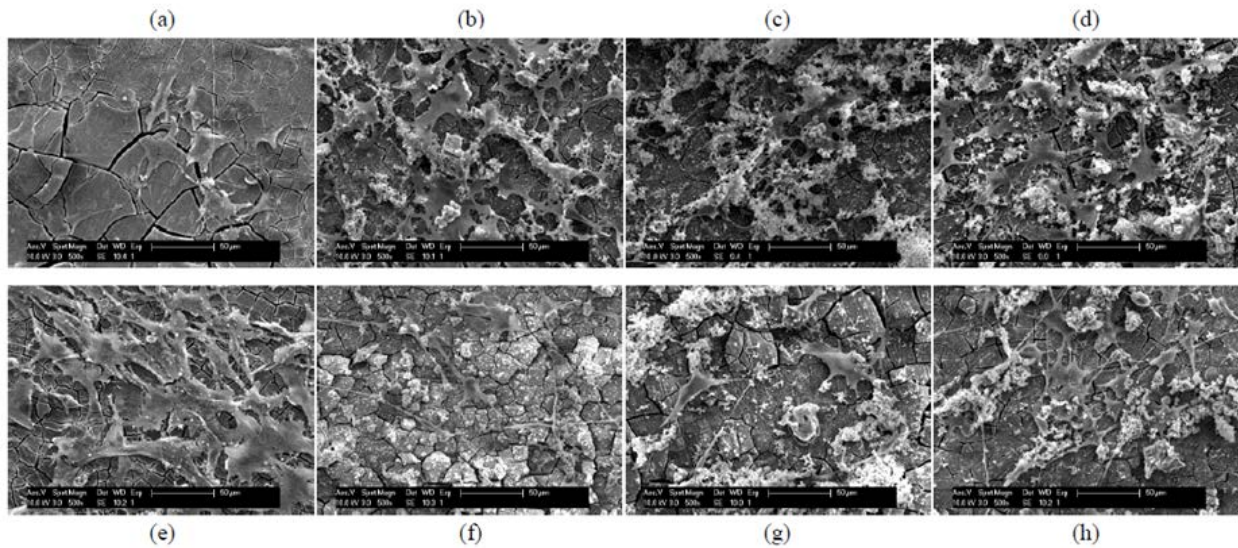


Figure B.5 SEM images of fixed samples at a magnification of 500X on a) uncoated AZ31 and AZ31 immersed in b) PB1, c) PB2, and d) PB3 as well as uncoated e) Mg4Y and Mg4Y immersed in f) PB1, g) PB2, and h) PB3 after 3 days of culture.

In comparing the two alloys it appears that the Mg-4Y alloy itself is more biocompatible than AZ31 based on the results for the two uncoated samples. Interestingly, after 3 days of cell culture, bubbles are clearly visible on the degrading Mg-4Y and AZ31 control samples and less on most of the coated sample live/dead images. On the coated substrates it is interesting that the PB2 condition for both alloy systems showed the least cell attachment. This coating procedure was optimized for AZ31, which is evident by the increased attachment on the two best AZ31 conditions in comparison to the two best Mg-4Y conditions, however, it is obvious that the presence of silicon in the coating indeed plays a role in increasing cell attachment as PB3, the

coating with the greatest silicon substitution, consistently shows an increased cell attachment compared to the other conditions on both alloys.

B.4 CONCLUSIONS

Ca, P, and Si were deposited onto the surface of both AZ31 and Mg-4Y by phosphating bath methods. A much larger amount of Si was deposited on Mg-4Y. These fairly inhomogeneous coatings did not greatly reduce the corrosion of magnesium alloys based on the pH measurements alone, however, the amount of Mg and Zn released from coated AZ31 surfaces were much lower than the uncoated control. As a result, PB coatings were much more effective at influencing the bioactivity of AZ31 substrates compared to Mg-4Y possibly due to the surface condition and compositional variations on the surface of Mg-4Y alloys. While the phase composition and crystallinity remain unknown, the presence of silicon in the coatings appeared to have a favorable influence on cell attachment for both alloy systems. Therefore, these results illustrate that the doping of CaP coatings on degradable alloy substrates with Si may be a useful approach to enhance cell attachment and proliferation.

APPENDIX C

NOVERL SOL-GEL DERIVED CALCIUM PHOSPHATE COATINGS ON A MG4Y ALLOY

C.1 INTRODUCTION

Each year a few million patients need a bone graft or bone graft substitute to repair and remodel a bone defect resulting from trauma or disease. In spite of a large number of available bone graft substitutes, resorbable implants with adequate mechanical strength have gained considerable interest in the field of orthopedic and craniofacial bone regeneration [101, 237]. Recently, many researchers have advocated the use of magnesium alloys as a promising biodegradable metal based implant material. The interest in magnesium alloys has been particularly motivated due to their comparable mechanical properties to natural bone [59, 187, 238]. The biocompatibility and biodegradability of Mg also make them attractive. Recently, many researchers have reported the *in vitro* and *in vivo* biocompatibility and degradability of magnesium based alloys [59, 187, 188, 239-243], however, the clinical applications of Mg based implants at present are very limited due to their relatively high degradation rate accompanied by hydrogen evolution under physiological conditions and limited bioactivity [188, 238, 244]. One approach to control the high corrosion rates of magnesium based alloys is the development of novel alloy compositions [59, 243, 245,

246]. Witte et al reported that Mg alloys containing rare earth elements seemed to be suitable for orthopedic applications [59, 243, 245, 246]. Recently, MgZnCa metallic glasses have been reported to have excellent degradation characteristics without any clinically observable hydrogen evolution and better cyto-compatibility in comparison to pure magnesium and other crystalline magnesium alloys [188, 247]. Another approach to reduce the corrosion rates of these novel alloys is coating with aluminum or titanium, and magnesium fluoride [114, 225, 240-242, 248, 249].

Although these different techniques of alloying, processing, and coating may improve the bio-corrosion resistance of magnesium alloys to a great extent, it is unlikely that these techniques can significantly alter the cell and tissue response, especially at the early stage of the implant [250]. Therefore, distinct alterations of implant surfaces may lead to different and unique chemical as well as physical surface properties, that eventually could lead to changes in the bone-to-implant interactions [250]. Thus, tailoring of the magnesium based biomaterials surfaces with a suitable inorganic and organic coatings may be of immense importance in increasing biocompatibility and osteo-conductivity [250, 251]. These goals can be achieved by coating the Mg alloy surface with a porous layer of bioactive materials of calcium phosphates (CaPs), especially hydroxyapatite (HA), which is the major inorganic mineralized component of natural bone. To improve the bioactivity of these calcium phosphate coatings further, elements such as Zn, Mg, Si, etc. can be incorporated into the calcium phosphate structure [238, 252-257]. In this regard, several studies have alluded to the important role of silicon on bone formation and growth under in vitro and in vivo conditions [253]. It is also well established that bio-ceramics including Bioglass [252], calcium silicate [258, 259] as well as Si-containing calcium phosphates [253] show superior bio-activity and bone forming ability. However, it should be noted that the

exact role of silicon on bone formation remains controversial [228]. In recent years, some efforts have been made to coat and modify surfaces of different Mg alloys using various phases of calcium phosphates (CaPs). Many methods are known for generating CaPs coatings on metallic substrates, especially on Ti alloys, namely immersion in simulated body fluids, wet chemical method, sol-gel method, plasma spraying method, RF sputtering, electrophoresis, cathodic deposition, etc [63, 251]. However, only a few of these techniques can be used to coat magnesium based alloys as most of these alloys are reactive to water based solutions and are very sensitive to high temperature processes due to their low melting points. To minimize some of these problems most of the techniques used so far to coat magnesium alloys have been electro-deposition, deposition in simulated body fluids and phosphating bath (solution of phosphoric acid, calcium phosphate, zinc phosphate and sodium nitrates) coatings [115, 225, 248, 249, 260-262]. Results showed that these CaPs based coatings improve the in vitro and in vivo bio-activity and biocompatibility of the Mg-based alloys [241, 261-264]. Although it has been reported that these coatings also alter the corrosion characteristics of native alloys, most of these CaPs based coatings are porous and contain cracks, therefore, they are not expected to significantly alter corrosion characteristics [114, 115, 225, 241, 249, 260, 261].

Sol-gel coatings are well studied for coating titanium-based orthopedic complex shaped scaffolds and generally result in porous, nano-crystalline, and thin to thick coatings with controlled micro-structure at relatively low processing temperatures [63, 265-267]. The other major advantage of sol-gel coating is that different elements can easily be included in the gel formation process and thus can be incorporated in the final structure of CaPs coatings. Interestingly, to the best of our knowledge no attempts so far have been reported on coating Mg alloys with CaPs structures using the sol-gel technique. This article reports the preliminary

results on an ethanol based sol-gel derived un-substituted calcium phosphates (CaPs) and different Si-containing CaPs (Si-CaPs) coatings on Mg-4Y substrates and subsequent characterization of the obtained coated films using different analytical techniques. Furthermore, this work also evaluates the in vitro biocompatibility and the influence of these coatings on the degradation characteristics of the alloy.

C.2 MATERIALS AND METHODS

C.2.1 Preparation of CaPs and Si-CaPs Coatings

Mg containing 4% Y (Mg4Y) ingots were obtained from GKSS Research Centre, Institute of Materials Research. These ingots were machined to obtain substrates of 10 mm x 10 mm x 0.8 mm and these substrates were annealed at 525°C under an inert atmosphere for 8 h to avoid any segregation of the alloying elements prior to coating. The substrates were cleaned using acid etching (3% nitric acid in ethanol) and washed repeatedly with acetone. The substrates were then polished with 800 grit and finally with 1200 grit SiC paper and cleaned under ultra-sonication using acetone. Calcium phosphate sol-gels were synthesized using calcium nitrate (Acros Organics, Thermo Fisher Scientific, USA) and phosphorus pentoxide (Sigma Aldrich) as precursors, with a Ca/P ratio of 1.67 as described by Kim et al. [267], corresponding to the hydroxyapatite (HA) composition, $\text{Ca}_{10}(\text{PO}_4)_6(\text{OH})_2$. Si-containing samples were prepared by mixing 0.01 mol of calcium nitrate, $(6-x) \times 0.0005$ mol of phosphorus pentoxide, and $x \times 0.001$ mol of Tetraethyl orthosilicate (TEOS, Aldrich) in 5ml 190 proof ethanol (Pharmco-AAPER), where $x= 0.0, 1, 2, \text{ and } 3$ and Ca/P+Si ratio of 1.67. The wt% of silicon was calculated assuming

full conversion of TEOS into silicon dioxide (SiO₂) using Equation C.1, where M_{Si} and M_{SiO₂} are the molecular weights of Si and SiO₂, respectively, and M_{HA} is the gram molecular weight of HA expressed as Ca₁₀(PO₄)₆(OH)₂. The value of wt. % of Si for x=0.0, 1, 2 and 3 were found to be 0.0, 2.6, 5.0 and 7.1, respectively.

$$\text{Equation C.1 Wt. \% Si} = (xM_{\text{Si}}100)/(M_{\text{HA}}+xM_{\text{SiO}_2})$$

For all the compositions, viscous gels were formed and these viscous gels were heated to 60°C and coated on the substrates using a dip coater (Desktop Dip Coater, Model No. EQ-HWTL-01-A, MTI Corporation, USA) with a withdrawal speed of 450 μm/sec. Coated substrates were dried at 60°C for 1.0 h and subsequently heat treated to 450 °C for 24.0 h in argon, depositing a layer of CaPs onto the surface of the alloy. These singly coated substrates were used for all the materials characterizations and in-vitro studies except X-ray diffraction. Multiple coated films (three coatings) were used for X-ray diffraction studies. For multiple gel coated films substrates were dried at 60°C for 1.0 h after each coating and re-coated. Total three gel coatings were done before heat treatment to 450 °C for 24 h in argon.

C.2.2 Characterization of CaPs and Si-CaPs Coatings and Powders

After completion of the coatings, the gels were dried overnight on a hot plate at 60°C in air. A part of the as dried gel powders were heated to 450°C for 24.0 h in argon and the other part of the as dried gels were heated to 750°C for 6.0 h in argon. The as dried powder, heat treated powders and coatings were characterized by X-ray diffraction (XRD) in a Philips X'Pert PRO diffractometer using Cu Kα radiation with a Si-detector (X'celerator). The X-ray generator was operated at 45 kV and 40 mA at a 2Θ range of 10-90 employing a step size of 0.033 and 90.17 *sec* time step. The surface morphology of the coatings were studied using a scanning electron

microscope (Philips-XL30 FEG, Philips) operating at 10.0 kV and all the samples used for SEM analysis were coated with Pd using a sputter coater system. FT-IR was performed on the different heat treated sample powders as well as on the obtained films using a Nicolet 6700 spectrophotometer (Thermo Electron Corporation) using a diamond ATR Smart orbit. Spectra were obtained at 1.0 cm^{-1} resolution averaging 32 scans. The chemical compositions of the films were studied by energy dispersive X-ray spectroscopy (EDX Genesis, EDAX Inc.). The thermal analysis (TG-DSC) of the dried gel powders were carried out in a STA 409 PC thermal analyzer (NETZSCH Instruments) under argon atmosphere employing a heating rate of $10^{\circ}\text{C}\cdot\text{min}^{-1}$.

C.2.3 *In-Vitro* Biodegradation

The *in vitro* degradation characteristics of the uncoated and coated substrates (weight 175 ± 25 mg) were tested in DMEM media without 10% Fetal Bovine Serum (FBS). In order to determine the pH, magnesium ion and yttrium ion concentration, each scaffold was completely immersed in 2.0 ml of media and the media was changed and replaced with fresh media after each 24.0 h. For each coating groups (i.e. $x=0.0, 1, 2$ and 3), three samples were used. The extracted media was used to measure the pH (ϕ 350, Beckman Coulter) and was stored at 4°C before they were used for Mg and Y ions concentration analysis using Inductively Coupled Plasma (ICP, iCAP 6000 series, Thermo Electron Corporation). Each ICP sample was measured in triplicate. The surface morphology of the uncoated and coated samples kept for a desired period of time in media were dried overnight in air and analyzed using SEM and EDX.

C.2.4 Cell Culture

Murine osteoblast cell line, MC3T3-E1, was obtained from ATCC (Manassas, VA). Cells were cultured under 37°C, 5% CO₂, and 95% relative humidity in minimum essential medium alpha (MEM α , Gibco, Grand Island, NY) containing 10% fetal bovine serum (FBS, Atlanta Biologicals, Lawrenceville, GA) and penicillin streptomycin (P/S, Gibco, Grand Island, NY). Cells at third to seventh passage were used in this experiment. For each group, at each time points, three coated substrates were used. All the substrates were sterilized under UV for at least 60 min. These sterilized substrates were placed in 12 well plates following which cells were seeded on them at a concentration of 120,000 cells/well. 1 milliliter of media per cm² of surface area was used and the culture media was changed daily.

C.2.5 Live-Dead Assay

Cell viability was assessed using live/dead staining (Invitrogen, Live/Dead Staining Kit). After day 1, 2 and 3 of culture during which media was changed daily, each sample was washed with phosphate buffered saline (PBS, Lonza BioWhittaker* Buffers and Buffered Salines, 1x, 0.0067M (PO₄) without Calcium or Magnesium) and then incubated for 40 minutes with the live/dead stain diluted in PBS. After incubation, samples were washed twice with PBS prior to imaging. Cells were then imaged by an inverted microscope with the fluorescence illuminator (CKX41, Olympus, Olympus America Inc.). Photos of the cells were obtained with a digital camera (Olympus DP25 Microscope Camera, Olympus, Olympus America Inc.). For each substrate images were taken from three to six different locations to obtain an overview of the cell attachments. Numbers of live, dead cells and % area coverage by live cells were counted from

the images using ImageJ software (National Institutes of Health, USA, rsbweb.nih.gov). For live dead analysis at least 2000 cells were counted for each sample. Cells were then fixed by using 4% paraformaldehyde and incubating for 20 minutes. After fixing, samples were subjected to alcohol dehydration and coated with palladium in order to observe cell morphology by SEM.

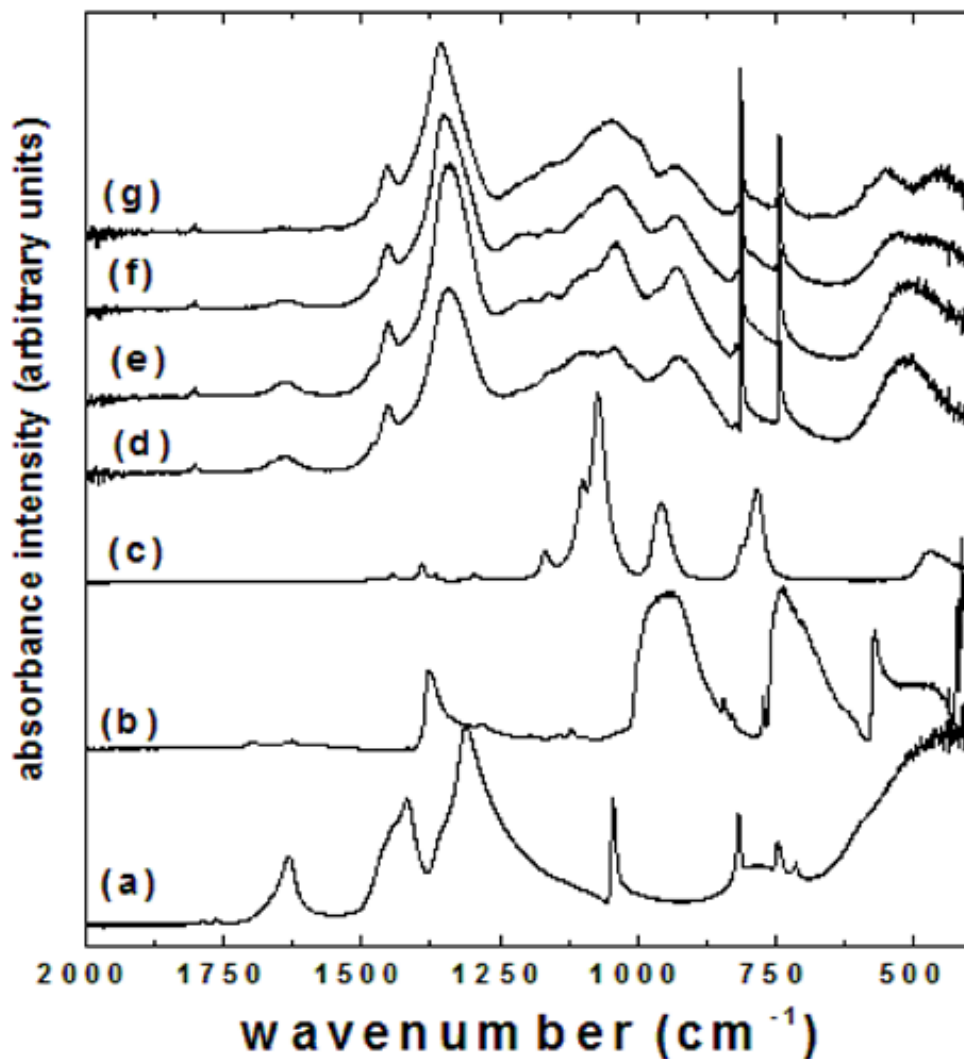


Figure C.1 FT-IR spectra of (a) $\text{Ca}(\text{NO}_3)_2 \cdot 4\text{H}_2\text{O}$, (b) P_2O_5 , (c) tetraethyl orthosilicate (TEOS), (d) dried gel of $x = 0$, (e) dried gel of $x = 1$, (f) dried gel of $x = 2$, and (g) dried gel of $x = 3$.

C.2.6 Cytoskeletal Staining

Cells were fixed with 4% paraformaldehyde for 15 minutes at room temperature. After washing three times with PBS to remove any remnants of paraformaldehyde, cells were stained with Tetramethylrhodamine B isothiocyanate conjugated phalloidin (Sigma-Aldrich) and washed with PBS three times. Subsequently, cells were counterstained with DAPI for nuclear staining. The

stained cells were viewed by an inverted microscope with the fluorescence illuminator (CKX41, Olympus, Olympus America Inc.). Photos of the cells were obtained with a digital camera (Olympus DP25 Microscope Camera, Olympus, Olympus America Inc.).

C.3 RESULTS AND DISCUSSION

The reaction of calcium nitrate with phosphorous pentoxide or with stoichiometric mixture of P_2O_5 and TEOS in ethanol resulted in the formation of a transparent gel at ambient temperature. All these gels showed a reversible and reproducible flow behavior, i.e. high viscosity at low temperature and low viscosity on heating; only when the heating and cooling operations were performed under an air tight sealed glass containers. On heating these gels in air lead to the formation of a translucent gel due to formation of few nanometers sized small colloidal sols, and upon further heating over time, this translucent gel changed to a sol solution. In order to understand the gelation process, FTIR analyses were performed on the dried gel powders together with the starting precursors and are shown in Figure C.1. The presence of a broad band 3450 (not shown) and 1638 cm^{-1} can be assigned to -OH stretching modes for all the dried gels [265-269]. The presence of bands at 741, 812, 1045, 1350 and 1450 cm^{-1} are the characteristics peaks of the nitrate as evident from the spectrum of calcium nitrate as shown in Figure C.1a [268]. The presence of bands from $925\text{ to }1080\text{ cm}^{-1}$ is related to the P-O-C stretching modes [265-269]. It is generally believed that during dissolution in ethanol, phosphorous pentoxide and calcium nitrate react to form a complex compound $[(OCH_2CH_3)_y (NO_3)_{2-y} Ca]_z [P(OCH_2CH_3)_5 \cdot x(OH)_x]_z$, where the z/z' ratio is determined by the Ca/P ratio and the degree of the polymerizations determined by the gel structure [265-269]. The addition of TEOS in the gelation

process does not change the FTIR spectra much, however, the peaks between 850 and 1250 cm^{-1} becomes more distinct with the appearance of two peaks at 540 and 445 cm^{-1} for $x=3$ (Figure C.1, g). The peak at 540 cm^{-1} is due to the Si-O-Si vibration and peak at 445 cm^{-1} assigned to a combination of Si-O-P and Si-O-Si bending vibrations [270, 271]. The weak and broad bands $\sim 1100 \text{ cm}^{-1}$ can be assigned to a combination of P-O stretching of the P-O-P and P-O-Si bridging units [270, 271]. From these results it can be said that the structure of the Si containing gels consists of a mixed frame work, built of $[\text{SiO}_4]$ and $[\text{PO}_4]$ tetrahedral networks, and can thus be constituted to be integrated with the complex polymeric chain discussed above.

Figure C.2 shows the results of DSC-TG analysis for as prepared dried gel for pure ($x=0$) and for a representative Si-containing ($x=2$) dried gel powders in the temperature range 25 to 1000 $^{\circ}\text{C}$ under argon atmosphere. The nature of the DSC-TG curves for un-substituted and Si-containing gels do not show any striking differences and the plots look similar to those reported in the literature [267, 269]. The TG curves for both the samples show a constant weight loss up to 550 $^{\circ}\text{C}$ and the weight remains constant on further increase in temperatures. However, there are some changes in the exothermic peak positions in the temperature ranges of 250-400 $^{\circ}\text{C}$ for the pure and Si-containing gels and these changes reflect some major rearrangements in the bonding and interactions in the gel structures due to the incorporation of the silicon. The major endothermic peak at 550 $^{\circ}\text{C}$ associated with a rapid weight loss in the TG (Figure C.2) is believed to be due to the decomposition of nitrates and organics [267, 269]. From these thermal analysis results it appears that a temperature of $\sim 550^{\circ}\text{C}$ is required for the formation of calcium phosphate. Hence it was concluded that the gel coated substrates should be heated to at least at 550 $^{\circ}\text{C}$ to get an impurity free coating. However, present experimental studies indicate that heating the Mg4Y substrates to higher temperatures, especially above 500 $^{\circ}\text{C}$ for extended period

of time, may lead to deformation of the substrates due to the temperatures being close to the melting point, and thus demand a lower gel decomposition temperature. Since the major decomposition peak due to the nitrates decomposition occurs at $\sim 450^{\circ}\text{C}$, it is reasonable to believe that maintaining coatings at 450°C for a long time would result in complete decomposition of the precursors.

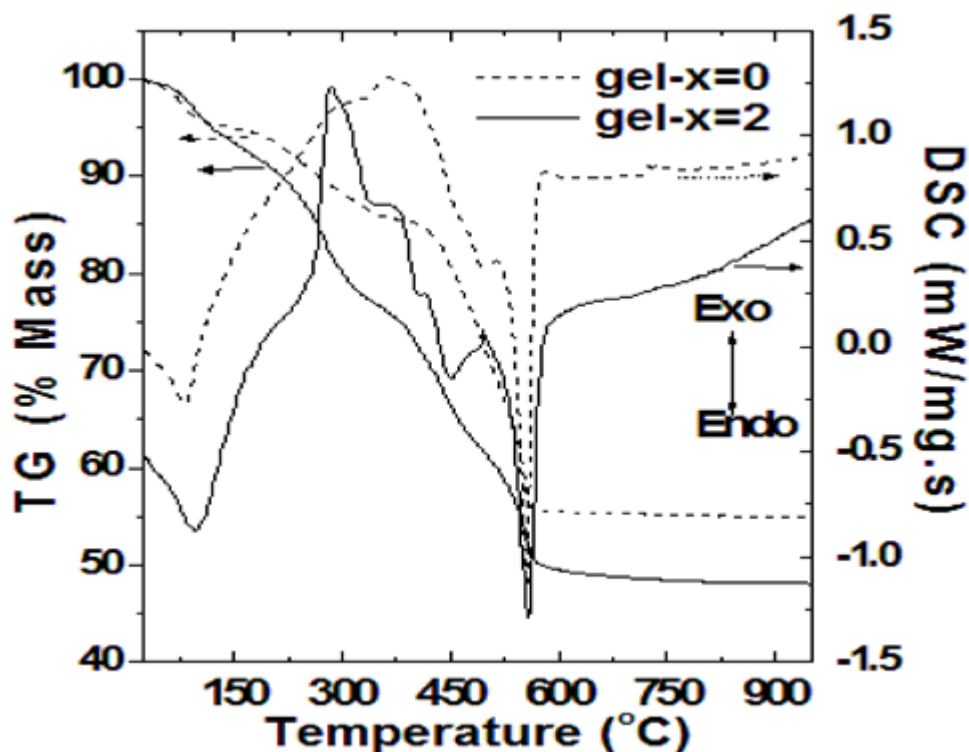


Figure C.2 The DSC and TG curves of the as dried gels.

To verify this, as dried gel powders were heated to 450°C for 24 h in argon and thermal analyses were performed on these heat treated gel powders. The DSC-TG of the heated treated samples show (not shown here) a weight loss of $\sim 4\%$ and $\sim 6\%$ in TG, for $x=0$ and $x=3$, respectively, and absence of any characteristics endo- or exothermic peaks for decomposition of the precursors. This weight change can be due to the presence of some un-decomposed nitrates and

carbonates [268]. These results indicate that the decompositions of the precursors were not fully completed and all the gel coated Mg4Y substrates were heated to 450 °C for 24 h in argon atmosphere may contain traces of impurities, however, any higher temperature heat treatments were not performed to avoid any deformation of the substrates.

The X-ray diffraction (XRD) patterns of the heat treated multiple-coated Mg4Y substrates are shown in Figure C.3. XRD patterns of the film corresponding to $x=0$ (Figure C.3b) shows presence of peaks other than the substrates corresponding closely to β -tricalcium phosphate (β -TCP) and hydroxyapatite (HA). The presence of β -TCP in the multiple coated films can be due to the diffusion of magnesium from the substrate underneath. It is well known that magnesium ions stabilize β -TCP in preference over HA [134]. It should be also noted that the reaction of magnesium with phosphate leads to the generation of excess calcium, the overall Ca/P ratio goes up and hence can favor the formation of HA. For all the silicon containing films, XRD patterns show the presence of HA only (Figure C.3d-f). The XRD results also indicate that silicon possibly stabilizes the HA phase and diffusion of magnesium from the substrate has no effect on the crystalline phase evaluation. It is generally believed that single phase silicon substituted HA (Si-HA) can be formed for Si addition up to 1.97 wt% [253, 272]. Addition of excess silicon generally leads to a mixed phase system of Si-TCP, Si-HA, β -TCP and an amorphous phase of variable Si-Ca-P composition [253, 273]. In the present work, the amounts of Si that have been used (2.6 and 7.1wt % for $x=1$ and $x=3$, respectively) are in excess than the amount of silicon that can be incorporated into the HA structure, and thus formation of mixed phases can be expected. However, the absence of any crystalline peaks other than HA in the coated films heated to 450°C does not obviate the presence of amorphous phases and the

presence of amorphous phase of variable Si-Ca-P compositions or amorphous SiO₂ cannot certainly be discounted.

FTIR spectra of the coated substrates corresponding to x=0, 1, 2 and 3 heated to 450°C for 24 h in argon are shown in Figure C.4. For all the samples the major bands in the range 570 and 605 cm⁻¹ are due to O-P-O bending mode and the intense band in the range 960-1088 can be attributed to P-O stretching vibration modes [265, 266, 269]. Carbonate group substituting the PO₄³⁻ ions in the apatite structure can be detected in all the heat treated coatings by the appearance of bands at 875, 1410 and 1450 cm⁻¹[270]. In spite of these similarities in the FTIR spectra between the non-silicon and silicon containing coatings (Figure C.4 b, d-f), some differences can also be observed. A weak absorption band at 630 cm⁻¹ attributable to the OH⁻¹ vibration mode can be seen in the spectra corresponding to the x=0, but absent in samples where silicon is introduced. This is due to the substitution of PO₄³⁻ by SiO₄⁴⁻ which will lead to a decrease in OH⁻¹ group to maintain the charge balance. For the silicon substituted samples, appearance of a weak band at ~ 520 cm⁻¹ can be observed and this band can be assigned to Si-O-Si vibration [270, 271]. The substitution of phosphate by silicon will lead to incorporation of silicate ions into some of the phosphate sites of the lattice, which will consequently change the bonding and symmetry of the PO₄³⁻ groups and this should be reflected in the FTIR spectra of these Si-substituted samples.

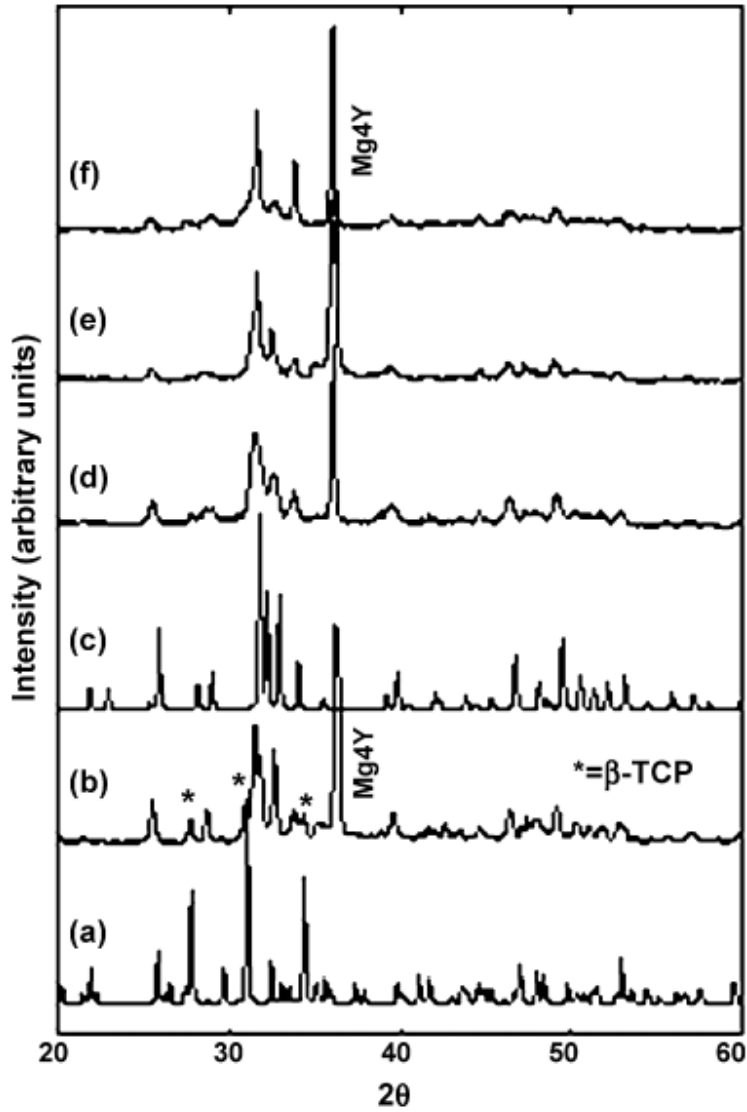


Figure C.3 X-ray diffraction patterns of coated samples heat treated to 450°C, 24 h, in argon together with the standard diffraction patterns (a) JCPDS# 9-169 of β -tricalcium phosphate (β -TCP), (b) $x = 0$, (c) JCPDS #9-432 for hydroxyapatite, (d) $x = 1$, (e) $x = 2$, and (f) $x = 3$.

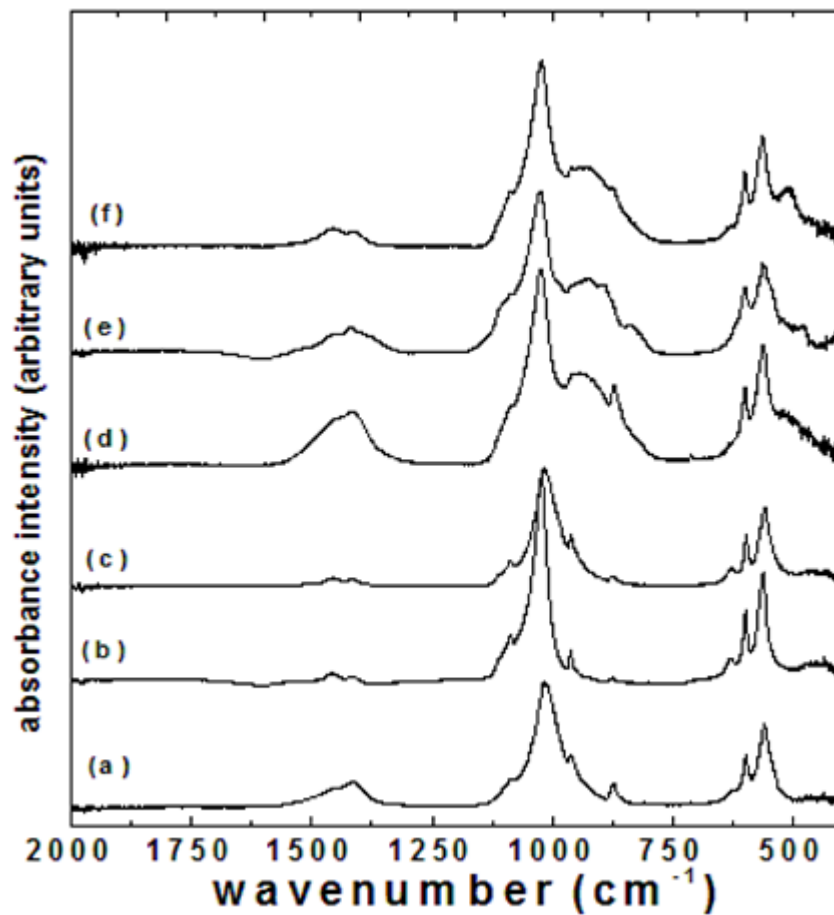


Figure C.4 FTIR spectra for the standard β -tricalcium phosphate (β -TCP), standard hydroxyapatite (HA) powders and gel coated substrates treated to 450°C, 24 h, in argon (a) β -TCP (HIMED, New York, USA), (b) $x = 0$, (c) HA (ACROS organics), (d) $x = 1$, (e) $x = 2$, and (f) $x = 3$.

These changes were indeed observed in the FTIR spectra for silicon containing coatings, the contribution of the intense Si–O–Si asymmetric stretching mode around 1080 cm^{-1} leads to broadening of the bands and the appearance of three weak additional peaks at 940, 890 and 830 cm^{-1} [270, 271]. Presence of these peaks leads to broadening of the band between 780 to 1140 cm^{-1} (Figure C.4, b-d). Similar observations have also been reported for Si-HA powders and coatings [270, 274]. From the analysis of XRD and FTIR results it can be concluded that Si-containing CaPs coatings on the Mg4Y substrates are of calcium phosphate having hydroxyapatite structure (HA) and also confirm the incorporation of silicate ions into the apatite lattice. The present coatings contain excess Si than required to substitute into the HA structure completely as discussed above and thus there may be some other phases of Ca-Si-P and SiO_2 which may also be present in the coatings. However, from these FTIR results it is difficult to confirm that all these phases are indeed present. From these XRD and FTIR results it is also difficult to ascertain that all the silicate ions have entered into the apatite lattice and there is a possibility that certain amount of silicon remains on the HA surface in the form of monomeric or polymeric SiO_4^{4-} [275].

Figure C.5 shows the surface microstructure and the EDX results of the calcium phosphate coated Mg4Y substrates. The thickness of these coatings from the cross sectional SEM images were found to be $\sim 50 (\pm 10)\ \mu\text{m}$. Although the coating looks continuous and homogeneous at low magnification for un-substituted coatings (Figure C.5 a), several cracks can be seen at higher magnifications (Figure C.5 b). Also at higher magnifications, a porous netlike coating was clearly observed and the coating layer consists of nano-sized calcium phosphate (Figure C.5c, 5f). Very similar results were obtained for all the Si-CaPs coated substrates, however, with higher silicon content more cracks on the coatings can be seen (Figure C.5e). The

EDX spectrum, as shown in Figure C.5g, for the un-substituted coating shows the presence of Ca and P and the ratio of Ca/P was ~1.6, thus confirming the presence of calcium phosphate. For the Si-containing coatings, the EDX clearly show the presence of silicon in these coatings and the amounts (weight percentage) of silicon in the coatings were very close to the starting stoichiometric amounts (Figure C.5h). Thus the EDX and FTIR results show the incorporation of silicon in the coatings.

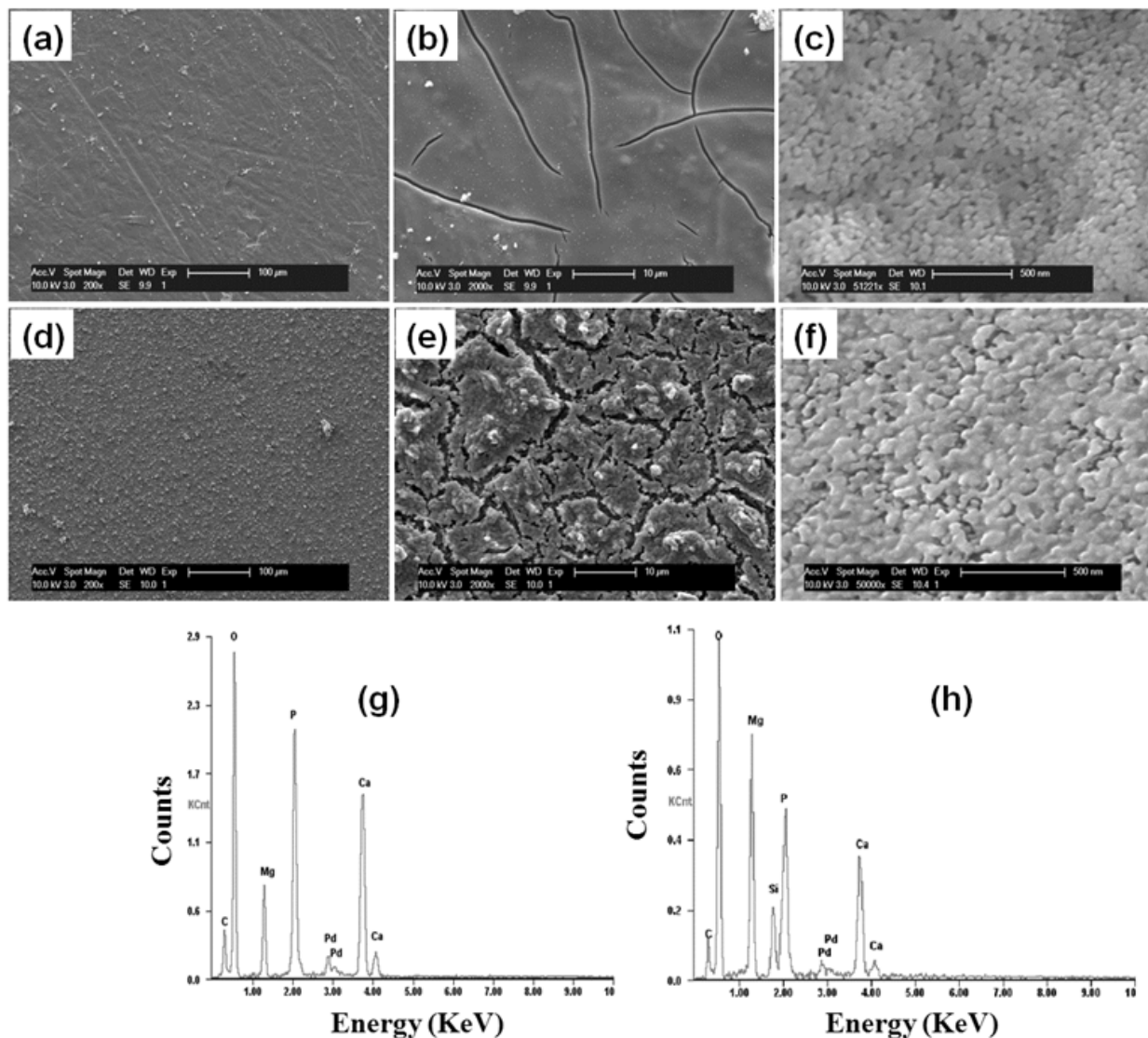


Figure C.5 SEM micrographs at different magnifications and EDX results on the coated substrates heat treated to 450°C, 24 h, argon, (a) SEM of x = 0 coatings; scale bar = 100 μm , (b) SEM of x = 0 coatings; scale bar = 10 μm , (c) SEM of x = 0 coatings; scale bar = 500 nm, (d) SEM of x = 2 coatings; scale bar = 100 μm , (e) SEM of x = 2 coatings; scale bar = 10 μm , (f) SEM of x = 2 coatings; scale bar = 500 nm, (g) EDX spectrum of x = 0 coatings, and (h) EDX spectrum of x = 2 coatings.

The pH values of the DMEM solutions (without any protein) in which the bare and coated substrates were immersed are shown in Figure C.6 a. For all samples the pH values were close to 8.2 and no definitive trend in the changes to the pH value changes can be observed. The magnesium and yttrium ions concentrations, as determined by the ICP, have been shown in Figure C.6 b and c, respectively. Similar to pH, no trend can be observed for these ions. It should also be noted that the concentration of both these ions, especially yttrium, varies over few orders of magnitudes. This large variation of yttrium concentration is most probably due to the irregular corrosion behavior of the native Mg4Y alloy itself and this corrosion rate is not affected much by the presence of calcium phosphate coatings.

These results clearly indicate that the CaPs coatings hardly play any role in changing the degradation behavior of the Mg4Y substrates as the pH and the concentration of Mg and Y ions are very similar for both the bare metal and coated substrates. These observations are not very surprising as all the coated films are porous in nature and these films contain many cracks. The presence of pores and cracks do not prevent the underlying bare substrate from being exposed to the surrounding DMEM and thus the coated substrates behave in a very similar manner to the uncoated substrate when it is in contact with media.

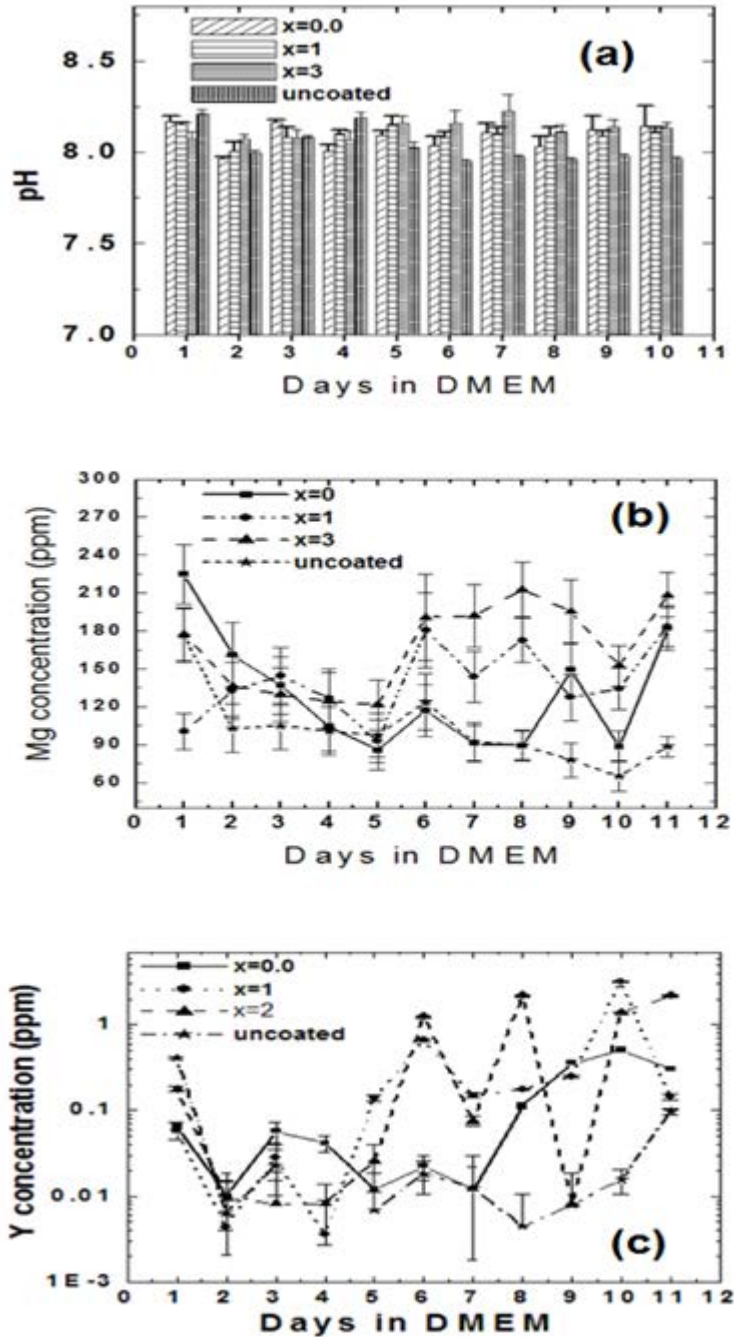


Figure C.6 SEM micrographs at different magnifications and EDX results on the coated substrates heat treated to 450°C, 24 h, argon, (a) SEM of x = 0 coatings; scale bar = 100 m, (b) SEM of x = 0 coatings; scale bar = 10 m, (c) SEM of x = 0 coatings; scale bar = 500 nm, (d) SEM of x = 2 coatings; scale bar = 100 m, (e) SEM of x = 2 coatings; scale bar = 10 m, (f) SEM of x = 2 coatings; scale bar = 500 nm, (g) EDX spectrum of x = 0 coatings, and (h) EDX spectrum of x = 2 coatings.

Other reports of CaPs based coating on magnesium alloys were also found to be porous and contain cracks and thus are not expected to alter the corrosion characteristics of the Mg alloys drastically [114, 115, 225, 241, 249, 260, 261]. Previous studies have reported the formation of a degradation layer during the corrosion process of magnesium alloys and it is assumed that this degradation layer itself also reduces the rate of the corrosion [240, 243, 245, 264]. Witte et al. assumed that this layer is composed of calcium phosphate precipitates and other corrosion products such as magnesium oxide or magnesium hydroxide [245]. A solution with high calcium and magnesium concentration appear to be good environmental conditions for the formation of calcium phosphate precipitates due to the increase in pH of the solution [240]. Thus, in this present study it is reasonable to assume that a similar protective layer should form on the coated and uncoated substrates which may alter the degradation characteristics of the substrates in vitro with time.

Figure C.7 shows the SEM images of the bare and coated samples kept in DMEM under in vitro conditions. The polished surface of the bare metal was slowly covered with layers of corrosion products. SEM studies also indicate that the coatings grew thicker with time. The FTIR results show the presence of $\text{Mg}(\text{OH})_2$ and PO_4^{3-} on these coatings, whereas EDX shows the presence Ca and P together with Mg on the coatings formed on the pristine metals. Interestingly, the atomic percentage of phosphorous was always much higher than calcium, albeit the amount of calcium in DMEM contains twice the amount of phosphorous. This possibly indicates that presence of phosphate in the media not only allows the calcium phosphate to precipitate out due to increase in pH value, but also reacts with the magnesium hydroxide coating that formed initially by reacting with water to deposit a coating of magnesium phosphate.

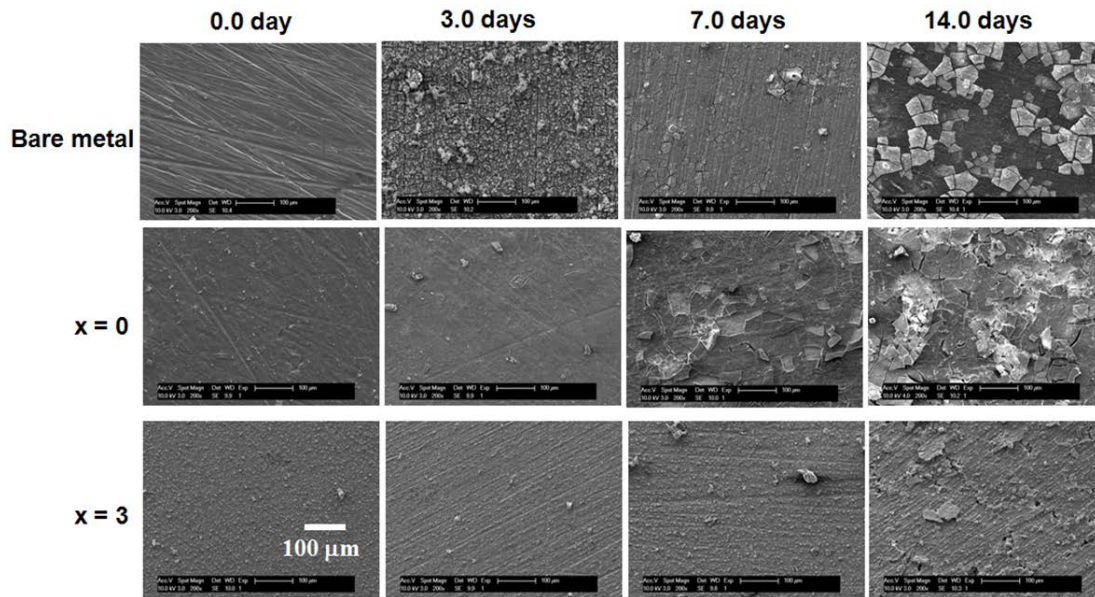


Figure C.7 SEM images of the pristine Mg4Y, CaPs coated (x=0) and Si-CaPs coated (x=3) substrates after incubation in DMEM for different times. The scale bar for all the images is 100 μm.

For CaPs and Si- CaPs coated samples, the coating seems to be very stable up to 3 days and at 7 days some part of the coating begins to peel off. At 14 days, although some of the coatings have degraded, most of the substrates remain coated with HA. Interestingly, the coatings were found to be much more adherent to the substrates for the Si-substituted HA coatings, especially for high silicon containing samples (x=2, 3). However, the exact role of silicon on adherence properties of the coatings is not very clear. As discussed earlier all these CaPs films are porous in nature and thus it is unlikely that they will be able to prevent the interaction between the substrates and the media. This will lead to the degradation of the substrates and eventually detachment of the coatings. This may cause the appearance of loose crystalline CaPs particles and debris around the implant that may cause a foreign body response [276-278]. Resorption of the CaPs coating and particles occurs in most clinical cases; initially by dissolution followed by cell mediated resorption [63, 279]. The biodegradation of these CaPs

particles is controlled by numerous factors, including crystal structure, microporosity, crystallinity, chemical compositions, Ca/P ration, lattice defects, particle size, and purity [63, 277, 280]. In the case of non-degradable alloys such as Ti-6Al-4V, it is generally believed that CaPs coatings should be mechanically stable and strongly adherent to the surface [63]. In the case of degradable metals such as magnesium alloys both the metal and the CaPs coatings should degrade and be replaced by natural bone. Thus the CaPs coatings for degradable metals should have high dissolution and re-precipitation rates, so that it locally provides an ideal site for the cell to adhere, grow and form new bone. In the present study we believe that the coatings peel off due to the rapid corrosion of the Mg4Y in the serum free DMEM, as have been shown by the ICP analyses. The rate of degradation of the alloy can change considerably in the presence of different proteins as shown recently [187, 281]. Thus it is reasonable to assume that the magnesium alloys, and hence the CaP coatings, can be more stable in-vivo than in-vitro. The present CaPs coatings can be resorbed at a much faster rate due to nano-crystalline particle sizes as well as the presence of Si in the structure. It has been reported that Si inhibits the growth of HA crystal and this effect is more significant as the Si level increased [228, 282, 283]. It has also been suggested that increased Si content would cause the HA crystal to be more soluble, releasing more Ca^{2+} , P^{5+} , and Si^{4+} ions into the surroundings [284]. The release of Si^{4+} ions has been shown to alter the surface properties of Si-containing HA [285, 286], which in turn have a positive effect on protein adsorption [287] and hence bioactivity of the coatings [284]. Many published reports suggest that CaPs particles, if present, would not cause any adverse problems as nano-particles can be easily resorbed by macrophages and bone cells [288, 289], and larger particle agglomerates act like a bone graft surrounded by new bone [279, 290].

Cell adhesion to the scaffolds is essential to the development, maintenance, and remodeling of osseous tissues. Adhesive interactions play a critical role in osteoblast survival, proliferation, differentiation, and matrix mineralization. These interactions also play an important role in bone formation, osteoclast function, and bone resorption [291-296]. Fluorescence microscopy in Figure C.8 shows that the live cell attachment was higher on scaffolds with coatings than on bare metal surfaces at day 1 and the number of dead cells are also high on the bare metal in comparison to the coated samples and tissue culture plastics. On day 3, comparatively, more live cells can be seen on the bare metal than the day 1 samples; however, there are also many dead cells. Figure C.8 clearly shows that the number of live cells (green) on the coated substrates is much more than on day 1 and only few dead cells (red) can be seen. The ratio of live cells to dead cells and the average percentage area covered by the live cells on the bare (Mg4Y), CaPs, Si-CaPs coated and normal tissue culture plastics (control) at different time point are shown in Figure C.9. Figure C.9a shows that the ratios of live to dead cells for the coated samples are always better compared to bare metal, especially at 48 h. The number of live cells on Si-CaPs coating seem to be better than the non-Si- containing or low Si-containing coatings. The percentage area covered by the live cells on the substrate increases with time for all the coated substrates and is shown in Figure C.9b. The area covered by the live cells in the case of bare metal was very similar to the CaPs coated substrates after 24 h of cell seeding; however, this value for bare metal does not change much with time. This is also consistent with the ratio of the live to dead cells as shown in Figure C.9a. These live to dead cells ratio values and percentage area coverage by live cells results demonstrate that cells adhered more easily to the coated substrates and grew considerably with time on these substrates in comparison to the bare metal. For the coated substrates the area coverage by the live cells increased considerably

with time. Similar to live to cell ratio results, the Si-CaPs coatings, especially $x=2$ and 3, show better area coverage by the live cells compare to bare metal and CaPs coating. These live dead ratio and live cell area coverage possibly indicate better in-vitro bioactivity of the Si-CaPs coatings. These results do not reflect any possible cytotoxic effect of any un-decomposed nitrates and carbonates that may remain in the coatings as found by the DSC-TG analyses. From these results it is also not possible to assess the role and effect of any amorphous Ca-Si-P or SiO_2 phases that may present in the Si-containing coated substrates on the cytotoxicity and cell viability.

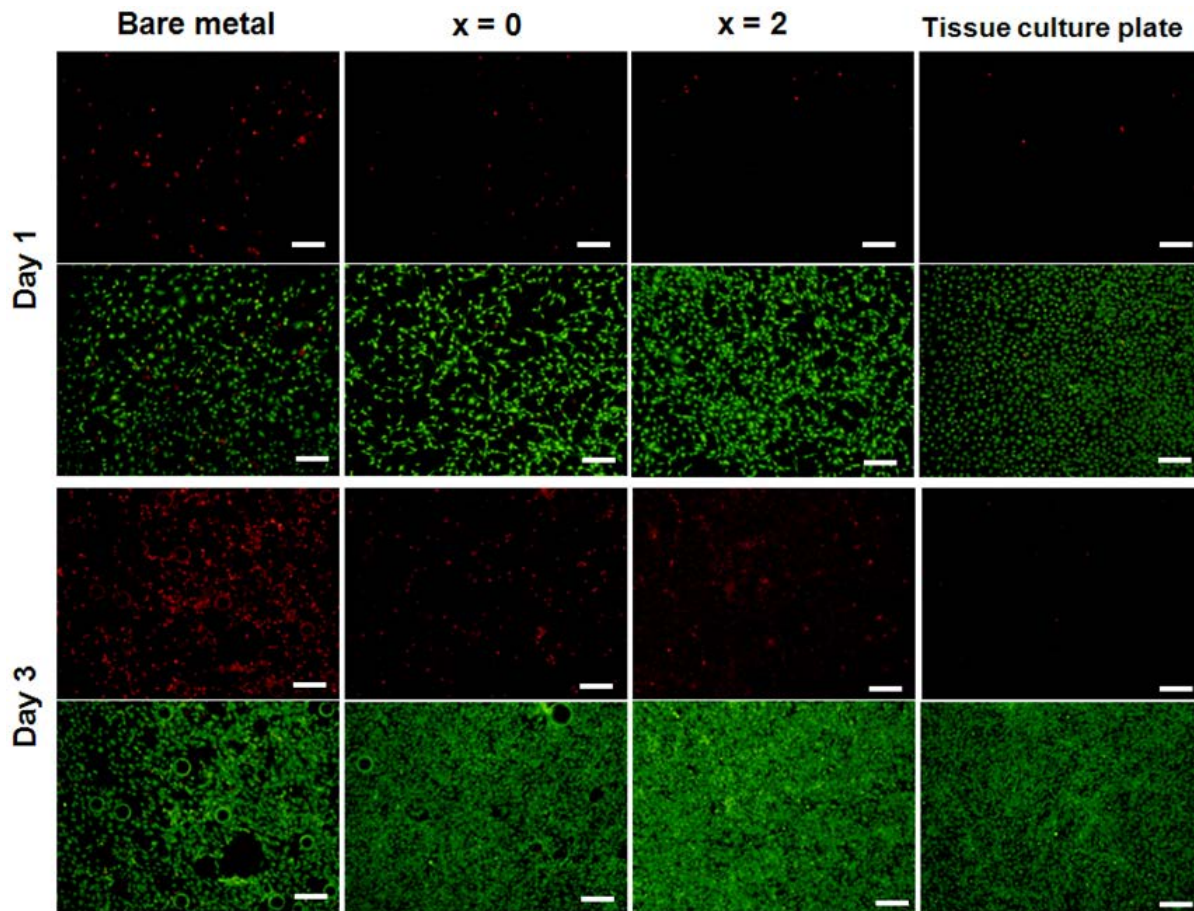


Figure C.8 MC3T3-E1 cells were seeded onto uncoated, CaPs coated ($x=0$) and Si-CaPs coated ($x=2$) substrates, and tissue culture polystyrene plate, incubated for 24h and 72h, and double-stained to be green for live cells and red for dead cells. The scale bar for all the images is 100 μ m.

Figure C.10 shows the SEM images of the osteoblast cells cultured for 1 day and after 3 days on CaPs coated magnesium substrates. The images show that the number of cells attached to the coated substrates after 3 days is much larger compared to the cells seen on day 1 and very similar to the results obtained by direct live-dead cell imaging. For uncoated samples however, not many cells were found after 1-day of incubation and only few cells can be seen after 3 days of culture. For CaPs coated 1 day culture samples, many cells were observed and cells seemed to be interconnected. After 3 days of culture on CaPs and Si-CaPs coated samples, more cells were found on the surface and the cells have connected each other and covered most of the samples (Figure C.10, b and d). Also, after 3 days of culture, the cells and the excreted matrixes were connected together and it is hard to distinguish between the cell and the matrix.

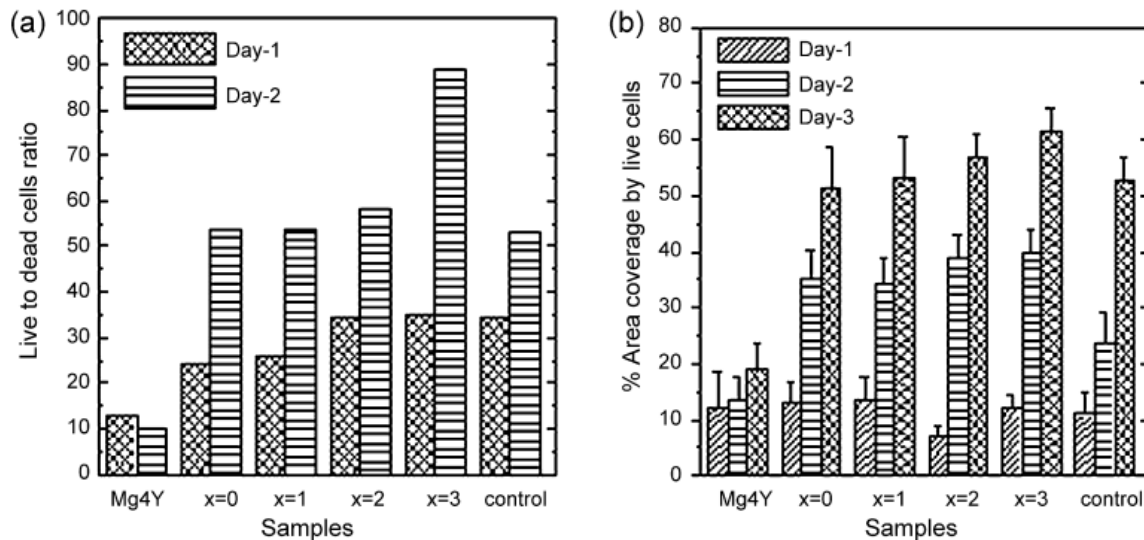


Figure C.9 Plots of (a) live to dead MC3T3-E1 cells ratio and (b) % area coverage by live MC3T3-E1 cells for bare metal (Mg4Y), CaPs coated (x = 0) and Si-CaPs coated (x = 1, 2, and 3) substrates together with tissue culture plastics as control.

In some parts of the coatings as shown in the high magnification SEM image (Figure C.10, c), the cells develop cytoplasmic extensions with lengths of 20–30 μm that appear to anchor onto the CaPs coating. These cytoplasmic extensions are regions of the cell plasma membrane that contain a meshwork or bundles of actin-containing microfilaments which permit the movement of the migrating cells along a substratum [102, 297]. Figure C.10 c also shows that the cells have formed cell–cell junctions (shown by arrow) and developed extensions that bridged the cracks of the porous films. In some cases (figure not shown) it was also observed that the cells had resided into a crack of the films and the tip of the cytoplasmic extension attached firmly to the CaPs and Si-CaPs coatings. Thus these SEM results together with live dead results on the cell attachment clearly demonstrate that CaPs and Si-CaPs coated substrates show better cell response in contrast to the pristine uncoated Mg4Y samples during the whole incubation time.

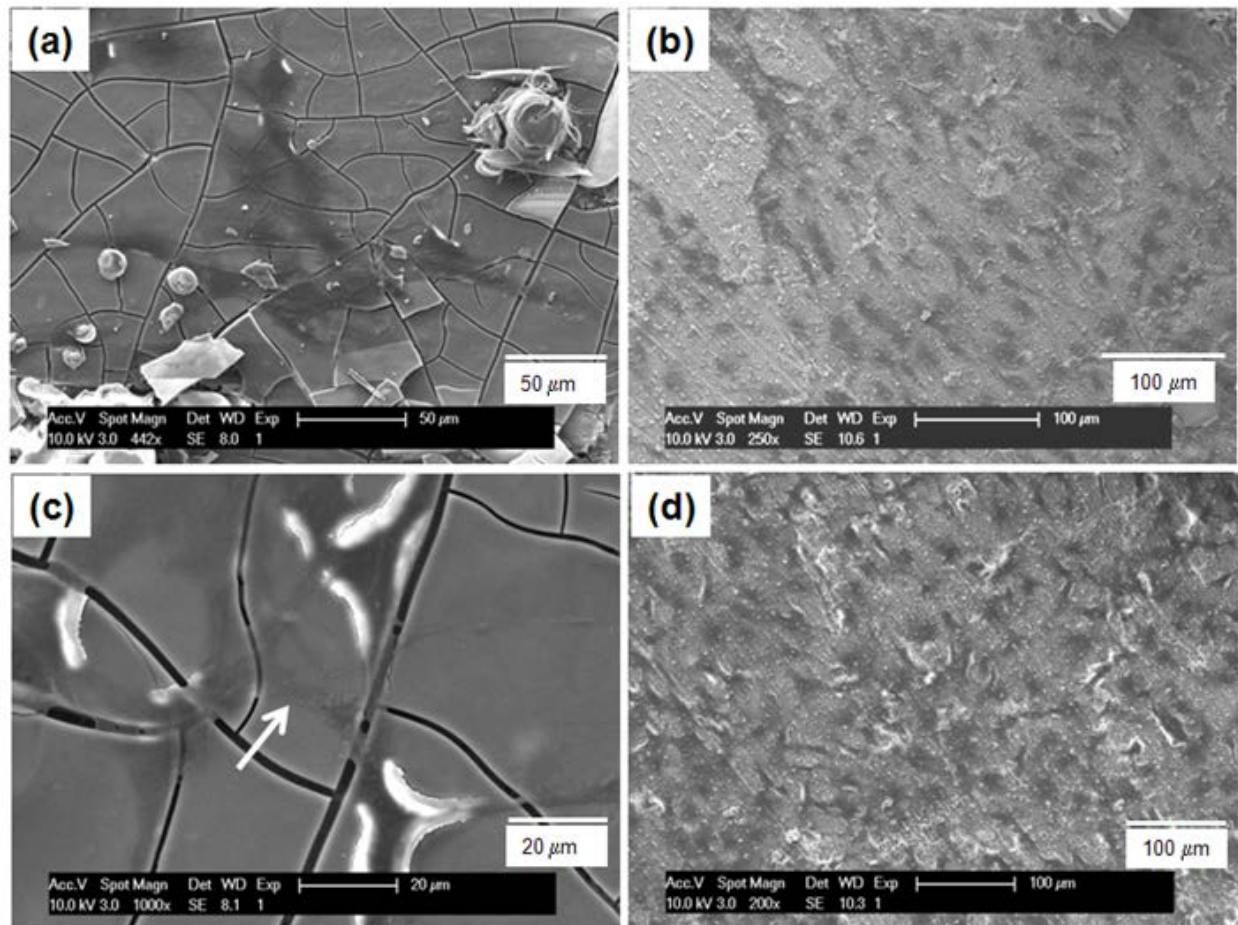


Figure C.10 SEM images of MC3T3-E1 cells on (a) CaPs coated ($x=0$) substrate at day 1, (b) CaPs coated ($x=0$) substrate at day 3, (c) CaPs coated ($x=0$) substrate at day 3, arrow showing cell junction and extension that bridges the crack in the porous films, and (d) Si-CaPs coated ($x = 3$) substrate at day 3.

The surface bioactivity of any biomaterial is mainly controlled by the physical and chemical properties of the surface [291-296]. It is generally accepted that a porous surface contributes greatly to the increased cell adhesion and growth resulting in a significantly stronger bond to the host tissue. Moreover, the porous structure of the coatings consists of nano-sized calcium phosphates with increased surface area, boundaries, and roughness that most likely facilitate an increase in numerous protein interactions and adsorption, thereby aiding cell adhesion, alignment, and finally tissue integration [291-296, 298]. In the present study, porous surface coatings consisting of nano-sized CaPs were successfully prepared on magnesium substrates by the sol-gel method, as shown in Figure C.5, which would definitely contribute to the good surface bioactivity.

In addition to the physical properties, chemical properties of the surface also play a very important role in determining the surface bioactivity. In order to improve the surface biocompatibility, various calcium phosphate coatings including brushite, tricalcium phosphate and hydroxyapatite have been successfully applied to magnesium alloys and it has been shown that the bioactivity of these coated substrates are better compared to the bare magnesium alloys [241, 261-264]. Our current results also show that cells attach and grow more favorably on the CaPs or Si-CaPs coated substrates than the bare metal as shown in Figure C.8, Figure C.9 and Figure C.10. The present work also indicates that Si-containing CaPs coatings show slightly improved bioactivity compared to non-Si-containing CaPs coating.

C.4 CONCLUSIONS

Porous thick (~50 μm) coatings consisting mostly of nano-sized calcium phosphate and Si-containing calcium phosphate were successfully deposited on magnesium alloy by sol-gel technique to improve the bioactivity of the magnesium alloy surfaces. Structural characterizations using XRD and FTIR show the formation of β -TCP and HA for non-Si containing coating and formation of mainly HA for Si-containing coatings. In vitro biodegradation test show that these films were not efficient in reducing the degradation of the substrate which is due to the porous nature as well presence of several cracks in the films. The films were found to be stable on the surfaces for at least 3 days under in vitro conditions and then some parts of the coatings were observed to peel off from the substrates. This is most probably due the corrosion of the underlying alloy surface due to the porosity and cracked nature of the coatings. In vitro biocompatibility experiments clearly demonstrate that the CaPs and Si-CaPs coated substrates are more cytocompatible than the uncoated alloy surfaces and thus can be useful for rapid osseo-integration in vivo.

APPENDIX D

CALCIUM PHOSPHATE COATINGS FORMED ON MICROARC OXIDIZED MAGNESIUM ALLOY SUBSTRATES

D.1 INTRODUCTION

In the previous work studying calcium phosphate coatings on magnesium alloys using aqueous approaches, it was observed that pretreatment processing is crucial to the overall coating stability and microstructure. Pretreatment using phosphate containing solutions and HF were studied. In the current Section, the use of micro-arc oxidation (MAO), also referred to as plasma electrolytic oxidation (PEO), was studied as a pretreatment protocol to subsequently deposit calcium phosphate coatings. MAO treatment results in the formation of highly porous, several micron thick, homogeneous oxide coatings with good adhesion on Mg alloys. To date, MAO coatings have only recently been studied as a pretreatment option to deposit CaP coatings. The coatings deposited on MAO treated substrates are yet to be studied either *in vitro* or *in vivo*.

D.2 MATERIALS AND METHODS

D.2.1 Formation of MAO Coatings

AZ31 substrates were etched and polished, as previously described. Electrical contacts were then prepared using a conductive silver paste and epoxy to provide insulation upon exposure to aqueous media. The electrolyte solution consisted of 9 g L⁻¹ Na₂SiO₃, 6 g L⁻¹ KF, and 3 g L⁻¹ Na₃PO₄. Insulated samples were immersed into this solution while connected to a power supply. Once fixed, a potential of approximately 200 V was applied. The coatings were deposited for 5, 10, and 20 minute periods.

D.2.2 Formation of CaP Coatings on MAO Treated Substrates

CaP coatings were deposited on MAO treated substrates by immersing these substrates into solutions kept at 70°C prepared with CaCl₂, Na₂HPO₄, and SrCl₂, as previously described. The substrates were immersed in these solutions for a period of 6 hours resulting in the deposition of CaP on their surfaces.

D.2.3 Analysis of Coating Microstructure

After applying CaP coatings, the samples were then sputter coated with palladium ((Cressington sputter coater 108A). The coating microstructure was then analyzed by imaging using scanning electron microscopy (Philips XL30 FEG ESEM).

D.2.4 Electrochemical Corrosion Analysis

Electrochemical corrosion experiments were performed at 37°C in Hank's buffered solution using a CH604a electrochemical workstation (CH Instruments, Austin TX). A three electrode cell comprising of platinum as a counter electrode and a Ag/AgCl reference electrode was used. Open circuit potential (OCP) was first established for all the samples after at least 1 h of stabilization in 125 ml of DMEM. Potentiodynamic polarization tests were then performed at a scan rate of 1 mV s⁻¹. Corrosion current and potential were determined using a Tafel extrapolation added into the OriginPro 8 data analysis and graphing software.

D.2.5 MC3T3-E1 Cell Culture

Murine preosteoblast cell line, MC3T3-E1, was obtained from ATCC (Manassas, VA). Cells were cultured under 37°C, 5% CO₂, and 95% relative humidity in minimum essential medium alpha (α -MEM, Gibco, Grand Island, NY) containing 10% FBS and 1% penicillin streptomycin (P/S, Gibco, Grand Island, NY). Cells after third passage were used in experiments and were seeded at a density of 50,000 cells per pellet/scaffold.

D.2.6 Live/Dead Staining

Cell viability was assessed using live/dead staining (Invitrogen, Live/Dead Staining Kit). After 3 days of culture on heat treated pellets, samples were washed with phosphate buffered saline (PBS) and incubated for 40 minutes with the live/dead stain. After incubation, the samples were once again gently washed with PBS prior to imaging using fluorescence (Olympus CKX41).

D.3 RESULTS AND DISCUSSION

The corrosion protection provided by the coatings formed on polished AZ31 substrates after subjecting to MAO treatment was analyzed using Tafel analysis. The data collected for bare AZ31 and the coatings formed after 5, 10, and 20 minutes are illustrated in Figure D.1. The experiments were performed using Hank's buffer solution kept at 37°C. Interestingly, a more negative corrosion potential (E_{corr}) was observed for all coated samples in comparison to AZ31. However, the greatest difference in potential observed between two conditions was roughly 100 mV. Therefore, this difference in potential alone may be too small to confirm which coating condition provides the best corrosion potential.

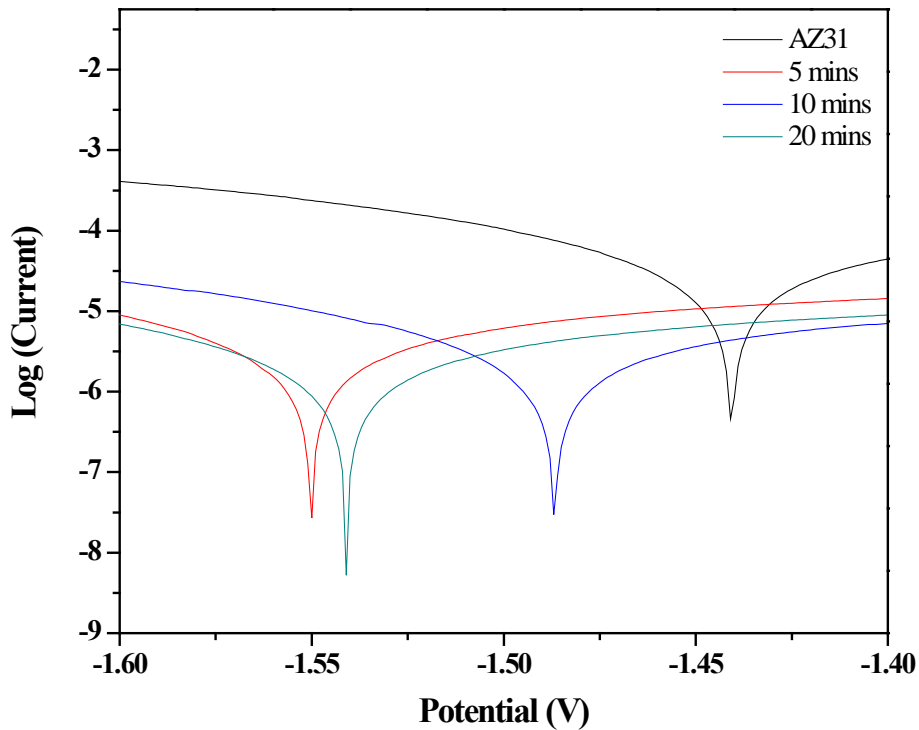


Figure D.1 Tafel plots of MAO treated AZ31 for coatings deposited after various amounts of time in Hank's buffer solution kept at 37°C.

The corrosion current was therefore analyzed to further study the capability of these MAO coatings to provide corrosion protection. In comparison to AZ31, a substantially reduced corrosion current (I_{corr}) was observed for all MAO coatings conditions. A slightly lower I_{corr} was obtained upon increasing the time of coating deposition. The decrease observed with increasing time may be due to the formation of coatings with increased thickness. Nonetheless, for all future experiments, the coatings formed after 10 minutes were chosen as the condition to deposit CaP coatings on due to the similar I_{corr} value in comparison to the coating deposited after 20 minutes and the more positive E_{corr} obtained.

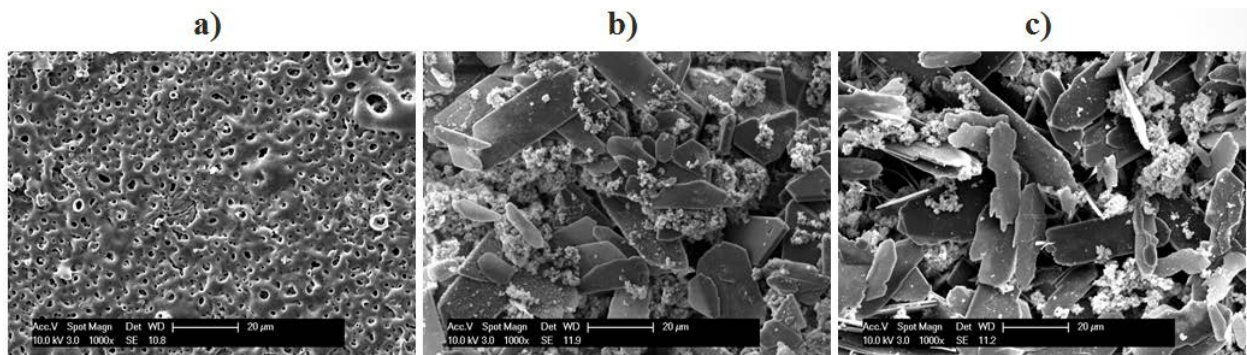


Figure D.2 The microstructure of a) MAO coated AZ31 after 10 minutes, b) the CaP coating formed on top of MAO treated AZ31, and c) the CaP coating formed in the presence of 10% Sr on MAO treated AZ31 at 1000X.

The microstructure of the coatings formed after 10 minutes of MAO treatment and subsequent CaP treatment with or without Sr is illustrated in Figure D.2. As expected, the typical porous structure of MAO coatings was observed prior to depositing CaP coatings (Figure D.2 a)). After immersion in CaP containing solutions (Figure D.2 b) and c)), a quite different microstructure consisting of plate like particles was observed. The coated substrates were then imaged at a slightly higher magnification (Figure D.3). The 2-5 µm pores of the coating formed

after MAO treatment were clearly observed (Figure D.3 a)). For the CaP coated substrates, in addition to the plate like particles previously detected, much smaller round particles were also observed (Figure D.3 b) and c)).

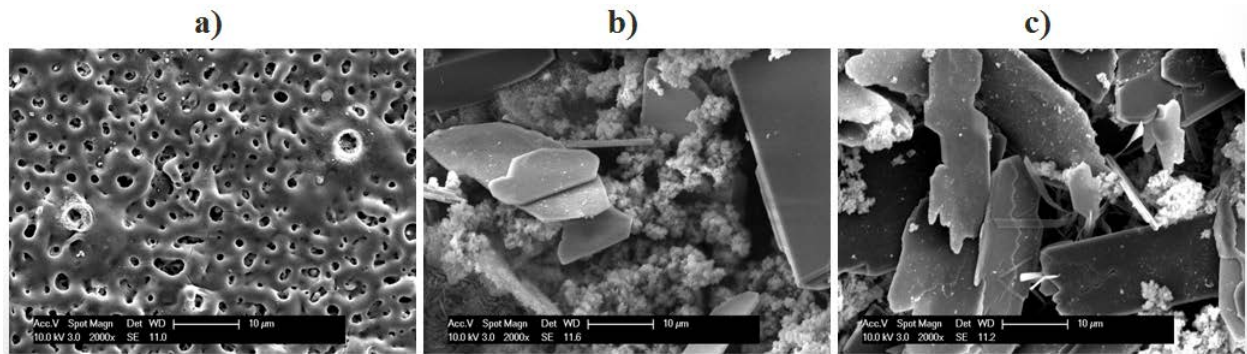


Figure D.3 The microstructure of a) MAO coated AZ31 after 10 minutes, b) the CaP coating formed on top of MAO treated AZ31, and c) the CaP coating formed in the presence of 10% Sr on MAO treated AZ31 at 2000X.

After confirming the formation of CaP coatings on the MAO treated substrates, MC3T3-E1 murine preosteoblasts were seeded directly on the coated substrates to evaluate the capability of these coatings to support cell proliferation. Live/dead staining was performed after 3 days (Figure D.4). Quite a few live cells were observed on tissue culture plastic, used as a positive control (Figure D.4 a)). However, very few live cells were observed on the MAO treated substrates without CaP coatings (Figure D.4 b)). A substantial improvement in live cell attachment was observed on both CaP coated substrates (Figure D.4 c) and d)). In comparing the CaP coatings formed with and without Sr, very little difference was observed between the two different coating conditions.

The live/dead assay was performed once again after 7 days of culture. The images collected are illustrated in Figure D.5. In comparison to the data collected after 3 days, the cells

seeded on culture plastic are much more confluent and very few dead cells were observed. (Figure D.5 a)). For the MAO coated substrates, several rounded dead cells were observed and either very few or no live cells were detected (Figure D.5 b)). For the CaP coated substrates, an increase in live cell density was observed for both conditions (Figure D.5 c) and d)). However a much larger increase in live cell density was observed on the substrates prepared with Sr in comparison to those prepared without Sr.

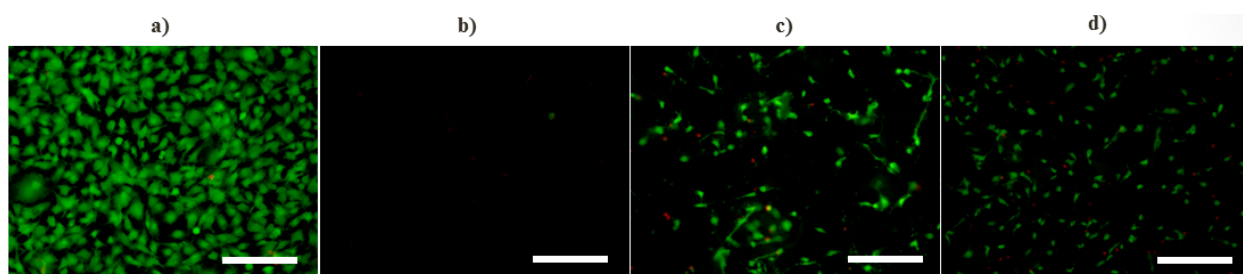


Figure D.4 Live/dead staining of MC3T3-E1 cells on a) tissue culture plastic, b) MAO treated AZ31, c) CaP coated MAO treated AZ31, and d) SrCaP coated MAO treated AZ31 after 3 days of culture. Scale bars are 200 μm .

In summary, CaP and SrCaP coatings were formed on MAO treated AZ31 substrates. MAO coated substrates alone were incapable of supporting MC3T3-E1 proliferation. This is most likely due to the highly porous nature of these coatings resulting in increased Mg^{2+} concentration. Both CaP and SrCaP coatings supported cell attachment and proliferation. Increased proliferation was observed on the coating prepared with Sr in comparison to those prepared without Sr.

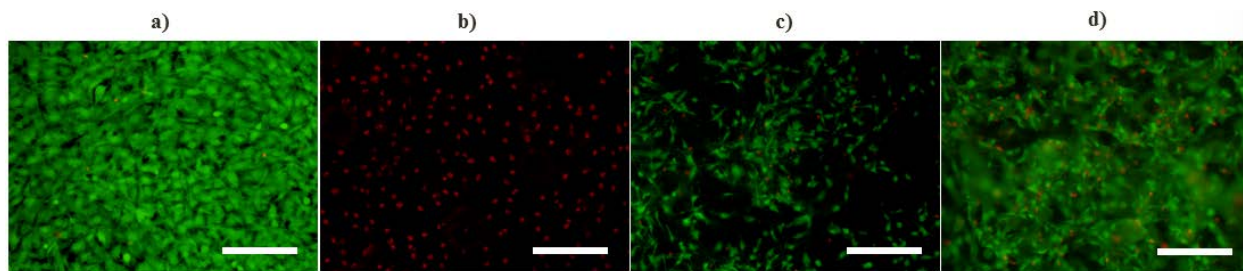


Figure D.5 Live/dead staining of MC3T3-E1 cells on a) tissue culture plastic, b) MAO treated AZ31, c) CaP coated MAO treated AZ31, and d) SrCaP coated MAO treated AZ31 after 7 days of culture. Scale bars are 200 μm .

D.4 CONCLUSIONS

MAO treatment proved to be a useful pretreatment technique to prior to depositing CaP coatings on AZ31 degradable substrates. Although the presence of Sr in the CaP coatings deposited has not been confirmed, the coatings prepared in Sr containing solutions were capable of supporting enhanced proliferation. In future work, this pretreatment protocol will be compared to other pretreatment regimes, such as Na_2HPO_4 immersion and heat treatment, previously studied to determine its role in providing corrosion protection and supporting improved cytocompatibility on CaP coated AZ31 with and without Sr.

BIBLIOGRAPHY

- [1] C. M. Weaver and R. K. Fuchs, "Chapter 12 - Skeletal Growth and Development," in *Basic and Applied Bone Biology*, D. B. Burr and M. R. Allen, Eds., ed San Diego: Academic Press, 2014, pp. 245-260.
- [2] F. Long, "Chapter 3 - Prenatal Bone Development," in *Pediatric Bone (Second Edition)*, F. H. Glorieux, J. M. Pettifor, and H. Jüppner, Eds., ed San Diego: Academic Press, 2012, pp. 39-53.
- [3] C. Sfeir, L. Ho, B. Doll, K. Azari, and J. Hollinger, "Fracture Repair," in *Bone Regeneration and Repair*, J. Lieberman and G. Friedlaender, Eds., ed: Humana Press, 2005, pp. 21-44.
- [4] A. C. Karaplis, "Chapter 3 - Embryonic Development of Bone and Regulation of Intramembranous and Endochondral Bone Formation," in *Principles of Bone Biology (Third Edition)*, J. P. Bilezikian, L. G. Raisz, and T. J. Martin, Eds., ed San Diego: Academic Press, 2008, pp. 53-84.
- [5] T. Mclau, R. Schneider, B. Frank Eames, and J. Helms, "Common Molecular Mechanisms Regulating Fetal Bone Formation and Adult Fracture Repair," in *Bone Regeneration and Repair*, J. Lieberman and G. Friedlaender, Eds., ed: Humana Press, 2005, pp. 45-55.
- [6] P. Fratzl and R. Weinkamer, "Nature's hierarchical materials," *Progress in Materials Science*, vol. 52, pp. 1263-1334, 2007.
- [7] R. Z. LeGeros, "Calcium Phosphate-Based Osteoinductive Materials," *Chemical Reviews*, vol. 108, pp. 4742-4753, 2008.
- [8] P. Fratzl, H. S. Gupta, E. P. Paschalis, and P. Roschger, "Structure and mechanical quality of the collagen-mineral nano-composite in bone," *Journal of Materials Chemistry*, vol. 14, pp. 2115-2123, 2004 2004.

- [9] H. Gao, B. Ji, I. L. Jäger, E. Arzt, and P. Fratzl, "Materials become insensitive to flaws at nanoscale: Lessons from nature," *Proceedings of the National Academy of Sciences of the United States of America*, vol. 100, pp. 5597-5600, 2003.
- [10] P. Zioupos, J. D. Currey, and A. J. Hamer, "The role of collagen in the declining mechanical properties of aging human cortical bone," *Journal of Biomedical Materials Research*, vol. 45, pp. 108-116, 1999.
- [11] J. D. Currey, "The design of mineralised hard tissues for their mechanical functions," *Journal of Experimental Biology*, vol. 202, pp. 3285-3294, 1999.
- [12] J. Li and D. L. Stocum, "Chapter 10 - Fracture Healing," in *Basic and Applied Bone Biology*, D. B. Burr and M. R. Allen, Eds., ed San Diego: Academic Press, 2014, pp. 205-223.
- [13] A. R. Shrivats, P. Alvarez, L. Schutte, and J. O. Hollinger, "Chapter 55 - Bone Regeneration," in *Principles of Tissue Engineering (Fourth Edition)*, R. Lanza, R. Langer, and J. Vacanti, Eds., ed Boston: Academic Press, 2014, pp. 1201-1221.
- [14] M. R. Allen and D. B. Burr, "Chapter 4 - Bone Modeling and Remodeling," in *Basic and Applied Bone Biology*, D. B. Burr and M. R. Allen, Eds., ed San Diego: Academic Press, 2014, pp. 75-90.
- [15] J. Hollinger, "Bone Dynamics," in *Bone Regeneration and Repair*, J. Lieberman and G. Friedlaender, Eds., ed: Humana Press, 2005, pp. 1-19.
- [16] D. B. Burr and O. Akkus, "Chapter 1 - Bone Morphology and Organization," in *Basic and Applied Bone Biology*, D. B. Burr and M. R. Allen, Eds., ed San Diego: Academic Press, 2014, pp. 3-25.
- [17] P. Jayakumar and L. Di Silvio, "Osteoblasts in bone tissue engineering," *Proceedings of the Institution of Mechanical Engineers, Part H: Journal of Engineering in Medicine*, vol. 224, pp. 1415-1440, 2010.
- [18] E. Karner, C.-M. Backesjo, J. Cedervall, R. V. Sugars, L. Ahrlund-Richter, and M. Wendel, "Dynamics of gene expression during bone matrix formation in osteogenic cultures derived from human embryonic stem cells in vitro," *Biochimica Et Biophysica Acta-General Subjects*, vol. 1790, pp. 110-118, Feb 2009.

- [19] T. J. Martin, K. Wah Ng, and N. A. Sims, "Chapter 2 - Basic Principles of Bone Cell Biology," in *Translational Endocrinology of Bone*, G. Karsenty, Ed., ed San Diego: Academic Press, 2013, pp. 5-26.
- [20] J. P. T. M. van Leeuwen, B. C. J. van der Eerden, J. van de Peppel, G. S. Stein, and J. B. Lian, "Chapter 9 - Osteoblast Biology," in *Osteoporosis (Fourth Edition)*, R. Marcus, D. Feldman, D. W. Dempster, M. Luckey, and J. A. Cauley, Eds., ed San Diego: Academic Press, 2013, pp. 161-207.
- [21] K. Jähn and L. F. Bonewald, "Chapter 1 - Bone Cell Biology: Osteoclasts, Osteoblasts, Osteocytes," in *Pediatric Bone (Second Edition)*, F. H. Glorieux, J. M. Pettifor, and H. Jüppner, Eds., ed San Diego: Academic Press, 2012, pp. 1-8.
- [22] R. Detsch and A. R. Boccaccini, "The role of osteoclasts in bone tissue engineering," *Journal of Tissue Engineering and Regenerative Medicine*, 2014.
- [23] R. Faccio, Y. Choi, S. L. Teitelbaum, and H. Takayanagi, "6 - The Osteoclast: The Pioneer of Osteoimmunology," in *Osteoimmunology*, J. Lorenzo, Y. Choi, M. Horowitz, and H. Takayanagi, Eds., ed San Diego: Academic Press, 2011, pp. 141-185.
- [24] T. R. Arnett, "Chapter 8 - Osteoclast Biology," in *Osteoporosis (Fourth Edition)*, R. Marcus, D. Feldman, D. W. Dempster, M. Luckey, and J. A. Cauley, Eds., ed San Diego: Academic Press, 2013, pp. 149-160.
- [25] J. Klein-Nulend and L. Bonewald, "Chapter 8 - The Osteocyte," in *Principles of Bone Biology (Third Edition)*, J. P. Bilezikian, L. G. Raisz, and T. J. Martin, Eds., ed San Diego: Academic Press, 2008, pp. 153-174.
- [26] T. Bellido, "Osteocyte-driven bone remodeling," *Calcified Tissue International*, vol. 94, pp. 25-34, 2014.
- [27] L. F. Bonewald, "Chapter 10 - Osteocyte Biology," in *Osteoporosis (Fourth Edition)*, R. Marcus, D. Feldman, D. W. Dempster, M. Luckey, and J. A. Cauley, Eds., ed San Diego: Academic Press, 2013, pp. 209-234.
- [28] F. Barrere, T. A. Mahmood, K. de Groot, and C. A. van Blitterswijk, "Advanced biomaterials for skeletal tissue regeneration: Instructive and smart functions," *Materials Science & Engineering R-Reports*, vol. 59, pp. 38-71, Feb 29 2008.

- [29] H. Yuan, H. Fernandes, P. Habibovic, J. de Boer, A. M. C. Barradas, A. de Ruiter, *et al.*, "Osteoinductive ceramics as a synthetic alternative to autologous bone grafting," *Proceedings of the National Academy of Sciences of the United States of America*, vol. 107, pp. 13614-13619, Aug 3 2010.
- [30] V. M. Goldberg, *Biology of Bone Allograft and Clinical Application*, 2008.
- [31] U. Meyer and H. P. Wiesmann, *Bone and Cartilage Engineering*, 2006.
- [32] V. Devescovi, E. Leonardi, G. Ciapetti, and E. Cenni, "Growth factors in bone repair," *La Chirurgia degli organi di movimento*, vol. 92, pp. 161-8, 2008-Dec 2008.
- [33] E. Gruskin, B. A. Doll, F. W. Futrell, J. P. Schmitz, and J. O. Hollinger, "Demineralized bone matrix in bone repair: History and use," *Advanced Drug Delivery Reviews*, vol. 64, pp. 1063-1077, Sep 2012.
- [34] L. Wolfinbarger, Jr., L. M. Eisenlohr, and K. Ruth, *Demineralized Bone Matrix: Maximizing New Bone Formation for Successful Bone Implantation*, 2008.
- [35] S. B. Nicoll, *Materials for Bone Graft Substitutes and Osseous Tissue Regeneration*, 2011.
- [36] W. Habraken, J. G. C. Wolke, and J. A. Jansen, "Ceramic composites as matrices and scaffolds for drug delivery in tissue engineering," *Advanced Drug Delivery Reviews*, vol. 59, pp. 234-248, 2007.
- [37] D. Eyrich, F. Brandl, B. Appel, H. Wiese, G. Maier, M. Wenzel, *et al.*, "Long-term stable fibrin gels for cartilage engineering," *Biomaterials*, vol. 28, pp. 55-65, 2007.
- [38] J. F. A. Valente, T. A. M. Valente, P. Alves, P. Ferreira, A. Silva, and I. J. Correia, "Alginate based scaffolds for bone tissue engineering," *Materials Science and Engineering C*, vol. 32, pp. 2596-2603, 2012.
- [39] A. J. Mieszawska, N. Fournaligas, I. Georgakoudi, N. M. Ouhib, D. J. Belton, C. C. Perry, *et al.*, "Osteoinductive silk-silica composite biomaterials for bone regeneration," *Biomaterials*, vol. 31, pp. 8902-8910, 2010.

- [40] C. Li, C. Vepari, H. J. Jin, H. J. Kim, and D. L. Kaplan, "Electrospun silk-BMP-2 scaffolds for bone tissue engineering," *Biomaterials*, vol. 27, pp. 3115-3124, 2006.
- [41] A. R. Costa-Pinto, R. L. Reis, and N. M. Neves, "Scaffolds based bone tissue engineering: The role of chitosan," *Tissue Engineering - Part B: Reviews*, vol. 17, pp. 331-347, 2011.
- [42] K. E. Tanner, "Bioactive ceramic-reinforced composites for bone augmentation," *Journal of the Royal Society Interface*, vol. 7, pp. S541-S557, 2010.
- [43] A. M. Ferreira, P. Gentile, V. Chiono, and G. Ciardelli, "Collagen for bone tissue regeneration," *Acta Biomaterialia*, vol. 8, pp. 3191-3200, 2012.
- [44] F. Tamimi, B. Kumarasami, C. Doillon, U. Gbureck, D. Le Nihouannen, E. L. Cabarcos, *et al.*, "Brushite-collagen composites for bone regeneration," *Acta Biomaterialia*, vol. 4, pp. 1315-1321, 2008.
- [45] J. F. Mano, G. A. Silva, H. S. Azevedo, P. B. Malafaya, R. A. Sousa, S. S. Silva, *et al.*, "Natural origin biodegradable systems in tissue engineering and regenerative medicine: Present status and some moving trends," *Journal of the Royal Society Interface*, vol. 4, pp. 999-1030, 2007.
- [46] A. Butscher, M. Böhner, S. Hofmann, L. Gauckler, and R. Müller, "Structural and material approaches to bone tissue engineering in powder-based three-dimensional printing," *Acta Biomaterialia*, vol. 7, pp. 907-920, 3// 2011.
- [47] F. Croisier and C. Jérôme, "Chitosan-based biomaterials for tissue engineering," *European Polymer Journal*, vol. 49, pp. 780-792, 2013.
- [48] J. E. Lee, K. E. Kim, I. C. Kwon, H. J. Ahn, S. H. Lee, H. Cho, *et al.*, "Effects of the controlled-released TGF- β 1 from chitosan microspheres on chondrocytes cultured in a collagen/chitosan/glycosaminoglycan scaffold," *Biomaterials*, vol. 25, pp. 4163-4173, 2004.
- [49] C. Xu, C. Lei, L. Meng, C. Wang, and Y. Song, "Chitosan as a barrier membrane material in periodontal tissue regeneration," *Journal of Biomedical Materials Research - Part B Applied Biomaterials*, vol. 100 B, pp. 1435-1443, 2012.

- [50] X. Liu and P. X. Ma, "Polymeric scaffolds for bone tissue engineering," *Annals of Biomedical Engineering*, vol. 32, pp. 477-486, 2004.
- [51] I. O. Smith, X. H. Liu, L. A. Smith, and P. X. Ma, "Nanostructured polymer scaffolds for tissue engineering and regenerative medicine," *Wiley Interdisciplinary Reviews: Nanomedicine and Nanobiotechnology*, vol. 1, pp. 226-236, 2009.
- [52] J. C. J. Webb and R. F. Spencer, "The role of polymethylmethacrylate bone cement in modern orthopaedic surgery," *Journal of Bone and Joint Surgery - Series B*, vol. 89, pp. 851-857, 2007.
- [53] H. Deramond, C. Depriester, P. Galibert, and D. Le Gars, "Percutaneous vertebroplasty with polymethylmethacrylate: Technique, indications, and results," *Radiologic Clinics of North America*, vol. 36, pp. 533-546, 1998.
- [54] L. Wang, D. M. Yoon, P. P. Spicer, A. M. Henslee, D. W. Scott, M. E. Wong, *et al.*, "Characterization of porous polymethylmethacrylate space maintainers for craniofacial reconstruction," *Journal of Biomedical Materials Research - Part B Applied Biomaterials*, vol. 101 B, pp. 813-825, 2013.
- [55] M. A. Lopez-Heredia, Y. Sa, P. Salmon, J. R. De Wijn, J. G. C. Wolke, and J. A. Jansen, "Bulk properties and bioactivity assessment of porous polymethylmethacrylate cement loaded with calcium phosphates under simulated physiological conditions," *Acta Biomaterialia*, vol. 8, pp. 3120-3127, 2012.
- [56] M. Sokolsky-Papkov, K. Agashi, A. Olaye, K. Shakesheff, and A. J. Domb, "Polymer carriers for drug delivery in tissue engineering," *Advanced Drug Delivery Reviews*, vol. 59, pp. 187-206, 2007.
- [57] J. S. Park, H. N. Yang, S. Y. Jeon, D. G. Woo, K. Na, and K. H. Park, "Osteogenic differentiation of human mesenchymal stem cells using RGD-modified BMP-2 coated microspheres," *Biomaterials*, vol. 31, pp. 6239-6248, 2010.
- [58] N. Saito and K. Takaoka, "New synthetic biodegradable polymers as BMP carriers for bone tissue engineering," *Biomaterials*, vol. 24, pp. 2287-2293, 2003.
- [59] F. Witte, N. Hort, C. Vogt, S. Cohen, K. U. Kainer, R. Willumeit, *et al.*, "Degradable biomaterials based on magnesium corrosion," *Current Opinion in Solid State & Materials Science*, vol. 12, pp. 63-72, 2008.

- [60] H. B. Wen, J. R. de Wijn, F. Z. Cui, and K. de Groot, "Preparation of calcium phosphate coatings on titanium implant materials by simple chemistry," *Journal of Biomedical Materials Research*, vol. 41, pp. 227-236, 1998.
- [61] R. Zeng, W. Dietzel, F. Witte, N. Hort, and C. Blawert, "Progress and challenge for magnesium alloys as biomaterials," *Advanced Engineering Materials*, vol. 10, pp. B3-B14+702, 2008.
- [62] M. Niinomi, M. Nakai, and J. Hieda, "Development of new metallic alloys for biomedical applications," *Acta biomaterialia*, vol. 8, pp. 3888-3903, 2012.
- [63] R. Narayanan, S. K. Seshadri, T. Y. Kwon, and K. H. Kim, "Calcium phosphate-based coatings on titanium and its alloys," *Journal of Biomedical Materials Research Part B-Applied Biomaterials*, vol. 85B, pp. 279-299, Apr 2008.
- [64] L. Le Guehennec, A. Soueidan, P. Layrolle, and Y. Amouriq, "Surface treatments of titanium dental implants for rapid osseointegration," *Dental Materials*, vol. 23, pp. 844-854, 2007.
- [65] M. Niinomi and M. Nakai, "Titanium-based biomaterials for preventing stress shielding between implant devices and bone," *International Journal of Biomaterials*, 2011.
- [66] R. Swaminathan, "Magnesium metabolism and its disorders," *The Clinical biochemist. Reviews / Australian Association of Clinical Biochemists*, vol. 24, pp. 47-66, 2003-May 2003.
- [67] S. Castiglioni, A. Cazzaniga, W. Albisetti, and J. A. M. Maier, "Magnesium and osteoporosis: Current state of knowledge and future research directions," *Nutrients*, vol. 5, pp. 3022-3033, 2013.
- [68] M. Leidi, F. Deller, M. Mariotti, and J. A. M. Maier, "High magnesium inhibits human osteoblast differentiation in vitro," *Magnesium Research*, vol. 24, pp. 1-6, // 2011.
- [69] E. G. Kovaleva and J. D. Lipscomb, "Versatility of biological non-heme Fe(II) centers in oxygen activation reactions," *Nature Chemical Biology*, vol. 4, pp. 186-193, 2008.
- [70] F. B. Jensen, "Comparative analysis of autoxidation of haemoglobin," *Journal of Experimental Biology*, vol. 204, pp. 2029-2033, 2001.

- [71] A. M. C. Barradas, H. Yuan, C. A. van Blitterswijk, and P. Habibovic, "Osteoinductive biomaterials: current knowledge of properties, experimental models and biological mechanisms," *European Cells & Materials*, vol. 21, pp. 407-429, 2011 May 2011.
- [72] S. V. Dorozhkin, "Calcium orthophosphate cements for biomedical application," *Journal of Materials Science*, vol. 43, pp. 3028-3057, 2008.
- [73] M. N. Rahaman, D. E. Day, B. Sonny Bal, Q. Fu, S. B. Jung, L. F. Bonewald, *et al.*, "Bioactive glass in tissue engineering," *Acta Biomaterialia*, vol. 7, pp. 2355-2373, 2011.
- [74] J. R. Jones, "Review of bioactive glass: From Hench to hybrids," *Acta Biomaterialia*, vol. 9, pp. 4457-4486, 2013.
- [75] A. Hoppe, N. S. Gldal, and A. R. Boccaccini, "A review of the biological response to ionic dissolution products from bioactive glasses and glass-ceramics," *Biomaterials*, vol. 32, pp. 2757-2774, 2011.
- [76] G. Kaur, O. P. Pandey, K. Singh, D. Homa, B. Scott, and G. Pickrell, "A review of bioactive glasses: Their structure, properties, fabrication and apatite formation," *Journal of Biomedical Materials Research - Part A*, vol. 102, pp. 254-274, 2014.
- [77] D. G. Gillam, J. Y. Tang, N. J. Mordan, and H. N. Newman, "The effects of a novel Bioglass® dentifrice on dentine sensitivity: A scanning electron microscopy investigation," *Journal of Oral Rehabilitation*, vol. 29, pp. 305-313, 2002.
- [78] L. L. Hench, "Bioceramics," *Journal of the American Ceramic Society*, vol. 81, pp. 1705-1728, 1998.
- [79] A. Roy, S. S. Singh, M. K. Datta, B. Lee, J. Ohodnicki, and P. N. Kumta, "Novel sol-gel derived calcium phosphate coatings on Mg4Y alloy," *Materials Science and Engineering B-Advanced Functional Solid-State Materials*, vol. 176, pp. 1679-1689, Dec 15 2011.
- [80] C. Moseke and U. Gbureck, "Tetracalcium phosphate: Synthesis, properties and biomedical applications," *Acta Biomaterialia*, vol. 6, pp. 3815-3823, 2010.
- [81] D. Lee, C. Sfeir, and P. N. Kumta, "Novel in-situ synthesis and characterization of nanostructured magnesium substituted beta-tricalcium phosphate (beta-TCMP)," *Materials Science & Engineering C-Biomimetic and Supramolecular Systems*, vol. 29, pp. 69-77, 2009.

- [82] S. Kannan, F. Goetz-Neunhoeffler, J. Neubauer, S. Pina, P. M. C. Torres, and J. M. F. Ferreira, "Synthesis and structural characterization of strontium- and magnesium-co-substituted beta-tricalcium phosphate," *Acta Biomaterialia*, vol. 6, pp. 571-576, Feb 2010.
- [83] S. V. Dorozhkin, "Calcium orthophosphate cements and concretes," *Materials*, vol. 2, pp. 221-291, 2009.
- [84] M. T. Fulmer and P. W. Brown, "Hydrolysis of dicalcium phosphate dihydrate to hydroxyapatite," *Journal of Materials Science: Materials in Medicine*, vol. 9, pp. 197-202, // 1998.
- [85] R. G. Carrodeguas and S. De Aza, "alpha-Tricalcium phosphate: Synthesis, properties and biomedical applications," *Acta Biomaterialia*, vol. 7, pp. 3536-3546, Oct 2011.
- [86] R. C. Richard, M. S. Sader, J. Dai, R. M. S. M. Thiré, and G. D. A. Soares, "Beta-type calcium phosphates with and without magnesium: From hydrolysis of brushite powder to robocasting of periodic scaffolds," *Journal of Biomedical Materials Research - Part A*, vol. 00A, pp. 000-000, // 2013.
- [87] U. Gbureck, T. Hozel, U. Klammert, K. Wurzler, F. A. Muller, and J. E. Barralet, "Resorbable dicalcium phosphate bone substitutes prepared by 3D powder printing," *Advanced Functional Materials*, vol. 17, pp. 3940-3945, 2007.
- [88] M. Roy and S. Bose, "Osteoclastogenesis and osteoclastic resorption of tricalcium phosphate: Effect of strontium and magnesium doping," *Journal of Biomedical Materials Research Part A*, vol. 100A, pp. 2450-2461, Sep 2012.
- [89] M. Bohner, F. Theiss, D. Apelt, W. Hirsiger, R. Houriet, G. Rizzoli, *et al.*, "Compositional changes of a dicalcium phosphate dihydrate cement after implantation in sheep," *Biomaterials*, vol. 24, pp. 3463-3474, 2003.
- [90] Y. K. Liu, Q. Z. Lu, R. Pei, H. J. Ji, G. S. Zhou, X. L. Zhao, *et al.*, "The effect of extracellular calcium and inorganic phosphate on the growth and osteogenic differentiation of mesenchymal stem cells in vitro: Implication for bone tissue engineering," *Biomedical Materials*, vol. 4, // 2009.
- [91] P. Jungbluth, M. Wild, J. P. Grassmann, E. Ar, M. Sager, M. Hertel, *et al.*, "Platelet-rich plasma on calcium phosphate granules promotes metaphyseal bone healing in mini-pigs,"

Journal of orthopaedic research : official publication of the Orthopaedic Research Society, vol. 28, pp. 1448-1455, 2010.

- [92] G. Daculsi, A. P. Uzel, P. Weiss, E. Goyenvalle, and E. Aguado, "Developments in injectable multiphasic biomaterials. the performance of microporous biphasic calcium phosphate granules and hydrogels," *Journal of Materials Science: Materials in Medicine*, vol. 21, pp. 855-861, 2010.
- [93] M. Schmitt, P. Weiss, X. Bourges, G. Amador Del Valle, and G. Daculsi, "Crystallization at the polymer/calcium-phosphate interface in a sterilized injectable bone substitute IBS," *Biomaterials*, vol. 23, pp. 2789-2794, 2002.
- [94] H. H. K. Xu, E. F. Burguera, and L. E. Carey, "Strong, macroporous, and in situ-setting calcium phosphate cement-layered structures," *Biomaterials*, vol. 28, pp. 3786-3796, 2007.
- [95] Y. C. Chai, A. Carlier, J. Bolander, S. J. Roberts, L. Geris, J. Schrooten, *et al.*, "Current views on calcium phosphate osteogenicity and the translation into effective bone regeneration strategies," *Acta Biomaterialia*, vol. 8, pp. 3876-3887, Nov 2012.
- [96] G. S. Lee, J. H. Park, U. S. Shin, and H. W. Kim, "Direct deposited porous scaffolds of calcium phosphate cement with alginate for drug delivery and bone tissue engineering," *Acta Biomaterialia*, vol. 7, pp. 3178-3186, 2011.
- [97] P. Habibovic, U. Gbureck, C. J. Doillon, D. C. Bassett, C. A. van Blitterswijk, and J. E. Barralet, "Osteoconduction and osteoinduction of low-temperature 3D printed bioceramic implants," *Biomaterials*, vol. 29, pp. 944-953, 2008.
- [98] U. Gbureck, E. Vorndran, F. A. Muller, and J. E. Barralet, "Low temperature direct 3D printed bioceramics and biocomposites as drug release matrices," *Journal of Controlled Release*, vol. 122, pp. 173-180, 2007.
- [99] M. Bohner, J. Lemaitre, and T. A. Ring, "Effects of sulfate, pyrophosphate, and citrate ions on the physicochemical properties of cements made of beta-tricalcium phosphate-phosphoric acid-water mixtures," *Journal of the American Ceramic Society*, vol. 79, pp. 1427-1434, 1996.
- [100] C. D. Friedman, P. D. Costantino, S. Takagi, and L. C. Chow, "Bonesource(TM) hydroxyapatite cement: A novel biomaterial for craniofacial skeletal tissue engineering

- and reconstruction," *Journal of Biomedical Materials Research*, vol. 43, pp. 428-432, 1998.
- [101] M. Bohner, "DESIGN OF CERAMIC-BASED CEMENTS AND PUTTIES FOR BONE GRAFT SUBSTITUTION," *European Cells & Materials*, vol. 20, pp. 1-12, 2010.
- [102] J. L. Moreau, M. D. Weir, and H. H. K. Xu, "Self-setting collagen-calcium phosphate bone cement: Mechanical and cellular properties," *Journal of Biomedical Materials Research Part A*, vol. 91A, pp. 605-613, 2009.
- [103] H. H. K. Xu, L. E. Carey, C. G. Simon Jr, S. Takagi, and L. C. Chow, "Premixed calcium phosphate cements: Synthesis, physical properties, and cell cytotoxicity," *Dental Materials*, vol. 23, pp. 433-441, 2007.
- [104] S. Bose and S. Tarafder, "Calcium phosphate ceramic systems in growth factor and drug delivery for bone tissue engineering: A review," *Acta Biomaterialia*, vol. 8, pp. 1401-1421, Apr 2012.
- [105] H. H. K. Xu, J. B. Quinn, S. Takagi, L. C. Chow, and F. C. Eichmiller, "Strong and macroporous calcium phosphate cement: Effects of porosity and fiber reinforcement on mechanical properties," *Journal of Biomedical Materials Research*, vol. 57, pp. 457-466, 2001.
- [106] P. J. ter Brugge, J. G. C. Wolke, and J. A. Jansen, "Effect of calcium phosphate coating crystallinity and implant surface roughness on differentiation of rat bone marrow cells," *Journal of Biomedical Materials Research*, vol. 60, pp. 70-78, Apr 2002.
- [107] P. J. ter Brugge, J. G. C. Wolke, and J. A. Jansen, "Effect of calcium phosphate coating composition and crystallinity on the response of osteogenic cells in vitro," *Clinical Oral Implants Research*, vol. 14, pp. 472-480, Aug 2003.
- [108] S. Shadanbaz and G. J. Dias, "Calcium phosphate coatings on magnesium alloys for biomedical applications: A review," *Acta Biomaterialia*, vol. 8, pp. 20-30, Jan 2012.
- [109] H. Hornberger, S. Virtanen, and A. R. Boccaccini, "Biomedical coatings on magnesium alloys - A review," *Acta Biomaterialia*, vol. 8, pp. 2442-55, 2012-Jul 2012.
- [110] R. A. Surmenev, "A review of plasma-assisted methods for calcium phosphate-based coatings fabrication," *Surface and Coatings Technology*, vol. 206, pp. 2035-2056, 2012.

- [111] P. Habibovic, F. Barrere, C. A. van Blitterswijk, K. de Groot, and P. Layrolle, "Biomimetic hydroxyapatite coating on metal implants," *Journal of the American Ceramic Society*, vol. 85, pp. 517-522, 2002.
- [112] X. B. Chen, N. Birbilis, and T. B. Abbott, "Review of Corrosion-Resistant Conversion Coatings for Magnesium and Its Alloys," *Corrosion*, vol. 67, Mar 2011.
- [113] I. S. Kim and P. N. Kumta, "Sol-gel synthesis and characterization of nanostructured hydroxyapatite powder," *Materials Science and Engineering B: Solid-State Materials for Advanced Technology*, vol. 111, pp. 232-236, 2004.
- [114] C. L. Wen, S. K. Guan, L. Peng, C. X. Ren, X. Wang, and Z. H. Hu, "Characterization and degradation behavior of AZ31 alloy surface modified by bone-like hydroxyapatite for implant applications," *Applied Surface Science*, vol. 255, pp. 6433-6438, 2009.
- [115] Y. W. Song, D. Y. Shan, and E. H. Han, "Electrodeposition of hydroxyapatite coating on AZ91D magnesium alloy for biomaterial application," *Materials Letters*, vol. 62, pp. 3276-3279, 2008.
- [116] T. Hayakawa, M. Kawashita, and G. H. Takaoaka, "Coating of hydroxyapatite films on titanium substrates by elect rodeposition under pulse current," *Journal of the Ceramic Society of Japan*, vol. 116, pp. 68-73, 2008.
- [117] R. S. Lima and B. R. Marple, "Thermal spray coatings engineered from nanostructured ceramic agglomerated powders for structural, thermal barrier and biomedical applications: A review," *Journal of Thermal Spray Technology*, vol. 16, pp. 40-63, 2007.
- [118] E. Boanini, M. Gazzano, and A. Bigi, "Ionic substitutions in calcium phosphates synthesized at low temperature," *Acta Biomaterialia*, vol. 6, pp. 1882-1894, Jun 2010.
- [119] P. Habibovic and J. E. Barralet, "Bioinorganics and biomaterials: Bone repair," *Acta Biomaterialia*, vol. 7, pp. 3013-3026, Aug 2011.
- [120] H. S. Ryu, K. S. Hong, J. K. Lee, D. J. Kim, J. H. Lee, B. S. Chang, *et al.*, "Magnesia-doped HA/beta-TCP ceramics and evaluation of their biocompatibility," *Biomaterials*, vol. 25, pp. 393-401, Feb 2004.

- [121] S. Kannan, J. M. Ventura, and J. M. F. Ferreira, "Aqueous precipitation method for the formation of Mg-stabilized beta-tricalcium phosphate: An X-ray diffraction study," *Ceramics International*, vol. 33, pp. 637-641, 2007.
- [122] J. C. Araujo, M. S. Sader, E. L. Moreira, V. C. A. Moraes, R. Z. LeGeros, and G. A. Soares, "Maximum substitution of magnesium for calcium sites in Mg-beta-TCP structure determined by X-ray powder diffraction with the Rietveld refinement," *Materials Chemistry and Physics*, vol. 118, pp. 337-340, Dec 15 2009.
- [123] S. Takaoka, T. Yamaguchi, S. Yano, M. Yamauchi, and T. Sugimoto, "The Calcium-sensing Receptor (CaR) is Involved in Strontium Ranelate-induced Osteoblast Differentiation and Mineralization," *Hormone and Metabolic Research*, vol. 42, pp. 627-631, Aug 2010.
- [124] M. Schumacher, A. Lode, A. Helth, and M. Gelinsky, "A novel strontium(II)-modified calcium phosphate bone cement stimulates human-bone-marrow-derived mesenchymal stem cell proliferation and osteogenic differentiation in vitro," *Acta Biomaterialia*, vol. 9, pp. 9547-9557, 2013.
- [125] I. S. Berglund, H. S. Brar, N. Dolgova, A. P. Acharya, B. G. Keselowsky, M. Sarntinoranont, *et al.*, "Synthesis and characterization of Mg-Ca-Sr alloys for biodegradable orthopedic implant applications," *Journal of Biomedical Materials Research Part B-Applied Biomaterials*, vol. 100B, pp. 1524-1534, Aug 2012.
- [126] S. Yoshizawa, A. Brown, A. Barchowsky, and C. Sfeir, "Magnesium ion stimulation of bone marrow stromal cells enhances osteogenic activity, simulating the effect of magnesium alloy degradation," *Acta Biomaterialia*.
- [127] R. Zeng, W. Dietzel, F. Witte, N. Hort, and C. Blawert, "Progress and challenge for magnesium alloys as biomaterials," *Advanced Engineering Materials*, vol. 10, pp. B3-B14, Aug 2008.
- [128] S. S. Singh, A. Roy, B. Lee, and P. N. Kumta, "Aqueous deposition of calcium phosphates and silicate substituted calcium phosphates on magnesium alloys," *Materials Science and Engineering B-Advanced Functional Solid-State Materials*, vol. 176, pp. 1695-1702, Dec 15 2011.
- [129] C. J. Wu, Z. H. Wen, C. S. Dai, Y. X. Lu, and F. X. Yang, "Fabrication of calcium phosphate/chitosan coatings on AZ91D magnesium alloy with a novel method," *Surface & Coatings Technology*, vol. 204, pp. 3336-3347, 2010.

- [130] X. B. Chen, D. R. Nisbet, R. W. Li, P. N. Smith, T. B. Abbott, M. A. Easton, *et al.*, "Controlling initial biodegradation of magnesium by a biocompatible strontium phosphate conversion coating," *Acta Biomaterialia*, 2013.
- [131] X. Lin, X. Yang, L. Tan, M. Li, X. Wang, Y. Zhang, *et al.*, "In vitro degradation and biocompatibility of a strontium-containing micro-arc oxidation coating on the biodegradable ZK60 magnesium alloy," *Applied Surface Science*, vol. 288, pp. 718-726, 2014.
- [132] A. López, M. Montazerolghaem, M. K. Ott, and C. Persson, "Calcium phosphate cements with strontium halides as radiopacifiers," *Journal of Biomedical Materials Research - Part B Applied Biomaterials*, vol. 102, pp. 250-259, 2014.
- [133] M. Schumache, A. Henß, M. Rohnke, and M. Gelinsky, "A novel and easy-to-prepare strontium(II) modified calcium phosphate bone cement with enhanced mechanical properties," *Acta Biomaterialia*, vol. 9, pp. 7536-7544, // 2013.
- [134] R. Enderle, F. Gotz-Neunhoeffler, M. Gobbels, F. A. Muller, and P. Greil, "Influence of magnesium doping on the phase transformation temperature of beta-TCP ceramics examined by Rietveld refinement," *Biomaterials*, vol. 26, pp. 3379-3384, Jun 2005.
- [135] A. A. Chaudhry, J. Goodall, M. Vickers, J. K. Cockcroft, I. Rehman, J. C. Knowles, *et al.*, "Synthesis and characterisation of magnesium substituted calcium phosphate bioceramic nanoparticles made via continuous hydrothermal flow synthesis," *Journal of Materials Chemistry*, vol. 18, pp. 5900-5908, 2008 2008.
- [136] M. Diba, F. Tapia, A. R. Boccaccini, and L. A. Strobel, "Magnesium-Containing Bioactive Glasses for Biomedical Applications," *International Journal of Applied Glass Science*, vol. 3, pp. 221-253, // 2012.
- [137] X. Li, A. Ito, Y. Sogo, X. Wang, and R. Z. LeGeros, "Solubility of Mg-containing beta-tricalcium phosphate at 25 degrees C," *Acta Biomaterialia*, vol. 5, pp. 508-517, Jan 2009.
- [138] D. H. Yassuda, N. F. M. Costa, G. O. Fernandes, G. G. Alves, J. M. Granjeiro, and G. D. A. Soares, "Magnesium incorporation into β -TCP reduced its in vivo resorption by decreasing parathormone production," *Journal of Biomedical Materials Research - Part A*, vol. 101 A, pp. 1986-1993, // 2013.

- [139] M. S. Sader, R. Z. LeGeros, and G. A. Soares, "Human osteoblasts adhesion and proliferation on magnesium-substituted tricalcium phosphate dense tablets," *Journal of Materials Science-Materials in Medicine*, vol. 20, pp. 521-527, Feb 2009.
- [140] W. Xue, K. Dahlquist, A. Banerjee, A. Bandyopadhyay, and S. Bose, "Synthesis and characterization of tricalcium phosphate with Zn and Mg based dopants," *Journal of Materials Science: Materials in Medicine*, vol. 19, pp. 2669-2677, // 2008.
- [141] G. A. Fielding, W. Smoot, and S. Bose, "Effects of SiO₂, SrO, MgO, and ZnO dopants in tricalcium phosphates on osteoblastic Runx2 expression," *Journal of Biomedical Materials Research - Part A*, vol. 00A, pp. 000-000, 2013.
- [142] K. S. Vecchio, X. Zhang, J. B. Massie, M. Wang, and C. W. Kim, "Conversion of sea urchin spines to Mg-substituted tricalcium phosphate for bone implants," *Acta Biomaterialia*, vol. 3, pp. 785-793, // 2007.
- [143] R. Z. LeGeros, A. M. Gatti, R. Kijkowska, D. Q. Mijares, and J. P. LeGeros, "Mg-substituted Tricalcium Phosphates: Formation and Properties," vol. 254-256, ed, 2004, pp. 127-130.
- [144] B. Dickens, Schroede.Lw, and W. E. Brown, "CRYSTALLOGRAPHIC STUDIES OF ROLE OF MG AS A STABILIZING IMPURITY IN BETA-CA₃(PO₄)₂ .1. CRYSTAL-STRUCTURE OF PURE BETA-CA₃(PO₄)₂," *Journal of Solid State Chemistry*, vol. 10, pp. 232-248, 1974 1974.
- [145] R. Z. LeGeros, "Calcium phosphates in oral biology and medicine," *Monographs in oral science*, vol. 15, pp. 1-201, // 1991.
- [146] S. Gomes, G. Renaudin, E. Jallot, and J. M. Nedelec, "Structural Characterization and Biological Fluid Interaction of Sol-Gel-Derived Mg-Substituted Biphasic Calcium Phosphate Ceramics," *Acs Applied Materials & Interfaces*, vol. 1, pp. 505-513, 2009.
- [147] S. Kannan, F. Goetz-Neunhoeffler, J. Neubauer, and J. M. F. Ferreira, "Ionic substitutions in biphasic hydroxyapatite and beta-tricalcium phosphate mixtures: Structural analysis by rietveld refinement," *Journal of the American Ceramic Society*, vol. 91, pp. 1-12, Jan 2008.
- [148] L. W. Schroeder, B. Dickens, and W. E. Brown, "CRYSTALLOGRAPHIC STUDIES OF ROLE OF MG AS A STABILIZING IMPURITY IN BETA-CA₃(PO₄)₂ .2.

- REFINEMENT OF MG-CONTAINING BETA- $\text{Ca}_3(\text{PO}_4)_2$," *Journal of Solid State Chemistry*, vol. 22, pp. 253-262, 1977 1977.
- [149] M. Yashima, A. Sakai, T. Kamiyama, and A. Hoshikawa, "Crystal structure analysis of beta-tricalcium phosphate $\text{Ca}_3(\text{PO}_4)_2$ by neutron powder diffraction," *Journal of Solid State Chemistry*, vol. 175, pp. 272-277, Nov 2003.
- [150] C. Combes and C. Rey, "Amorphous calcium phosphates: Synthesis, properties and uses in biomaterials," *Acta Biomaterialia*, vol. 6, pp. 3362-3378, Sep 2010.
- [151] D. Lee and P. N. Kumta, "Chemical synthesis and characterization of magnesium substituted amorphous calcium phosphate (MG-ACP)," *Materials Science & Engineering C-Materials for Biological Applications*, vol. 30, pp. 1313-1317, 2010.
- [152] M. J. Olszta, X. Cheng, S. S. Jee, R. Kumar, Y.-Y. Kim, M. J. Kaufman, *et al.*, "Bone structure and formation: A new perspective," *Materials Science & Engineering R-Reports*, vol. 58, pp. 77-116, Nov 28 2007.
- [153] C. Combes and C. Rey, "Adsorption of proteins and calcium phosphate materials bioactivity," *Biomaterials*, vol. 23, pp. 2817-2823, Jul 2002.
- [154] F. Barrere, C. A. van Blitterswijk, and K. de Groot, "Bone regeneration: molecular and cellular interactions with calcium phosphate ceramics," *International Journal of Nanomedicine*, vol. 1, pp. 317-332, 2006 2006.
- [155] J. Fischer, M. H. Prosenč, M. Wolff, N. Hort, R. Willumeit, and F. Feyerabend, "Interference of magnesium corrosion with tetrazolium-based cytotoxicity assays," *Acta Biomaterialia*, vol. 6, pp. 1813-1823, May 2010.
- [156] E. E. Golub, "Role of matrix vesicles in biomineralization," *Biochimica Et Biophysica Acta-General Subjects*, vol. 1790, pp. 1592-1598, Dec 2009.
- [157] S. Castiglioni, M. Leidi, E. Carpanese, and J. A. M. Maier, "Extracellular magnesium and in vitro cell differentiation: Different behaviour of different cells," *Magnesium Research*, vol. 26, pp. 24-31, // 2013.
- [158] W. Zhang, Y. Shen, H. Pan, K. Lin, X. Liu, B. W. Darvell, *et al.*, "Effects of strontium in modified biomaterials," *Acta Biomaterialia*, vol. 7, pp. 800-808, Feb 2011.

- [159] F. Yang, D. Yang, J. Tu, Q. Zheng, L. Cai, and L. Wang, "Strontium Enhances Osteogenic Differentiation of Mesenchymal Stem Cells and In Vivo Bone Formation by Activating Wnt/Catenin Signaling," *Stem Cells*, vol. 29, pp. 981-991, Jun 2011.
- [160] X. Lü, J. Wang, B. Li, Z. Zhang, and L. Zhao, "Gene expression profile study on osteoinductive effect of natural hydroxyapatite," *Journal of Biomedical Materials Research - Part A*, 2013.
- [161] Y. R. V. Shih, Y. Hwang, A. Phadke, H. Kang, N. S. Hwang, E. J. Caro, *et al.*, "Calcium phosphate-bearing matrices induce osteogenic differentiation of stem cells through adenosine signaling," *Proceedings of the National Academy of Sciences of the United States of America*, vol. 111, pp. 990-995, 2014.
- [162] B. Bracci, P. Torricelli, S. Panzavolta, E. Boanini, R. Giardino, and A. Bigi, "Effect of Mg²⁺, Sr²⁺, and Mn²⁺ on the chemico-physical and in vitro biological properties of calcium phosphate biomimetic coatings," *Journal of Inorganic Biochemistry*, vol. 103, pp. 1666-1674, 2009.
- [163] A. Bigi, E. Foresti, M. Gandolfi, M. Gazzano, and N. Roveri, "Isomorphous substitutions in beta-tricalcium phosphate: The different effects of zinc and strontium," *Journal of Inorganic Biochemistry*, vol. 66, pp. 259-265, 1997.
- [164] S. Kannan, S. Pina, and J. M. F. Ferreira, "Formation of strontium-stabilized beta-tricalcium phosphate from calcium-deficient apatite," *Journal of the American Ceramic Society*, vol. 89, pp. 3277-3280, Oct 2006.
- [165] D. D. Deligianni, N. D. Katsala, P. G. Koutsoukos, and Y. F. Missirlis, "Effect of surface roughness of hydroxyapatite on human bone marrow cell adhesion, proliferation, differentiation and detachment strength," *Biomaterials*, vol. 22, pp. 87-96, 2001.
- [166] "Bone Research Protocols, Second Edition," in *Bone Research Protocols, Second Edition*. vol. 816, M. H. Helfrich and S. H. Ralston, Eds., ed, 2012.
- [167] J. Sodek, B. Ganss, and M. D. McKee, "Osteopontin," *Critical Reviews in Oral Biology & Medicine*, vol. 11, pp. 279-303, Aug 2000.
- [168] C. M. Giachelli and S. Steitz, "Osteopontin: a versatile regulator of inflammation and biomineralization," *Matrix Biology*, vol. 19, pp. 615-622, Dec 2000.

- [169] K. Vaananen, "Mechanism of osteoclast mediated bone resorption - rationale for the design of new therapeutics," *Advanced Drug Delivery Reviews*, vol. 57, pp. 959-971, May 25 2005.
- [170] N. Bucay, I. Sarosi, C. R. Dunstan, S. Morony, J. Tarpley, C. Capparelli, *et al.*, "osteoprotegerin-deficient mice develop early onset osteoporosis and arterial calcification," *Genes & Development*, vol. 12, pp. 1260-1268, May 1 1998.
- [171] J. Zhao, Y. Liu, W.-b. Sun, and H. Zhang, "Amorphous calcium phosphate and its application in dentistry," *Chemistry Central Journal*, vol. 5, Jul 8 2011.
- [172] C. E. Boumah, N. Selvamurugan, and N. C. Partridge, "Transcription in the Osteoblast: Regulatory Mechanisms Utilized by Parathyroid Hormone and Transforming Growth Factor-Beta," in *Progress in Nucleic Acid Research and Molecular Biology*. vol. Volume 80, M. Kivie, Ed., ed: Academic Press, 2005, pp. 287-321.
- [173] L. F. Bonewald and S. L. Dallas, "The Role of Growth Factors in Bone Formation," in *Advances in Organ Biology*. vol. Volume 5, ed: Elsevier, 1998, pp. 591-613.
- [174] K. Azari, J. S. Doctor, B. A. Doll, and J. O. Hollinger, "Bone morphogenetic proteins: A review for cranial and maxillofacial surgery," *Oral and Maxillofacial Surgery Clinics of North America*, vol. 14, pp. 1-14, 2// 2002.
- [175] G. J. Anderson and D. Darshan, "Small-molecule dissection of BMP signaling," *Nature Chemical Biology*, vol. 4, pp. 15-16, 2008.
- [176] R. Derynck and Y. E. Zhang, "Smad-dependent and Smad-independent pathways in TGF- β family signalling," *Nature*, vol. 425, pp. 577-584, 2003.
- [177] H. Gu, F. Guo, X. Zhou, L. Gong, Y. Zhang, W. Zhai, *et al.*, "The stimulation of osteogenic differentiation of human adipose-derived stem cells by ionic products from akermanite dissolution via activation of the ERK pathway," *Biomaterials*, vol. 32, pp. 7023-7033, 10// 2011.
- [178] S. V. Dorozhkin, "Amorphous calcium (ortho)phosphates," *Acta Biomaterialia*, vol. 6, pp. 4457-4475, Dec 2010.

- [179] A. S. Posner, F. Betts, and N. C. Blumenthal, "Role of ATP and Mg in the stabilization of biological and synthetic amorphous calcium phosphates," *Calcified Tissue Research*, vol. 22, pp. 208-212, 1976/12/01 1976.
- [180] Y. Li and W. Weng, "In vitro synthesis and characterization of amorphous calcium phosphates with various Ca/P atomic ratios," *Journal of Materials Science: Materials in Medicine*, vol. 18, pp. 2303-2308, 2007/12/01 2007.
- [181] A. Hanifi, M. H. Fathi, H. M. M. Sadeghi, and J. Varshosaz, "Mg²⁺ substituted calcium phosphate nano particles synthesis for non viral gene delivery application," *Journal of Materials Science-Materials in Medicine*, vol. 21, pp. 2393-2401, Aug 2010.
- [182] W. L. Suchanek, K. Byrappa, P. Shuk, R. E. Riman, V. F. Janas, and K. S. TenHuisen, "Preparation of magnesium-substituted hydroxyapatite powders by the mechanochemical-hydrothermal method," *Biomaterials*, vol. 25, pp. 4647-4657, 8// 2004.
- [183] G. C. Qi, S. Zhang, K. A. Khor, C. M. Liu, X. T. Zeng, W. J. Weng, *et al.*, "In vitro effect of magnesium inclusion in sol-gel derived apatite," *Thin Solid Films*, vol. 516, pp. 5176-5180, 2008.
- [184] D. Lee and P. N. Kumta, "Chemical synthesis and stabilization of magnesium substituted brushite," *Materials Science and Engineering: C*, vol. 30, pp. 934-943, 8/30/ 2010.
- [185] S. Mandel and A. C. Tas, "Brushite (CaHPO₄·2H₂O) to octacalcium phosphate (Ca₈(HPO₄)₂(PO₄)₄·5H₂O) transformation in DMEM solutions at 36.5 degrees C," *Materials Science & Engineering C-Materials for Biological Applications*, vol. 30, pp. 245-254, Jan 30 2010.
- [186] N. T. Kirkland, "Magnesium biomaterials: past, present and future," *Corrosion Engineering Science and Technology*, vol. 47, pp. 322-328, Aug 2012.
- [187] Y. Xin, T. Hu, and P. K. Chu, "In vitro studies of biomedical magnesium alloys in a simulated physiological environment: A review," *Acta Biomaterialia*, vol. 7, pp. 1452-1459, Apr 2011.
- [188] B. Zberg, P. J. Uggowitzer, and J. F. Löffler, "MgZnCa glasses without clinically observable hydrogen evolution for biodegradable implants," *Nature Materials*, vol. 8, pp. 887-891, Nov 2009.

- [189] F. Feyerabend, J. Fischer, J. Holtz, F. Witte, R. Willumeit, H. Druecker, *et al.*, "Evaluation of short-term effects of rare earth and other elements used in magnesium alloys on primary cells and cell lines," *Acta Biomaterialia*, vol. 6, pp. 1834-1842, May 2010.
- [190] Y. K. Xu, H. Ma, J. Xu, and E. Ma, "Mg-based bulk metallic glass composites with plasticity and gigapascal strength," *Acta Materialia*, vol. 53, pp. 1857-1866, Apr 2005.
- [191] X. N. Gu, N. Li, W. R. Zhou, Y. F. Zheng, X. Zhao, Q. Z. Cai, *et al.*, "Corrosion resistance and surface biocompatibility of a microarc oxidation coating on a Mg-Ca alloy," *Acta Biomaterialia*, vol. 7, pp. 1880-1889, Apr 2011.
- [192] H. Chai, L. Guo, X. Wang, X. Gao, K. Liu, Y. Fu, *et al.*, "In vitro and in vivo evaluations on osteogenesis and biodegradability of a ss-tricalcium phosphate coated magnesium alloy," *Journal of Biomedical Materials Research Part A*, vol. 100A, pp. 293-304, Feb 2012.
- [193] P. Ammann, I. Badoud, S. Barraud, R. Dayer, and R. Rizzoli, "Strontium ranelate treatment improves trabecular and cortical intrinsic bone tissue quality, a determinant of bone strength," *Journal of Bone and Mineral Research*, vol. 22, pp. 1419-1425, Sep 2007.
- [194] X. B. Chen, D. R. Nisbet, R. W. Li, P. N. Smith, T. B. Abbott, M. A. Easton, *et al.*, "Controlling initial biodegradation of magnesium by a biocompatible strontium phosphate conversion coating," *Acta Biomaterialia*.
- [195] M. Gunasekaran, N. Vijayan, R. R. Babu, R. Gopalakrishnan, P. Ramasamy, and C. W. Lan, "Growth and characterization of di-sodium hydrogen phosphate," *Journal of Crystal Growth*, vol. 244, pp. 194-199, Oct 2002.
- [196] G. Mestres and M.-P. Ginebra, "Novel magnesium phosphate cements with high early strength and antibacterial properties," *Acta Biomaterialia*, vol. 7, pp. 1853-1861, Apr 2011.
- [197] T. Ishizaki, R. Kudo, T. Omi, K. Teshima, T. Sonoda, I. Shigematsu, *et al.*, "Corrosion resistance of multilayered magnesium phosphate/magnesium hydroxide film formed on magnesium alloy using steam-curing assisted chemical conversion method," *Electrochimica Acta*, vol. 62, pp. 19-29, Feb 15 2012.

- [198] T. Ishizaki, R. Kudo, T. Omi, K. Teshima, T. Sonoda, I. Shigematsu, *et al.*, "Magnesium hydroxide/magnesium phosphate compounds composite coating for corrosion protection of magnesium alloy by a combination process of chemical conversion and steam curing," *Materials Letters*, vol. 68, pp. 122-125, Feb 1 2012.
- [199] N. T. Kirkland, N. Birbilis, and M. P. Staiger, "Assessing the corrosion of biodegradable magnesium implants: A critical review of current methodologies and their limitations," *Acta Biomaterialia*, vol. 8, pp. 925-936, Mar 2012.
- [200] Q. Q. Hoang, F. Sicheri, A. J. Howard, and D. S. C. Yang, "Bone recognition mechanism of porcine osteocalcin from crystal structure," *Nature*, vol. 425, pp. 977-980, Oct 30 2003.
- [201] Z. Saidak and P. J. Marie, "Strontium signaling: Molecular mechanisms and therapeutic implications in osteoporosis," *Pharmacology & therapeutics*, vol. 136, pp. 216-26, 2012-Nov 2012.
- [202] G. X. Ni, W. W. Lu, B. Tang, A. H. W. Ngan, K. Y. Chiu, K. M. C. Cheung, *et al.*, "Effect of weight-bearing on bone-bonding behavior of strontium-containing hydroxyapatite bone cement," *Journal of Biomedical Materials Research - Part A*, vol. 83, pp. 570-576, // 2007.
- [203] D. Guo, K. Xu, X. Zhao, and Y. Han, "Development of a strontium-containing hydroxyapatite bone cement," *Biomaterials*, vol. 26, pp. 4073-4083, // 2005.
- [204] S. Panzavolta, P. Torricelli, L. Sturba, B. Bracci, R. Giardino, and A. Bigi, "Setting properties and in vitro bioactivity of strontium-enriched gelatin-calcium phosphate bone cements," *Journal of Biomedical Materials Research - Part A*, vol. 84, pp. 965-972, // 2008.
- [205] E. Boanini, S. Panzavolta, K. Rubini, M. Gandolfi, and A. Bigi, "Effect of strontium and gelatin on the reactivity of α -tricalcium phosphate," *Acta Biomaterialia*, vol. 6, pp. 936-942, // 2010.
- [206] S. Jegou Saint-Jean, C. L. Camiré, P. Nevsten, S. Hansen, and M. P. Ginebra, "Study of the reactivity and in vitro bioactivity of Sr-substituted α -TCP cements," *Journal of Materials Science: Materials in Medicine*, vol. 16, pp. 993-1001, 2005.

- [207] G. Dagang, K. Xu, and Y. Han, "The influence of Sr doses on the in vitro biocompatibility and in vivo degradability of single-phase Sr-incorporated HAP cement," *Journal of Biomedical Materials Research - Part A*, vol. 86, pp. 947-958, 2008.
- [208] N. Temizel, G. Giriskan, and A. C. Tas, "Accelerated transformation of brushite to octacalcium phosphate in new biomineralization media between 36.5 °c and 80 °c," *Materials Science and Engineering C*, vol. 31, pp. 1136-1143, // 2011.
- [209] E. Rokita, C. Hermes, H. F. Nolting, and J. Ryczek, "Substitution of calcium by strontium within selected calcium phosphates," *Journal of Crystal Growth*, vol. 130, pp. 543-552, // 1993.
- [210] M. H. Alkhalsat, F. T. Marino, C. R. Rodriguez, L. B. Jerez, and E. L. Cabarcos, "Combined effect of strontium and pyrophosphate on the properties of brushite cements," *Acta Biomaterialia*, vol. 4, pp. 664-670, 2008.
- [211] R. Z. LeGeros and J. P. LeGeros, "Brushite crystals grown by diffusion in silica gel and in solution," *Journal of Crystal Growth*, vol. 13-14, pp. 476-480, // 1972.
- [212] E. F. Burguera, H. H. K. Xu, S. Takagi, and L. C. Chow, "High early strength calcium phosphate bone cement: Effects of dicalcium phosphate dihydrate and absorbable fibers," *Journal of Biomedical Materials Research - Part A*, vol. 75, pp. 966-975, // 2005.
- [213] S. Takagi, L. C. Chow, and K. Ishikawa, "Formation of hydroxyapatite in new calcium phosphate cements," *Biomaterials*, vol. 19, pp. 1593-1599, // 1998.
- [214] Y. E. Greish and P. W. Brown, "Phase Evolution during the Formation of Stoichiometric Hydroxyapatite at 37.4 °C," *Journal of Biomedical Materials Research - Part B Applied Biomaterials*, vol. 67, pp. 632-637, // 2003.
- [215] U. Gbureck, J. E. Barralet, M. P. Hofmann, and R. Thull, "Nanocrystalline tetracalcium phosphate cement," *Journal of Dental Research*, vol. 83, pp. 425-428, 2004.
- [216] E. F. Burguera, F. Guitián, and L. C. Chow, "A water setting tetracalcium phosphate-dicalcium phosphate dihydrate cement," *Journal of Biomedical Materials Research - Part A*, vol. 71, pp. 275-282, 2004.

- [217] N. Chattopadhyay, S. J. Quinn, O. Kifor, C. Ye, and E. M. Brown, "The calcium-sensing receptor (CaR) is involved in strontium ranelate-induced osteoblast proliferation," *Biochemical Pharmacology*, vol. 74, pp. 438-447, // 2007.
- [218] C. A. Hemingway, R. P. Shellis, D. M. Parker, M. Addy, and M. E. Barbour, "Inhibition of hydroxyapatite dissolution by ovalbumin as a function of pH, calcium concentration, protein concentration and acid type," *Caries Research*, vol. 42, pp. 348-353, 2008.
- [219] P. J. Meunier, C. Roux, E. Seeman, S. Ortolani, J. E. Badurski, T. D. Spector, *et al.*, "The Effects of Strontium Ranelate on the Risk of Vertebral Fracture in Women with Postmenopausal Osteoporosis," *New England Journal of Medicine*, vol. 350, pp. 459-468, // 2004.
- [220] Y. Honda, T. Anada, S. Kamakura, S. Morimoto, T. Kuriyagawa, and O. Suzuki, "The effect of microstructure of octacalcium phosphate on the bone regenerative property," *Tissue Engineering - Part A*, vol. 15, pp. 1965-1973, 2009.
- [221] S. C. Mendes, J. M. Tibbe, M. Veenhof, S. Both, F. C. Oner, C. A. Van Blitterswijk, *et al.*, "Relation between in vitro and in vivo osteogenic potential of cultured human bone marrow stromal cells," *Journal of Materials Science: Materials in Medicine*, vol. 15, pp. 1123-1128, 2004.
- [222] G. Hulsart-Billström, W. Xia, E. Pankotai, M. Weszl, E. Carlsson, C. Forster-Horváth, *et al.*, "Osteogenic potential of Sr-doped calcium phosphate hollow spheres in vitro and in vivo," *Journal of Biomedical Materials Research - Part A*, vol. 101 A, pp. 2322-2331, 2013.
- [223] Y. Huang, X. Jin, X. Zhang, H. Sun, J. Tu, T. Tang, *et al.*, "In vitro and in vivo evaluation of akermanite bioceramics for bone regeneration," *Biomaterials*, vol. 30, pp. 5041-5048, 10// 2009.
- [224] J. E. Gray-Munro, C. Seguin, and M. Strong, "Influence of surface modification on the in vitro corrosion rate of magnesium alloy AZ31," *Journal of Biomedical Materials Research Part A*, vol. 91A, pp. 221-230, 2009.
- [225] J. E. Gray-Munro and M. Strong, "The mechanism of deposition of calcium phosphate coatings from solution onto magnesium alloy AZ31," *Journal of Biomedical Materials Research Part A*, vol. 90A, pp. 339-350, 2009.

- [226] A. Drynda, N. Deinet, N. Braun, and M. Peuster, "Rare earth metals used in biodegradable magnesium-based stents do not interfere with proliferation of smooth muscle cells but do induce the upregulation of inflammatory genes," *Journal of Biomedical Materials Research Part A*, vol. 91A, pp. 360-369, Nov 2009.
- [227] C. L. Camire, S. J. Saint-Jean, C. Mochales, P. Nevsten, J. S. Wang, L. Lidgren, *et al.*, "Material characterization and in vivo behavior of silicon substituted alpha-tricalcium phosphate cement," *Journal of Biomedical Materials Research Part B-Applied Biomaterials*, vol. 76B, pp. 424-431, 2006.
- [228] M. Bohner, "Silicon-substituted calcium phosphates - A critical view," *Biomaterials*, vol. 30, pp. 6403-6406, 2009.
- [229] C. T. Wu, J. A. Chang, J. Y. Wang, S. Y. Ni, and W. Y. Zhai, "Preparation and characteristics of a calcium magnesium silicate (bredigite) bioactive ceramic," *Biomaterials*, vol. 26, pp. 2925-2931, 2005.
- [230] M. Liu, P. Schmutz, P. J. Uggowitzer, G. L. Song, and A. Atrens, "The influence of yttrium (Y) on the corrosion of Mg-Y binary alloys," *Corrosion Science*, vol. 52, pp. 3687-3701, Nov 2010.
- [231] S. C. Bondy, "The neurotoxicity of environmental aluminum is still an issue," *Neurotoxicology*, vol. 31, pp. 575-581, Sep 2010.
- [232] W. Maret and H. H. Sandstead, "Zinc requirements and the risks and benefits of zinc supplementation," *Journal of Trace Elements in Medicine and Biology*, vol. 20, pp. 3-18, 2006.
- [233] R. Willumeit, J. Fischer, F. Feyerabend, N. Hort, U. Bismayer, S. Heidrich, *et al.*, "Chemical surface alteration of biodegradable magnesium exposed to corrosion media," *Acta Biomaterialia*, vol. 7, pp. 2704-2715, Jun 2011.
- [234] A. Yamamoto and S. Hiromoto, "Effect of inorganic salts, amino acids and proteins on the degradation of pure magnesium in vitro," *Materials Science & Engineering C-Biomimetic and Supramolecular Systems*, vol. 29, pp. 1559-1568, Jun 1 2009.
- [235] D. D. Deligianni, N. Katsala, S. Ladas, D. Sotiropoulou, J. Amedee, and Y. F. Missirlis, "Effect of surface roughness of the titanium alloy Ti-6Al-4V on human bone marrow cell response and on protein adsorption," *Biomaterials*, vol. 22, pp. 1241-1251, 2001.

- [236] K. Anselme, M. Bigerelle, B. Noel, E. Dufresne, D. Judas, A. Iost, *et al.*, "Qualitative and quantitative study of human osteoblast adhesion on materials with various surface roughnesses," *Journal of Biomedical Materials Research*, vol. 49, pp. 155-166, 2000.
- [237] S. R. Paital and N. B. Dahotre, "Calcium phosphate coatings for bio-implant applications: Materials, performance factors, and methodologies," *Materials Science & Engineering R-Reports*, vol. 66, pp. 1-70, 2009.
- [238] M. P. Staiger, A. M. Pietak, J. Huadmai, and G. Dias, "Magnesium and its alloys as orthopedic biomaterials: A review," *Biomaterials*, vol. 27, pp. 1728-1734, 2006.
- [239] X. N. Gu, Y. F. Zheng, Y. Cheng, S. P. Zhong, and T. F. Xi, "In vitro corrosion and biocompatibility of binary magnesium alloys," *Biomaterials*, vol. 30, pp. 484-498, 2009.
- [240] M. Thomann, C. Krause, N. Angrisani, D. Bormann, T. Hassel, H. Windhagen, *et al.*, "Influence of a magnesium-fluoride coating of magnesium-based implants (MgCa0.8) on degradation in a rabbit model," *Journal of Biomedical Materials Research Part A*, vol. 93A, pp. 1609-1619, 2010.
- [241] L. P. Xu, F. Pan, G. N. Yu, L. Yang, E. L. Zhang, and K. Yang, "In vitro and in vivo evaluation of the surface bioactivity of a calcium phosphate coated magnesium alloy," *Biomaterials*, vol. 30, pp. 1512-1523, 2009.
- [242] H. M. Wong, K. W. K. Yeung, K. O. Lam, V. Tam, P. K. Chu, K. D. K. Luk, *et al.*, "A biodegradable polymer-based coating to control the performance of magnesium alloy orthopaedic implants," *Biomaterials*, vol. 31, pp. 2084-2096, 2010.
- [243] F. Witte, J. Fischer, J. Nellesen, H. A. Crostack, V. Kaese, A. Pisch, *et al.*, "In vitro and in vivo corrosion measurements of magnesium alloys," *Biomaterials*, vol. 27, pp. 1013-1018, 2006.
- [244] H. S. Brar, M. O. Platt, M. Sarntinoranont, P. I. Martin, and M. V. Manuel, "Magnesium as a biodegradable and bioabsorbable material for medical implants," *Jom*, vol. 61, pp. 31-34, 2009.
- [245] F. Witte, V. Kaese, H. Haferkamp, E. Switzer, A. Meyer-Lindenberg, C. J. Wirth, *et al.*, "In vivo corrosion of four magnesium alloys and the associated bone response," *Biomaterials*, vol. 26, pp. 3557-3563, 2005.

- [246] R. C. Zeng, W. Dietzel, F. Witte, N. Hort, and C. Blawert, "Progress and challenge for magnesium alloys as biomaterials," *Advanced Engineering Materials*, vol. 10, pp. B3-B14, 2008.
- [247] X. N. Gu, Y. F. Zheng, S. P. Zhong, T. F. Xi, J. Q. Wang, and W. H. Wang, "Corrosion of, and cellular responses to Mg-Zn-Ca bulk metallic glasses," *Biomaterials*, vol. 31, pp. 1093-1103, 2010 2010.
- [248] Y. Wang, M. Wei, J. C. Gao, J. Z. Hu, and Y. Zhang, "Corrosion process of pure magnesium in simulated body fluid," *Materials Letters*, vol. 62, pp. 2181-2184, 2008.
- [249] F. Geng, L. L. Tan, X. X. Jin, J. Y. Yang, and K. Yang, "The preparation, cytocompatibility, and in vitro biodegradation study of pure beta-TCP on magnesium," *Journal of Materials Science-Materials in Medicine*, vol. 20, pp. 1149-1157, 2009.
- [250] L. T. de Jonge, S. C. G. Leeuwenburgh, J. G. C. Wolke, and J. A. Jansen, "Organic-inorganic surface modifications for titanium implant surfaces," *Pharmaceutical Research*, vol. 25, pp. 2357-2369, 2008.
- [251] G. Lewis, "Hydroxyapatite-coated bioalloy surfaces: Current status and future challenges," *Bio-Medical Materials and Engineering*, vol. 10, pp. 157-188, 2000.
- [252] A. Hoppe, N. S. Gueldal, and A. R. Boccaccini, "A review of the biological response to ionic dissolution products from bioactive glasses and glass-ceramics," *Biomaterials*, vol. 32, pp. 2757-2774, 2011 2011.
- [253] A. M. Pietak, J. W. Reid, M. J. Stott, and M. Sayer, "Silicon substitution in the calcium phosphate bioceramics," *Biomaterials*, vol. 28, pp. 4023-4032, 2007.
- [254] H. Zreiqat, C. R. Howlett, A. Zannettino, P. Evans, G. Schulze-Tanzil, C. Knabe, *et al.*, "Mechanisms of magnesium-stimulated adhesion of osteoblastic cells to commonly used orthopaedic implants," *Journal of Biomedical Materials Research*, vol. 62, pp. 175-184, Nov 2002.
- [255] R. Z. LeGeros, "Properties of osteoconductive biomaterials: Calcium phosphates," *Clinical Orthopaedics and Related Research*, pp. 81-98, Feb 2002.

- [256] S. D. Miao, N. Lin, K. Cheng, D. S. Yang, X. Huang, G. R. Han, *et al.*, "Zn-Releasing FHA Coating and Its Enhanced Osseointegration Ability," *Journal of the American Ceramic Society*, vol. 94, pp. 256-261, Jan 2011.
- [257] A. Ito, K. Ojima, H. Naito, N. Ichinose, and T. Tateishi, "Preparation, solubility, and cytocompatibility of zinc-releasing calcium phosphate ceramics," *Journal of Biomedical Materials Research*, vol. 50, pp. 178-183, May 2000.
- [258] W. C. Xue, X. Y. Liu, X. B. Zheng, and C. X. Ding, "In vivo evaluation of plasma-sprayed wollastonite coating," *Biomaterials*, vol. 26, pp. 3455-3460, 2005.
- [259] J. Y. Sun, L. Wei, X. Y. Liu, J. Y. Li, B. E. Li, G. C. Wang, *et al.*, "Influences of ionic dissolution products of dicalcium silicate coating on osteoblastic proliferation, differentiation and gene expression," *Acta Biomaterialia*, vol. 5, pp. 1284-1293, 2009.
- [260] L. P. Xu, E. L. Zhang, and K. Yang, "Phosphating treatment and corrosion properties of Mg-Mn-Zn alloy for biomedical application," *Journal of Materials Science-Materials in Medicine*, vol. 20, pp. 859-867, Apr 2009.
- [261] Y. Song, S. X. Zhang, J. A. Li, C. L. Zhao, and X. N. Zhang, "Electrodeposition of Ca-P coatings on biodegradable Mg alloy: In vitro biomineralization behavior," *Acta Biomaterialia*, vol. 6, pp. 1736-1742, 2010 2010.
- [262] S. Zhang, X. Zhang, C. Zhao, J. Li, Y. Song, C. Xie, *et al.*, "Research on an Mg-Zn alloy as a degradable biomaterial," *Acta Biomater*, vol. 6, pp. 626-40, 2010 2010.
- [263] H. X. Wang, S. K. Guan, X. Wang, C. X. Ren, and L. G. Wang, "In vitro degradation and mechanical integrity of Mg-Zn-Ca alloy coated with Ca-deficient hydroxyapatite by the pulse electrodeposition process," *Acta Biomaterialia*, vol. 6, pp. 1743-1748, 2010.
- [264] E. L. Zhang, L. P. Xu, G. N. Yu, F. Pan, and K. Yang, "In vivo evaluation of biodegradable magnesium alloy bone implant in the first 6 months implantation," *Journal of Biomedical Materials Research Part A*, vol. 90A, pp. 882-893, 2009.
- [265] W. J. Weng and J. L. Baptista, "Sol gel derived porous hydroxyapatite coatings," *Journal of Materials Science-Materials in Medicine*, vol. 9, pp. 159-163, Mar 1998.

- [266] W. J. Weng and J. L. Baptista, "Preparation and characterization of hydroxyapatite coatings on Ti6Al4V alloy by a sol-gel method," *Journal of the American Ceramic Society*, vol. 82, pp. 27-32, Jan 1999.
- [267] I. S. Kim and P. N. Kumta, "Sol-gel synthesis and characterization of nanostructured hydroxyapatite powder," *Materials Science and Engineering B-Solid State Materials for Advanced Technology*, vol. 111, pp. 232-236, Aug 2004.
- [268] D. M. Liu, Q. Z. Yang, T. Troczynski, and W. J. J. Tseng, "Structural evolution of sol-gel-derived hydroxyapatite," *Biomaterials*, vol. 23, pp. 1679-1687, Apr 2002.
- [269] J. X. Wang, H. C. Zhao, S. B. Zhou, X. Lu, B. Feng, C. H. Duan, *et al.*, "One-step in situ synthesis and characterization of sponge-like porous calcium phosphate scaffolds using a sol-gel and gel casting hybrid process," *Journal of Biomedical Materials Research Part A*, vol. 90A, pp. 401-410, Aug 2009.
- [270] N. Hijon, M. V. Cabanas, J. Pena, and M. Vallet-Regi, "Dip coated silicon-substituted hydroxyapatite films," *Acta Biomaterialia*, vol. 2, pp. 567-574, Sep 2006.
- [271] M. D'Apuzzo, A. Aronne, S. Esposito, and P. Pernice, "Sol-gel synthesis of humidity-sensitive P₂O₅-SiO₂ amorphous films," *Journal of Sol-Gel Science and Technology*, vol. 17, pp. 247-254, Mar 2000.
- [272] S. Langstaff, M. Sayer, T. J. N. Smith, S. M. Pugh, S. A. M. Hesp, and W. T. Thompson, "Resorbable bioceramics based on stabilized calcium phosphates. Part I: rational design, sample preparation and material characterization," *Biomaterials*, vol. 20, pp. 1727-1741, Sep 1999.
- [273] M. Sayer, A. D. Stratilatov, J. Reid, L. Calderin, M. J. Stott, X. Yin, *et al.*, "Structure and composition of silicon-stabilized tricalcium phosphate," *Biomaterials*, vol. 24, pp. 369-382, Feb 2003.
- [274] I. R. Gibson, S. M. Best, and W. Bonfield, "Chemical characterization of silicon-substituted hydroxyapatite," *Journal of Biomedical Materials Research*, vol. 44, pp. 422-428, Mar 1999.
- [275] F. Balas, J. Perez-Pariente, and M. Vallet-Regi, "In vitro bioactivity of silicon-substituted hydroxyapatites," *Journal of Biomedical Materials Research Part A*, vol. 66A, pp. 364-375, Aug 2003.

- [276] R. Y. Whitehead, W. R. Lacefield, and L. C. Lucas, "STRUCTURE AND INTEGRITY OF A PLASMA-SPRAYED HYDROXYLAPATITE COATING ON TITANIUM," *Journal of Biomedical Materials Research*, vol. 27, pp. 1501-1507, 1993.
- [277] B. L. a. J. A. Janson, Ed., *Thin Calcium Phosphate Coatings for Medical Implants*. Springer Sciences+Business Media, LLC 2009, 2009, p.^pp. Pages.
- [278] R. D. Bloebaum, L. Zou, K. N. Bachus, K. G. Shea, A. A. Hofmann, and H. K. Dunn, "Analysis of particles in acetabular components from patients with osteolysis," *Clinical Orthopaedics and Related Research*, pp. 109-118, 1997.
- [279] L. M. Sun, C. C. Berndt, K. A. Gross, and A. Kucuk, "Material fundamentals and clinical performance of plasma-sprayed hydroxyapatite coatings: A review," *Journal of Biomedical Materials Research*, vol. 58, pp. 570-592, 2001.
- [280] K. Degroot, R. Geesink, C. Klein, and P. Serekian, "PLASMA SPRAYED COATINGS OF HYDROXYLAPATITE," *Journal of Biomedical Materials Research*, vol. 21, pp. 1375-1381, 1987.
- [281] N. T. Kirkland, N. Birbilis, J. Walker, T. Woodfield, G. J. Dies, and M. P. Steiger, "In-vitro dissolution of magnesium-calcium binary alloys: Clarifying the unique role of calcium additions in bioresorbable magnesium implant alloys," *Journal of Biomedical Materials Research Part B-Applied Biomaterials*, vol. 95B, pp. 91-100, 2010.
- [282] D. Arcos, J. Rodriguez-Carvajal, and M. Vallet-Regi, "Silicon incorporation in hydroxyapatite obtained by controlled crystallization," *Chemistry of Materials*, vol. 16, pp. 2300-2308, Jun 2004.
- [283] A. E. Porter, C. M. Botelho, M. A. Lopes, J. D. Santos, S. M. Best, and W. Bonfield, "Ultrastructural comparison of dissolution and apatite precipitation on hydroxyapatite and silicon-substituted hydroxyapatite in vitro and in vivo," *Journal of Biomedical Materials Research Part A*, vol. 69A, pp. 670-679, Jun 2004.
- [284] E. S. Thian, J. Huang, S. M. Best, Z. H. Barber, R. A. Brooks, N. Rushton, *et al.*, "The response of osteoblasts to nanocrystalline silicon-substituted hydroxyapatite thin films," *Biomaterials*, vol. 27, pp. 2692-2698, 2006.
- [285] C. M. Botelho, M. A. Lopes, I. R. Gibson, S. M. Best, and J. D. Santos, "Structural analysis of Si-substituted hydroxyapatite: zeta potential and X-ray photoelectron

- spectroscopy," *Journal of Materials Science-Materials in Medicine*, vol. 13, pp. 1123-1127, Dec 2002.
- [286] A. E. Porter, N. Patel, J. N. Skepper, S. M. Best, and W. Bonfield, "Comparison of in vivo dissolution processes in hydroxyapatite and silicon-substituted hydroxyapatite bioceramics," *Biomaterials*, vol. 24, pp. 4609-4620, 2003.
- [287] C. M. Botelho, R. A. Brooks, T. Kawai, S. Ogata, C. Ohtsuki, S. M. Best, *et al.*, "In vitro analysis of protein adhesion to phase pure hydroxyapatite and silicon substituted hydroxyapatite," *Bioceramics 17*, vol. 284-286, pp. 461-464, 2005.
- [288] O. Rahbek, S. Kold, K. Bendix, S. Overgaard, and K. Soballe, "No effect of hydroxyapatite particles in phagocytosable sizes on implant fixation: An experimental study in dogs," *Journal of Biomedical Materials Research Part A*, vol. 73A, pp. 150-157, 2005.
- [289] Y. R. Cai, Y. K. Liu, W. Q. Yan, Q. H. Hu, J. H. Tao, M. Zhang, *et al.*, "Role of hydroxyapatite nanoparticle size in bone cell proliferation," *Journal of Materials Chemistry*, vol. 17, pp. 3780-3787, 2007.
- [290] J. S. Wang, S. Goodman, and P. Aspenberg, "BONE FORMATION IN THE PRESENCE OF PHAGOCYTOSABLE HYDROXYAPATITE PARTICLES," *Clinical Orthopaedics and Related Research*, pp. 272-279, 1994.
- [291] H. Assender, V. Bliznyuk, and K. Porfyarakis, "How surface topography relates to materials properties," *Science*, vol. 297, pp. 973-976, Aug 2002.
- [292] B. Kasemo, "Biological surface science," *Surface Science*, vol. 500, pp. 656-677, Mar 2002.
- [293] T. J. Webster and J. U. Ejiolor, "Increased osteoblast adhesion on nanophase metals: Ti, Ti6Al4V, and CoCrMo," *Biomaterials*, vol. 25, pp. 4731-4739, Aug 2004.
- [294] M. P. Lutolf and J. A. Hubbell, "Synthetic biomaterials as instructive extracellular microenvironments for morphogenesis in tissue engineering," *Nature Biotechnology*, vol. 23, pp. 47-55, Jan 2005.
- [295] M. M. Stevens and J. H. George, "Exploring and engineering the cell surface interface," *Science*, vol. 310, pp. 1135-1138, Nov 2005.

- [296] S. R. Paital and N. B. Dahotre, "Laser surface treatment for porous and textured Ca-P bio-ceramic coating on Ti-6Al-4V," *Biomedical Materials*, vol. 2, pp. 274-281, Dec 2007.
- [297] B. A. Lodish H, Zipursky SL, Matsudaira P, Baltimore D, Darnell J, *J. Molecular Cell Biology*, vol. 4th ed. : Freeman and Company, 2000.
- [298] L. Meirelles, A. Arvidsson, M. Andersson, P. Kjellin, T. Albrektsson, and A. Wennerberg, "Nano hydroxyapatite structures influence early bone formation," *Journal of Biomedical Materials Research Part A*, vol. 87A, pp. 299-307, 2008.